Institute of Engineering Surveying and Space Geodesy
School of Civil Engineering

Mapping The Underworld: Integrated GNSS Based Positioning and GIS Based GNSS Simulation

by
Ahmad Adnan Mohammad Taha
Diploma, BA, MSc

Thesis submitted to the University of Nottingham for
the degree of Doctor of Philosophy

November 2008

To My Mother and My Family
&
In Memory of My Father Adnan Mohammad Taha (1934 – 1994)

Abstract

The United Kingdom utility services are facing the challenge of "mapping the underworld" over four million kilometres of buried pipes and cables (a combination of water, sewage, gas, electricity and drainage). Having accurately mapped pipes and cables increases the efficiency of street works projects, but many existing pipes and cables were only mapped relative to other topographic map features and to varying levels of accuracy.

The aim of this thesis is to research various means of improving the positional accuracy of underground utilities in built-up areas through the use of Global Navigation Satellite System (GNSS), integrated with other positioning systems such as Inertial Navigation Systems (INS) and total stations. The reliability and accuracy of the integrated system is an underpinning issue and this thesis looks at testing both current and future GNSS constellations in a controlled environment at the University of Nottingham campus. GNSS integrated with an INS in the first instance, and integrated with a total-station in the second instance, are tested using a network of established points in urban canyon environments on the campus. Several, new technologies were developed by the author including: Urban Canyon GNSS Simulation (UCGS) – a GIS tool; Multiple Step Integration Technique (MSIT) – a methodology for GNSS/INS data collection and processing; and Continuous Updating Technique (CUPT) – a software for GNSS/total-station integration.

The results of different simulations provide evidence that using more than one GNSS constellation will significantly increase the availability of GNSS positions in urban canyon environments. However, position availability using the criteria of 5 or more satellites with a Position Dilution Of Precision (PDOP) value of 6 or less for centimetre level is not guaranteed 100% of the time when using GNSS alone. Considering the results of the integrated GNSS/INS system, the position availability was guaranteed 100% of the time in all environments, but the accuracy is not enough to meet utility service requirements. The best results used GNSS integrated with a total-station and showed that, in this case, position availability to a centimetre level of accuracy can be guaranteed 100% of the time in all environments.

Acknowledgments

In the name of Allah, most Gracious, most Merciful.

The Author wishes to thank the Engineering and Physical Sciences Research Council (EPSRC) for sponsoring the Mapping The Underworld project. Likewise, I would like to thank the Arab British Chamber of Commerce for awarding me a bursary in my last year.

The work presented could not have been possible without the guidance and support of many people. In the first place, I would like to thank my supervisors Dr Gethin Roberts and Dr Xiaolin Meng, for directing my efforts to complete this work.

Likewise, I would like to thanks Professor Terry Moore for his support and presenting the ION paper. Also, many thanks go to Dr Chris Hide for his expert advice and training on INS device and software. The unlimited support from Dr Andrew Sowter is also highly appreciated. Similarly, the support of Dr Martin Smith is gratefully acknowledged.

The efforts of Mr Craig Hancock, Dr Oluropo Ogundipe, Mr Nikolaos Kokkas, Mr Huib de-Ligt, Dr Waugh Samantha, Dr Chris Hill, Dr Caroline Noakes, Mr Sean Ince and other IESSG staff are gratefully acknowledged as well. In addition, the services of the Natural Environment Research Council (NERC) British Isles GPS archive Facility (BIGF) are gratefully acknowledged for providing archived GPS data.

Many thanks are due to my mother and all members of my family, specially my brother Mahmoud and my sister Ruwaida for their generous prayers and financial support. Also my gratitude goes to my wife Rawda and my kids for being a source of support, motivation and patience.

Contents

List of Figures

List of Tables

List of Publications

Taha, A., Hancock, C., Roberts, G.. W. and Meng, X. (2008) The Use of GPS and INS for Centimeter Positioning Accuracy during Long GPS Outages. *Proceedings of the International Symposium of GPS/GNSS 2008, 11-14 November, Tokyo, Japan,(Paper accepted as reviewed paper).*

Taha, A., Kokkas, N., Hancock, C., Roberts, G.. W., Meng, X. and Uff, J. (2008) A GIS Approach to GNSS Simulation in Urban Canyons. *Proceedings of the European Navigation Conference 2008, 23-25 April, Toulouse, France, CD-ROM.*

Ogundipe, O., Hancock, C., Taha, A. and Roberts, G. W. (2008) The Use of High Sensitivity GPS for Mapping Sub-surface Utilities. *Proceedings of the European Navigation Conference 2008, 23-25 April, Toulouse, France, CD-ROM.*

Roberts, G. W., Hancock, C., Ogundipe, O., Meng, X., Taha, A. and Montillet, J-P. (2007) Positioning Buried Utilities Using an Integrated GNSS Approach. *Proceedings of the International Global Navigation Satellite Systems Society (IGNSS) Symposium 2007, 4 – 6 December, The University of New South Wales, Sydney, Australia. CD-ROM*

Taha, A., Ogundipe, O., Hancock, C., Roberts, G. W. and Meng, X. (2007) Kinematic Positioning Through Continuous Updating Technique. *Proceedings of the Royal Institute of Navigation's Nav'07 Conference, 30 October – 1 November, London. CD-ROM*

Taha A. (2007). A Continuous Updating Technique for Loosely Coupled RTK GPS with Total Station Observations. *Proceedings of the ION GNSS 2007, 24-25 September, Texas, USA, CD-ROM, pp. 1491-1500.*

Montillet, J-P., Taha, A. Meng, X. and Roberts, G. W. (2007) Mapping the Underworld – Testing GPS and GSM in Urban Canyons. *GIS/GPS 2007 – A Supplement to Civil Engineering Surveyor, September, pp. 4-8.*

Taha A., Roberts G. W. and Meng X., (2007). Integrating RTK GPS with Total Station for High Accuracy and High Reliability Positioning in Urban Canyons. *RIN meeting, Imperial College, June, 2007.*

Montillet, J-P., Taha, A. Meng, X. and Roberts, G. W. (2007). Buried Assets: Testing GPS and GSM in Urban Canyons. *GPS World, March 2007, pp. 39-43.*

Roberts G. W., Meng X., Taha A. and Montillet J-P. (2006). The Location and Positioning of Buried Pipes and Cables in Built up Areas. *Proceedings of FIG XXIII Congress, 8-13 October, Munich, Germany, CD-ROM.*

Taha A., Meng X., Roberts G. W., Hide C. and Montillet J-P (2006). Using SmartStation and GPS Integrated with INS to Map Underground Pipes and Cables. *Proceedings of the ION GNSS 2006, 26-29 September, Texas, USA, CD-ROM.*

Chapter 1: Introduction

The UK has a massive network of buried pipes and cables – a combination of water, sewage, gas, electricity and drainage (Figure 1.1). Many of them are 50 years old or more – some even date from the Victorian era, like many of London's sewage systems. Although recently installed assets may have been well mapped, location and attribute data on older services can be very poor, in some cases even non-existent. Furthermore, records of such utility locations are relatively limited and, even when records are available, they almost always refer to positions relative to ground-level physical features that may no longer exist or that may have been moved or altered. This is due to a variety of factors in the creation and maintenance of records as management practices have changed over the last century. Therefore, the exact positions of many assets are either unknown or very inaccurate (up to several meters). This means that locating these assets in order to carry out maintenance is a difficult task. In addition, disturbances such as weather conditions, traffic volume, and other road works can be detrimental to locating these buried assets. Ideally, therefore, all pipes and cables must be located accurately to ensure that streetworks projects are carried out quickly, efficiently and safely.

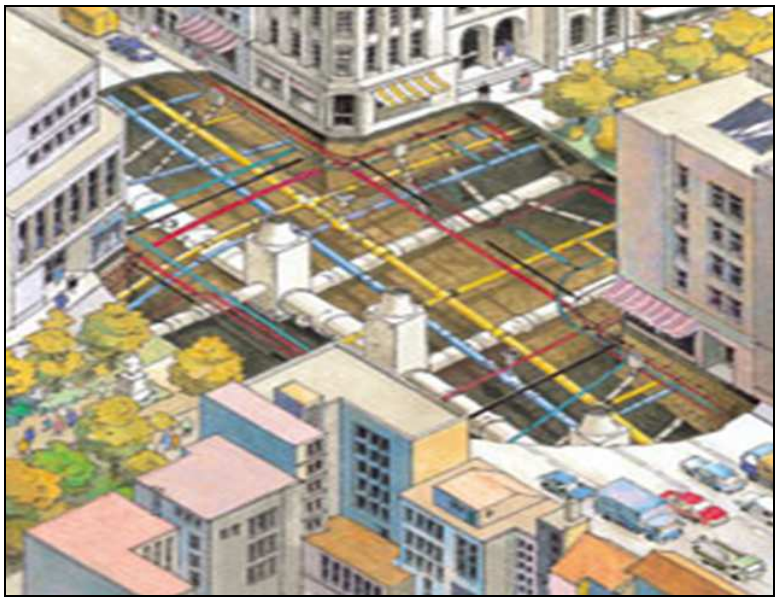

Figure 1.1: Massive network of pipes and cables in built-up environment [MTU, 2008]

A four-year EPSRC funded initiative called the Mapping The Underworld (MTU) project, originally instigated by the UK Water Industry Research (UKWIR) on behalf of the utility companies, aims to solve the problems associated with the difficulty in finding buried infrastructure. The overall aim of the MTU project is to investigate the feasibility of several novel approaches, alongside greatly enhanced existing approaches, to be combined in a single multi-modal approach to the location, identification and condition assessment of buried assets.

The contribution of the University of Nottingham to this project is to research various means of improving the accuracy and availability of positioning underground pipes and cables in built-up areas through a GNSS based system, integrated with other systems such as INS and total-stations. The reliable and accurate positioning of the overall system is an underpinning issue.

Buried asset research faces the challenge of positioning in city centres to a high-level of accuracy, down to the centimetre level. Furthermore, finding and mapping pipes or cables close to a target pipe to prevent any damage to nearby utilities may even need positioning accuracy at the centimetre level.

Locating/finding buried utilities can be performed through the use of different techniques such as old maps, trial holes, detection devices or to stake-out the coordinates. As mentioned previously, old maps/records in most cases are either inaccurate or non-existent. Digging trial holes is a practical solution but time consuming solution and can result in delays in road works, affecting the public. The problem that continues to challenge the industry is currently that there is no available geophysical/detection technology that can locate accurately all underground utility services [Costello et al., 2007]. If absolute coordinates of the buried utilities are known, their position can be accurately located on the surface of the ground using any standard surveying techniques.

Several standard surveying techniques can be employed for this. However, the choice of suitable technique is limited by several factors such as the location of the utilities and the available surveying equipment. The utilities can be situated either in an open area such as a rural area or in a restricted area such as a built-up area. When

positioning in open areas, satellite based systems (i.e. GNSS) can be a powerful tool providing a precise position of a specific feature. GNSS systems offer attractive measurement devices that are portable, stand-alone and easy to operate. Besides, they can also be used in all weather, any time, and, in kinematic mode, can give a centimetre level of accuracy. Nevertheless, most utilities are located in built-up areas where GNSS signals can be lost, unavailable or have large errors due to multipath. In addition, poor satellite geometry could degrade the quality and accuracy of the GNSS position. Traditional surveying instruments such as total-stations can be employed for positioning purposes in such areas. However, the use of total-stations requires a professional to operate the instrument and, in general, the system suffers from several limitations. For example, it requires two intervisible points to start the surveying and it can be time consuming, especially if traverse is being used. In addition, errors could be accumulated if multiple set-ups are compulsory to complete the survey.

To overcome the limitations of accurately positioning in built up areas, a combination of the forthcoming GNSS systems could be one step forward. Current GNSS systems (i.e. GPS and GLONASS) can be tested under a control environment for availability and accuracy assessments. However, the forthcoming GNSS satellites such as a full constellation of GLONASS, Galileo and COMPASS require a simulation tool to check real time positioning performance in built up areas. Satellite visibility of the current and the future constellations in different trajectory scenarios, i.e. kinematic and stop & go, within various 3D city models are required for the current research. Current available simulation tools could be extended to add more constellations, but they are not available to be used in the research at the IESSG. Hence a new Geographic Information System (GIS) tool called Urban Canyon GNSS Simulation (UCGS) has been developed as part of the research in this thesis to calculate satellites visibility and the Dilution Of Precision (DOP) values for both current and the forthcoming GNSS constellations along a trajectory path within a 3D city model (a Triangulated Irregular Network (TIN) or a Raster surface). This tool was written in the Microsoft Visual Basic for Application (VBA) embedded within ArcView/ArcScene and based on several ArcObjects classes.

Another solution that can be used for dynamic positioning in built up areas is GNSS integrated with an Inertial Navigation System (INS). GNSS/INS integration provides a survey system that exhibits superior performance in comparison with either GNSS or INS stand-alone. GNSS and high grade INS are widely used to determine aircraft position and rotation angles for geo-referencing purposes in photogrammetry. Another major area of research focuses on the accuracy of the integrated solution during GNSS outage using a GNSS and a low cost MEMS INS system. Using such a system, metre-level positioning accuracy was reported by several studies over short GNSS outages, i.e. over 3 minutes [Hide and Moore, 2004]. The research in this thesis studies the integration of kinematic carrier phase GPS positions with a high grade INS for the purpose of achieving centimetre-level positioning accuracy in city centre environments, which has not been previously researched. In such environments, long GPS outages for several minutes, i.e. 20 minutes, could occur. Centimetre level positioning accuracy during such long GPS outages has been achieved through the development of a Multiple Step Integration Technique (MSIT) - a methodology for the GNSS/INS data collection and processing. While collecting GNSS/INS data, it is necessary to monitor the GNSS availability. When GNSS positions are available, it is possible to collect kinematic positions. However, when working in outages, a stop-and-go technique to initialize, called Zero Velocity Update (ZUPT), which assists the reduction of the INS drift, must be employed.

GNSS integrated with a total-station can also be used for positioning in built-up areas. GNSS can provide an accurate real time position wherever it is available using reference network (e.g. SmartNet) or local base station corrections. Besides, the user operates the total-station to measure points that have to be surveyed in restricted areas. Similar to the integration of GNSS/INS, GNSS/total-station integration hopes to provide a survey system that exhibits superior performance in comparison with either GNSS or total-station alone. There are different devices that can serve for such integration. For example, a Leica SmartStation, a Leica SmartPole or an IntegratedPole equipped with HSGPS receiver. There could be several Real Time Kinematic (RTK) points, with centimetre-level accuracy, available when setting-up the SmartStation multiple times or when moving the SmartPole/Integrated pole from one surveying point to another. Furthermore, it could be required to collect multiple total-station observations for the same point from different set-ups for data checking.

In some environments, it can be difficult to collect two intervisible RTK points with strong geometry to be used as starting points for the total-station and, in general, the GNSS/total-station integration could suffer from the limitations of both GNSS and total-station systems. Therefore, it was believed to be necessary to develop a technique to overcome, to some extent, the previous limitations and to integrate the GNSS and total-station observations which has not been previously researched. Hence, a new software called Continuous Updating Technique (CUPT) has been developed for the previous purposes. The CUPT was based on the theory of loosely coupled integrating which combines the RTK positions with total-station observations by building stochastic and functional least squares models. To do this, several Matlab functions were written to perform the CUPT calculations and to output an adjustment report and various statistical figures for further analysis. Three types of integrations are offered by CUPT: direct, indirect and network integrations.

The research in this thesis focuses on the above positioning technologies that use GNSS based positioning systems. Nevertheless, other techniques could be used for positioning some of which have been researched in the DTI Vista project, such as Locatalites and GPS integrated with Group Signal Mobile (GSM) system. Other non-GNSS based system (such as OS mapping and laser offset, OS mapping and tape, laser scanners, photogrammetry and other systems) can also be used for positioning buried utilities. However, each of these systems has various limitations such as accuracy, speed, efficiency, etc. (more information can be found in [Parker, 2006]) as well as being unable to use these systems in a dynamic real-time mode. Therefore, they were considered unsuitable for the requirements of this research.

Overall, numerous tests using GNSS alone, various simulations of the current and the forthcoming constellations and several tests using GNSS integrated with INS in the first instance and with a total-station in the second instance have been carried out under control environments in order to assess the position availability and accuracy in built-up areas. This research has resulted in developing several novel approaches to provide a centimetre level of positioning accuracy and 100% of the time positioning availability in urban canyons, that meets the research requirements.

1.1 Research Aim and Objectives

The overall aim of the research in this thesis is to investigate various means of improving the position accuracy and availability for positioning underground utilities in built-up areas through a GNSS based system, integrated with other systems such as INS and total-stations. The following objectives have been drawn to achieve this aim:

- A review of the scientific principles and historical research underpinning the technologies.
- Establishment of 'truth' coordinates for a network encompassing a range of conditions similar to that which would be found in city centres.
- Testing of current GNSS (GPS and GLONASS) satellites and simulating of the future GNSS (GPS, full GLONASS constellation, Galileo and COMPASS) satellites.
- Testing of GPS integrated with a high grade INS for positioning in built-up areas.
- Testing of GPS integrated with a total-station using three configurations: the Leica SmartStation; a robotic total-station with an IntegratedPole equipped with the Leica 1200 GPS receiver in the first instance; and equipped with High Sensitivity GPS (HSGPS) in the second instance.

1.2 The Novelty of the Research

The novelty of the research in this thesis is in addressing and overcoming the limitations of using GNSS-based positioning for mapping underground utilities in built-up areas through the following:

- There is no available tool that can perform satellite visibility for all GNSS constellations along a desired trajectory in a 3D city model. Hence, a new GIS tool -**Urban Canyon GNSS Simulation** (UCGS) - has been developed in this research. This tool simulates satellite visibility (the number of available satellites) and DOP values, for both current and the future GNSS constellations, along a desired trajectory path within a 3D city model environment. UCGS is a unique tool in its ability to perform the following:

- Provide a powerful link between GIS and GNSS.
- Build and modify an Almanac file for any GNSS constellation.
- Add building to TIN, taking into the account the gable type roofs.
- Simulate the number of available satellites and DOP values for multiple GNSS Constellations.
- Perform simulation within either a TIN or a Raster 3D city model.
- Conduct simulation in different trajectory scenarios including: static point or grid of points, kinematic points along polyline, stop and go points along polyline or file of points.
- Easy to operate (no professional GIS knowledge is required to use this tool) and used to filter the required layers within a GIS project, such as find all available TIN/Raster layers and find all available polylines.

No such tool currently exists that can perform all of the previous tasks. Most of the current tools perform satellite visibility predictions without considering the terrain or structures that block GNSS signals, a major issue in urban areas.

- To the author's knowledge, GNSS integrated with high grade INS has not been previously tested for positioning in city centres to map the under ground utilities. This system will be tested along a city centre-like trail route. In such environments, long GNSS outages for several minutes, i.e. 20 minutes, could occur. Centimetre level positioning accuracy during such long GNSS outages has been achieved through the development of a **Multiple Step Integration Technique** (MSIT) - a methodology for the GNSS/INS data collection and processing. While being used for collecting GNSS/INS data, it is necessary to monitor the GNSS positioning availability. When GNSS positions are available, it is possible to collect kinematic positions. However, when working in outages, a stop-and-go technique to initialize, called Zero Velocity Update (ZUPT), which assists the reduction of the INS drift, must be employed.
- A new software called **Continuous UPdating Technique** (CUPT) has been developed by the author to combine RTK GNSS positions with total-station observations. Such an integration technique has the following advantages when used with GPS:

- Offers three types of integration between RTK GPS positions with total-station observations: direct, indirect and network integration.
- Increases the overall accuracy for the integrated positions as well as reducing the position uncertainties compared with a GPS or total station only solution.
- Eliminates the need of two control points to start the surveying, as required in conventional total-station and SmartStation surveying.
- Takes advantage of all RTK GPS points that could be available if the SmartStation is utilised in multiple setups technique, and hence breaks down growth of the errors in this technique.
- Can be used with a robotic total station and an IntegratedPole, equipped with dual frequency Leica GPS in the first instance, and equipped with HSGPS in the second instance, where several RTK GPS points could be available when moving the IntegratedPole from one point to another.
- Combines multiple total-station observations with RTK GPS positions, if available, for the same point and calculates the best coordinates for this point
- Can be used for error detection and correction if redundant observations are available
- Outputs an adjustment report and various statistical figures for further analysis.

1.3 Organization of the Thesis

In order to report on the research caned out by the author, the thesis is organized in eight chapters as follows:

- **Chapter 1** introduces the thesis and provides an overview of the aim and objectives, as well as the thesis outline used to complete the project.
- **Chapter 2** looks at the problem of utility monitoring and solutions detailed in existing literature.

- **Chapter 3** addresses GNSS. It provides an overview of the current and the forthcoming GNSS constellations. Also, it presents the results of testing the current GNSS capability and analyses these results in terms of accuracy and availability.
- **Chapter 4** provides an overview about GIS, programming under the ArcGIS environment and how 3D city models have been built on this thesis. It also discusses the limitations of current satellite visibility prediction tools. The results from Chapter 3 show there is a need to develop a simulation tool for future GNSS satellites. This Chapter describes and evaluates a simulation tool developed by the author for this purpose.
- **Chapter 5** focuses on the specific availability of GNSS in urban canyons using the simulation tool and analyses the results of simulations.
- **Chapter 6** addresses GNSS and INS integration. It gives an overview of the technique and discusses the limitations of previous research. Then, it describes a methodology developed by the author and the results of applying this methodology using GPS/INS in numerous tests.
- **Chapter 7** addresses GNSS and total-station integration. It provides an overview of the technique and discusses the limitations of previous research. After that, it presents software and algorithms developed by the author for processing various data and an analysis of the results of the processing when using GPS and total stations.
- **Chapter 8** concludes the research and recommends possible areas for further research activities.

Chapter 2: Background

This Chapter begins with a description of underground utilities and the economic impact of their maintenance, followed by an overview of the Mapping The Underworld (MTU) project. Existing methods for the position and location of buried utilities will then be discussed and the accuracy requirement for the MTU project will be defined. Finally, an overview of the positioning techniques that could be used for positioning in built up areas will be given.

2.1 Utilities and Economic Distribution

The UK has over four million kilometres of buried pipes and cables – a combination of water, sewage, gas, electricity, drainage, telecoms, misc. e.g. oil, hot water, lighting, etc.. Every year, it is estimated that, on average, four million holes are dug in UK highway and footpaths by utilities to repair assets, provide connecting services to new premises and to lay new cables and pipes [McMahon et al., 2005]. Although recently installed assets are usually well mapped, location and attribute data on older services can be very poor and in some cases even non-existent. This is due to a variety of factors in the creation and maintenance of records as management practises have changed over the last century. Poor data quality can lead to unnecessary holes dug in the wrong place and third party damage to other underground services.

While most utility companies maintain records for their asset data in digital vector formats, it is common for third party users to only have access to printed versions (some of this data may be hardcopy derived from a vector web GIS) [Beck et al., 2007]. Furthermore, the records are sometimes incompatible between various companies, with the result that, for example, positioning one company's pipes relative to another's cables is difficult.

The problem that continues to challenge the industry is that there is uncertainty of GIS data with no available single technology that can locate accurately all existing

underground utility services or that can provide a means of condition assessment that is generally applicable [Costello et al., 2007]. In addition, due to the inaccurate data and location knowledge of the services, more excavation is carried out than would be required if the coordinates of these buried utilities were known more accurately. This is true for excavation as well as trench-less technology.

Utility companies require quick and efficient access to their assets in order to assess or repair damage and replace any degraded material. Particularly in urban environments, the bulk of utility infrastructure is buried in the highway. Therefore disruption and congestion is likely when excavation occurs. Due to the use of trial holes to find the utilities in the first place, and the fact that other utilities are sometimes damaged during excavation, accurate knowledge of the locations of such utilities would be of great benefit. This would reduce the direct, indirect and social costs associated with excavation. The social costs of just traffic congestion caused by excavation are estimated to be between £2 and £4 billion per annum in the UK [McMahon et al., 2005].

Further to this, the direct costs of trenching and reinstatement of approximately four million street openings each year is estimated at approximately £1 billion per annum. Equally important, there are also considerable indirect costs (about £2 billion per annum or maybe more according to some estimates) to society owing to disruption on the roads caused by works, waste and pollution [McMahon et al., 2005]. From June 2008, it was expected that the Traffic Management Act will require all owners of underground assets to provide asset location information in GIS format on request [DFT, 2006; NUAG, 2006]. However, this has not happened yet and is still subject to a final decision.

Overall, the lack of real-time accurate knowledge of a utility's location results in an increased number and size of street openings, plus longer duration of excavation with an undesirably high number of "hits" on third party assets, over and above those caused by poor practice. Given these statistics, it is rather surprising that it has taken until the 21st century for a serious initiative to do something about properly locating and recording the position of buried services, so that pipes and cables are located

accurately to ensure that streetworks projects are carried out quickly, efficiently and safely.

2.2 The Mapping The Underworld Project

A four-year EPSRC funded initiative, the Mapping The Underworld (MTU) project, originally instigated by UK Water Industry Research (UKWIR) on behalf of the utility companies, aims to solve the problems associated with the difficulty in finding buried infrastructure. Five integrated research projects were funded to lay the foundation for a programme of work that will ultimately need direct stakeholder involvement in developing and proving the system:

- Buried asset location, identification and condition assessment – a multi-sensor approach.
- Mapping and Positioning.
- Knowledge and Data Integration.
- Enhanced Methods of Detection of Buried Assets.
- Mapping the Underworld Network.

The Universities of Bath, Birmingham, Leeds, Nottingham, Oxford, Sheffield and Southampton, with funding from EPSRC and support from UKWIR, were charged with undertaking the above projects. The overall work is to last for 4 years, and started in the summer of 2005. In addition to research work, the projects also organise workshops on a regular basis in order to disseminate findings and ideas. The project has a web page www.mappingtheunderworld.ac.uk.

The overall aim of the MTU project is to investigate the feasibility of several novel approaches, alongside greatly enhanced existing approaches, to be combined in a single multi-modal approach to the location, identification and condition assessment of buried assets. These include developing Ground Penetrating Radar (GPR), Acoustic Quasi-static field techniques, interaction of the soil in previously excavated areas, as well as the interaction of the soil with the utility, and integrating their combined information with the location of the data. More information about these technologies can be found in [Metje et al., 2007]. The devices will be both surface

based, whereby a suite of sensors will sweep across an area, as well as pipe based, so that the sensors are taken through a sewer pipe and the surrounding utilities detected.

The University Nottingham's contribution is to research various means of improving the position accuracy and availability in built-up areas through a GNSS based system, integrated with other systems such as INS and total station. The reliability and accuracy of the overall positioning system is an underpinning issue.

Related research was carried out at the IESSG by a second PhD student, Jean-Philippe Montillet, under another project called Visualising Integrated Information on Buried Assets to Reduce Streetworks (VISTA). This DTI funded project focuses on enhancement and integration of existing legacy asset information, together with dynamically acquired accurately geo-referenced data in the street, and development of novel techniques to display the resulting knowledge to digging teams and network planners. Both MTU and VISTA are proof of concept projects that evaluate the range of technical challenges and approaches to position, particularly in urban canyons.

2.3 Positioning and Locating Buried Utilities

Obtaining accurate information on underground infrastructure is becoming more critical during the planning and design phases of construction projects. Information on buried assets has been recorded in many different forms over time. Early records were paper-based which have been digitised in some way over the past thirty years. Not all of this information is recorded against the OS National Grid; much was originally recorded with reference to ground-level physical features, many of which have been changed or removed**.** More recent records are in digital format with reference to OS National Grid. Utility companies provide information about their facilities in different formats: secure WebGIS, CD-Roms, microfiche, faxed copies of paper records or marked out in-situ.

Currently, positioning new assets is carried out before the burial process using, in most cases, total-stations and levels (relative positioning). Three-dimensional OS national grid coordinates are usually recorded for these assets along with attribute

information such as asset type, diameter, material, owner, etc.. The surrounding area and the existing physical landmarks, such as roads, buildings, or bridges for example are also surveyed. This process, which is usually referred to as as-built or as-laid drawing, allows utility companies to relate their maps to OS maps in order to show the location of the assets with regards to the surrounding environment. However, when OS mapping is overlaid with as-built drawings, some significant spatial discrepancies can be observed. As a result the OS have just completed a Positional Accuracy Improvement (PAI) programme to correct the errors within their data. The OS product MasterMap is now PAI corrected and will overlay, to some extent, with absolute coordinates (the urban and rural mapping have a 95% accuracy confidence of 1 and 2.5 metres respectively) [NUAG, 2006].

Jeong et al. [Jeong et al., 2002] and NUAG [2006], in their survey, report that most utility companies are looking to use GPS-based positioning system to produce absolute 3D coordinates for the assets. This will allow having a fixable scale, if the data is captured by GPS and stored electronically. In addition, it will increase the overall accuracy of locating the buried assets.

In order to locate/find the buried assets, several methods have been or are currently employed as follows:

- *Historical utility records*: These records were drawn in different media including: paper, tracing cloth and drafting film. In the UK, OS mapping was generally used as a reference source with companies tracing their records directly onto map sheets [Beck et al., 2008]. These records provide basic information on possible locations, congestion and orientation of utilities. Such information may be incomplete or inaccurate and therefore inadequate to be used by a contractor on their own, but are useful to plan density and orientation of survey lines, choose the right equipment, and plan the survey operations.
- *Scanned maps*: According to Arnott and Keddie [1992], in the late 1980s and early 1990s most utility companies made significant progress towards scanning and digitising their utility records and tying them in to a relative position system. However, information loss, inaccuracies in the scanning, poor digitising methods, human error, and the benchmarks used in the

identification systems can all lead to errors. Also, scanned maps very often locate the utility line in only two dimensions (E, N), usually in the form of a line on a map. The third dimension (Ht), depth, is critically important for the construction of accurate three-dimensional (3D) plans of buried assets [NETTWORK, 2002].

- *Digital maps related to physical features and OS maps*: Unfortunately, utilising a physical landmark as a reference point for locating a buried underground utility does not always facilitate accurate location of the asset. Occasionally, physical landmarks undergo a change. For example, a road may undergo widening or repair that may alter its relative distance to the buried assets. A building may undergo renovation or even demolition, precluding the ability to utilise such a structure as a point of reference for a location measurement. As mentioned before, relating assets to OS map backgrounds produces an accuracy similar to the OS map, i.e. 1.0m in city centres and 2.5m in rural areas, if the latest background is used, which can lead to inaccurate locating of the utility assets. However, some information was transferred from earlier maps with lesser accuracy.
- *Trial holes*: The severe consequences of not accurately positioning a buried asset, frequently forces utility contractors to dig trial holes with very great caution which results in delays in road works, affecting the public [Cumberbatch, 2005].
- *Geophysical detection tools*: Geophysical methods provide information about the physical properties of the earth's subsurface. There are two general types of methods: Active, which measure the subsurface response to electromagnetic, electrical, and seismic energy; and passive, which measure the earth's ambient magnetic, electrical, and gravitational fields. In general, Jeong et al. [2002] summarises the widely used geophysical methods in practice as illustrated in Table 2.1.

Table 2.1: Summary of widely used geophysical methods in practice [Jeong et al., 2002]

Method		Principle of the Method	Energy Propagation over Utility	Interpretation of the Data	Application Information
Electromagnetic methods (EM)	Pipe and Cable Locator	A transmitter emits an electromagnetic wave (radio frequency, normally ranging from 50 Hz to 480 kHz) to the ground or directly to the pipe and a receiver detects reflected waves from the underground utility.	Electromagnetic current is produced on the underground metallic object by the emitting wave. This current generates a radio frequency through the utility.	The receiver detects the reflected wave and gives an indication such as beep sound or visual sign on the screen for an operator to detect the existence of underground utility.	- Only metallic objects can be detected. - Various application techniques (Conductive, Inductive, Passive, Sonde insertion, Tracing wire /metallic marking tape). - Good for tracing utilities. - Crew size of 1~2 people.
	Terrain Conductivity	A transmitter emits an electromagnetic wave to the ground and a receiver detects reflected waves from the underground utility.			- Only metallic objects can be detected. - Effective depth is typically 15 feet or so. - Good for searching utilities - Crew size of 1 person.
	E-line locator	Same as pipe and cable locator but digging a hole and installing an E-line through a mechanical fitting is needed.			- Used for plastic gas pipe. - Exact location of pipe is required. - Relatively expensive.
	Metal Detectors	A transmitter emits an AC magnetic field into the ground and a receiver analyzes a corresponding magnetic field.	Metallic object reflects a slightly different magnetic field from the current reflected from the surrounding soil	A receiving unit detects the different magnetic field and emits a noise, alerting the operator to the presence of the metallic object	- Only metallic objects can be detected. - Only applicable for shallow manhole lids, valve box covers and so on. - Crew size of 1 person.
	Electronic Marker System (EMS)	A locator transmits electromagnetic signal to the electro marker and a receiver detects the reflected signal from the electronic marker	Electronic marker reflects the electromagnetic signal back to the locator	The location is indicated with both visual reading and audible tone.	- Usually installed for non-metallic utilities. - Different frequency of electro markers for different type of utility.
Ground Penetration Radar (GPR)		The radar sends electromagnetic waves (commonly between 10 - 1,000 MHz) and receives reflected waves from subsurface material. Responds to changes in electrical properties (dielectric and conductivity).	GPR profile is generated when the antenna is moved along the surface.	The data to interpret is changes in the materials electrical properties, through which GPR waves travel. The interpretation is to be made with computer programs by skilled geologists.	- Both metallic and non-metallic utilities may be imaged. - Rule of thumb: from surface to 6 feet of depth and very low conductivity and highly different impedances, a round utility whose diameter in inches does not exceed the depth in feet can be imaged.
Magnetic Methods		It measures the intensity of the earth's magnetic field. Deviation of magnetic intensity caused by ferrous objects is detected by the equipment	Ferrous objects radiates its own magnetic field	The different intensity of the magnetic field captured by two sensors creates a beep sound or high numeric number on the screen for an operator to detect the existence of metallic object.	- Useful for detecting and tracing ferrous (steel or iron) utilities. - Good for searching utilities. - Crew size of 1 person. - Effective depth is typically 10 to 20 feet.
Acoustic Emission Method		An acoustic transducer applies a sound wave into the pipeline. The sound wave travels along the utility lines and special sensors on the ground detect the sound wave that reach the surface.	The utility line emits the sound wave to the surface.	Special sensors such as geophones or accelerometers are used to detect the sound emitted from the pipe.	- The method is useful for designating plastic pipe (typically water/gas pipe). - The method can service up to 1000 ft (300m) distance for gas pipe and 500 ft for water pipe. - Crew size of 1~2 people.

In addition to the widely used methods, there are other geophysical methods that can be used for locating buried utilities. They include resistivity method, infrared thermography method, micro gravitational method and seismic refraction/reflection method. More details about these methods can be found in Jeong et al. [2002]. In order to effectively select an appropriate geophysical method, it is crucial to establish a set of criteria based on the characteristics of each method and information that can be obtained from drawings and site visits. Ten criteria were identified by Jeong et al. [2002] for the selection of appropriate geophysical methods as follows: type of utility, material of utility, joint type of metallic pipe, special materials for detection, access point to utility, ground surface condition, inner state of pipe, soil type, depth of utility and diameter/depth ratio.

Highly trained technicians or geophysicists are usually required to operate and to effectively interpret the images/data collected by the geophysical technologies. The complexity existing in the selection of the most appropriate imaging technology stems from the shortcomings of each imaging technology. Further, none of the geophysical methods are able to provide accurate and comprehensive data on the location of non-metallic buried pipes [ITRC, 2003]. Plastic pipes and fibre optics cables are the most difficult to detect because they do not emit energy and therefore cannot be located using current methods. Services buried in concrete cause similar difficulties and require more thorough investigation.

- *GPS and total-stations*: Since the adverse effect of mis-locating or utility hits is becoming more and more apparent, utility companies are now starting to consider the ease of locating utilities prior to construction. For instance, providing absolute positions and correct records of the newly constructed utilities at the time of construction can be one of the most effective solutions. Currently, traditional survey methods, using levels and total-stations, and CAD are the prevailing data management system, but GPS and GIS appear to be the next generation for data management systems, due to their apparent advantages over traditional surveying methods and CAD [Jeong et al., 2002; (NUAG), 2006]. If absolute coordinates are known for the utility asset

(positioned before the burial process), GPS and/or total stations can be employed to determine, i.e. to centimetre level, the asset location on the surface of the ground very precisely. Knowing the 3D coordinates of the asset and the height coordinate of the surface, the depth of asset can also be simply calculated.

2.4 Accuracy Requirements and Factors Affecting Accuracy

A questionnaire about the accuracy requirement for mapping underground utilities was developed by Birmingham University [MTU, 2006]. This included both the accuracy of the positioning system and the accuracy of detection devices (i.e. GPR). 59 questionnaire responses provided input. The results of these responses are shown in Figure 2.1.

A significant majority of respondents said that they require horizontal and vertical absolute accuracy to be within a margin of 100mm, for all service types. Similarly, NUAG [2006] and Parker [2006] recommended that all future spatial data includes the 3rd dimension and is captured with a minimum standard of 100mm in all three dimensions. While a horizontal accuracy of up to 300mm would be acceptable for many respondents, a greater error margin appears acceptable only to a small proportion of stakeholders. Also, 300mm provides an acceptable vertical accuracy for many respondents (although for electricity and gas infrastructure this generally reduced to 200mm), with limited support for the acceptability of accuracy margins greater than 300mm.

As mentioned before, the required accuracy includes both the accuracy of the positioning system and the accuracy of detection devices (i.e. GPR). Therefore, the positional accuracy needs to be in the range of a few centimetres, as the GPR accuracies are typically a few centimetres.

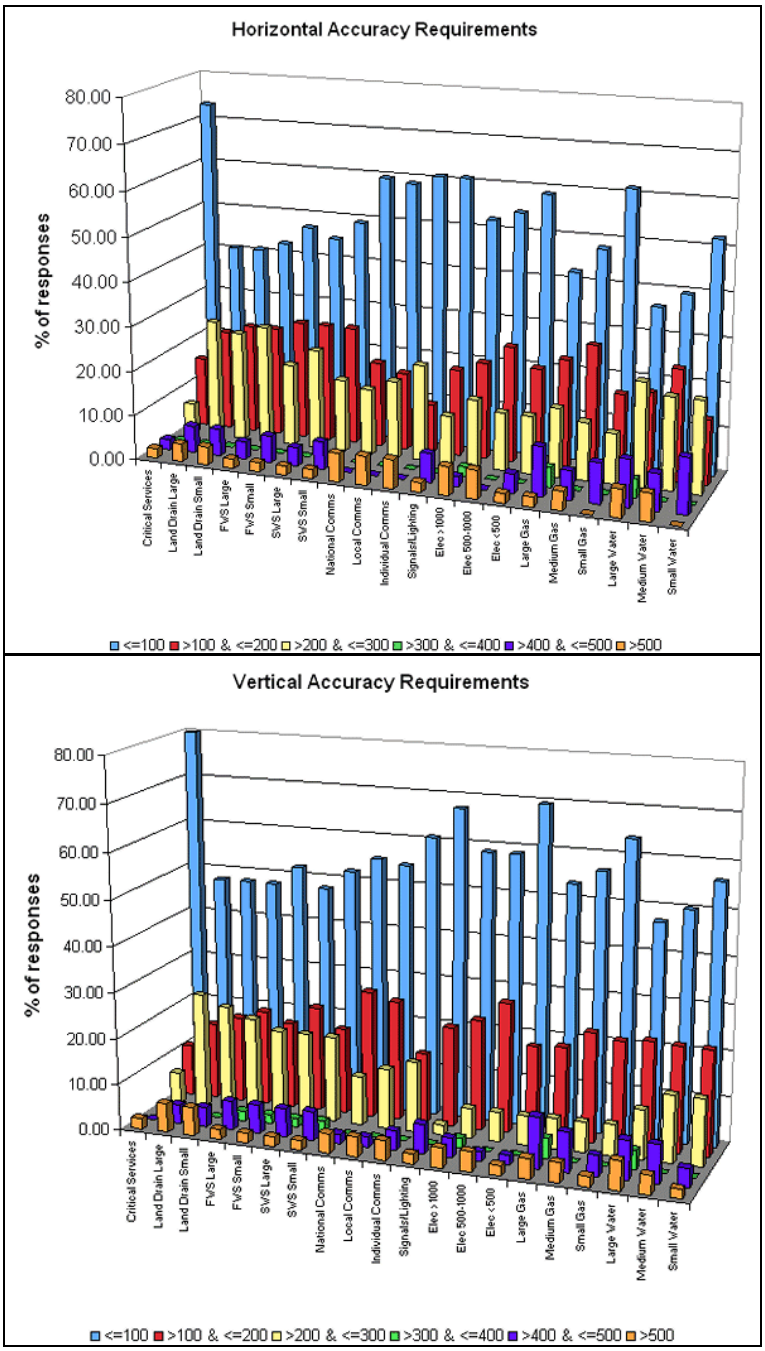

Figure 2.1: Horizontal (top) and vertical (down) accuracy requirements for underground utilities based on MTU questionnaire

In order to achieve the positional accuracy requirements, GNSS systems can be employed. Such systems can provide a superior accuracy in open areas. However, buried asset research faces the challenge of positioning in urban canyons where GNSS signals can be lost, unavailable or have large errors. Therefore, GNSS integrated with other systems such as INS or total station could be the optimal solution. In this case, the integrated systems could aid the GNSS system or provide a position when GNSS fails. Such systems will be discussed in the next section.

2.5 Positioning Techniques in Difficult Environments

There are many surveying techniques available which could be used for positioning. The use of these techniques depends on several factors such as the cost of the instruments, the precision of the procedure and the area of interest (open or built-up area). For example, when positioning in an open area, it is possible to achieve a high degree of 3D positional accuracy using traditional surveying instruments such as total station, satellite based systems (i.e. GNSS) or Leica's SmartStation. However, when positioning in some areas, such as urban canyons, some of the above systems do not work as effectively. For example, GNSS signals may be lost, unavailable or have large errors in built up areas. Since the majority of the utilities are located in city centres with a prevalence of urban canyons; the following section will discuss the positioning techniques that could be used for positioning in these built up areas.

2.5.1 Total-Station

A total-station is an electronic digital theodolite with an electronic distance measurer (EDM) and an on-board microprocessor. In addition there is either a built-in data collector (on-board data card) or interfaced data collector (connected by cable or wireless) incorporated in the instrument.

For several years, total-stations have been widely used for positioning in built up areas. These devices have advantages such as high precision, the ability to perform computations in the field, they work well in both open and closed areas, and they are cost effective. However, they suffer from several drawbacks such as the fact that errors are cumulative if multiple steps are required, the network geometry can affect the position accuracy and they are a two person system. Furthermore, they require a trained surveyor, intervisibility between total-station and target, and control points to start work from.

The theodolite used in a total-station, measures horizontal and vertical angles while the EDM measures the distance. A modern total-station, such as the Leica TCR1201, can have angular precision of 1 second with 0.1 seconds display resolution and

distance measurement precision in standard mode of (2mm+2ppm) with 1.5 seconds measurement time [Leica-Geosystems-AG, 2006d].

The total-station microprocessor automatically monitors the instrument's operating status and manages built-in surveying programs [Kavanagh, 2006]. Hence, computations and adjustments for the collected field data can be performed immediately in the field. The basic concept of a total-station is based on measuring angles and distances, and it is not dependant on whether the area to be surveyed is open or closed. This is a great advantage for the system. However, a line-of-sight (intervisibility) between the total-station and the objects being measured is essential.

The average cost of a total-station ranges in price from £3,000 to £10,000. The price is dependant on the total-station precision, distance measurement range, reflectorless features, data collector capacity and other features.

Traditionally for all forms of legal, mapping and engineering surveys, techniques of traversing are used as control surveys and to establish control points. However, the multiple measurements, used in traversing, can lead to the accumulation of systematic and constant errors [Irvine and Maclennan, 2006]. In addition, the traverse/network shape (geometry) can affect the position accuracy. Besides, building the traverse requires much effort and takes a long time, which reduces the overall productivity of the total-station system.

For efficient surveying, a two-person team needs to be employed. One person (a surveyor) operates the total station while the other (an assistant) carries a pole with a reflector target on the required points to be measured. However, using either a robotic total-station (significantly more expensive than conventional units) or a reflectorless total-station (measures distances directly to an object) can potentially remove the need for an assistant surveyor.

2.5.2 Satellite Based Systems

The attractive features offered by GNSS techniques include working in all weathers, 24 hours a day, a high level of relative accuracy, intervisibility between control stations is not required, ease of operation and high productivity. However when using a GNSS system for positioning in dense urban areas, this system has limiting factors such as the number of tracked satellites, spatial geometry and multipath errors. Furthermore, GPS instrumentation is approximately twice the cost of a total-station while a GNSS set can be even more expensive. These issues will be discussed in this section as well as the combination of GNSS satellites.

GNSS satellites transmit electromagnetic waves which pass through cloud and rain, and can be used globally wherever they are visible, on the ground, in the air and at sea, day or night. Dual frequency and carrier phase measurements from at least 5 well distributed satellites are required to achieve a real time relative position with a high level of precision. Relative position employs two GPS receivers (base and rover) simultaneously tracking satellite's observables (code and carrier phase signals). An example of relative positioning is the Real-Time-Kinematic (RTK) technique, with communication links between base and rover receivers. A user with minimum experience can operate the rover receiver using this technique. Centimetre accuracy can be achieved for a dual frequency geodetic receiver such as the Leica GX1230 (RTK precision of 10mm+1ppm for horizontal and 20mm+1ppm vertical) [Leica-Geosystems-AG, 2007a]. It should be noted that intervisibility between control points is not required because both base and rover receivers collect observations from satellites. However, GNSS receivers do need to be located within an open sky area where satellites are visible from it.

When using a GNSS system for positioning, there is no need for traversing and hence there are no cumulative errors to propagate into consequent GNSS points. In addition, after setting up a local base station or using an RTK GPS network, the operator can start surveying at the required points. As a result high productivity with little effort is guaranteed when using this system.

It has long been recognised that the accuracy, availability and reliability of satellite based positioning are very dependent on the number of tracked satellites and their spatial geometry [Santerre, 1991]. Line of sight to a sufficient number of satellites is not always possible when working in built up areas due to different obstructions such as buildings and trees.

The reflected signals from different obstructions can also introduce multipath errors which, as a result, can decrease the position accuracy. In order to reduce the impact of multipath, several techniques have been developed as receivers and antennas have evolved, however, multipath remains a problem in urban areas.

The combination of GNSS systems makes it possible to provide better accuracy, reliability and availability especially where satellite signals may be obscured, such as in urban canyons [Rizos et al., 2005; Daghay et al., 2005]. In addition, future GNSS systems will emit signals on 3 frequencies whereas the current GPS and GLONASS systems uses only 2 carrier frequencies [Moore, 2006]. These extra frequencies will allow a better correction of the atmospheric disturbances as well as increase the number of observations available for ambiguity resolution. As a result, positioning at locations with bad visibility will become more accurate and feasible as more than 100 positioning satellites will be available for use.

Previous research about GNSS integration carried out by Rizos et al [2005] showed that '*the visibility improvements of the combined systems with respect to GPS-only are therefore approximately 200%, 250% and 350% for GPS/GLONASS, GPS/Galileo and GPS/GLONASS/Galileo respectively'*. In addition, the Positional Dilution of Position (PDOP) levels of the combined system are approximately 50% of the levels for the standalone GPS scenario. Therefore, the GPS/GLONASS/Galileo system is expected to strengthen the geometry and contribute a twofold improvement in the levels of precision [Rizos et al., 2005].

Another research project conducted by Daghay et al in [2005] showed that '*using GPS+Galileo more visible satellites are available worldwide and the combined system reduces or even eliminates the presence of problem locations worldwide*'. In addition, the contribution of the satellite geometry to the total positioning error

budget is reduced to about 40% when using the demonstrated combined DOP values [Daghay et al., 2005]. However, these results were obtained under free-ideal conditions.

The above results show the potential benefit of GNSS integration. Therefore, it is worth while to test such integration under a controlled environment but it is also imperative to simulate the future satellites in an urban environment with different obstruction levels, i.e. the University of Nottingham campus trial route, as carried out as part of the research in this thesis.

2.5.3 GNSS and INS Integration

An inertial navigation system (INS) is a self-contained navigation system that primarily measures position, velocity and altitude. The system's inertial frame measures the accelerations and the angular velocities by using an inertial measurement unit (IMU). The IMU is a group of six inertial sensors which are three linear accelerometers and three gyroscopes (gyros). An INS also contains a computer system to perform the position calculations.

The problem with IMUs is that the error from sensors (noise, bias, scale factors, temperature sensitivity etc.) results in a drift of the position solution over time. To overcome this, other sensors (such as odometer, speedometer, magnetic compass or GPS) can be integrated with the INS to provide additional information such as speed, heading and position. By using one or more of these sensors, the augmentation can be extended which will improve the system's performance. For instance, GPS can be used for real-time calibration of the INS by global Latitude and Longitudinal coordinates. In addition, GPS and INS are ideal for integration, as their error dynamics are totally different and uncorrelated [Kaplan and Hegarty, 2006]. This integration between GPS and INS improves significantly the overall accuracy and reliability compared with the stand alone units [Cramer, 1997].

GPS and INS have been integrated for such a long time, and in so many ways, that it is difficult to detail all the possible methods and results. However, in summary there

are two primary integration schemes performed through the process of Kalman filtering: loosely and tightly coupled mode. In the loosely coupled mode, the GPS receiver and the INS are treated as separate navigation systems. The GPS provides a position, velocity, and time solution. The INS implements its navigation/attitude algorithms to give a position, velocity, and attitude. An integrated Kalman filter is then applied to combine the GPS and INS solutions. However, in the tightly coupled mode, only a single Kalman filter is applied to process both sets of GPS observables (code and/or phase) and INS measurements (more information can be found in Chapter 6).

The major advantage to a loosely coupled system is its design simplicity relative to a tightly coupled system. In addition, only high quality position can be chosen for updating, which ensures no GPS position errors will affect the combined GPS/INS position. However, tightly coupled, based on centralized Kalman filter, is preferred [Gautier and Parkinson, 2003] and proved from previous researches (see, for example,[Hide and Moore, 2004]) to have several theoretical advantages over a loosely coupled system. The main advantage being that any number of GPS measurements may be used in the filter to help bind INS error growth. Although, the disadvantage to such a system is the complexity of the design and the ability to make such a system functional in practice.

Other advantages are that zero velocity measurements can be used with GPS/INS integration to increase the accuracy of such a system. In addition, the use of a Kalman filter smoothing algorithm can significantly reduce the errors across the GPS gaps [Zarchan and Musoff, 2005]. However, smoothing is a post-processing algorithm that is used when all of the data (forward and backward data) are available.

Generally, for a high level of accuracy, a high quality IMU, such as Honeywell CIMU with a gyro bias specification of 0.0035 degree/hour, is required. However, such a high specification system can cost the user over £100,000.

2.5.4 SmartStation and SmartPole

The Leica SmartStation comprises of a Leica TPS1200 total station with an ATX1230 SmartAntenna. The SmartAntenna is a 12 channel dual frequency GPS RTK receiver that fits on and communicates with the total station [Leica-Geosystems-AG, 2006c]. The SmartAntenna can be attached to a pole equipped with a prism to produce the SmartPole. SmartStation or SmartPole with a total-station can cost the region of £30,000 depending on the total station used (i.e. robotic total station, 1 or 5 seconds precision, etc).

Typically, the GPS provides the user with a real time high accuracy position wherever it is available using either reference network (e.g. SmartNet) or local base station corrections. A minimum of two inter-visible SmartStation points (one as a base station and one as a reference object) are required to complete the survey. Then the user operates the total-station to measure angles and distances to the objects that have to be surveyed in restricted areas. Alternatively subject to position availability, the SmartPole can be utilised to measure positions using either GPS or total-station techniques as required.

The SmartStation and SmartPole eliminate the need for traversing to propagate control points into the survey area by providing RTK GPS positioning of the total station [Cranenbroeck, 2005].

Previous work by Hill [2005] showed that surveying using a SmartStation completed work 38% faster than conventional traversing on a topographic survey whilst maintaining an accuracy of better than 15mm in both horizontal and vertical components. Using the Leica SmartStation in urban areas, Parker [2006] reported an absolute accuracy of 15mm in 3D and showed the advantages of using this system over others.

GPS coordinates are provided in an earth-centred, earth-fixed coordinate system defined by the GPS satellite ephemerides (the WGS84 system when the broadcast ephemeris is used). Thus, these coordinates need to be transformed into a local

geodetic system before they can be integrated with results from conventional surveys (total-station), which can introduce some errors.

All set-up possibilities within the SmartStation, determined by Hill [2005], require having a minimum of two inter-visible control points. However, when positioning in densely settled urban areas, it is often difficult to find two inter-visible RTK fixed points with good geometry. In addition, if multiple set-ups are required to complete the survey, it is possible to have several points where RTK position is available. Similarly, when moving the SmartPole from one surveying point to another, it is possible to collect numerous RTK points with position fixed. Traversing techniques could be used in the multiple set-up case, although this could result in cumulative errors. After testing the current SmartStation and SmartPole, none of them make use of all available RTK positions that could be available during the data collection.

In addition to the previous unused positions, there is not any research which studies the integration of RTK GPS positions with total-station observations. Therefore, it is worth investigating a technique to integrate the GPS positions with the total-station observations. Such a technique would overcome the previous limitations as well as taking advantage of the several RTK points that could be available when SmartStation or SmartPole are utilised. For the research in this thesis, it was decided that this technique should allow the operator to:

- start from points with temporary coordinates
- collect all necessary details (temporary coordinates)
- collect RTK positions wherever it is possible on any point
- measure distances horizontal and vertical, in two directions, for control points
- combine all observation to produce adjusted integrated positions
- update all positions as new observations are collected from the GPS or the total-station.

2.5.5 Other Techniques

Locatalite networks and/or pseudolites integrated with GPS can also be used for positioning. GSM signals can also be integrated with GPS in order to aid positioning.

Other non-GNSS based system (such as OS mapping and laser offset, OS mapping and tape, laser scanners, photogrammetry and other systems) can also be used for positioning buried utilities. However, each of these systems has various limitations such as accuracy, speed, efficiency, etc (more information can be found in [Parker, 2006]) and were considered to be not suitable to the satisfy research requirements of the MTU project.

2.6 Summary

This Chapter has described the situation and economic impact of buried assets. Accurate positions of the buried assets are essential especially for utility companies which require quick and efficient access to their assets in order to assess or repair damage and replace any degraded material. Particularly in urban environments, the bulk of utility infrastructure is buried in the highway. Therefore disruption and congestion is likely when excavation occurs. The MTU project is a four year EPSRC funded initiative aimed at solving the problems associated with finding buried infrastructure. Seven universities are working with different tasks within the project. The University of Nottingham's contribution to this project is to research various means of improving the position accuracy and availability in built-up areas through a GNSS-based system, integrated with other systems such as a total station and an INS.

This Chapter has also discussed the current methods of positioning new assets and of locating the buried utilities. Most utility companies are looking to use a GPS-based positioning system to produce absolute 3D coordinates for the assets. This will allow a fixed scale to be used if the data is captured by GPS and stored electronically. Several methods were discussed that are used to locate buried utilities: historical utility records, scanned maps, existing maps related to OS map and physical features, trial holes, geophysical detection tools and GPS and total-stations.

The accuracy requirement for the MTU project has been defined, based on a questionnaire developed, as 100mm for both locating and positioning the buried utilities. However, finding and mapping pipes or cables close to a target pipe to prevent any damage to nearby utilities may need absolute positioning accuracy at the

centimetre level. An overview of the positioning techniques that could be used to achieve such accuracies in the built up areas was given, in the context of the research and development carried out in this thesis.

Chapter 3: Review of GNSS Positioning Technology

3.1 Introduction

Global Navigation Satellite System (GNSS) is the generic term for any autonomous space-based radio positioning system providing navigation and timing information worldwide. GNSS is comprised of several satellite constellations that are either operational or are in the process of implementation (developmental). Currently, as of 2008, the only fully operational GNSS is the Global Positioning System (GPS) deployed by the U.S.A. With help from India, the Russian Federation is in the process of restoring the constellation of their deteriorated GLONASS to full operation. Meanwhile, China has indicated it will expand its regional Beidou navigation system into a global system called COMPASS. Separately, the European Galileo is a next generation GNSS in the initial deployment phase. Other developing systems are Indian Regional Navigational Satellite System (IRNSS) of India and Quasi-Zenith Satellite System (QZSS) of Japan.

GNSS satellites transmit radio signals which pass through the atmosphere, and can be used globally wherever they are visible, on the ground, in the air and at sea, day or night. In their simplest form, GNSS receivers can pick up these signals and calculate a three-dimensional position by the simple process of resection, using distances measured to the satellites. The attractive features offered by GNSS techniques include working in all weathers, 24 hours a day, a high level of relative accuracy, intervisibility between control stations is not required, ease of operation and high productivity. However when using GNSS for positioning in dense urban areas, there may be limiting factors such as the number of tracked satellites, spatial geometry and multipath errors.

This chapter provides an overview of both operational and developmental GNSS. It describes how GNSS-based positioning can be performed. The results of three tests of the current GNSS satellites (GPS and GLONASS) along Nottingham's Campus trial route are then discussed and analysed.

3.2 Current Operational GNSS

This section provides an overview about the current operational GNSS satellites: GPS and GLONASS.

3.2.1 GPS: an Overview

The Global Positioning System was developed and is operated by the United States Department of Defence and usually known simply as GPS. The first GPS operational satellite was launched in 1978 and global availability was reached at the end of 1994 [Groves, 2008]. GPS is currently the world's most widely utilized satellite navigation system.

The GPS system can be separated into three segments: space, control and user equipment segments. The space segment is the satellite constellation which is summarised in Table 3.1 [Proakis, 2001; Kaplan and Hegarty, 2006].

Table 3.1: GPS constellation parameters

No of satellites	24 (nominal constellation, today 30 satellites)
No of orbital planes	6 Medium Earth Orbit (MEO) planes evenly spaced 60 degrees
Inclination	55° with respect to the equatorial plane
Semi-major axis	26,599.7 Km
Orbit Period	11 hours, 58 minutes

There are 10 different GPS navigation signals, broadcast across three bands, known as link 1 (L1), L2 and L5 [Groves, 2008]. Most of these signals are being introduced under the GPS modernization program, such as a second civil code on L2 and the third civil code on a new carrier, L5 [Leick, 2004]. Broadcasting more GPS signals on more frequencies will improve the positional accuracy and robustness of GPS, especially in built up areas. GPS uses Code Division Multiple Access (CDMA) to distinguish between satellites. This means that each satellite transmits a different

pseudorandom noise code in its signal but all satellites have access to the whole spectrum.

The control segment is a network of ground stations that monitor and operate the GPS satellites. There are six monitor stations (one of them is a master control station located in Colorado Springs, Colorado) and four ground antennas spaced around the globe [El-Rabbany, 2006]. The user segment consists of an unlimited number of users equipped with GPS receivers (signal receiving and tracking equipments) which can be used for navigation purposes and/or geodetic positioning. At least four satellites are required to calculate position, velocity, and time estimates. A full description about the GPS segments can be found in any of the GPS text books such as [Seeber, 2003; Kaplan and Hegarty, 2006; El-Rabbany, 2006; Groves, 2008].

3.2.2 GLONASS an Overview

The Global Navigation Satellite System (GLONASS) is managed for the Russian Federation Government by the Russian Space Forces and the system is operated by the Coordination Scientific Information Centre (KNITs) of the Ministry of Defence of the Russian Federation. The first satellites for GLONASS were launched in 1982, but the system was not a fully functional navigation constellation until 1995 [Groves, 2008]. Due to economic difficulties, the GLONASS system has deteriorated to only 15 satellites (as of 2008), leading to gaps in coverage and only partial availability. Since December 2004, India has been a partner in the operation of GLONASS and full operational capability (24 satellites) is proposed to be completed by 2010 [Revnivykh, 2005]. Similar to GPS, GLONASS can be separated into space, control and user equipment segments. The operational space segment of GLONASS is summarised in Table 3.2 [ICA, 2002].

Table 3.2: GLONASS constellation parameters

No of satellites	24 (21 operational and 3 spares, today 15 active satellites)
No of orbital planes	3 MEO planes evenly spaced 120 degrees
Inclination	64.8° with respect to the equatorial plane
Semi-major axis	25,440 Km
Orbit Period	11 hours, 15 minutes

There are 6 different GLONASS navigation signals, broadcast across three bands: L1, L2 and L3 [Groves, 2008]. As with GPS, most of these signals are being introduced under the GLONASS modernization program such as a second civil signal on L2, since GLONASS-M satellites in 2003, and a third civil signal on L3, since GLONASS-K satellites in 2008 [Revnivykh, 2005]. In contrast to GPS, GLONASS uses Frequency Division Multiple Access (FDMA) to distinguish between satellites. Using this method each satellite transmits the same code, the receivers knows which satellite the signal is coming from because each satellite transmits on a different frequency. However, use of CDMA for future GLONASS signals is under consideration [Anon, 2007].

Unlike the ground control segment of GPS, which is spaced around the globe, the ground control segment of GLONASS is entirely located within the former Soviet Union territory. It comprises the GLONASS system control centre located near Moscow, two monitor stations in Moscow and four Telemetry, Tracking and Control (TTC) stations. However, as part of the modernization program, a network of at least 12 monitor stations are planned to be used to determine the orbits of GLONASS satellites [Revnivykh, 2005].

Despite its lack of development and any uncertainty about its future, there are many manufacturers that produce GNSS receivers making use of both GPS and GLONASS satellites such as Leica, Trimble, Topcon, JAVAD, Magellan Navigation and NovAtel.

3.3 Developmental and Proposed GNSS and RNSS

3.3.1 Galileo

Galileo is a planned GNSS, being developed by the European Union (EU) and European Space Agency (ESA). After the recent launch of GIOVE-B (Galileo In-Orbit Validation Element B) on the 27th April 2008, to add to the already launched GIOVE-A, there are two Galileo test satellites in orbit, and there is a possibility that a third test satellite, GIOVE-A2, will be launched in the second half of 2008 (this was not launched yet), with Galileo scheduled to be fully operational by 2014 [Groves, 2008].

Similar to GPS and GLONASS, Galileo can be separated into space, control and user segments. The proposed fully deployed Galileo system is summarised in Table 3.3 [European-Space-Agency, 2008].

Table 3.3: Galileo constellation parameters

No of satellites	30 (27 operational and 3 spares, today two experimental satellite)
No of orbital planes	3 MEO planes evenly spaced 120 degrees
Inclination	56° with respect to the equatorial plane
Semi-major axis	29,601.297 Km
Orbit Period	14 hours, 5 minutes

Similar to GPS signals, there will be 10 different Galileo navigation signals, broadcast across three bands: E5 (E5a and E5b), E6 and E1-L1-E2 [Falcone et al., 2006]. All the Galileo satellites will share the same nominal frequency, making use of CDMA technique compatible with the GPS approach.

The ground control segment of Galileo will be two Galileo Control Centres. Each will manage 'control' functions supported by a dedicated Ground Control Segment (GCS), and 'mission' functions supported by a dedicated Ground Mission Segment (GMS). The GCS will use a worldwide network of nominally 5 TTC stations and

will handle satellite housekeeping and constellation maintenance [ESA, 2006]. The GMS will use a global network of nominally 30 stations and will handle the navigation and timing system [ESA, 2006]. Currently, there are a few manufacturers producing Galileo ready receiver that can be updated, using updating software, when Galileo is in operation. These manufacturers include JAVAD, NovAtel and U-blox.

3.3.2 Beidou and COMPASS

The Chinese regional navigation satellite system (RNSS) Beidou (Big Dipper) is made up of a constellation of three geostationary (GEO) satellites [Groves, 2008]. It has a limited coverage (spanning China and neighbouring countries) and applications (due to the use of two-way ranging which limits the number of users and introduces a lag of about a second).

In 2007, China began a program to develop and expand Beidou into a GNSS, called COMPASS. The nominal COMPASS constellation is summarised in Table 3.4 [Groves, 2008]. Additionally, COMPASS will include Beidou GEO satellites as well as two further GEO satellites launched in 2007 (a total of five GEO satellites at longitudes of 58.75° E, 80° E, 110.5° E, 140°E and 160° E) [Hein et al., 2007]. Further three satellites are proposed to be positioned in inclined geosynchronous orbits (IGSO), at 55° with respect to the equator and crossing it at a longitude of 118° [Hein et al., 2007].

Table 3.4: COMPASS constellation parameters

No of satellites	30 (nominal constellation, today one experimental satellite)
No of orbital planes	3 MEO planes evenly spaced 120 degrees
Inclination	55° with respect to the equatorial plane
Semi-major axis	27,840 Km
Orbit Period	13 hours, 14 minutes

There will be 6 different COMPASS navigation signals, broadcast across three bands: E5b, E6 and E2 [Grelier et al., 2007]. All the COMPASS satellites will share

the same nominal frequency, making use of CDMA technique compatible with the GPS and Galileo approaches.

The current Beidou ground segment is within the region of China and consists of a central control station, three ground tracking stations for orbit determination, and ground correction stations [SinoDefence, 2007]. COMPASS user terminals are intended to be compatible with GPS, GLONASS, and Galileo receivers. Recently, Javad Company has manufactured a GNSS receiver that is capable of tracking all current and future GNSS signals using the TRIUMPH Chip with 216 channels [JAVAD, 2008].

3.3.3 IRNSS

The Indian Regional Navigational Satellite System (IRNSS) is a proposed satellite navigation system to provide India with a fully independent GNSS service. The system is planned to be operational between 2009 and 2012 [Groves, 2008].

The proposed system would consist of a constellation of seven satellites: three GEO and four IGSO satellites [Hein et al., 2007]. The space segment, ground segment and user receivers will all be built in India.

3.3.4 QZSS

The Quasi-Zenith Satellite System (QZSS) is a proposed enhancement for GPS in Japan. It is intended to increase the number of satellites visible in Japan especially in difficult areas such as urban canyons. Additionally, it will provide a GPS differential corrections service to a higher resolution than the existing Multi-functional Satellite Augmentation System (MSAS).

The proposed system would consist of a constellation of three IGSO satellites with the first satellite scheduled to be launched in 2009 [Groves, 2008]. Each satellite will be positioned on orbit so as to pass over the same ground track at a constant interval. In addition, QZSS was designed so as to guarantee that at any time at least one of the three satellites is close to the zenith direction over Japan.

3.4 Fundamentals of GNSS-Based Positioning

Each GNSS satellite continuously broadcasts microwave radio signals composed of carrier frequencies (two or more sine waves) modulated by digital / pseudorandom (PRN) codes (two or more) and a navigation message. The carrier and the code can be used to determine the distance from the user's antenna receiver to the satellite's antenna. The navigation message contains information regarding the satellite's orbital position, satellite's clock correction, and health and almanac data for all the satellites. Besides, the GNSS signals are Doppler (or frequency) shifted resulting from the relative dynamics of the transmitting satellite and the receiver (whether stationary or in dynamic motion) [Kaplan, 1996].

3.4.1 PRN Code and Carrier Phase Ranges

The accuracy of the GNSS-based positioning is highly dependant on accurate range measurements between the user's receiver antenna and the satellite's antenna. As stated before, the code and the carrier are used mainly to determine such ranges. A GNSS receiver measures the time offset between a PRN code received from a GNSS satellite and a replica PRN generated within the receiver by correlating the two codes [Leick, 2004]. The code-tracking loop within the receiver shifts the replica PRN generated within the receiver in time until maximum correlation occurs [Leick, 2004]. The measured range is the time offset multiplied by the speed of light. This range is contaminated by the lack of time synchronization between the clock in the GNSS satellite and the clock in the GNSS receiver, along with other errors and biases such as atmospheric delay, multipath and receiver noise. Therefore, the measured range is not very accurate and usually referred to as pseudo-range, rather than range.

More accurate ranges to satellites can be obtained through the carrier phases. When the GNSS receiver is switched on, it measures a fraction of a cycle of the received signal very accurately and continues tracking the phase changes. The initial number of complete cycles (or integer ambiguity) between the satellite and the receiver

remain unknown or ambiguous. This integer ambiguity can be resolved using relative (differential) positioning technique or precise point positioning (PPP) for absolute (stand-alone) positioning technique.

The process of obtaining the range from the carrier phase can be corrupted by the presence of the cycle slip. A cycle slip is a discontinuity or a jump in the measured carrier phase resulting from a temporary loss of lock in the carrier tracking loop of a GNSS receiver. This could be caused by obstructions, such as buildings, trees and other objects, radio interference, sever ionospheric disturbance, high receiver dynamics or due to a receiver malfunction [El-Rabbany, 2006]. Cycle slips must be identified and corrected to avoid large errors in the range based on carrier phase.

3.4.2 Various Positioning Techniques

Position determination using GNSS signals is well known. The basic principle of GNSS-based positioning is the process of trilateration using distances measured to the satellites. Theoretically, only three distances or three simultaneously tracked satellites are required to calculate a 3D position. However, the GNSS receiver is usually equipped with quartz clocks, which are less precise than the atomic clocks (highly stable rubidium or caesium) on board the satellites. Therefore, a fourth satellite is needed to account for the receiver clock offset [Kaplan and Hegarty, 2006]. The more satellites are available, the more redundant data and the better the accuracy of the position. In general, positioning with GNSS can be performed by either of two ways: absolute (stand-alone or point) positioning or relative (differential) positioning.

3.4.2.1 GNSS Point Positioning

GNSS point positioning, also known as the absolute, standalone or autonomous positioning, involves one GNSS receiver only. Either a classical approach or a precise point positioning (PPP) approach can be employed. The classical approach uses timing code (to calculate pseudoranges) from at least four satellites and the broadcast ephemeris (to determine the satellite coordinates) to calculate the

receiver's point position. As stated before, pseudoranges are contaminated by a number of biases and errors which are explained in the pseudo-range observation equation:

$$p = \rho + c*(dt - dT) + d_{ion} + d_{trop} + d_{eph} + v$$

where p is the pseudo-range, ρ is the geometric range to the satellite, c is the speed of light, dt and dT are the offsets of the satellite and receiver clock from the GPS time, d_{ion} and d_{trop} the delays imparted by the ionosphere and troposphere, d_{eph} is the errors in the satellite ephemeris and v represents observation residuals. The satellite clock is monitored by the control centre and the clock offset broadcast in the navigation message. The receiver clock offset is considered as unknown and solved for using the fourth pseudorange. The ionospheric delay can be removed, when using a dual frequency receiver, through the combination of the L1 and L2 measurements to generate the so-called ionosphere-free linear combination. However, Klobuchar model is usually used when a single frequency receiver is being employed, to mitigate the ionospheric delay to some extent. The tropospheric delays can be mitigated, to some extent, using models such as Hopfield and Saastamoinen [Leick, 2004]. In the classical approach, stand alone position does not attempt to mitigate the errors in the satellite ephemeris. Therefore, the accuracy of the classical GNSS point positioning is limited to several meters (i.e. up to 15 m) as a result of the presence of unmodelled errors and biases.

The three dimensional coordinates of the receiver are implicated in the geometric range ρ.

$$\rho = \sqrt{(X^s - X_r)^2 + (Y^s - Y_r)^2 + (Z^s - Z_r)^2}$$

where (X^s, Y^s, Z^s) are the coordinates of the satellite s and (X_r, Y_r, Z_r) are the coordinates of the receiver r. Usually, the receiver's coordinates are calculated through the process of least squares or Kalman filtering technique, with the observation equations linearized when they are used in the least squares. More details about linearization of observation equations can be found in [Strang and Borre, 1997].

To improve the accuracy of stand alone positioning, both carrier phase and pseudorange measurements are used in the PPP technique. Using PPP, most of the errors and biases described in the pseudorange equation can be modelled with sufficient accuracy. The exception is the tropospheric delay, which is usually treated as an additional unknown to be estimated along with the receiver coordinates, receiver clock and the ambiguity parameters [El-Rabbany, 2006]. The ionospheric delays are eliminated using the ionospheric-free function. An essential element in achieving high level of position accuracy with PPP is accurate satellite clock offsets, which are available for post processing as part of the precise ephemeris [Leick, 2004]. The accuracy of PPP can be of a centimetre level for a static receiver using a long observation series (i.e. 30 minutes) , and of sub-decimetre of a roving receiver [Leick, 2004].

3.4.2.2 GNSS Differential Positioning

GNSS differential positioning, also known as relative positioning, employs two (or more) GNSS receivers that are simultaneously tracking the same satellites. The measurements of two (or more) receivers simultaneously tracking a particular satellite, have more or less the same errors and biases. It is possible, therefore, to generate several types of simultaneous baseline solutions of combined measurements, known as differences, such as single-differencing (one satellite and two receivers or two satellites and one receiver), double-differencing (two satellites and two receiver) and triple-differencing (double-differencing across two epochs) [Van Sickle, 2001]. The differential positioning can be carried out using either pseudo-ranges or carrier phase observables.

The differential positioning using the pseudo-ranges is commonly known as DGPS (differential GPS) and mainly used for navigation purposes with accuracy in a range of sub meter to about several meters. The position of a receiver is computed using its differentially corrected pseudo-ranges. Local base station/s, with precisely known coordinates, are used in a Local Area DGPS (LADGPS), where the pseudo-range corrections are computed by a reference station and a differential message is continuously transmitted in real-time via special telemetry links in RTCM SC-104 format [Van Sickle, 2001]. Alternatively, Wide Area DGPS (WADGPS) can be used

in DGPS, where the corrected differential message is broadcast through a geostationary satellite. Unlike a LADGPS, a WADGPS can cover large areas, i.e. WAAS cover the USA and EGNOS cover Europe. Also, the ephemeris errors and ionospheric and tropospheric biases are known from the modelling carried out as part of the WADGPS system.

High precision relative positioning at centimetre-level, can be achieved through the use of carrier phase observables. A carrier phase-based relative positioning is accomplished by simultaneously tracking carrier phase observables at two (or more) GNSS receivers. As mentioned before, the GNSS receiver measures a fraction of a cycle very accurately and continues tracking the phase changes. The initial number of complete cycles (or integer ambiguity) between the satellite and the receiver remain unknown or ambiguous. The carrier phase observation equation explains the different parameters to measure the range between the satellite and the receiver:

$$N + \Phi = \frac{f}{c}\rho + f * (dt - dT) + d_{ion} + d_{trop} + d_{eph} + v$$

where N is the integer ambiguity between the satellite and the receiver (unknown), Φ is the carrier phase observed by the receiver and f is the frequency (known). Other terms are explained in the pseudo-range observation equation.

As mentioned before, most of the errors and biases can be eliminated or mitigated using differential positioning. A major issue facing carrier phase observables is to resolve the integer ambiguity. Several methods and algorithms have been developed to resolve the integer ambiguity based on the surveying technique (static or kinematic) used in the data collection. Static and fast (rapid) static surveying employ two or more receivers (at least one at a control point) which simultaneously track the same satellites for a certain period of time. The occupation time varies from several minutes to a few hours or even to a whole day, depending on several factors such as the baseline length, accuracy required, number of visible satellites, and the satellite geometry. The minimum time is required to assure a large enough amount of data are available to resolve the integer ambiguity. Measurements are made over a sufficiently long observation session so that there is a change in the geometry of the satellites. This facilitates the separation of ambiguity parameters from the baseline

solution as part of least-squares, or Kalman filtering [Leick, 2004; El-Rabbany, 2006].

To overcome the need for long observational time spans, several methods have been developed. One such method is to use a known baseline; where the ambiguity parameters are determined after a short period of time (known as receiver initialisation). With this method, the ambiguity parameters calculated in the initialisation period are used to solve the coordinates of new points. A disadvantage for such method is that if a loss of lock occurs, returning to a known position is required. A more advanced technique, developed to determine the integer ambiguity while the receiver is in motion, is On-The-Fly (OTF) ambiguity resolution. Resolving the ambiguities OTF can be performed using observational time span (initialisation) as short as a few seconds. OTF requires at least five satellites for ambiguity resolution, but four satellites can be used for positioning once the integer have been resolved.

Kim and Langley [2000] classified ambiguity resolution techniques into three categories. The first class of algorithms was the ambiguity resolution in the measurement domain, which uses C/A-code or P-code pseudoranges. The second class of algorithms was the search technique in the coordinate domain, which employs the Ambiguity Function Method (AFM) [Counselman and Gourevitch, 1981]. The third class of algorithms was the search technique in the ambiguity domain, which comprises the most abundant group of techniques that are based on the theory of integer least-squares. The following are some representative techniques in that class: the Least-Squares Ambiguity Search Technique (LSAST) [Hatch, 1990]; the Fast Ambiguity Resolution Approach (FARA) [Frei and Beutler, 1990]; the Least-Squares AMBiguity Decorrelation Adjustment (LAMBDA) [Teunissen, 1994]; the Fast Ambiguity Search Filter (FASF) [Chen and Lachapelle, 1995]; and the Optimal Method for Estimating GPS Ambiguities (OMEGA) [Kim and Langley, 1999].

A fixed or float phase solution can be calculated from the ambiguity resolution. The phase fixed solution is a solution with high level of accuracy, centimetre-level, and it is obtained when the baseline processor is able to resolve the integer ambiguity

search with enough confidence. The phase float solution is less accurate than the phase fixed solution and it is obtained when the baseline processor is not able to resolve the integer ambiguity search with enough confidence.

3.5 Satellite Constellation Geometry and Dilution of Precision

Satellite constellation geometry, i.e. the distribution of visible satellites relative to the user, plays a very important role in determining positioning precision and accuracy. The geometry is said to be strong when satellites are spread out in the sky (Figure 3.1 left) as opposed to close to each other or in a line (Figure 3.1 right). As the ranges measured between satellites and receiver all contain errors due to atmospheric delay and satellite ephemeris, intersection of the ranges will form an uncertainty area containing the user's position. This area is highly dependent on the satellites geometry. The better the satellite the geometry is, the small the uncertainty area is and the higher the precision and accuracy of the position is.

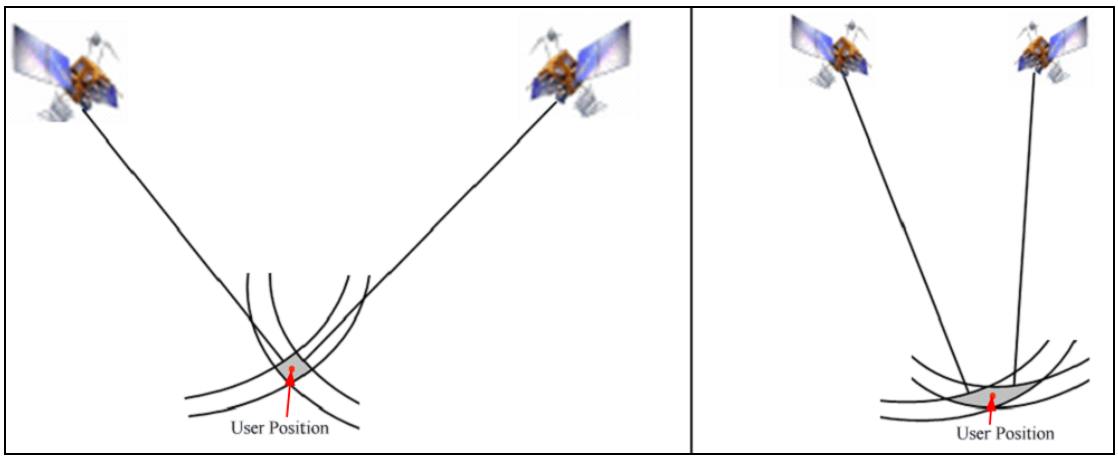

Figure 3.1: Strong satellite geometry (left) and poor satellite geometry (right)

The geometric strength of the satellite constellation can be quantified by a unit-less number called Dilution of Precision (DOP) [El-Rabbany, 2006]. The lower the value of DOP, the better the geometric strength is, and the higher the corresponding positional precision and accuracy becomes. The DOP indicators are Vertical (VDOP), Horizontal (HDOP), Positional (PDOP: HDOP & VDOP), Time clock offset (TDOP) and Geometric (GDOP: PDOP & TDOP). The DOP values are computed based on the relative receiver-satellite geometry at any instance. They are simple functions of the diagonal elements of the covariance matrix of the adjusted

parameters, containing the variance of the positional and receiver clock bias errors. The presence of obstructions, e.g. in an urban environments, can influence the DOP. A full explanation about DOP value calculation from the covariance matrix can be found in [Strang and Borre, 1997]; Leick, 2004; Kaplan and Hegarty, 2006].

3.6 Test of Current Global Navigation Systems

Three GNSS tests were conducted at The University of Nottingham to collect GNSS observables from current GNSS satellites (GPS and GLONASS) along the University's trial route (as an example of a built up area – see Appendix 2). The aim of the first test was to examine the improvement of the availability of obtaining phase fixed solutions, as the number of satellites is increased in a GNSS (GPS and GLONASS) solution when compared with a GPS only solution, in kinematic mode along the trial route. The accuracy improvement when using a GNSS solution when compared with a GPS only solution was then evaluated in the second and third tests.

3.6.1 GNSS Data Collection

The first GNSS test was carried out using a set of Leica GX1230 GG receivers (local base and rover) on 10th August 2006 (GPS week 1387). These receivers are multi-frequency geodetic receivers which are capable of collecting both GPS and GLONASS observables. They were used together with two Leica AX1202 GG antennas. On the other hand, data for the second and third tests were collected with the Trimble R8 System, consisting of multi-frequency base and rover receivers with their internal antennas. Collection for these two tests took place on two different days at different times: in the afternoon of 18th April 2008 (GPS week 1475) and in the morning of 22nd April 2008 (GPS week 1476). This was to allow the use of different satellites in the data collection.

In the three tests, GPS and GLONASS observables were collected, at one second epoch interval rate with an elevation mask of 10˚. Simultaneously, GPS and GLONASS observables were collected at the base receiver on a reference station (TOW) located on the turret of the IESSG building, while the rover receiver moved

along a predefined route, resulting in baselines ranging up to about 400 metres. In the first test, to be able to verify more fixed positions, breaks for re-initialisation were taken in case Loss Of Lock (LOL) to the satellites occurred. As a result of this, more fixed positions could be verified. In the second and third tests, the rover receiver was stationed above points located along the route for a period of two minutes per point.

3.6.2 GNSS Data Post-Processing

After collecting GNSS data along the trial route, all data sets were post-processed twice, using LGO v.6.0 software. This software is easy to use and allows the user to post-process GPS data and or a combined GPS and GLONASS data. KinPos software (the IESSG GNSS post-processing software) was not used as it does not support post-processing a combined GPS and GLONASS data, is still under development, and cannot cope with cycle slips in challenging environment such as urban canyons. The first processing with LGO was using only GPS data while the second processing was using both GPS and GLONASS data together. The processing strategy described in Appendix 1 was followed in both cases.

As mentioned in Appendix 1, Leica DBX file can be directly imported into LGO. However, in order to process the data collected with the Trimble R8 System, the proprietary Trimble DAT format had first to be converted to a combined GPS-GLONASS RINEX file using Trimble's 'Convert to RINEX' utility.

3.6.3 The First Test: Results and Analysis

The results and analysis of a GPS only solution and a GNSS solution are presented in the following section.

3.6.3.1 GPS only Solution: Results and Analysis

The post-processing results from LGO showed that several different solution types, i.e. phase, code and no solution, were calculated when using GPS only. The computed Cartesian coordinates for both the phase and code solution were converted

to National Grid OSGB36 coordinates using Grid InQuest software. The grid coordinates were then superimposed on an OS MasterMap as shown in Figure 3.2.

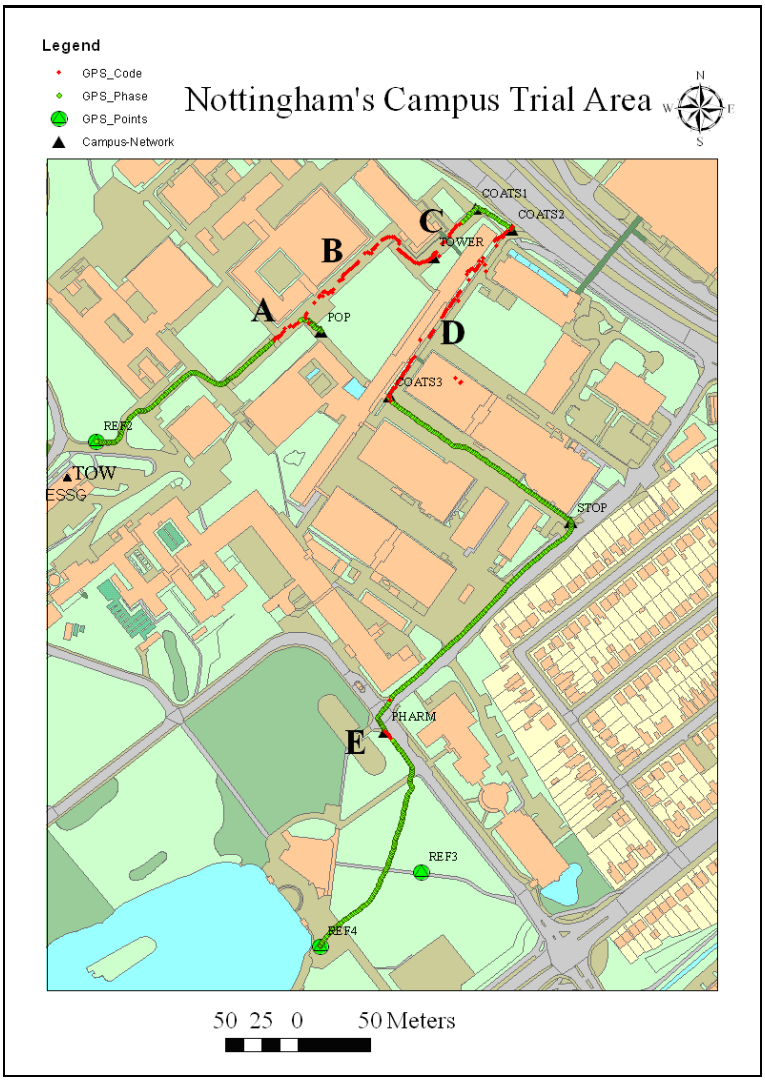

Figure 3.2: Availability of GPS only phase and code solutions for Test1 (© OS MasterMap)

Figure 3.2, shows that GPS only was successful in obtaining phase solutions in the more open sky areas along the trial route. However, in the difficult areas (areas with a large number of obstructions such as A, B, C and D), several epochs were calculated as either code solutions or without any solution (such as gaps under bridges or epochs where LOL occurred). Also, the area E which is located near a big tree (near the point PHARM in Figure 3.2) was also calculated as a code solution. In general, there were 52%, 34% and 14% epochs with phase solution, code and no solution respectively.

As mentioned before, in order to have a real time phase fixed solution using OTF technique, it is required to have observables from at least five satellites. Therefore, it is prudent to analyse the number of the satellites used during the tests. This is shown in Figure 3.3.

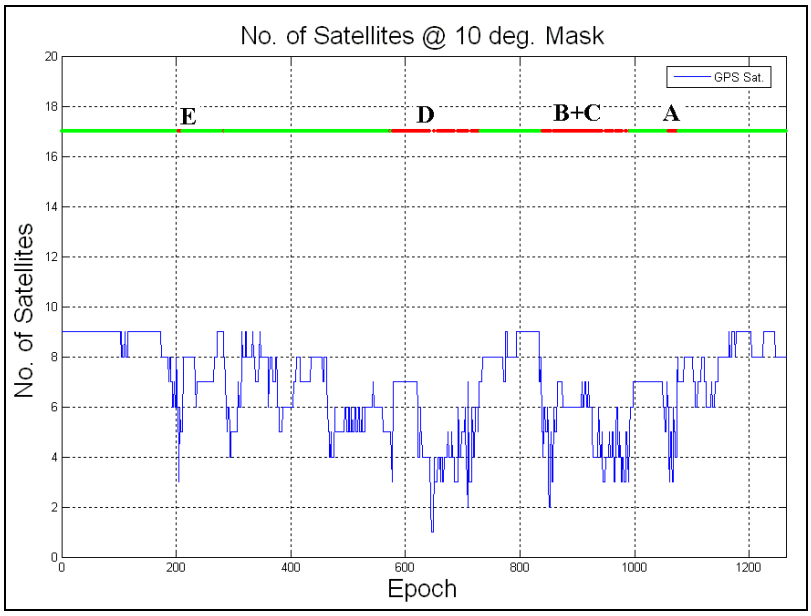

Figure 3.3: Number of GPS Satellites for Test1

From Figure 3.3, it is clear that the number of GPS satellites, at 10 degrees mask angle, is fluctuating between 1 and 9. When linking the number of satellites in Figure 3.3 with the locations, it is clear the number of visible satellites in the open areas is more than that in the difficult areas (i.e. A, B, C, D and E). In addition, it can be seen that the code solution and gaps mostly occurred when the number of satellites was less than 5. This shows the importance to have five or more satellites in order to be able to calculate a fixed position. However, other factors can also affect the position, such as the satellite geometry and the data quality.

3.6.3.2 GNSS Solution: Results and Analysis

Like the GPS only solution, the output Cartesian coordinates from processing both GPS and GLONASS data were converted to National Grid OSGB36 coordinates using Grid InQuest software. The Grid coordinates (both of the phase and the code solutions) were then superimposed on the OS Matermap (Figure 3.4).

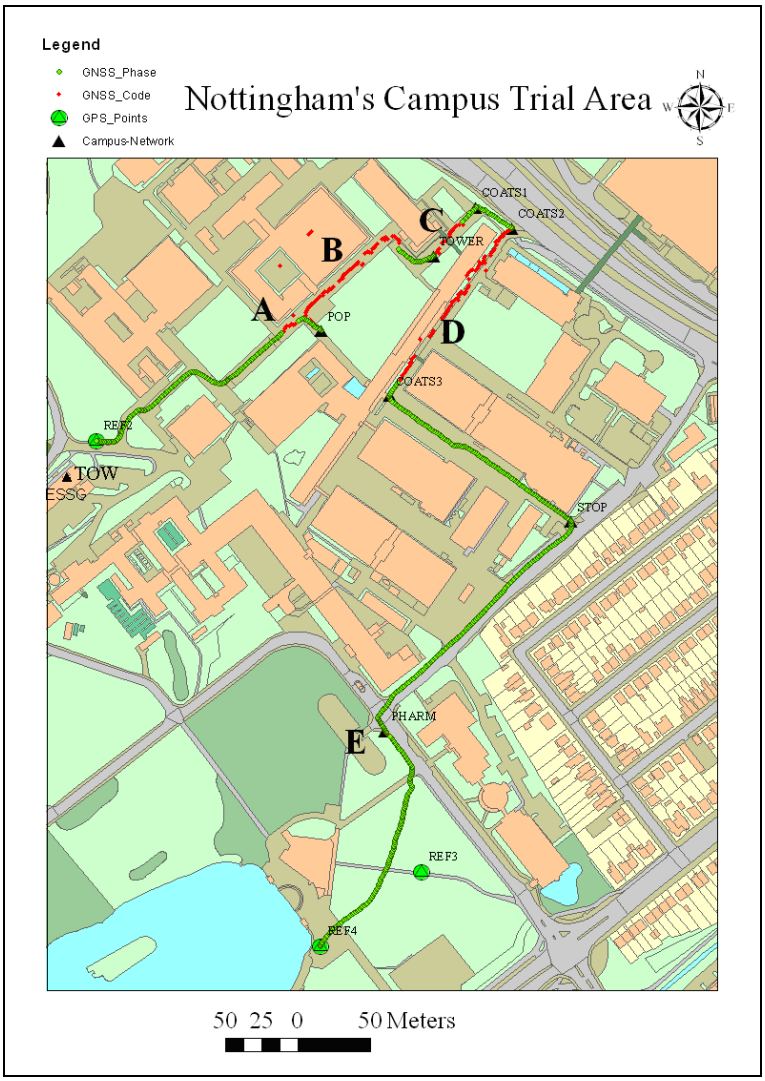

Figure 3.4: Availability of GNSS phase and code solutions for Test1 (© OS MasterMap)

Unlike the GPS only results, the GPS and GLONASS results produce more phase solutions in areas B and C. The percentage of phase solution is increased from 52% in the GPS only solution to 58% in the GNSS solution. Whereas the percentages of code and no solutions respectively, have dropped from 34% and 14% in the GPS only solution to 31% and 11% in the GNSS solution. This is evidence of the slight improvement in availability for centimetre-level positioning currently offered by the GNSS solution.

When analysing the number of satellites, a total of 12 GNSS satellites were found in some open areas of the trial route. In general, more satellites were found when GPS and GLONASS satellites are combined. However, as expected, no GLONASS satellites were also found under the bridges (Figure 3.5).

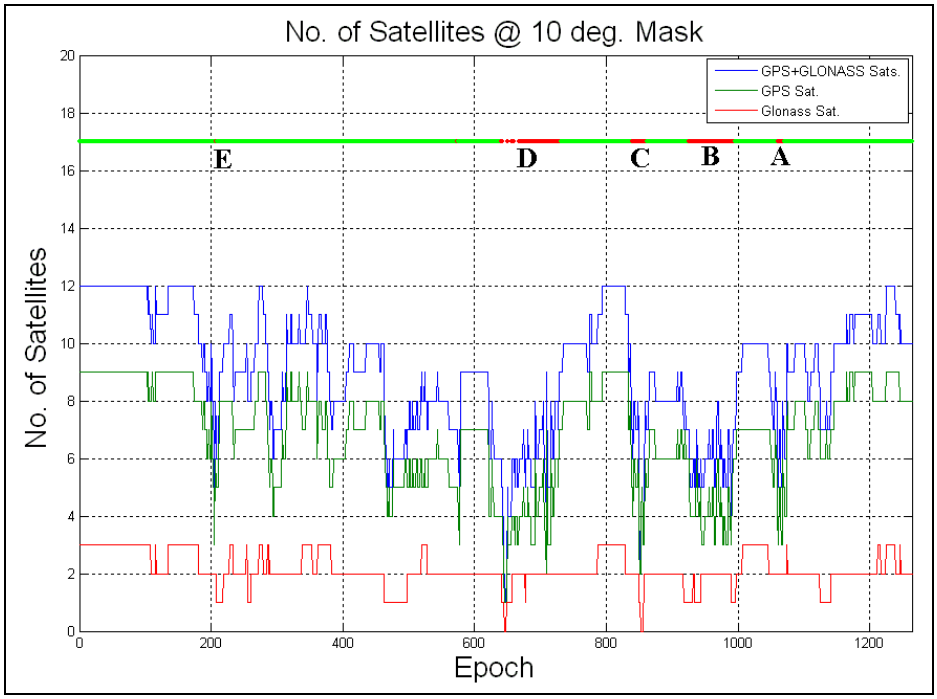

Figure 3.5: Number of the GNSS Satellites at 10 degrees mask angle

From the analysis above, although the combination of current GNSS satellites increased the availability of centimetre-level positioning when compared with GPS only, there are still large areas of degraded positioning accuracy.

3.6.4 The Second and Third Tests: Results and Analysis

The results of the GPS only solution and the GNSS solution were compared with the 'truth' coordinates established in Appendix 1 and analysed in the following section.

3.6.4.1 GPS only Solution: Results and Analysis

Similar to the first test, the processing results from LGO software show that several solution types (i.e. Phase, Code or no solution) were calculated. In addition, the output Cartesian coordinates were converted to National Grid OSGB36 coordinates. The average coordinates for all of the testing points were calculated and compared with the truth coordinates (Figure 3.6).

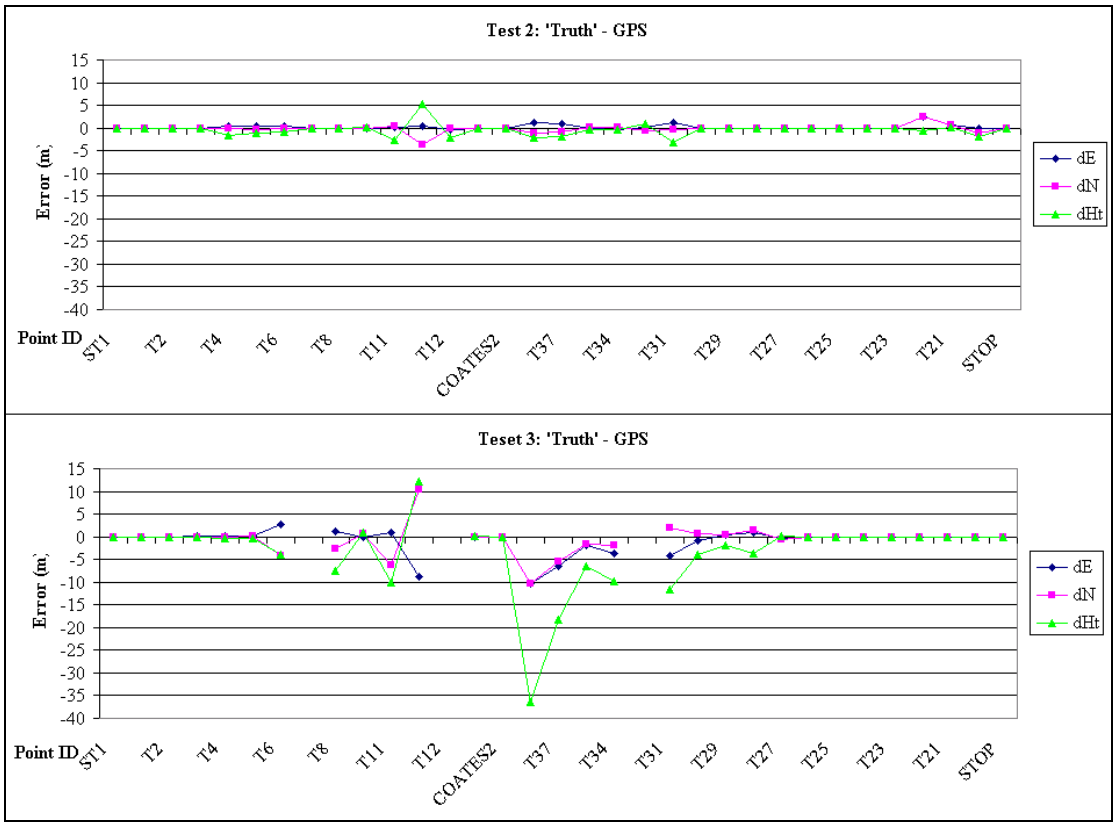

Figure 3.6: GPS only solution coordinates compared with the 'Truth' coordinates for Test 2 (up) and Test 3 (down)

From Figure 3.6, it is clear that there are differences in the GPS only solution due to the difference in the time of observation and the corresponding different satellite constellation. For example, some points have a phase solution in Test 2 (e.g. T8) while they have a code solution or no solution in Test 3 (e.g. T8) and vice-versa. Generally, it could be said that the time of the data collection in Test 2 was more favourable than the time of the data collection in Test 3.

In Test 2 and Test 3 there were respectively 17 and 14 points out of a total of 33 testing points for which a phase solution was found. In these cases, the maximum differences were found equal to 0.023m in E, 0.025 in N, and 0.059m in Ht in Test 2 and 0.059m in E, 0.077m N, and 0.064m in Ht in Test 3. These errors could be due to the high multipath errors and poor DOP that can be found in the urban canyons. Also, according to Taha et al. [2007], the variation about the mean of the phase positions in built up areas can be even greater than this say, up to 0.15m.

For further analysis and assessments of the phase solutions in built-up areas the COATES2 testing point was considered, since it was found to have maximum error

in the height coordinate on test 2. The variation of the coordinates around the mean, in E, N and Ht directions along with the standard error for this testing point are demonstrated in Figure 3.7.

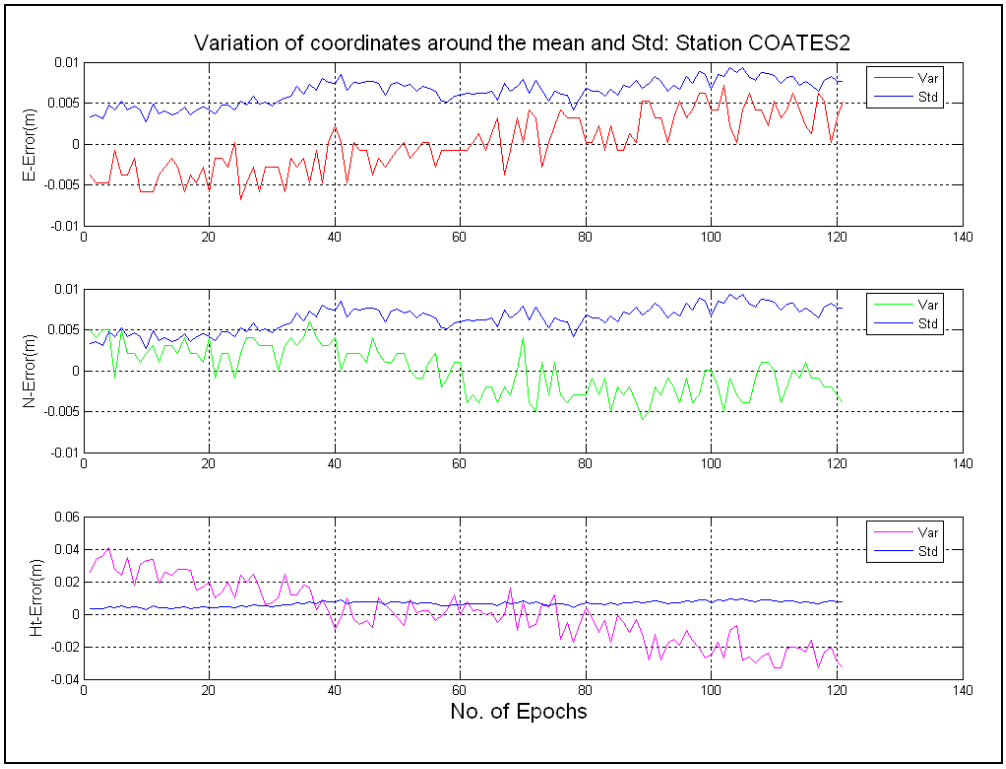

Figure 3.7: Variation of coordinates around the mean (and standard errors)in E (top), N (middle) and Ht (bottom) for COATS2 point in Test 2

Figure 3.7 clearly shows that the height error on COATS2 is significantly larger that the horizontal error. The standard error, however, shows that the uncertainty in this measurement is small (i.e. better than 0.01m). It is well known that the vertical precision and accuracy that is achieved with GPS is significantly lower than the horizontal precision and accuracy, due to the geometry of the constellation. Figure 3.8 shows the DOP values (PDOP, HDOP and VDOP) in TEST 2 for the GPS only solution.

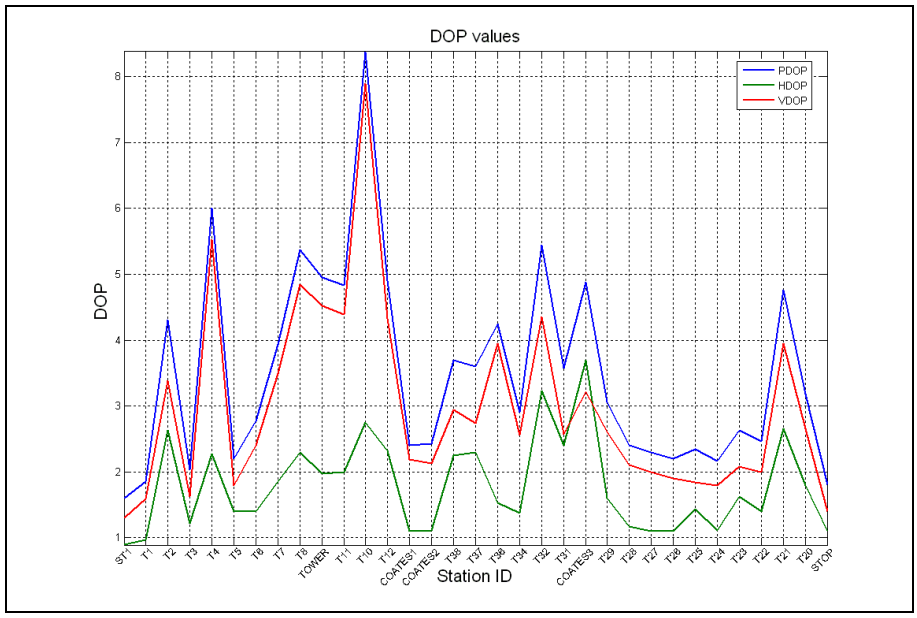

Figure 3.8: DOP values in Test 2 for GPS only solution

From Figure 3.8 it is clear that the VDOP value for COATES2 is much higher than the HDOP value, as expected. However, both of these values fall within the criteria of 'good geometry' and, therefore other factors such as multipath must be affecting the height.

3.6.4.2 GNSS Solution: Results and Analysis

Like the GPS only solution, the output Cartesian coordinates were converted to National Grid OSGB36 coordinates. The average coordinates for all of the testing points were calculated and compared with truth coordinates (Figure 3.9).

Figure 3.9: GNSS solution coordinates compared with the 'Truth' coordinates for Test 2 (top) and Test 3 (bottom)

From Figure 3.9, it is clear that there are differences in the GNSS solution due to the difference in the time of observation, in a similar way to the GPS only solution. The GNSS solution confirms that the time of the data collection in Test 2 was more favourable than the time of the data collection in Test 3 as all of the testing points have a solution in Test 2. For 20 points out of 33 points a phase solution was found in both Test 2 and Test 3. The maximum differences were found equal to 0.030m in E, 0.024 in N, and 0.097m in Ht in Test 2 and 0.058m in E, 0.076m N, and 0.114m in Ht in Test 3.

Comparing the GNSS solution with the GPS only solution, more points were calculated with a phase solution in the GNSS solution, in both Test 2 and Test 3. This is due to the use of the additional GLONASS satellites which make it possible to calculate phase solution on the points where the GPS only failed. However, the maximum error in the GNSS solution is higher than that of the GPS only solution. For example, in Test 2 the maximum error in the height was found equal to 0.059m in the GPS only solution while it was 0.098m in the GNSS solution. This is partly because the maximum error in the GNSS solution was found at a different point (T38

point) which has a code solution when using GPS only and in Test 3, the maximum error in the height was found equal to 0.064m in the GPS only solution while it was 0.114m in the GNSS solution. In both solutions, the maximum error was found at the same point T22. As mentioned before, these errors could be due to multipath and/or poor DOP. Therefore, it is important to consider the DOP values along the testing points in Test 3 Figure 3.10.

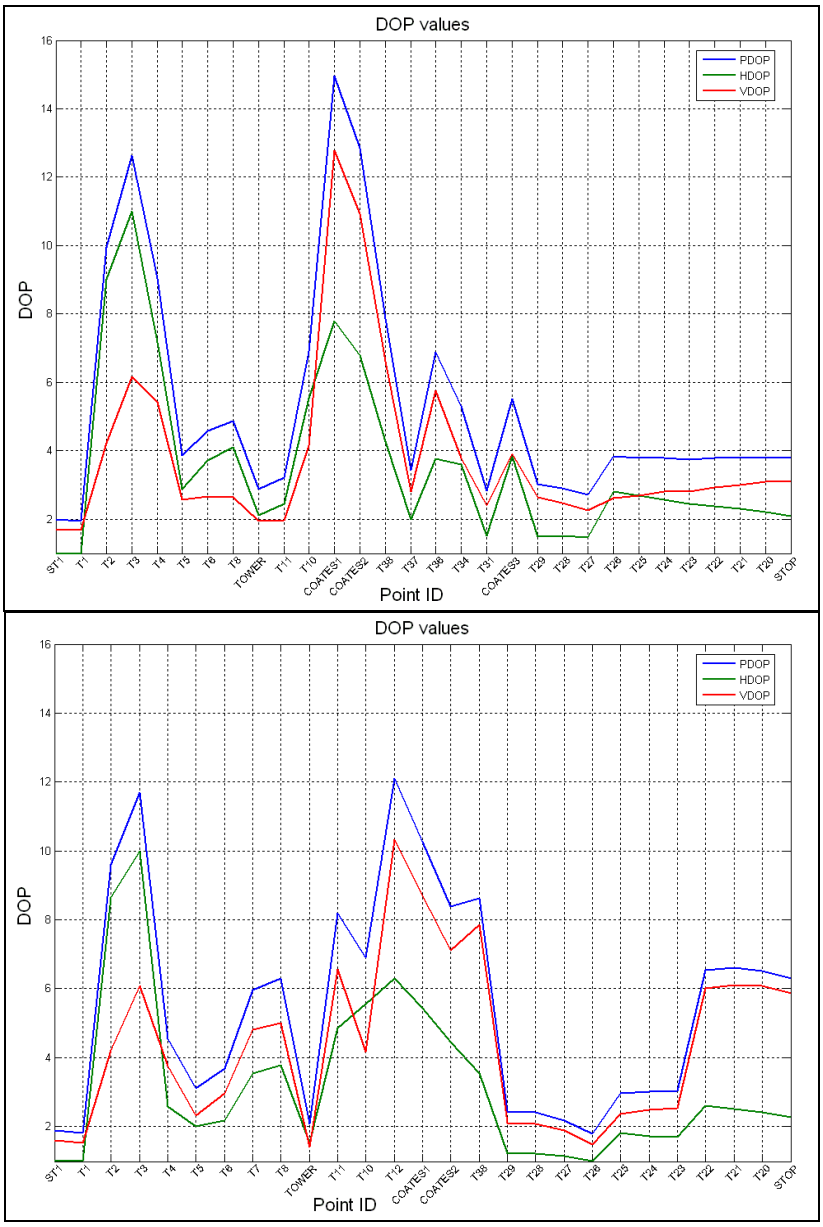

Figure 3.10: DOP values in Test3 for GPS only (top) and GNSS (bottom)

From Figure 3.10, the PDOP value at point T22 increased from about 4 in the GPS only to about 6.5 in the GNSS solution. This causes the accuracy of this point to be reduced. Additionally, this point had a limited sky view due to the surrounding

buildings on both sides of the road. More multipath error could have, therefore, propagated into this point solution as additional satellites (GLONASS satellites) were used. To investigate further, Figure 3.11 shows the L2 multipath (MP2) for each satellite when moving from point T22 to point STOP in Test3.

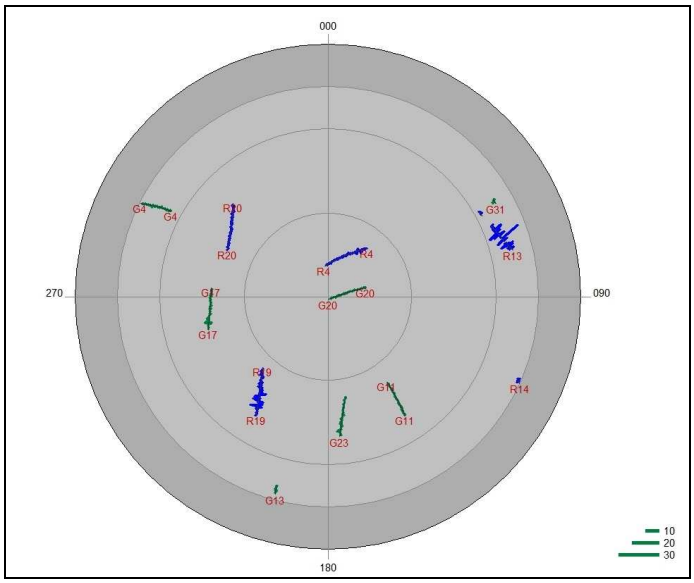

Figure 3.11: Skyplot depicting the position and MP2 values for both GPS (green) and GLONASS (blue) satellites

From Figure 3.11, it can be clearly seen that the GLONASS satellites have much larger multipath errors than their GPS counterparts; this is especially seen in R13 and R19. For further analysis and since all points in this subset of points have solutions (either phase or code) in Test 2, GNSS and GPS solutions were compared with 'truth' coordinates in Figure 3.12.

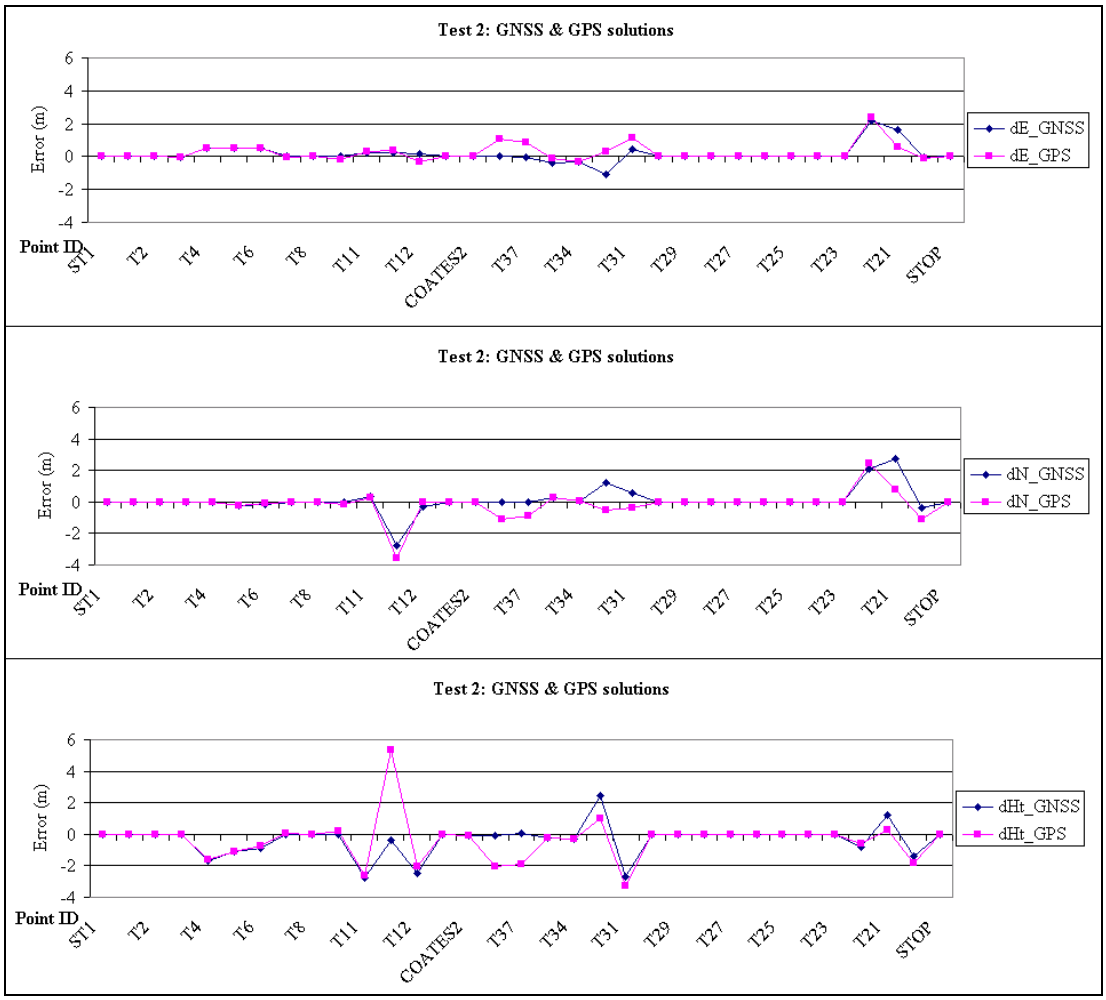

Figure 3.12: Test 2: GNSS and GPS solutions compared with 'truth' coordinates dE (top), dN (middle) and dHt (bottom) for a subset of points in Test2

From Figure 3.12, it is clear that the GNSS solution, in most testing points, is generally more accurate than the GPS only solution expect for points T21 and T31. For comparison purposes, the PDOP values estimated in GNSS and GPS only solution are illustrated in Figure 3.13.

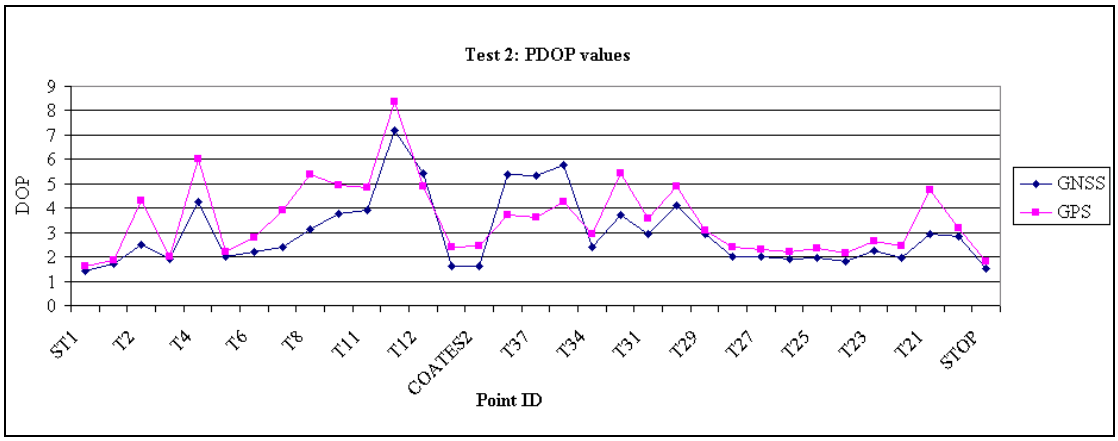

Figure 3.13: Test 2 PDOP values

From Figure 3.13, is clear that the PDOP values reduced, at most of the testing points, for the GNSS solution when compared with the GPS only solution. The improvement of the PDOP is due to the use of more GLONASS satellites that are well distributed over the testing area. However, the increase in the PDOP around the point T37 shows that this is not always the case.

3.7 Summary

This chapter provided an overview of both current operational GNSS (the US GPS and the Russian GLONASS) and the development GNSS (the European Galileo, the Chinese Beidou and COMPASS, the Indian IRNSS and the Japanese QZSS). The constellation parameters for the first four GNSS constellations were summarized within the chapter.

The basic principle of GNSS-based positioning were described and the accuracy of GNSS-based positioning was explained as being highly dependant on the accuracy of range measurements, which can be measured using the PRN code (low level range accuracy can be produced in this method) and/or carrier phase ranges (high level range accuracy can be produced in this method). Various positioning techniques (Point Positioning and Differential Positioning) were discussed along with the positioning solution (Phase Fixed, Float or Code solutions) that can be calculated. The effect of satellite geometry and DOP were also illustrated in this chapter.

The results of three tests using the current GNSS satellites (GPS and GLONASS) along Nottingham's Campus trial route were discussed and analysed. The first test proved that a GNSS solution can improve the availability of Phase fixed solutions in kinematic mode by increasing the number of satellites when compared to a GPS only solution. However, the second and third tests showed that although there were more testing points with a phase solution in the GNSS solution, when compared with the GPS only solution, this does not guarantee high accuracy, as more satellites can lead to higher multipath and the use of constellations with poor DOP; especially with GLONASS in urban canyons.

Chapter 4: Urban Canyon GNSS Simulation

4.1 Introduction

GPS and other GNSS (for example the Russian GLONASS, the emerging European Galileo and the Chinese COMPASS) are developing rapidly. In the future more than 100 satellites could be available for positioning. As a result, the ability to accurately position within a level of accuracy of a few centimetres, in difficult areas such as urban canyons, should be more feasible.

It is well known that the accuracy, availability and reliability of satellite based positioning are very dependent on the number of tracked satellites and their spatial geometry [Kleusberg and Langley, 1990; Santerre, 1991]. As mentioned in Chapter 3, satellite geometry is measured by the DOP statistics [Gopi, 2005c]. DOP, while acting as a general precision and accuracy indicator, does not necessary relate directly to accuracy. Rather, it is not the errors themselves that are directly increased by the DOP; it is the uncertainty of the GPS position that is increased [Van Sickle, 2001]. Position Dilution of Precision (PDOP) is one of the more commonly used factors in estimating the precision and accuracy of GPS.

Line of sight to a sufficient number of satellites is not always possible when working in built-up areas due to different obstructions such as buildings and trees. Under adverse conditions, for example, GNSS receivers may have difficulty tracking satellites, may track a reflected signal. It is generally accepted that conducting GNSS positioning in urban environments is problematic. Kleusberg and Langley [1990] address the urban environment generally while discussing the limitations of GPS:

"*In the inner city streets of urban areas lined with skyscrapers the 'visibility' of GPS satellites are very limited. In such areas the signals can be obstructed for extended periods of time or even continuously unavailable*."

The combination of current and future GNSS satellites will make it possible to provide better precision and accuracy, reliability and availability, especially where satellite signals may be obscured, such as in urban canyons [Daghay et al., 2005; Rizos et al., 2005]. As a result, positioning at locations with limited visibility should become more feasible and more accurate as more than 100 positioning satellites will be available to be used in the future.

As discussed in Chapter 3, although the combination of current GNSS satellites increased the availability of accurate positioning compared with GPS only, there are still large areas of degraded positioning accuracy. Therefore, simulation of forthcoming GNSS satellites in similar environments is necessary at this moment in time to evaluate the advantages of different GNSS combinations and predict what the future availability of GNSS satellites might be in difficult environments. In order to do this the Urban Canyon GNSS Simulation (UCGS) tool was developed by the author. This tool simulates satellite visibility and DOP for both the current and the future GNSS constellations within a 3D city model environment. Four GNSS constellations (current GPS, current and future GLONASS, Galileo and COMPASS) were tested for satellite visibility and DOP using UCGS and using a 3D model of Nottingham's University Park campus. In addition further tests were carried out using LiDAR data for the town of Upton Upon Severn.

This chapter commences with a background review about current satellite visibility prediction tools. An overview of GIS and programming within ArcGIS are given afterwards. After that, 3D city model creation based on photogrammetry and LiDAR data is discussed. Then the UCGS tool algorithms are described before the results of the simulations, conducted using UCGS within different 3D models, are presented and analysed.

4.2 Current Satellite Visibility Prediction Tools

Currently there are many tools available that perform satellite visibility predictions, however, these are limited when considering terrain or structures that block GPS signals, which is a major issue in urban areas (see for example [Wagner, 2000]).

Other tools, such as Trimble Planning Software [Trimble, 2008] are able to take the terrain into account, but require extensive manual user input to define the geographical terrain surrounding point locations. With the increased availability of high-resolution photogrammetric surface models, a number of researchers have proposed methods to overcome this issue. Boulianne et al. [1996] suggested generating obstruction diagrams based on the floating cones concept injected into a photogrammetric stereo model. Similarly, Walker and Sang [1997] used the elevation mask angles that were derived from a digital terrain model created based on a photogrammetric approach. The conclusion drawn in their work is that accurate Digital Terrain Model (DTM) information is invaluable to the users of high precision GPS planning in harsh environments.

More comprehensive mission planning software tools have been recently developed to perform visibility within digital surface models (DSMs) under a GIS environment. For example, the Satellite-Viewsheds tool developed by Germroth and Carstensen [2005] to perform visibility analysis for GPS satellites within a raster grid surface model. Another powerful tool, is the one developed by Taylor et al. [2007] for predicting the number of satellites visible to a GPS receiver along roads in urban areas within either raster or TIN models. However, each of these tools falls short, in one way or another, of the objectives of the UCGS. For instance, the simulation of multiple GNSS constellations was not discussed in any of the tools previously mentioned. Also none of these tools perform visibility analysis in different trajectory scenarios such as Static, Kinematic and Stop & Go.

4.3 GIS Overview

A Geographical Information System (GIS) represents the integration of many subject areas. De Mers [1997] stated that there is no absolutely agreed upon definition of a GIS. More recently, one accepted definition of GIS is the one provided by GIS.com [2007]:

"*GIS is a collection of computer hardware, software, and geographic data for capturing, managing, analyzing, and displaying all forms of geographically referenced information*".

GIS is extensively used in different areas such as urban planning and development [Easa et al., 2000], agriculture (acquisition, management and analysis of spatial data) [Pierce and Clay, 2007], utilities management, mapping, modelling, and planning [Shamsi, 2005], transportation and traffic planning, and many other applications.

The most commonly used conceptual model for a GIS is the overlay (layer) model (Figure 4.1). The layers are typically thematic, so one layer may be land usage, another may be elevation, another parcels, another streets and so on. By holding each theme as a separate layer they can be analyzed separately, and also in combination with each other.

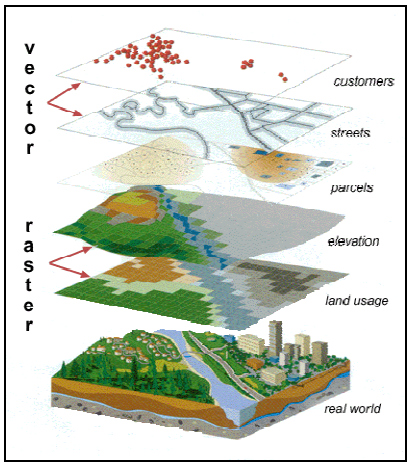

Figure 4.1: The concept of layers [ESRI, 1996]

There are many different GIS packages available around the world. These vary in their capabilities, features and applications. For example, Autodesk and Microstation were primarily developed for engineering and architectural applications whereas ERDAS IMAGINE and PCI are more used for remote sensing and photogrammetry [Longley, 2005]. Some of the most popular GIS software packages are ESRI ArcGIS, GE Smallworld, Intergraph GeoMedia and MapInfo.

ESRI is one of the world leaders in GIS modelling and mapping software and technology. ESRI uses the name ArcGIS to refer to its suite of GIS software products which consists of four primary frameworks: desktop, server, mobile and ESRI Developer Network (EDN) [ESRI, 2006a]. All four ArcGIS frameworks share a common architecture and are based on ArcObjects, the ArcGIS software component library and the core of all ArcGIS products. The current version of ArcGIS Desktop

suite is 9.2 which can be accessed using three software products (ArcView, ArcEditor and ArcInfo), each providing a high level of functionality.

ArcGIS Desktop 9.2 comprises a suite of integrated desktop applications, including ArcMap, ArcCatalog, ArcToolbox, and ArcScene [ESRI, 2006a]. Using these applications and their user interfaces in unison, it is possible to perform any GIS task, including mapping, geographical analysis, data editing and compilation, data management, visualization, and geoprocessing.

UCGS predicts satellite visibility by using ArcScene within either raster or vector models. Therefore, before discussing UCGS, it is necessary to understand the raster and vector data models and it is useful to discuss the programming within ArcGIS.

4.3.1 Geographical Datasets

Usually, there are two types of data associated with geographic features: non-spatial and spatial data [Singh and Fiorentino, 1996], both of which are termed geographic data [Davis, 2001]. Non-Spatial data refers to traditional tabular attributes (associated attribute tables) that containing descriptive information about geographic objects and features such as object ID, owner ID, owner name, length, area, parcel ID, value, etc (Figure 4.2). Usually, it is stored in a table and linked to the feature through an address or geo-code, which allows this non-spatial data to be viewed and analysed through its location.

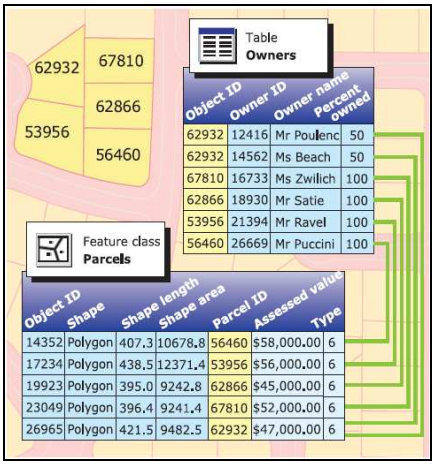

Figure 4.2: Associated attribute tables [ESRI, 2006a]

Spatial data represents real world objects (location, shape, size, and orientation of, and relationships among, geographic features) with digital data. There are two main models for storing and representing spatial data in GIS: vector and raster models [Easa et al., 2000; Wise, 2002].

4.3.1.1 Vector Data Model

The vector data model represents geographic features in a coordinate-based model as points, lines/arcs or polygons [Crosier et al., 2002] (Figure 4.3).

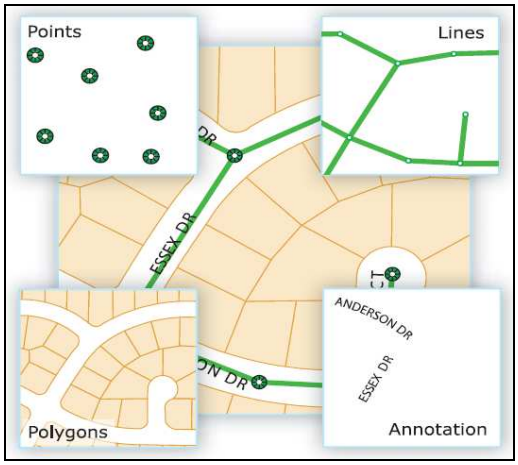

Figure 4.3: Vector data model: points, line and polyline [ESRI, 2006a]

Point data is most commonly used to represent nonadjacent features and abstract points as a single coordinate pair of x, y or a triplet of x, y, z, coordinates. For instance, point locations could represent city locations, or place names. Line/arc data is used to represent linear features. Common examples would be streams, roads and hydrology. Polygons are defined by borders and are represented by closed polygons. They can be legally defined, such as a parcel of land; administrative, such as counties; or naturally occurring boundaries, such as watersheds. Vector data are usually stored in feature classes and collections of topologically related feature classes [Crosier et al., 2002]. The attributes associated with the features are then stored in separate data tables[Brooks, 2004].

A vector data model can also represent a continuous surface as a set of TIN derived from irregularly spaced sample points and breakline features. The TIN data set includes topological relationships between points and their neighbouring triangles.

4.3.1.2 Raster Data Model

Raster data represent features as an array of cells arranged in rows and columns (Figure 4.4). Each cell must be rectangular in shape, but not necessarily square. Each cell contains an attribute value and location coordinates. Unlike a vector structure which stores coordinates explicitly, the spatial location of each cell is implicitly contained within the ordering of the matrix.

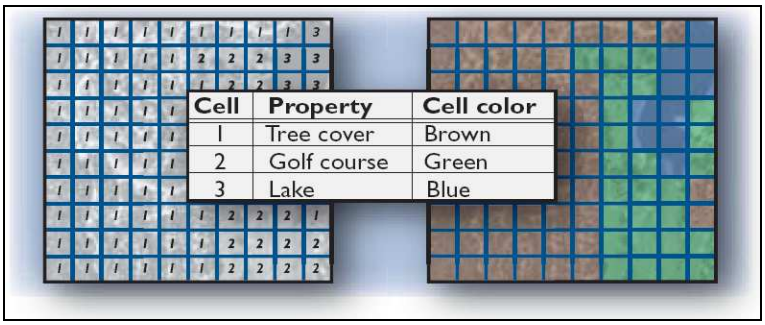

Figure 4.4: Raster data model [ESRI, 2006a]

Raster data stores point features as a single cell with a unique value, and line features as a string of cells with common values [Brooks, 2004]. Besides, polygonal features are stored as groups of adjacent cells with common values.

Most often, raster data are images (raster images) with each pixel (or cell) containing a colour value. In addition, values recorded for each cell may be a discrete value (such as land use) a continuous value (such as for an elevation surface) or a null value if no data is available. The resolution of the raster data set is its cell width in ground units. The smaller the cell size for the raster layer, the higher the resolution and the more detailed the map, however, the larger the storage required.

4.3.2 Programming within ArcGIS

Developers can create new custom extensions to ArcGIS Desktop by working with ArcObjects. ArcObjects includes a wide variety of programmable objects which were built using Microsoft's Component Object Model (COM) technology [Burke, 2003]. Therefore, it is possible to extend ArcObjects by writing COM components using any COM-compliant development language such as Visual Basic 6 (VB), .NET and

Visual C++. However, the most common method that developers use to customize the ArcGIS Desktop applications is through Visual Basic for Applications (VBA), which is embedded within ArcMap, ArcCatalog and ArcScene.

The UCGS tool was written by the author in the VBA version 6.3 editor of ArcScene in ArcGIS version 9.2. Developing such a tool for ArcGIS requires knowledge of both VBA and ArcObjects.

On the one hand, VBA provides the programming language and can normally only run code from within a host application, such as ArcGIS, rather than as a standalone application. It is fast and easy to extend ArcGIS with new modules, class modules and user forms. With VBA, it is possible to create extensive and sophisticated applications based on ArcObjects that run within the ArcMap and ArcScene application frameworks. The standard ESRI type libraries are already referenced within VBA, which helps to assemble code quickly.

On the other hand, ArcObjects consists of objects and classes. An object stands for spatial features such as points, lines, polygons, maps and layers. Objects are sets of classes. Classes are codes that are stored in Dynamic Linked Library (DLL) files. ArcGIS 9.2 has thousands of classes and interfaces. ESRI groups ArcObjects into more than 65 libraries [Chang, 2008]. Class has interfaces (all the ESRI class interfaces start with the letter 'I') and the interface is a logical grouping of properties and methods of a class. A Property describes an attribute or characteristic of an object such as get/read and put/write properties. A method, also called behaviour, performs a specific action, which may require some arguments and may return a value or values such as update contents method. ArcObjects includes three types of classes: abstract class, CoClass and class (Figure 4.5). Some of these classes were used in the UCGS tool, i.e. the TIN layer class (ITinLayer).

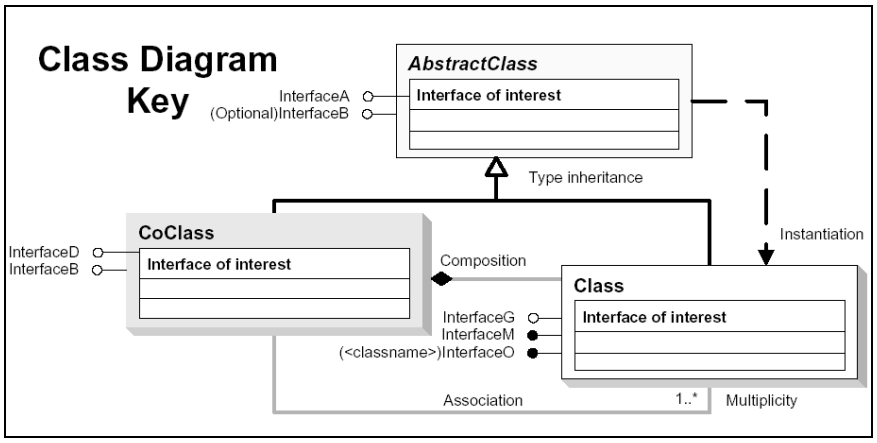

Figure 4.5: Class diagram key [ESRI, 2006b]

When working with classes that have interfaces, it is necessary to find out which interfaces a property or method is on before using it. Object model diagrams (Figure 4.5) are commonly used to make it easy to understand what ArcObjects are, what the relationship between different types of classes is and what individual objects do.

In order to make UCGS available to any map document, it was stored in the Normal project. The development of UCGS passed through several steps that are described in great detail in section 4.5 and Appendix 12.

4.4 Three Dimensional City Model Preparations

As mentioned in the previous section, the vector data model can represent a continuous surface as a set of TIN. Also, the elevation surface can be represented as a raster model.

A TIN surface is usually created from digital photogrammetric data. The fundamental principle of photogrammetry is based on the geometry of perspective scenes and on the principles of stereovision in which the three-dimensional coordinates of points are determined by measurements made in two or more overlapped photographic images taken from different positions [Mikhail et al., 2001]. In recent years, the rapid development of digital photogrammetry has led to increased productivity in generating topographic maps and the TIN. However, creating a very detailed and accurate TIN surface involves several steps, as discussed in the next sub section.

On the other hand, a raster data model can be created easily and quickly from remote sensing LiDAR data. This section describes how a 3D digital surface model can be built from photogrammetry data in order to be used for the simulation. In addition, it describes how LiDAR data was used for the simulation.

4.4.1 Photogrammetric Model Preparation

This sub section gives an overview of the workflow used to create a very detailed and accurate TIN surface of the University Campus 3D Urban Model. TIN surfaces are of particular significance when performing satellite visibility analysis studies. The amount of roof details represented in a TIN surface coupled with the horizontal and vertical accuracy can influence significantly the results of such analysis. Therefore an effective workflow for the generation of detailed TIN surfaces from airborne data is of great importance.

4.4.1.1 Aerial Images and Camera

For The University of Nottingham's Campus, a block of 86 UltraCamD images was provided by BlomAerofilms Ltd. [BLOM, 2008]. The block of images consists of 4 strips with 20% side overlap and 60% forward overlap. The images were acquired from an altitude of approximately 500m. The aerial survey was performed during November 2006 with the use of onboard GPS/IMU so that the position and attitude of each image is determined and used as initial values in the Aerial triangulation (AT).

The UltraCamD has an 86 Mega-Pixel resolution with Vexcel's UltraCamD digital sensor unit consisting of eight independent cameras [Gruber et al., 2004]. Four of them are on a line through the centre of the cone cluster and are used to capture the panchoromatic images which are made up of 9 overlapping sub-images. These overlapping sub-images are then post-processed to create a composite image [Gruber and Ladstädler, 2006; Kruck, 2006; Smith et al., 2007]. The composite panchromatic images have 11500x7500 pixels. Each pixel has 9μm physical dimensions while the calibrated focal length was equal to 101.4mm.

The ground sample distance (GSD) for the test site was approximately equal to 5 cm which is estimated by multiplying the pixel size (physical dimensions) with the image scale (focal length / flight altitude). GSD can be defined as the minimum distance between two adjacent targets on the ground or the smallest feature size that can be detected in the image. The lower the altitude of the flight the better GSD can be achieved.

4.4.1.2 Image Orientation and Feature Collection

Image orientation and feature collection were conducted using the Leica Photogrammetry Suite 9.0 (LPS) and the integrated Orientation Management (ORIMA) software. According to Leica-Geosystems-AG [2007b]:

'*LPS is a collection of seamlessly integrated software modules providing accurate and production oriented photogrammetric tools for a broad range of geospatial imaging applications. LPS's state-of-the-art photogrammetric and image processing algorithms for automatic point measurement, automatic terrain extraction and subpixel point positioning not only help you maintain accuracy, they increase it.*'

In photogrammetry, image orientations can be stored in three orientations: interior, relative, and exterior/absolute [Campbell and Wu, 2004]. Interior orientation (IO) aims at reconstructing the bundle of rays inherent in each image as that which exists at the instant of exposure. For the University of Nottingham's Campus block images, the interior orientation was reconstructed using the camera calibration report provided by BlomAerofilms. The parameters used for accurately describing the geometry of the UltaCamD model were the calibrated focal length, the position of the principal and the three polynomial co-efficient K0, K1, K2 representing radial lens distortions.

Relative orientation involves recreation of the relationship (geometry) between two photographs and hence forms a perfect, in a relative sense, three-dimensional model. The image-to-ground relationship should be established in order to relate the image to the real world. This can be accomplished through either the absolute orientation or exterior orientation process. Exterior orientation creates three dimensional ground coordinates, without the need to perform relative and absolute orientations. In

addition, it works by importing the exterior orientation parameters, positional and angular: for single image; for blocks of images from files such as those derived from GPS/IMU system (direct orientation); or from aerotriangulation packages a combination between relative and absolute orientations (indirect orientation) [Schenk, 1999].

The exterior elements can be determined if at least three ground control points are observed in the images through the absolute orientation or through the aerial triangulation process (where two of the ground control points have known horizontal coordinates to provide the scale and three of the points have known elevation) [Wolf and Dewitt, 2000; Mikhail et al., 2001]. For the University of Nottingham's Campus, static GPS data were collected on 33 ground control points (GCPs) for about 20 to 30 minutes on each point. Simultaneously, GPS static observations were collected on a reference station (TOW) fixed on the tower of the IESSG which is located approximately in the mid of the block. The GPS data were post-processed using LGO software and the output Cartesian coordinates (X,Y and Z) were then transformed to National Grid coordinates (E, N and H) using Grid-InQuest version 6.08 software. A total of 9 GCPs were used as control points and the rest (24 points) were used as check points during the AT. Figure 4.6 illustrates the arrangement of the block of photographs and the GCPs distributions.

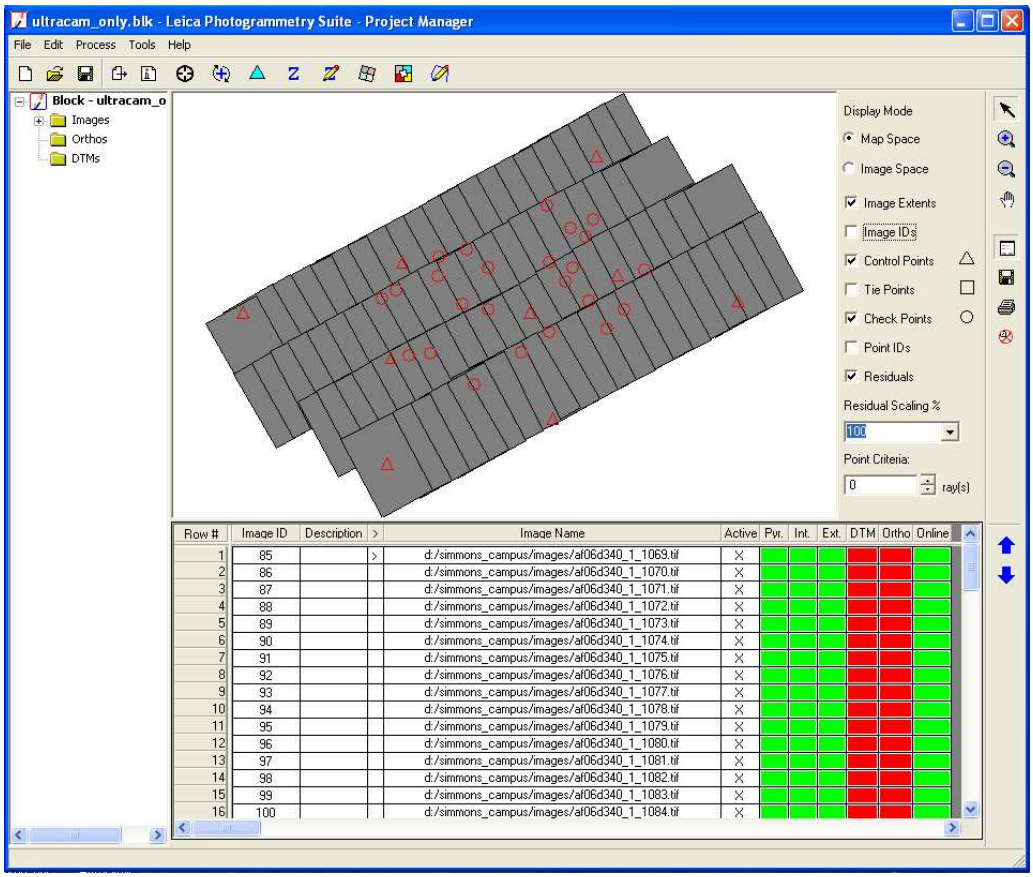

Figure 4.6: The University of Nottingham's Campus block images and GCPs distribution

Using LPS, a total of 806 tie points were automatically extracted using a stereo matching process employing a least squares correlation matching algorithm. Typically, this process uses a least squares estimation to derive parameters that best fit a search window to a reference window between two overlapping images.

In order to determine the information required to create ortho-images, DTMs, stereo-models (oriented images) and 3D features, the technique of aerial triangulation is employed. The aerial triangulation (AT) was performed within LPS based on GPS/IMU values as initial parameters with standard errors of 1000m and 360 degrees respectively. These standard error values left the block of images to float during the AT. Ebner's Orthogonal Model (12) (more information about this model can be found in [Ebner, 1976]) was used for self calibration and GCPs with 'Same weighted values' and standard errors of 0.05m for E, N and H used in AT. Figure 4.7 summarises the AT results.

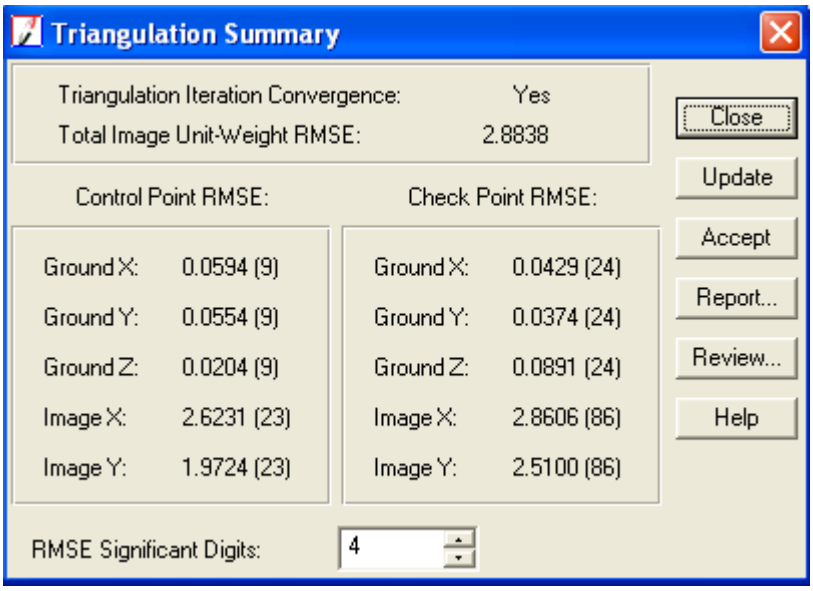

Figure 4.7: The University of Nottingham's Campus AT results summary

A total of 9,300 terrain points were manually measured for the requirements of the digital terrain model as well as a number of breaklines on streets and steep canyons streams. In addition, buildings were modelled at the highest possible level of detail regarding their roofs. Therefore chimneys, dormers, ventilation equipment and pipes were all modelled using 3D stereo modelling.

4.4.1.3 Digital Elevation Model based on TIN

A digital elevation model (DEM) - also sometimes called a digital surface model (DSM) - is a mathematical (or digital) representation of ground surface topography or terrain including features such as buildings, vegetations, bridges, etc. DEMs are commonly built using remote sensing or laser scanning techniques (raster DEM); however, they can also be built from land surveying or photogrammetric techniques (vector/TIN DEM). A digital terrain model (DTM) on the other hand is a filtered version of a DEM which provides a so-called bare-earth model, devoid of landscape features.

In order to create a DEM based on a TIN, terrain and feature points have to be connected by edges so that triangles are formed. There is no unique way to generate triangles from arbitrarily distributed points, so that a solution has to be found which is optimal in a certain sense. However, breaklines can be used to force the TIN to reflect significant breaks in topography. The most widely used optimization criterion

for irregular triangulation is the Delaunay criterion: the points are to be connected by edges to form triangles so that for each triangle no fourth point of the triangulation is within the circumscribing circle (circumcircle) [Li et al., 2005] . The Delaunay triangulation criterion yields triangles which are closest to equilateral ones. If the Delaunay criterion is satisfied everywhere on the TIN, the minimum interior angle of all triangles is maximized. There are a wide variety of algorithms available to create a Delaunay triangulation from a point cloud. The Bowyer-Watson algorithm [Bowyer, 1981; Watson, 1981], also called incremental algorithm, has been described as the simplest, most practical and the most robust triangulation algorithm [Li et al., 2005].

4.4.1.4 Workflow for TIN Generation of a 3D City Model

In order to carry out any kind of visibility analysis, the DEM surface should accurately represent the surface that includes buildings and other features. When a DEM is built from a vector model based on a TIN with a complex urban structure, it is considered more accurate to build a bare-earth TIN (i.e. DTM) first then to add the buildings or other features.

There are certain challenges when adding buildings and other features to a bare-earth TIN in a GIS. The first issue is that the vertical building facades cannot be represented as such in a TIN surface and the second issue is that the footprints of small roof details exist on the ground level rather than on the main rooftop. The first issue can be resolved by expanding the main footprint by a small distance using buffer regions. To tackle the second issue the individual small roof polygon level has to be categorised in a hierarchical way depending on its area and location inside other polygons. For example, if a smaller roof polygon is located inside five other bigger polygons with lower height, it will be in a higher level (Figure 4.8).

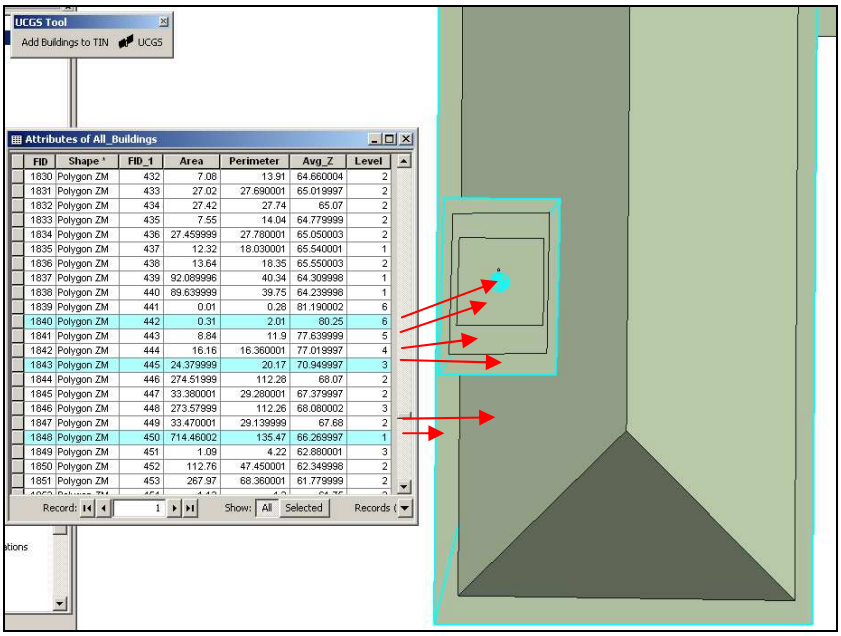

Figure 4.8: Complex urban structure: roof detail categorisation

Extraction of building levels was performed automatically for UCGS using the developed tool 'Auto Add Buildings to TIN' (Figure 4.9), as a result of running this option, a new field, 'Level', was added to the layer's attributes. The algorithms behind this option are discussed further in section 4.5.

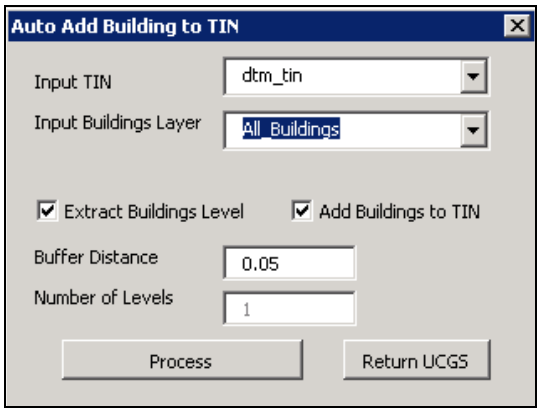

Figure 4.9 : GUI for the Auto Add Buildings to TIN tool

The adding building to TIN tool allows for an iterative TIN surface generation, where for each iteration an expanded footprint for roof level is created based on the previous level. More specifically, the TIN surface is first created using only the footprint of the main rooftop and then based on that TIN, a footprint of the 2nd roof level was created etc.. In general, the workflow in ArcGIS to build a TIN surface including complex structures is passed into several steps as follows:

- Employ Delaunay triangulation using the terrain points representing the ground surface to create a bare-earth TIN surface.
- Categorise the roof polygons in different levels using the tool 'Auto Add Buildings to TIN' within UCGS. A total of 6 roof level categories were created for the University of Nottingham's Campus grouping corresponding roof polygons.
- Also, using the developed tool 'Auto Add Buildings to TIN', the buildings can be added to the bare-earth TIN surface with a specific buffer distance such as 5 cm as follows:
  - Add the main rooftop - 1st level: Add 3D polygons and footprints on ground TIN.
  - For each subsequent roof level repeat loop using the TIN generated from the previous roof level.

With this workflow, it is possible to create very detailed TIN models of an urban area, i.e. very detailed 3D City Models. Nevertheless the proposed workflow has a limitation when modelling complex structures, especially when multiple buildings with different heights are sharing one or more building edges. This can cause errors when connecting Delaunay triangles. The available 'Add Buildings to TIN' tool doesn't account for gable roof and therefore the TIN model represents all the roof polygons as flat rooftops (Figure 4.10 right). When a gable roof is present the available tool will create a levelled roof using the average height value. However, the 'Auto Add Buildings to TIN' tool generates several layers, i.e. interpolated buffer layer and level layer, and uses them as brake-lines when adding them to a TIN. In this method, the resultant TIN will include the gable roof (Figure 4.10 left). More detail on this processing is given in section 4.5

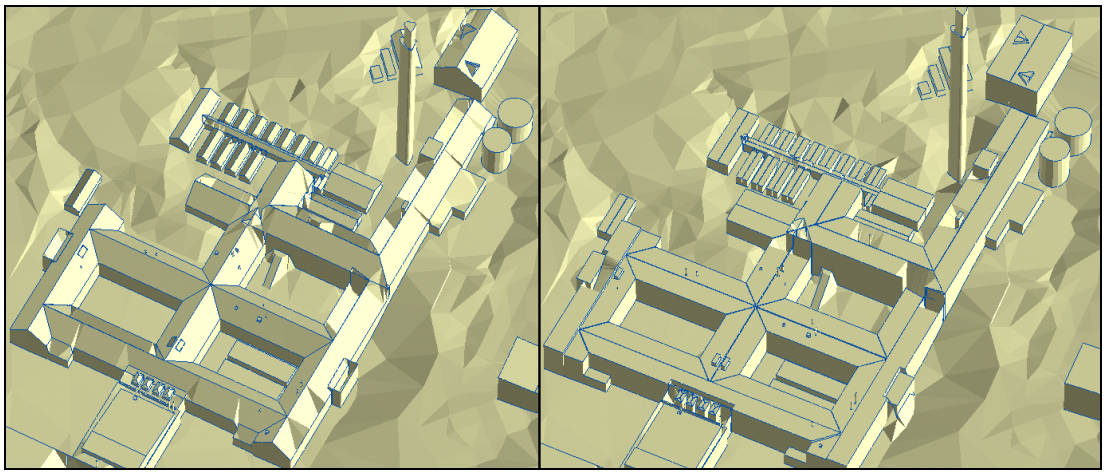

Figure 4.10 : Auto Add Buildings to TIN model (left) and available Add Buildings to TIN model (right)

GNSS signals can propagate through vegetation, however, this is very difficult to be implemented in a TIN; as vegetation can only be presented as an irregular solid shape which blocks signals. Therefore, vegetation was not accounted for in the University on Nottingham's Campus 3D model.

4.4.2 DEM Generation from LiDAR Data

Light Detection and Ranging (LiDAR), an emerging technology, is an active remote sensing technology that uses laser light to measure distances. It offers the capability of capturing high density 3D points and generating high accuracy DEMs in a fast and cost-effective way [Taylor et al., 2007]. The advantage of the LiDAR system is that collected data includes the first and last pulse return, which allows for the measurement of elevations both at the top and at the bottom of features such as tree canopies, and signal intensity data which provides some information about the texture of the reflected surface. LiDAR data can be collected using ground-based, satellite-borne or airborne techniques [Habib et al., 2004].

The ground-based LiDAR is usually using fixed or rotating laser scanner systems, i.e. Leica ScanStation 2 Laser Scanner, to scan building, rock formation or for mobile applications (LiDAR fixed on a car), to produce a 3D model.

Satellite-borne/space-borne LiDAR, such as the Geoscience Laser Altimeter System (GLAS), a new sensor onboard NASA's ICESat (Ice, Clouds, Elevation)

[CSR/TSGC, 2007], measures the surface elevations with an accuracy of sub-meter level and along track spatial resolution of 70m [Sang Hoon et al., 2005]. Also, Satellite-borne Synthetic Aperture Radar Interferometry (InSAR) can be used to generate 20-m resolution DEM [Lee et al., 2005].

Airborne LiDAR is usually mounted in an airplane or a helicopter and comprises three technologies: a laser scanner, GPS and INS. These technologies are combined and processed to generate densely spaced and highly accurate topographic points. By overlapping parallel flight paths, it is possible to survey large areas, producing millions of 3-dimensional data points known as 'point clouds' (Figure 4.11).

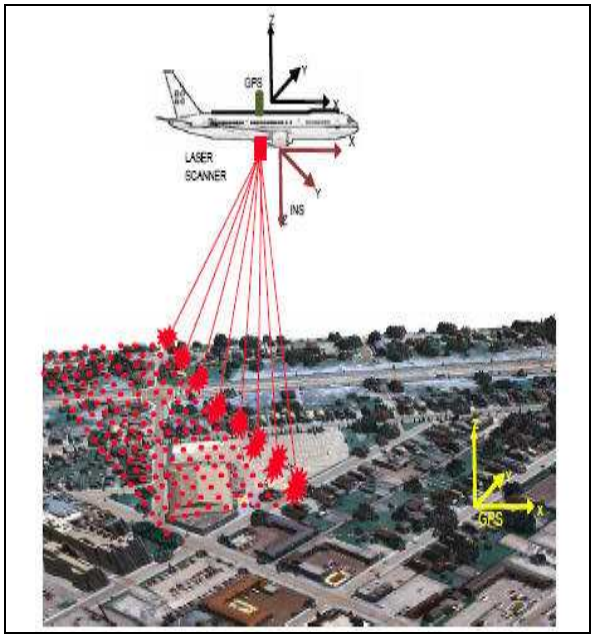

Figure 4.11: Airborne LiDAR [Lohani, 2008]

Processing large point sets of LiDAR data poses a number of computational challenges and complex algorithms have to be used. Most of these algorithms are proprietary to the companies using the LiDAR systems and most of the data preparation and processing is carried out in-house prior to distribution. Nevertheless LiDAR remains the preferred technique for accurate, high-resolution and fast terrain data collection which is only paralleled by photogrammetry because of its cheaper production costs. The airborne LiDAR data are accurate to about 0.10-0.15m RMSE in vertical [Lohani, 2001] and can be found in the form of a regular grid of points at 1 or 2m intervals [Stanfords, 2007]. Furthermore, according to Burton and Neill

[2007] FLI-MAP 400 (Fast Laser Imaging Mapping Airborne Platform) is an airborne low-level LiDAR that has an improved ranging accuracy of 0.01m and vertical accuracy in the order of 0.03m.

4.4.3 Integration of Photogrammetry and LiDAR

The combination of aerial photography and LiDAR has great potential. It benefits from high-resolution imagery and a very accurate, dense LiDAR-generated DEM. The building models can be reconstructed from LiDAR point clouds with aid of aerial photographs or ground plan maps, see for example by Verbree et al. [2004]. The reconstructed building model can then be used to predict the satellite visibility. However, fitting LiDAR points into segmented ground plans for rooftop reconstruction may have a bearing on the prediction accuracy [Taylor et al., 2007].

Taylor et al., [2007] suggested that 3D break-lines compiled photogrammetrically can be incorporated into the LiDAR data through the constrained Delaunay triangulation to produce more realistic digital surface models. Most recent research focuses on automated acquisition of 3D building models based on the integration of LiDAR data and aerial images.

4.5 UCGS Tool Algorithms

Appendix 12 presents an overview of the UCGS tool, as a 'user manual'; whereas this section concentrates on the algorithms developed for the tool and its three main processes: 'Constellation Builder', 'Auto Add Buildings to TIN' and 'Satellites Visibility Simulation'.

4.5.1 Constellation Builder

The first process, 'Constellation Builder', is loaded when the 'Almanac File Preparation' option is selected. The algorithms for this were developed using several VBA Modules, Sub Procedures and Functions, with none of the ArcObjects classes used. The output result of this tool is an almanac file in Yuma format. For future

constellations, it is possible to create a new almanac file using the 'New Constellation' option by defining some nominal constellation information. The information required are: Constellation ID, Number of orbital planes, Number of satellite vehicles (SV) on each orbit, SV start number from, Orbit Inclination, semi-major axis and almanac date (either UTC or GPS time) (Figure 4.12).

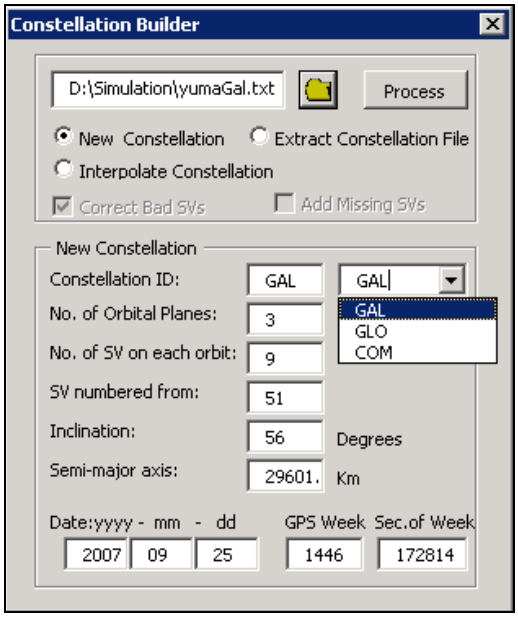

Figure 4.12: Constellation Builder form

Constellation information for three GNSS constellations (Galileo –GAL, GLONASS -GLO and COMPASS -COM) are included within 'Constellation Builder' based on GNSS constellation information for Galileo in [ESA, 2002], for GLONASS in [ICA, 2002] and for COMPASS/Beidou in [GPS-World, 2007].

The simulation for GNSS constellations assumes that satellites are in circular orbits around the earth. Almanac file in Yuma format consists of information line (start with stars) followed by the 13 lines described in Table 4.1. These lines are repeated for all satellites (a full description about definition of a Yuma Almanac can be found in [Navigation-Center, 2008a]).

Table 4.1: Almanac Yuma format and formulas

Line: Format	Formula
1: ID	0 to 'No of Satellites'
2: Health	000 (good)
3: Eccentricity	Set to the value 0
4: Time of Applicability(s)	GPS seconds of week calculated
5: Orbital Inclination(rad)	Inclination * Pi / 180
6: Rate of Right Ascen(r/s)	Set to the value 0
7: SQRT(A)	$\sqrt{SemiMajorAxis(A)}$
8: Right Ascen at Week(rad)	For i = 1 To 'No of Orbital Planes' Ω = (360 / No of Orbits) * (i - 1) * Pi / 180 Next i
9: Argument of Perigee(rad)	Set to the value 0 (circular orbit)
10: Mean Anom(rad)	For j = 1 To 'No of SV on each orbit' Delta = ((360 / No of SV) * Pi / 180) * (j - 1) Next j
11: Af0 (s)	Set to the value 0
12: Af1 (s/s)	Set to the value 0
13: week	GPS week routine

Any combined almanac file can be extracted in 'Constellation Builder' into separate files: e.g. almanac GPS and almanac GLONASS. Since GLONASS is operative, there are 14 GLONASS active satellites (Heath = 0), 8 inactive satellites (Heath = 1) and 2 missing satellites in almanac combined file which has been downloaded from [Magellan-Professional, 2008] on 31st March 2008 (GPS week of 1472). 'Interpolate Constellation' allows for interpolating bad satellites and/or adding missing satellites. The interpolation is conducted by searching to the closest active satellite in the same orbit and using it as a reference satellite for the interpolation. Some data from the reference satellite, such as time of applicability and inclination, are used in the interpolated satellite. However, the Mean Anomaly of the interpolated satellite is interpolated based on the Mean Anomaly of the reference satellite.

4.5.2 Auto Add Buildings to TIN

The second process is 'Auto Add Buildings to TIN' (summarised in Figure 4.13). This has been developed by the author to categorise the roof polygons in different levels which can then be used to add buildings to TIN. The algorithms in this tool were developed based on ArcObjects classes (such as Field class 'IField', point-collection class 'IPointCollection' and Polygon class 'IPolygon') and tools (such as

'Analysis' tool to create buffer, '3D Analyst' tool for interpolation and 'Management' tool to create layer). In addition, several VBA classes, Modules, Sub Procedures and Functions were also used.

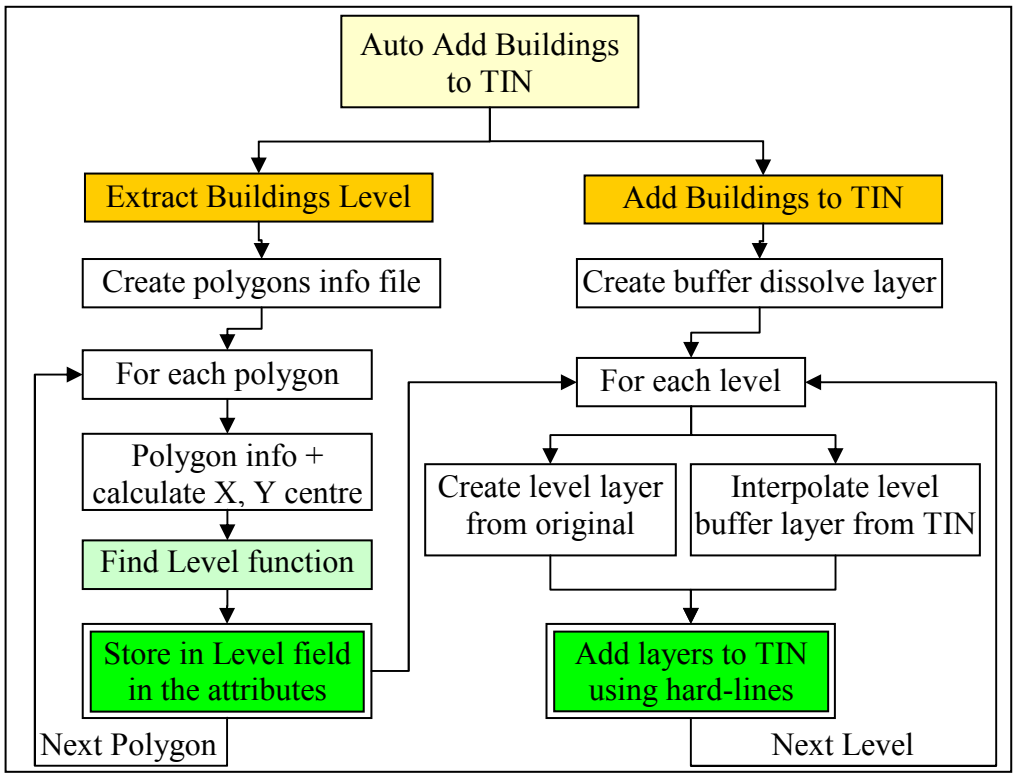

Figure 4.13: 'Auto Add Buildings to TIN' flowchart

Categorising the roof polygons can be done for each polygon layer in the ArcScene project as follows:

1: Loop through all polygons in the feature layer and store the following in a file (polygon's info file): Building index, Area, Average Z (Avg_Z), X and Y minimum and maximum values, and X and Y coordinates for the polygon. Some of the ArcObjects classes used here are 'IFeatureLayer', 'IField', 'IFeature', 'IEnumVertex' and 'IPointCollection'.

2: Loop through all polygons in the feature layer again and do the following:

   a. Get the polygon's information as in step 1: using some ArcObjects classes.

   b. Calculate X and Y centre values of the polygon from the minimum and maximum X and Y values.

   c. Call 'Find Level' function (new function written by the author) to calculate building level. All polygons' information explained in point 1: together with

the calculated X and Y centre in a. are used in this function. The algorithms within 'Find Level' function summarised in a flow chart in Figure 4.14.

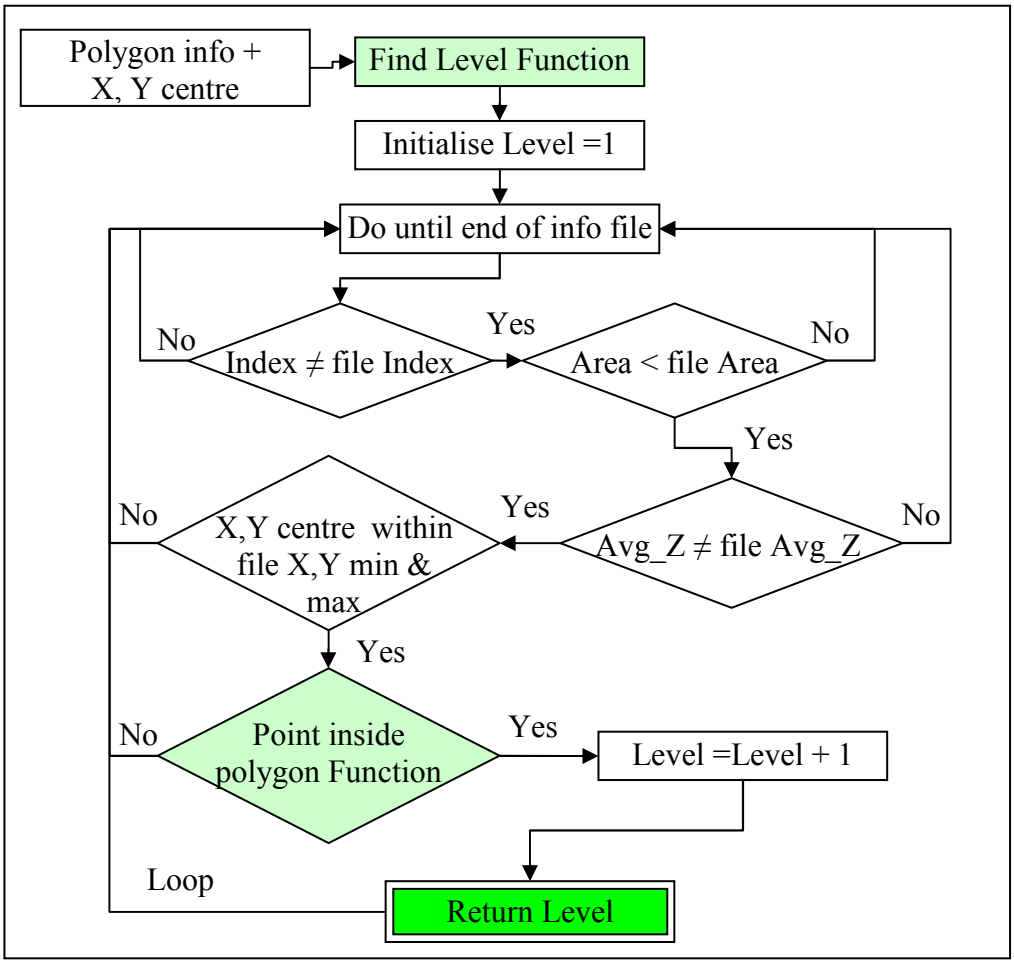

Figure 4.14: 'Find Level' Function flowchart

When the 'Find Level' function is called, it performs the following tasks:

- Initialise Level =1
- Do until end of the polygon's info file. For the current polygon check all polygons in the file:
  - If Building Index ≠ file Building Index then next check
  - If Area < file Area then next check. If the area of the polygon less than the area of the polygon in the file, it could located inside the bigger polygon
  - If Average Z difference (Avg_Z – Avg_Z in the file) is > 0 then next check. This means that the polygon/building is the higher than the polygon/building in the file

- If the X and Y centre coordinates are within the X and Y minimum and maximum of the polygon in the file then next check. This was done by checking if the X and Y centre coordinates are greater than the X and Y minimum and less than X and Y maximum
- Call function 'InOrOut', which has been written by the author to check if any point of the polygon is located inside the polygon in the file and return 1 if true or 0 if false. The inputs for this function are the polygon coordinates and X and Y for the point to be checked. This function calls 'Point In Polygon' (PIP) function which is based on the Jordan Curve Theorem [Haines, 1994]. Essentially, it tests how many times a ray starting from the point crossings the edges of the polygon. If the point in question is not on the boundary of the polygon, the number of intersections is odd number if the point is inside, else it is outside. This algorithm is sometimes also known as the crossing number algorithm. It is worth mentioning that there are other different methods described in [Haines, 1994] for testing whether a point is inside a polygon such as angle summation test and triangle tests. PIP function optimisations can be done as follows:
  - Consider a ray is shot from the test point along an axis (+X is commonly used)
  - Check the edges against this point, if the Y components of a polygon edge differ in sign, then the edge can cross the test ray
  - In this case, if both X components are positive, the edge and ray must intersect and a crossing is recorded
  - Else, if the X signs differ, then the X intersection of the edge and the ray is computed and if positive a crossing is recorded
- If the return value from 'Point In Polygon' = 1 then Level =Level +1. Loop.

- Return Level as the building level.

d. Store building level in Level field in the layer's attributes.

The 'Add buildings to TIN' process uses several ArcGIS tools and performs the following tasks:

- Create and dissolve a buffer of specific distance, i.e. 5 cm, around the original building layer using 'Analysis' tool. The commands used are:
  - Set GP = CreateObject("esriGeoprocessing.GpDispatch.1")

  - GP.Buffer_analysis InputShpFileName, OutputBuffFileName, BufferDistance, "", "", "LIST", "Level"

- For each level of the buildings, do the following:
  - Create level layer selected from the original building layer using 'Management' tool. The commands are:
    - GP.Toolbox = "management"
    - GP.MakeFeatureLayer_management OutputBuffFileName, "lyr"
    - GP.MakeFeatureLayer_management InputShpFileName, "lyr1"
  - Interpolate another level layer selected from buffer layer with the current TIN using '3D Analyst' tool. The commands are:
    - GP.Toolbox = "3D"
    - GP.InterpolateShape DTMLayerName, OutputLevelFileName, OutputIntrpFileName ' , "1", "0.3048"
  - Add the previous level layers to the TIN using hard-line technique using '3D Analyst' tool. The commands are:
    - AddBuildingFiles = OutputIntrpFileName + " shape <none> hardline true; " + OutputLevel1FileName + " shape <none> hardline true"
    - GP.edittin DTMLayerName, AddBuildingFiles
- Loop for next level.

4.5.3 Satellites Visibility Simulation

The third process is the satellite visibility simulation which performs visibility along a trajectory path using multiple GNSS constellations (stored in almanac files) within a 3D city model environment (either TIN or Raster models). The algorithms in this process have been developed based on several ArcObjects classes and VBA Modules, Sub Procedures and Functions and are summarised in a flow chart in Figure 4.15.

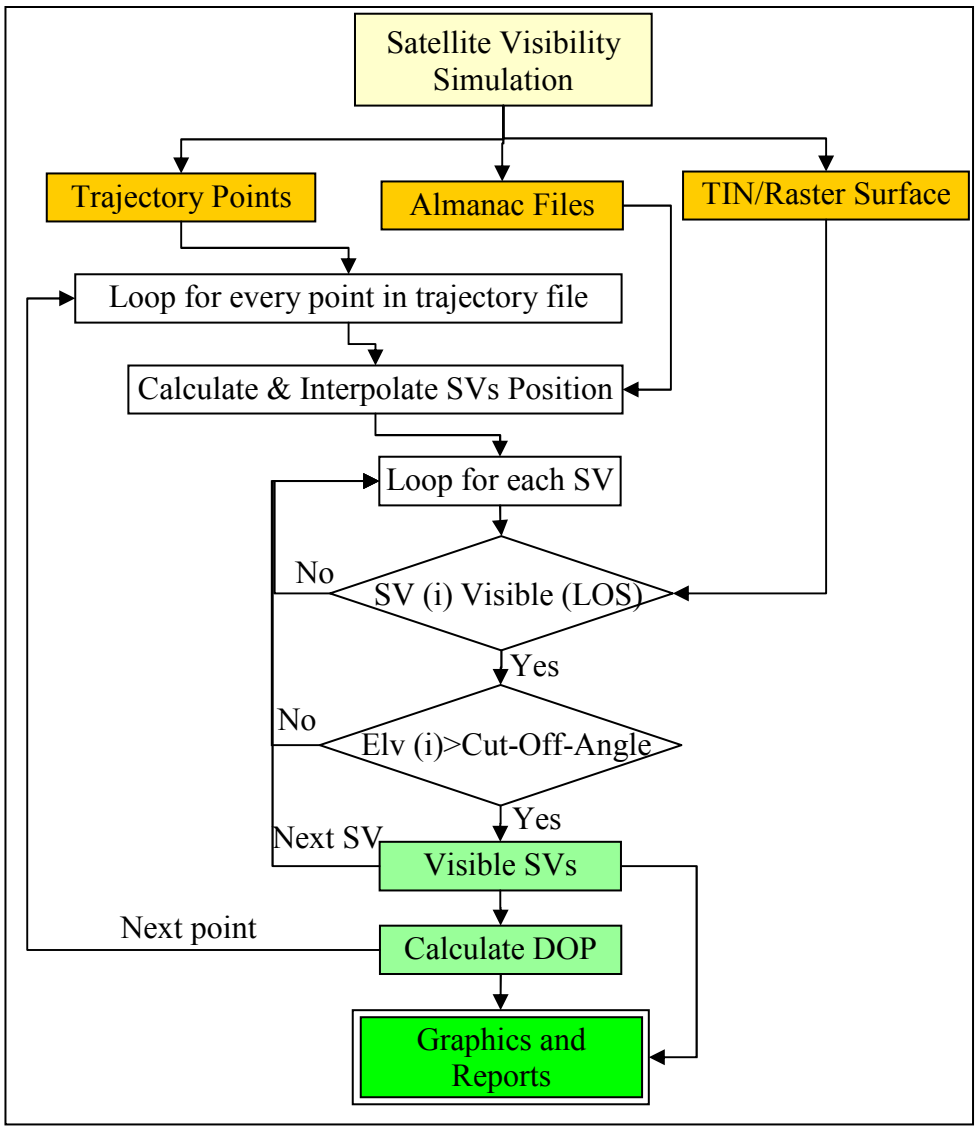

Figure 4.15: Satellite visibility simulation flowchart

In general, when the 'Run Simulation' button is clicked, the satellite visibility tool performs the following tasks:

- **Almanac files**: Store the names of the Almanac files in an array (e.g. AlmanacFiles).
- **Working surface**: Define the working surface (using ISurface class), either from TIN or Raster dataset, as selected in the Surface frame. This is done as follows:
    - Loop through all layers in the ArcView's table of contents.
    - If the name of the layer (i) equal the layer name in the Surface frame then next, else loop next layer.

  - Check if the layer type is TIN layer (ITinLayer class) then define the surface from TIN dataset and exit loop.
  - Check if the layer type is Raster layer (IRasterLayer class) then define the surface from Raster dataset and exit loop

- **Trajectory points**: Calculate grid coordinates and GPS time (GPS week and seconds of week) for the trajectory points (based on the selected scenario, static, kinematic or other scenarios) and store them in a big array (AllTrajPoints). This was done using the 'Trajectory Module' which includes several VBA Sub Procedures (such as Static_Trajectory and Kinematic_Trajectory) as well as some ArcObjects classes (such as IPolyline and IPointCollection). The coordinates in AllTrajPoints array should be interpolated to get elevation if the height of any point is equal to the default elevation (-1000m). This was done within the 3D surface model (pSurf) using the ArcGIS 'pSurf.GetElevation' Method. The points in the AllTrajPoints array are, after interpolation, stored in a file and then added to the ArcView's table of contents.
- **Main loop**: For each trajectory point in the AllTrajPoints array do the following:
  - Compute Cartesian coordinates for all satellites in the constellations based on almanac information in AlmanacFiles, using the procedure described in Verhagen [2006]. This was done using the VBA module 'ComputeSatPos' which includes several Sub Procedures (such as ReadEphemris and satpos) and several Functions for GPS time calculations (such as GPS_Time and Julian_day). Then for each satellite do:
    - Interpolate satellite coordinates at distance equal to value of the Interpolation Radius using the VBA Sub 'InterpolateSat'.
    - Transform satellite's Cartesian coordinates to British National Grid coordinates using the DLL of Grid InQuest tool (GIQ 6) using the VBA Sub 'XYZ2ENHt'.
    - Calculate Azimuth and Elevation angles of point to satellite vector using the VBA Sub 'AzimuthElevation'.
    - Check visibility between point and satellite within the 3D model surface (i.e. pSurf) using the ArcGIS

'pSurf.GetLineOfSight' Method. The command is: pSurf.GetLineOfSight pObserver, pTarget, pObstruct, pVisPolyline, pInVisPolyline, bIsVis, False, False

- Check the satellite's elevation angle against the cut-off-angle.
- Store visible satellites in an array.

- Loop next satellite.
- Calculate DOP values for the visible satellites following the equations described in [Verhagen, 2006] using the VBA Sub 'CompDop'.
- Write Report files.
- Loop next trajectory point.
- Draw graphics.

As explained above, the algorithms in the UCGS tool were developed from the available ArcObjects classes and tools as well as from several VBA classes, Modules, Sub Procedures and Functions that were developed to complete the objectives of this tool. These algorithms should make it easy for future development of UCGS, and in understanding how the different tools have been mixed together to perform different tasks.

4.6 UCGS Tool Evaluation

In order to test the reliability and to assess the UCGS tool performance in a real world scenario, the program was field-tested on the University of Nottingham campus.

The first step in the testing process was the collection of real GPS data (15 seconds interval) on 24th of September 2007 (in the GPS week of 1446) over a period of 24 hours starting at midnight at a fixed point on the IESSG building. An almanac file for the same date was then downloaded from Magellan-Professional [2008]. This file was converted to ASCII format using Ashtech Evaluate version 6.01 software, extracted to GPS and GLONASS almanac files using Almanac Builder and imported the GPS into the UCGS.

The photogrammetric model of the University of Nottingham's Campus was then imported into the UCGS to calculate which features would block signals. One Static Point scenario was selected and the grid coordinates (E, N and Ht) of the IESSG point were entered in the Static Options Form. Within the option frame, the default values of cut-off angle (10°) and interpolation radius (1000m) were used. However, the observation height was modified to 0.0m and the simulation date and time, as well as the interval, were modified to match the data collection.

The differences between the number of real and simulated GPS satellites over the same period of time are plotted in Figure 4.16.

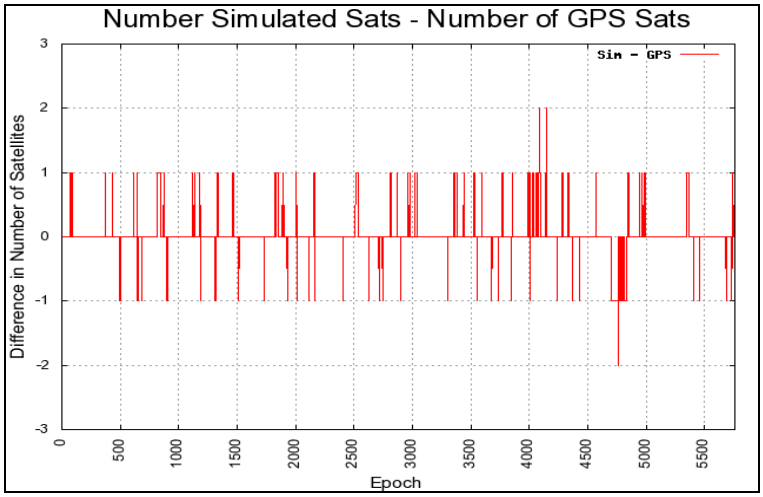

Figure 4.16: Differences between real and simulated number of GPS satellites

The results show that cases agree 91.7% of the time in terms of the number of satellites. There were 473 of 5,758 epochs with a difference of one satellite and four epochs with difference of two satellites.

These differences could be caused by errors in the 3D model, including the fact that vegetation was not modelled in the DEM, or by differences in the calculation of the satellite orbits given in the almanac (used by the UCGS) and the satellite orbits given in the ephemeris (used by the receiver).

To investigate this further, a sky plot for the simulated GNSS satellites is provided in Figure 4.17.

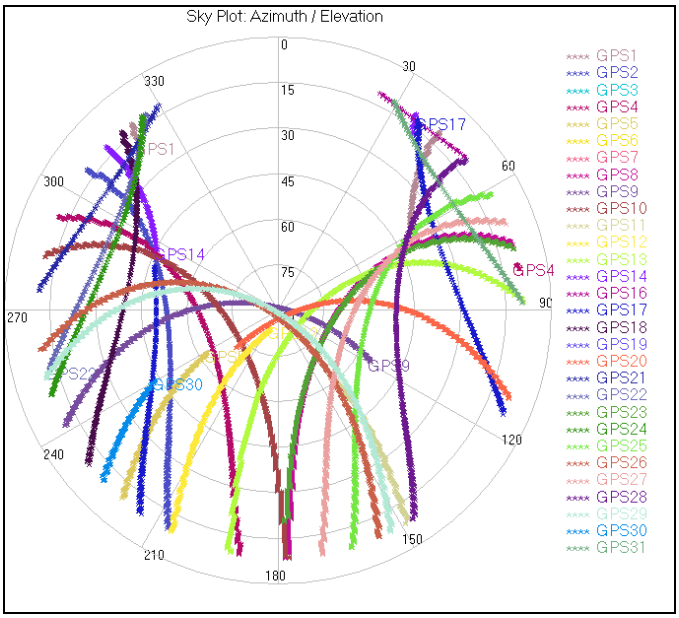

Figure 4.17: Simulated GNSS satellites over a period of 24 hours starting at midnight at a fixed point on the IESSG building

Considering a test epoch, epoch 4763, with a difference of two satellites; nine satellites (with numbers 3, 8,16,18,19,21,22,25 and 27) for the real data, but only seven satellites (with numbers 3, 8, 18, 19, 22, 25 and 27) for the simulated data, the azimuth (AZ.) and elevation (Elv.) angles for the actual and simulated (Sim.) GPS satellites, and their differences (Diff.), are given in Table 4.2.

Table 4.2: Azimuth and elevation angles, and their differences, for real and simulated GPS satellites

Sat. ID	Real Az.	Sim. Az.	Diff	Real Elv.	Sim. Elv.	Diff
16	172.53°	171.89°	0.64°	21.96°	21.85°	0.11°
21	63.90°	62.28°	1.62°	10.06°	9.97°	0.09°

From Table 4.2, it is clear that the differences between the azimuth and elevation angles based on an almanac and those based on an epehemeris are up to 1.62° and 0.11° respectively.

For satellite number 21, when considering that the real data was observed with an elevation cut off angle of 10 degrees, it is clear that this satellite is not appearing in the simulated data, at this one test epoch, due to the subtle difference in elevation angle. Whereas, for satellite number 16, when considering the environment surrounding the IESSG building it is clear from Figure 4.18 that a tall chimney is

located in the direction of this satellite, which is not appearing in the simulated data, at this one test epoch, due to the subtle difference in azimuth.

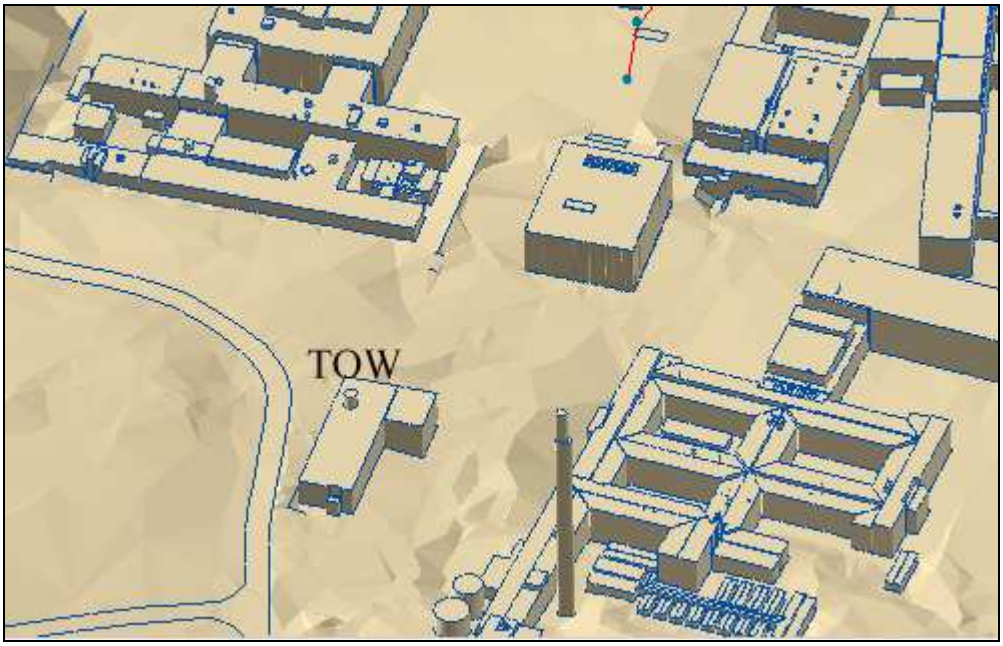

Figure 4.18: Obstructions of satellite number 16 by a tall chimney

From this limited analysis, it can be concluded, therefore, that for the urban canyon scenario on the University of Nottingham's campus, the main reason for the differences found is not due to the fact that vegetation was not modelled in the DEM, but due to differences in the satellite orbits given in the almanac (used by the UCGS) and the satellite orbits given in the ephemeris (used by the receiver).

4.7 Summary

This chapter introduced the UCGS tool developed by the author. The UCGS tool consists of three processes: Constellation Builder, Auto Add Buildings to TIN and Satellites Visibility Simulation. These make it possible to consider satellite visibility within a 3D model environment.

The chapter was started by providing a background about current Satellite prediction tools, each of which falls short, in one way or another, of the objective of UCGS. For instance, the simulation of multiple GNSS constellations was not discussed in any of these tools, and none consider visibility in different trajectory scenarios such as

Static, Kinematic and Stop & Go scenarios. Although these are not insurmountable, they are clearly shortcoming in these tools, which have been addressed in UCGS.

An overview of GIS and in particular ArcGIS was then given. UCGS predicts satellite visibility under ArcScene along a trajectory path within either raster or vector data models. Therefore, it was necessary to understand what raster and the vector data models are and how programming within ArcGIS, using the available ArcObjects classes within the embedded VBA, is carried out.

Three dimensional model preparations were discussed in great detail, especially the photogrammetric 3D model. 'Auto Add Buildings to TIN' one of the UCGS processes was described. This categorises building levels and uses these levels for adding buildings to a TIN in an iterative TIN surface generation, where for each iteration an expanded footprint for roof level is created based on the previous level. LiDAR data preparation was also briefly described.

A discussion of the algorithms used to build the different processes in UCGS was given and the UCGS tool was then briefly evaluated using real GPS data collected during a period of 24 hours at a fixed point on the IESSG building. The results showed a 91.7% match in the number of real and simulated satellites ,with subtle differences shown to be due to errors in azimuth and elevation angles calculated for satellites when using the satellite orbits given in an almanac.

Chapter 5: Applications of GNSS Simulation

5.1 Introduction

The previous Chapter described the development of the UCGS tool which can assess satellite visibility along a trajectory path within a 3D city model. This Chapter will focus on the applications of such a tool to perform satellite visibility in two different environments using two different datasets of 3D models. Firstly GNSS simulation was carried out using a 3D model of the University of Nottingham's Campus described in the previous section. A second simulation was then carried out using 1.0m resolution LiDAR data of Upton-upon-Severn. The purpose of simulating present and future GNSS constellations is to investigate the potential advantages given by using additional satellites when positioning in urban canyons. Building height data, for the area that is being investigated, is therefore required to be able to model any obstructions that might block the GNSS signals.

5.2 Campus Simulation

Using the 3D model, built using photogrammetric techniques, of the University of Nottingham's Campus and a trial route of testing points (Figure 5.1), the effect of additional satellite constellations that may be available in the near future was tested in three simulations. The first two simulations were carried out to test the number of satellites and their PDOP at two different times (morning and afternoon) along the trial route. The third simulation was performed over 24 hours on each of the testing points. In all simulations, several scenarios were tested: GPS only; GPS and GLONASS (a fully operational 24 satellite constellation) (GPS+GLO); GPS, GLONASS and Galileo (GPS+GLO+GAL); and finally all four constellations, namely GPS, GLONASS, Galileo and COMPASS (GPS+GLO+GAL+COM).

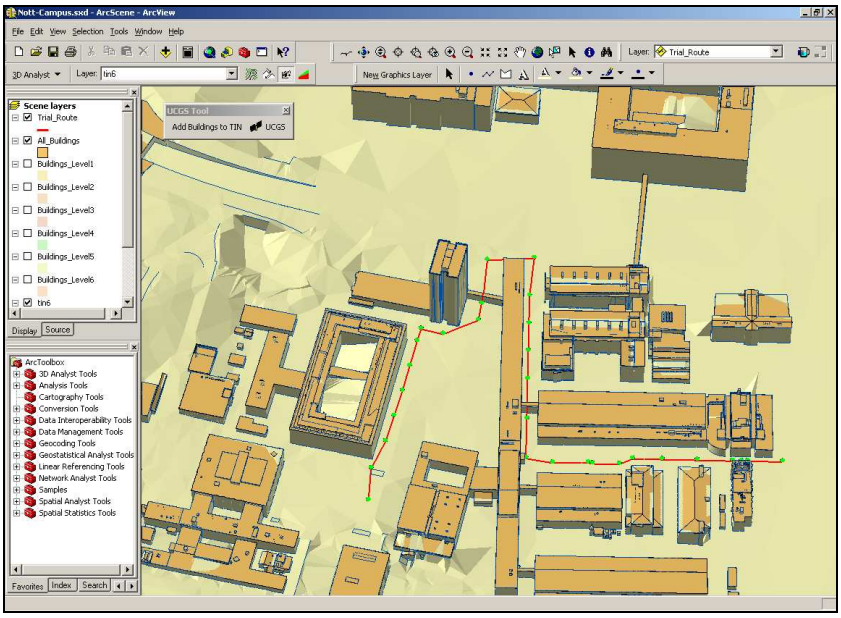

Figure 5.1: A 3D model of the University used in the GNSS simulator

In total, 31 of the testing points in the campus network were used in the simulation tests. It is worth mentioning that the points under the bridges (T10 and T33) were excluded from the simulation, since the bridges were modelled as walls in the TIN. The results of Morning and Afternoon simulations as well as of the 24 hours simulation are analysed in the next sections.

5.2.1 Campus Simulation: Morning and Afternoon Simulations

The simulation was performed on the 25th of September 2007 (in GPS week 1446) at the times of 9:00am and 1:00pm for the Morning and Afternoon simulation respectively. UCGS was used in its 'Stop & Go' mode; the receiver was simulated to move along the campus network (shown by the red line in Figure 5.1) at a speed of 1.5m/second and to stop on each of the 31 points for 120 seconds, with a 10 second observation interval. The simulation parameters used in both simulations were the UCGS default values which include: cut off angle of 10º, observer height of 1.8m and interpolation radius of 1000m. The simulated variation of the number of satellites is shown in Figure 5.2 for Morning (top) and Afternoon (bottom).

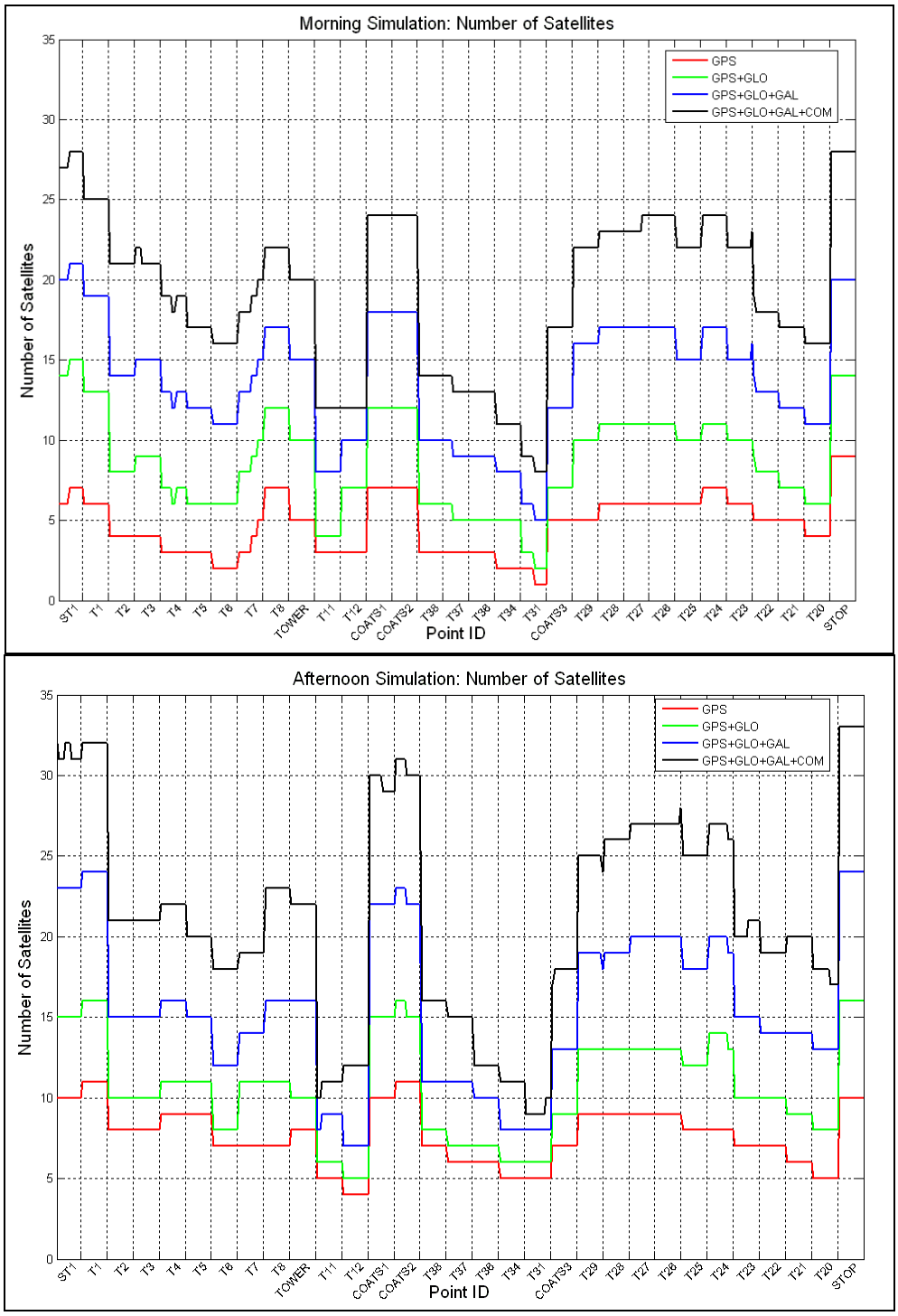

Figure 5.2: Number of satellites available in the Morning simulation (top) and Afternoon simulation (bottom)

As stated previously, at least five well distributed GNSS satellites are required for real time positioning of centimetre-level of accuracy. The Morning simulation (Figure 5.2 (top)) shows that using GPS only, 14 out of 31 points are predicted to have less than five satellites, due to building obstructions, and five points were found to have only five satellites. However, the Afternoon simulation (Figure 5.2 (bottom))

shows that using GPS only, only one point (T12 located close to a bridge) was found to have less than five satellites, and four points (three of them located close to a bridge and one point (T20) located in a narrow road) to have only five satellites. In general, therefore, the Afternoon simulation gave better availability results and shows the advantage of using simulation for planning data collection in the urban canyons, when using GPS only.

If both GPS and GLONASS were fully operational then the simulation predicts that only two points (T11 and T31) would have less than five satellites in the Morning and no points would have less than five satellites in the Afternoon. Furthermore, when adding Galileo satellites to the Morning simulation, then none of the testing points would have less than five satellites and with the addition of COMPASS, there would still be no points with less than five satellites. The average number of satellites available over the whole network in the Morning simulation increases from five for GPS only, to nine for GPS+GLO, to 14 for GPS+GLO+GAL, and finally to 19 when using all four constellations. Similarly, the average number of satellites available over the whole network in the Afternoon simulates increases from eight for GPS only, to 11 for GPS+GLO, to 16 for GPS+GLO+GAL, and finally to 21 when using all four constellations. Using all four constellations, the minimum number of satellites was found to be eight and nine in the Morning and in the Afternoon respectively, and the maximum number of satellites was found to be 28 and 33 in the Morning and the Afternoon respectively.

As well as the number of satellites affecting the availability of positions using GNSS, the PDOP is also critical. Figure 5.3 shows the variation of the PDOP values calculated for the Morning (top) and Afternoon (bottom) simulated satellite constellations.

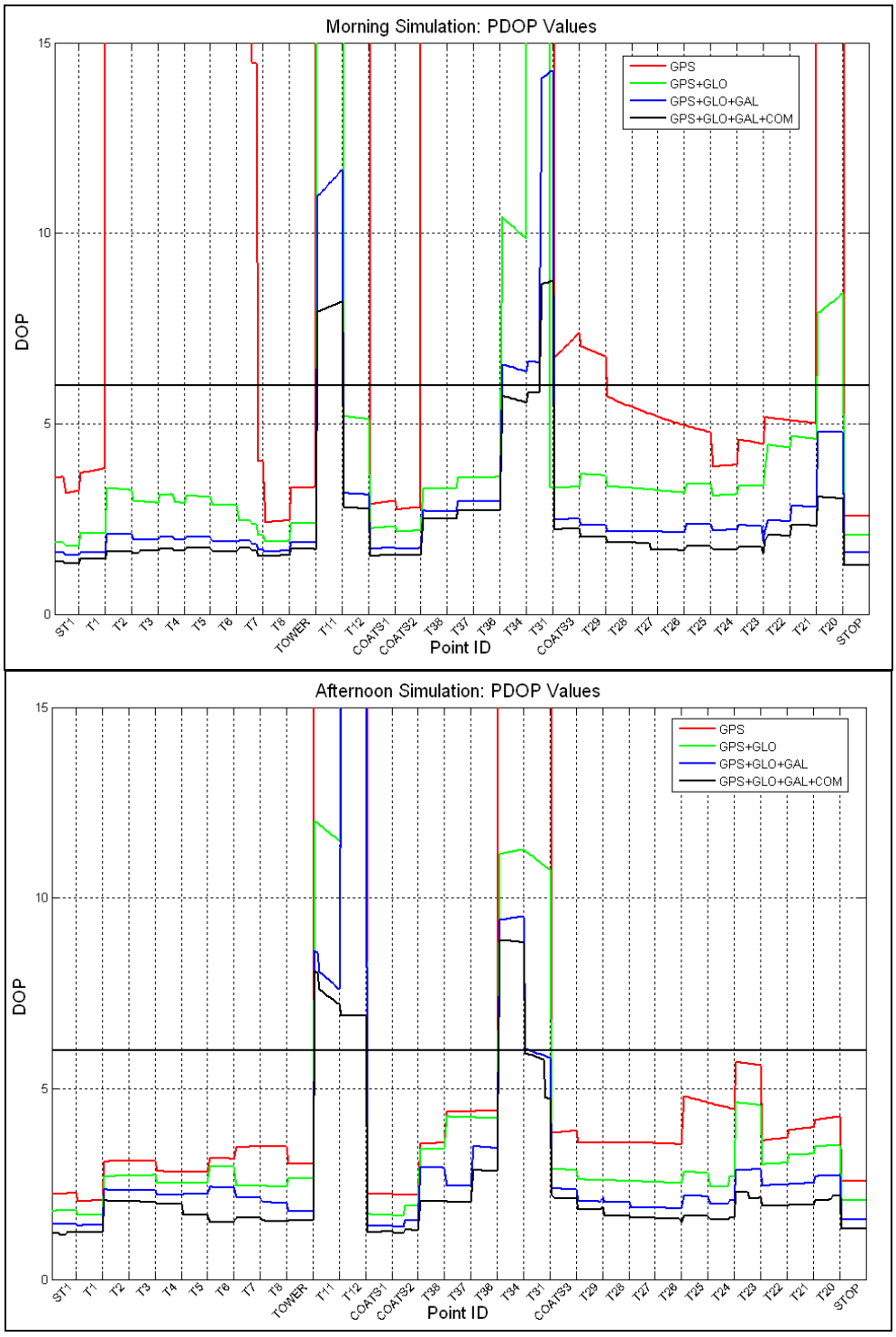

Figure 5.3: Variation of PDOP in the Morning simulation (top) and Afternoon simulation (bottom)

The black horizontal line running across the graphs represents a PDOP of 6, i.e. the normal cut off point for when the satellite geometry becomes unreliable for centimetre-level positioning, based on several text books (for example [Bossler, 2002; Kennedy, 2002; Spencer, 2003; Kaplan and Hegarty, 2006; Roddy and Ebrary Inc., 2006]). Immediately it can be seen from Figure 5.3 (top) that using GPS only

gives very large PDOP values on the same 14 points which had less than five satellites in the Morning simulation. Further, large PDOP values were found in the areas with four and five satellites in the Afternoon simulation. After introducing the GLONASS constellation into the Morning simulation, only one testing point (T31) gave a very large PDOP value, one testing point (T11) gave a large PDOP value (about 70) and two other testing points gave PDOP values of greater than 6 (green line, Figure 5.3 (top)). Noticeable drops in the PDOP vales were found for the four points (T11, T12, T34 and T31 which are located close to bridges between buildings) which had large PDOP in the GPS only Afternoon simulation after adding the GLONASS satellites. Further drops in the PDOP values were recorded in both simulations after using the three and four constellations. However even when using all four constellations, there are still a few points where a PDOP value of less than 6 is not guaranteed.

Overall, therefore, it can be concluded that the combination of satellite constellations can significantly improve the number of available satellites. However, although the minimum number of satellites when using all four constellations was found to be equal to eight and nine satellites (in the Morning and the Afternoon respectively), a PDOP value of less than 6 is still not guaranteed all of the time. As a result, position availability using the criteria of five or more satellites with a PDOP of 6 or less, is not guaranteed 100% of the time. For further analysis of the availability of satellites and the PDOP values in the urban canyons, 24 hours simulation on each of the testing points was carried out using UCGS as detailed in the next section.

5.2.2 Campus Simulation: 24 Hours Simulation

Similar to the Morning and Afternoon simulations, this simulation was also performed on the 25th of September 2007 (in GPS week 1446) over a 24 hour period starting at midnight and carrying on through that day. Each point was simulated individually, in static mode and with an observation interval of 60 seconds. Similar to the previous simulations, the UCGS default simulation parameters were used.

Figure 5.4 shows the maximum (red line) and minimum (green line) available positioning satellites when using GPS only along the trial route. According to the simulation results, there are only three points (ST1, T1 and STOP) along the trail route where, across the whole 24 hour period, it is guaranteed that five or more satellites will be in line of sight of the GPS receiver at all times. These points are located in reasonably open sky areas. In contrast, the minimum number of satellites (1 satellite) were found for five points (T11, T12, T36, T34 and T31) which are located close to bridges. On the other hand, it can be seen that all of the points have some time of the day when more than five satellites are available.

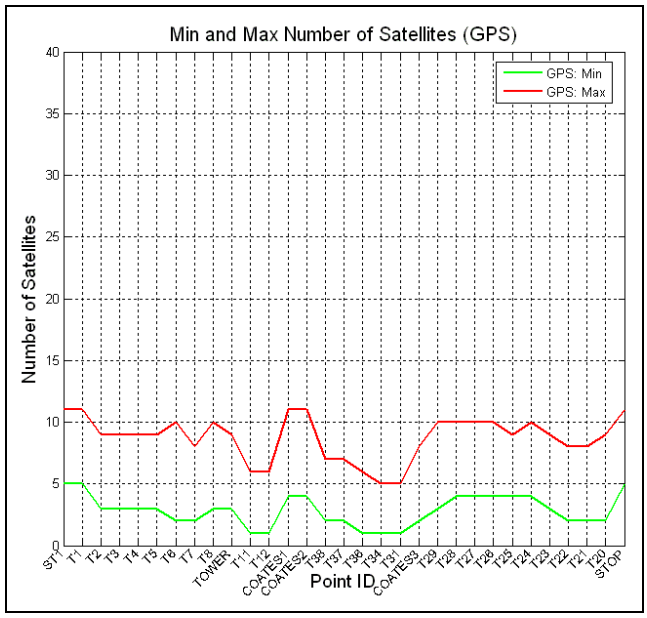

Figure 5.4: Maximum and minimum GPS satellites available around the trial route over a 24 hour period

Figure 5.5 shows the maximum and minimum available satellites when using a GPS+GLO constellation along the trial route. This simulation shows a significant improvement in the number of points that always have line of sight to five satellites or more. Although the minimum number of satellites increased from one (using GPS only) to two (using GPS + GLO), there are clearly still significant problems with the availability of satellites in the areas with the most restricted view of the sky, i.e. the points near the bridges.

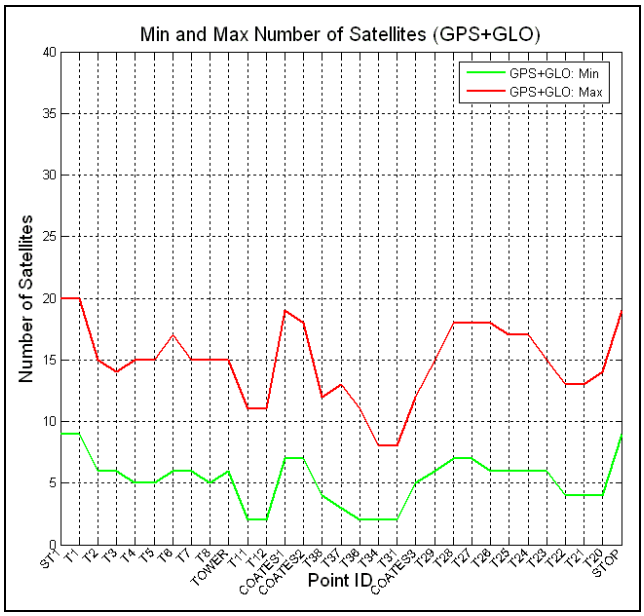

Figure 5.5: Maximum and minimum GPS + GLO satellites available around the trial route over a 24 hour period

Figure 5.6 shows the maximum and minimum available satellites when using a GPS+GLO+GAL constellation. If all three of these constellations were fully operational, UCGS predicts that only three of the points would have some epochs with less than five satellites available. These points are T11, T34 and T31, all of which are within a few metres of a bridge and thus have a significantly restricted view of the sky.

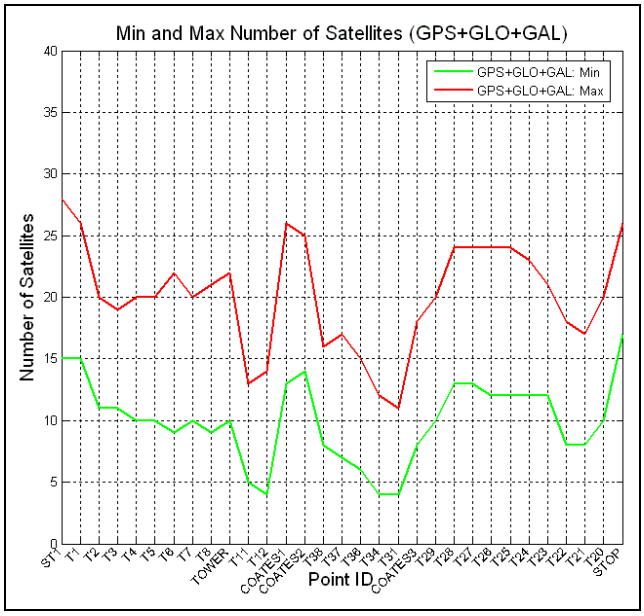

Figure 5.6: Maximum and minimum GPS + GLO + GAL satellites available around the trial route over a 24 hour period

Figure 5.7 shows the maximum and minimum available satellites for the three previously mentioned GNSS satellite constellations, augmented by the Chinese GNSS system that is currently under development, known as COMPASS. The simulation shows that only one point (T31) has a minimum of five satellites, two points have a minimum of six satellites (T12 and T34) and all other testing points have more than six satellites at all times. Again, the points with five and six satellites are located close to the bridges.

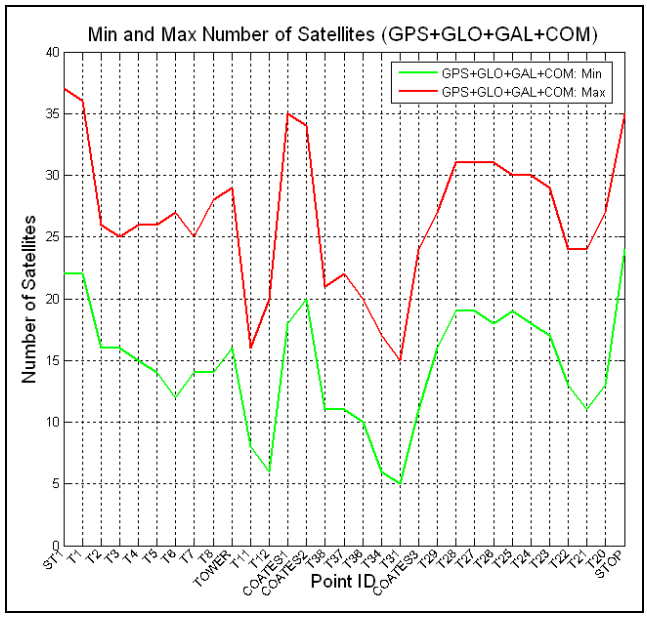

Figure 5.7: Maximum and minimum GPS+GLO+GAL+COM satellites available around the trial route over a 24 hour period

To summarise the results, Figure 5.8 shows, as a percentage for each point over the 24 hours simulation, the availability of more than five satellites.

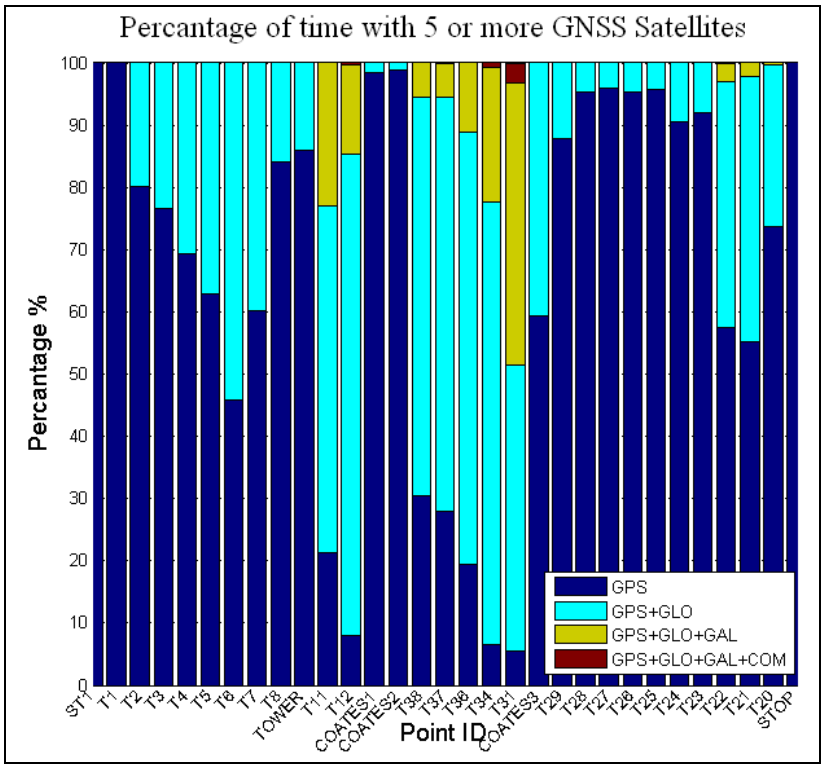

Figure 5.8: The percentage of time where five or more GNSS satellites were simulated to be available around the trial route

From Figure 5.8 it can be seen that, when using GPS only, only 3 out of the 31 points, two of which were specifically been placed in areas which have a clear view of the sky (ST1 and STOP), have greater than five satellites available 100% of the time. With the addition of a full GLONASS constellation, to the currently available GPS constellation, UCGS predicts that 21 of the 31 points will have five GNSS Satellites available 100% of the time. After adding the Galileo constellation to the simulation, there are now only a few epochs at points T31 and T34 where less than five satellites are available and the addition of a fourth GNSS constellation, COMPASS, means that all 31 of the test points have more than five satellites available 100% of the time.

However, using the combined criteria of five or more satellites being available with a PDOP value of less than 6, the percentage availability statistics are affected as seen in Figure 5.9.

Figure 5.9: Percentage of time where five or more GNSS satellites were available and PDOP is less than 6

From Figure 5.9 it is clear that point T31 will be very difficult to position, to a centimetre-level, even when using all four GNSS constellations. This difficulty is caused by the fact that the view of the sky at this position is obscured by the surrounding buildings as well as a bridge just to the east of the point. Therefore, T31 testing point will be further analysed as a worst case scenario. The simulated results for the number of satellites available on this point are plotted in Figure 5.10. Using GPS only, five GPS satellites were only available for 5% of the trial time. After adding GLONASS to the simulation this availability increased to just over 50%, with a further increase after adding Galileo to over 95% and then to 100% when all four constellations were used. However, as seen from Figure 5.9, when using the criteria of five or more satellites with a PDOP value of less than 6, this availability is reduced to 34% even when using all four constellations.

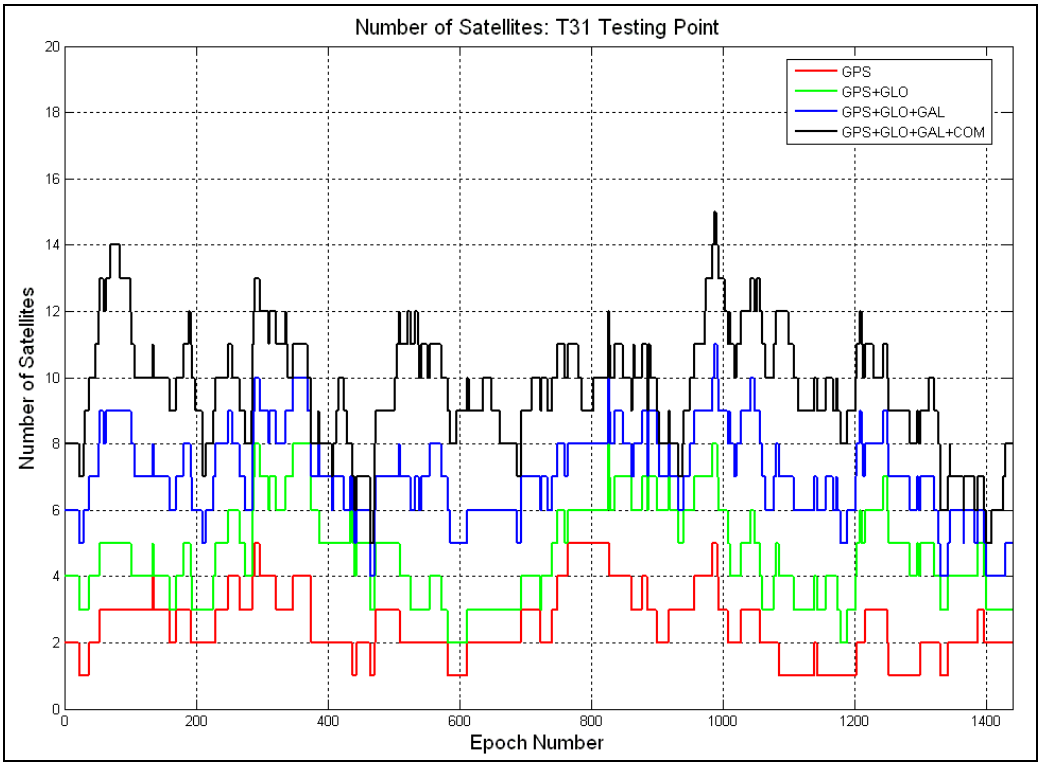

Figure 5.10: Variation of available satellites at point T31

Overall, the results of the Campus simulations provide evidence that using more than one GNSS constellation will significantly increase the availability of satellites in urban environments. However, an investigation of the PDOP values for one of the most obstructed positions (point T31) shows that with all four GNSS constellations fully operational, although five or more satellites will be available 100% of the time, the distribution of these satellites may still restrict the times of day when centimetre-level positioning is achievable.

5.3 Upton Simulation

In order to test the different GNSS constellations in a different area and with a different DEM, another simulation was conducted based on 1.0m resolution LiDAR data for Upton-upon-Severn, a small town in the West Midlands of England. A trial route through Upton was established and designed to encompass the variation in environments typical of towns in the United Kingdom. The trial route starts in an open area (car park – epoch 1) with a clear view of the sky and then heads into the town centre, which is typified by very narrow streets with three or four storey

buildings on either side of the road (epochs 40-50), that restrict the view of the sky a great deal. The route then continues to a modern housing estate with many two store houses that are relatively well spaced (epochs 80-290), and then heads back through the town centre (epochs 310-330) and to the open car park. The trial route can be seen in Figure 5.11. Unlike the University of Nottingham's Campus trial route, there are no bridges in the Upton trail route.

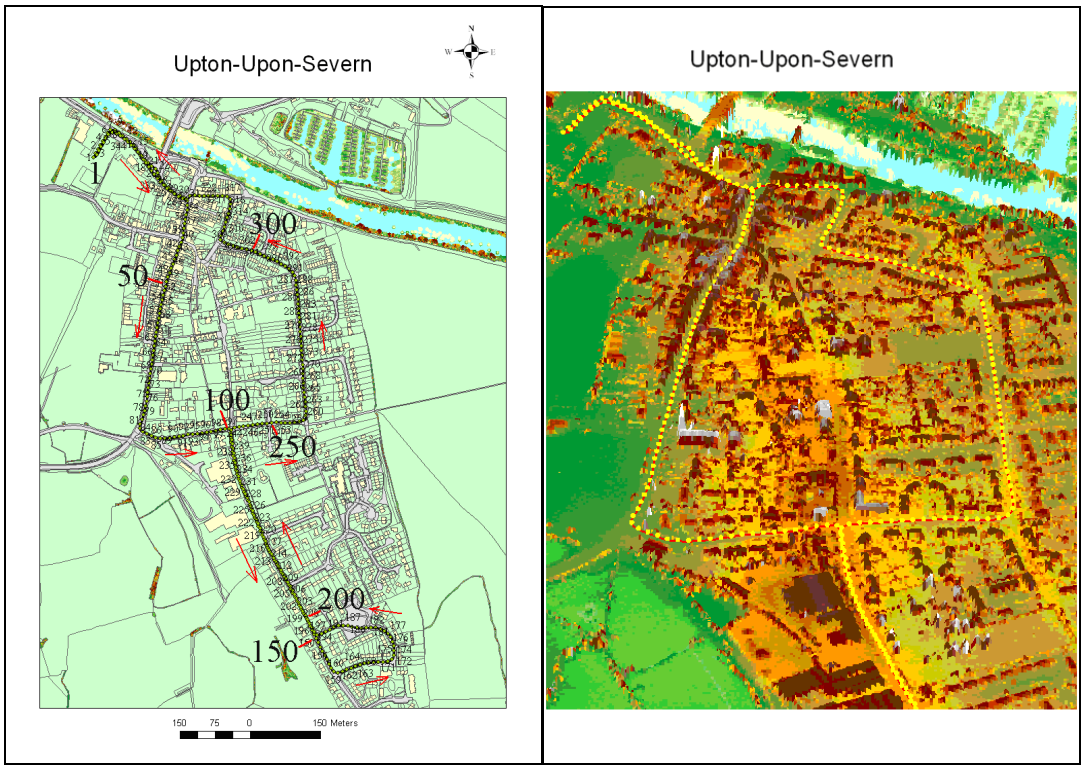

Figure 5.11: Upton trial route (left) and LiDAR Data (right)

Simulations along the Upton trial route were performed for the same scenarios as in the Campus simulation, namely GPS only, GPS + GLONASS, GPS + GLONASS + Galileo and finally all four constellations. In addition, two simulations (Morning and Afternoon simulations) were carried out using the same date and time, and the same simulation parameters and almanac files that were used in the previous Campus simulation. However, UCGS was used in its 'Kinematic' mode instead of 'Stop & Go' mode. The simulated variation of the number of satellites is shown below in Figure 5.12 for the Morning (top) and for the Afternoon (bottom).

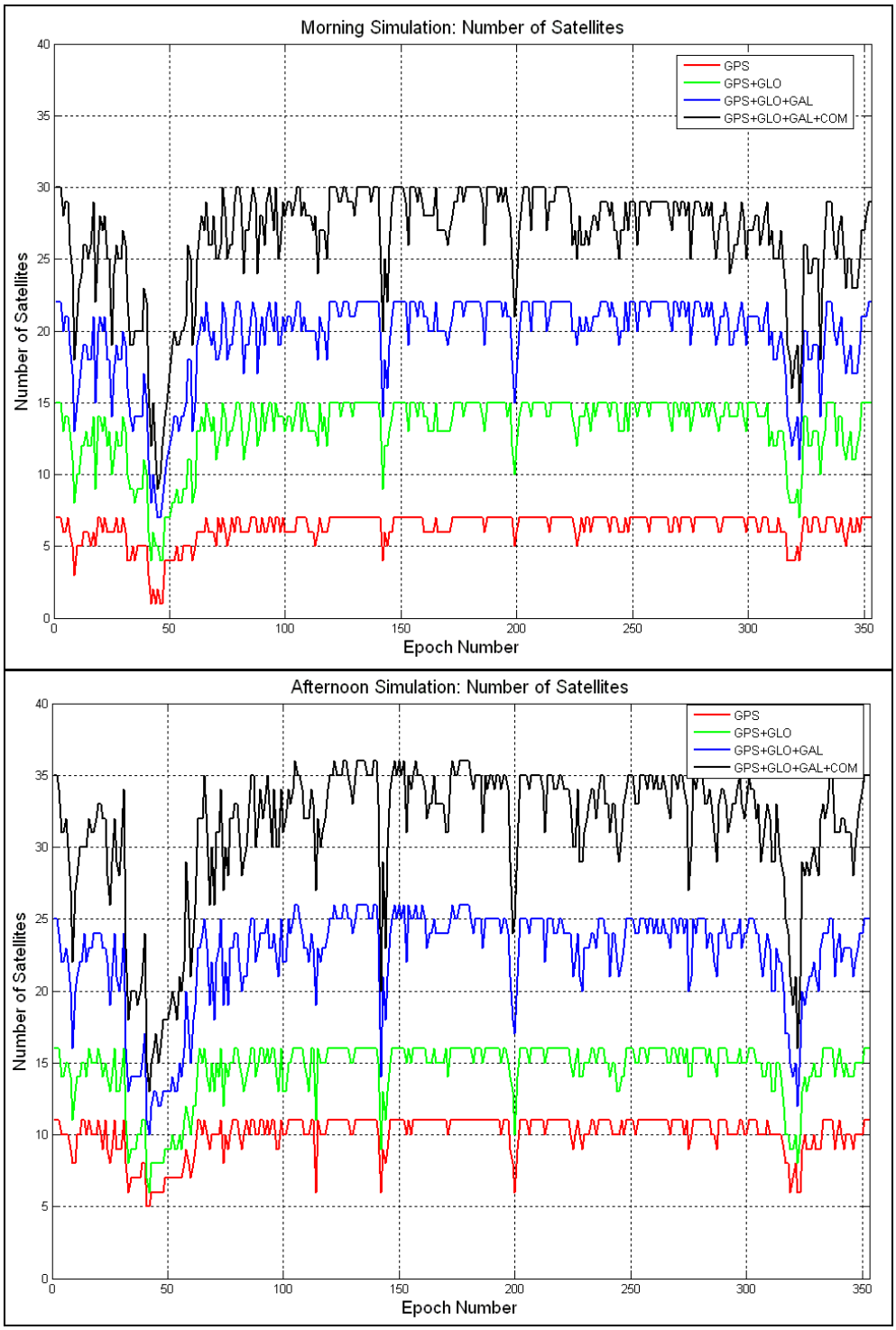

Figure 5.12: Number of satellites in the Morning (top) and Afternoon simulation (bottom)

The morning simulation showed that with GPS only there are four areas where less than the required five satellites are available. These areas are in the narrow streets of the town centre. However, the Afternoon simulation predicted none of the epochs to have less than five satellites. Once a second constellation (GLONASS) is added to the Morning simulation then only one area around the epochs 40-50 is still to have

less than five satellites. The addition of the Galileo constellation assures that there are no epochs with less than five satellites in both simulations. The average number of satellites available over the whole trial route in the Morning increases from six for GPS only, to 13 for GPS + GLO, to 20 for GPS + GLO + GAL, and finally to 27 when using all four constellations. Similarly, the average number of satellites available over the whole network in the Afternoon increases from 10 for GPS only, to 15 for GPS + GLO, to 23 for GPS + GLO + GAL, and finally to 31 when using all four constellations. Using all four constellations, the minimum number of satellites was found to be nine and 13 in the Morning and the Afternoon respectively, and the maximum number of satellites was found to be 30 and 36 in the Morning and the Afternoon respectively.

The variation of PDOP was also calculated along the same trial route over the same epochs, and the results are shown in Figure 5.13 for the Morning (top) and Afternoon (bottom). The PDOP values were found to be very large at times when using GPS only, especially in the Morning simulation. Furthermore, although there were not any epochs of less than five satellites in the Afternoon simulation, the PDOP was large in four areas. As in the Campus simulation, the PDOP values were reduced by adding more constellations. However, even when considering all four constellations, there is still an area around epoch 50 with PDOP of more than 6 in the Morning.

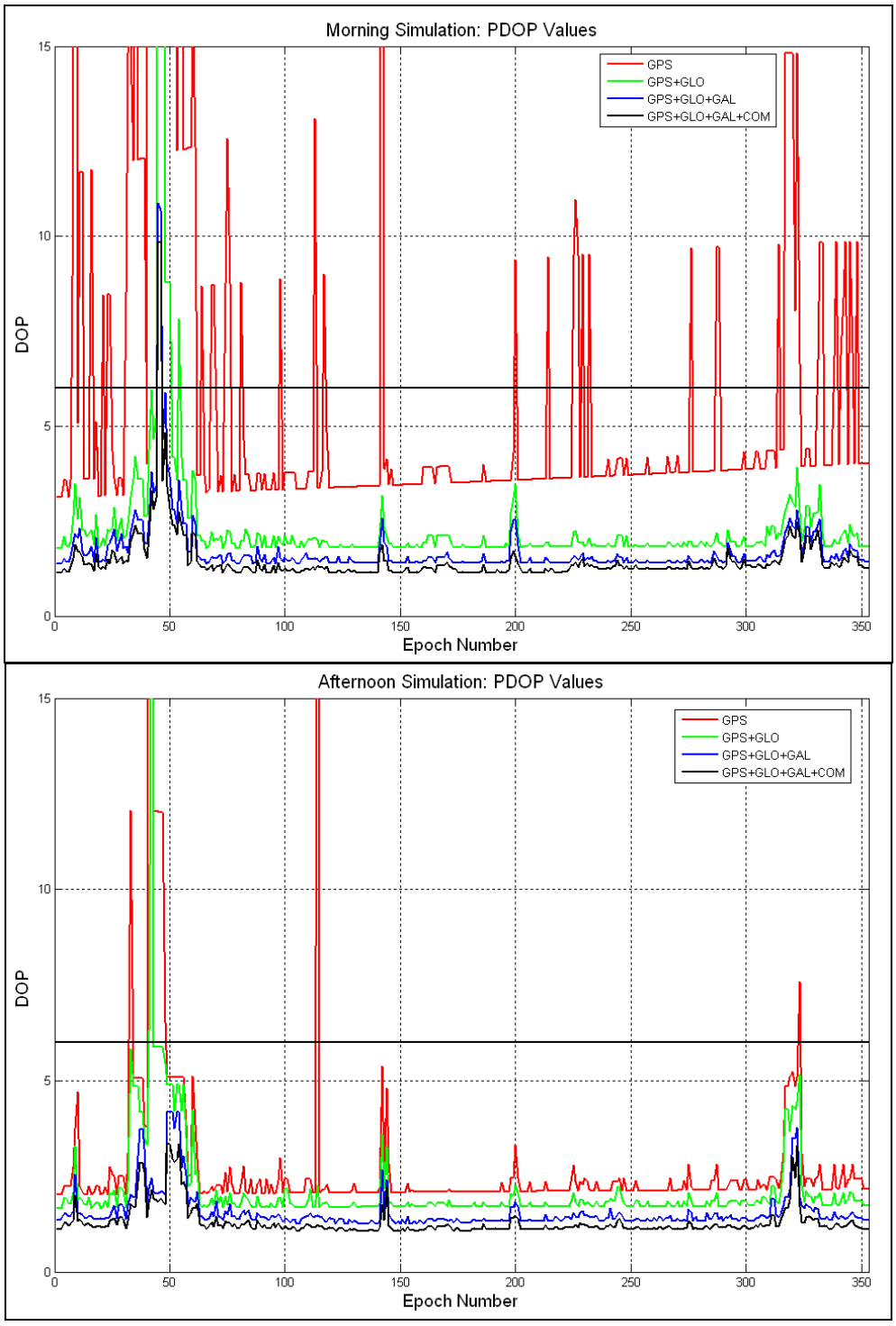

Figure 5.13: Variation of PDOP of Morning simulation (top) and Afternoon simulation (bottom)

Using the combined criteria of five or more visible satellites and PDOP values of 6 or less, the simulation results showed that when using GPS only, 78% of the Morning epochs and 97% of the Afternoon epochs would be likely to provide a centimetre-level position. When GPS and GLONASS were simulated together, this increased to 98% of Morning epochs and 99% of Afternoon epochs. With the further

satellites of Galileo and COMPASS, this increased further to 99% of the Morning epochs and 100% of the Afternoon epochs.

5.4 Summary

This Chapter introduced some applications of the UCGS tool to assess satellite visibility in two different environments, using two different datasets of 3D models. The purpose of simulating present and future GNSS constellations is to investigate the advantages given by using the additional satellites to positioning in urban canyons. Building height data, for the area that is being investigated, is therefore required to be able to model any obstructions that might block the GNSS signals. The first GNSS simulation was carried out using a 3D model of the University of Nottingham's Campus as described in the previous Chapter. A second simulation was then carried out using 1.0m resolution LiDAR data of Upton-upon-Severn.

The results of the Campus simulations gave evidence that using more than one constellation will significantly increase the availability of satellites in urban environments. However, although the minimum number of satellites when using four constellations was found to be equal to eight and nine satellites, a PDOP value of less than 6 was not guaranteed all the time. As a result, position availability using the criteria of five or more satellites with PDOP value of 6 or less for centimetre level, is not guaranteed 100% of the time.

The Upton simulation, as an example of a typical British town, gives evidence that in the future, with four constellations, it could be possible to achieve 99% positioning availability in such areas using the criteria of five or more satellites with PDOP values of 6 or less.

In addition to DOP, it should also be noted that the UCGS Tool does not consider the effects that multipath in 'urban canyons' might have on the quality of the GNSS positions. Modelling multipath within UCGS would require a great programming effort, but this Chapter has shown that PDOP is still the over-riding issue, even with four constellations.

Chapter 6: GNSS and INS Integration

6.1 Introduction

As discussed in the previous two Chapters, even when using a combination of four GNSS constellations, it is not guaranteed that centimetre-level positioning will be achievable 100% of the time in built-up areas. Furthermore, in areas where it is not possible to pick up directly GNSS signals such as under bridges or inside tunnels, a GNSS only solution would fail and in urban canyons there is also the issue of multipath, which can lead to available but degraded positions. For all of these reasons, the possible use of GNSS integrated with another system, such as an Inertial Navigation System (INS) is of great interest.

This Chapter introduces INS, discusses INS drift and alignment (both static and dynamic) and introduces different GNSS/INS integration strategies. These include the four most common approaches that are used for integration: uncoupled, loosely coupled, tightly coupled and deep/ultra tightly coupled. The Chapter then goes on to discuss the limitations of previous research before introducing the Multiple Step Integration Technique (MSIT), developed by the author as a methodology for GNSS/INS data collection and processing. Finally, the results from three sets of GPS and INS data, collected along the University of Nottingham's Campus trial route are discussed and analysed in great detail.

6.2 Inertial Navigation System (INS)

An INS is a self-contained navigation system that primarily estimates position, velocity and attitude over a short period of time (i.e. output rates of 100 Hz or higher) [Titterton and Weston, 2004]. An INS is a dead reckoning form of navigation that requires an initial starting position, velocity and attitude in order to navigate. The theory of inertial navigation is based on the application of Newton's laws of motion, in particular Newton's first and second laws [Farrell and Barth, 1999]. Since the

measuring device (i.e. an accelerometer) has a known mass (m), Newton's second law can be applied to determine the acceleration (a) as:

$$a=F/m$$

The measured force (F) of a moving vehicle with respect to an inertial frame can be obtained as a linear combination of the linear acceleration of the system and gravitational acceleration (g). When the gravitational acceleration is known, usually from gravity models, the linear acceleration can be calculated from the sensed force. These measurements are integrated to provide velocity followed by a second integration to provide position [Farrell and Barth, 1999].

The system's inertial frame measures the accelerations and the angular velocities by using an Inertial Measurement Unit (IMU). A typical IMU is made up of a group of six inertial sensors, namely, three linear accelerometers (measuring acceleration) and three gyros (measuring angular velocities). The gyros usually measure the angular rate rotation in reference to one or more axes (Pitch (X), Roll (Y) and Yaw (Z)). The rate measurements are integrated with respect to time to compute the attitude information. Some types of accelerometers are: Vibrating Beam (VBA), Quartz Resonating (QRA) and Pendulous Mass (PMA). Some types of gyros are: Dynamically tuned (DTG), Fibre Optic (FOG) and Ring laser (RLG). An INS also contains a computer system to perform the position calculations.

In general, there are two different types of INS in use: gimballed, or stabilized, systems and strapdown systems. The primary difference between these systems is the environment in which the accelerometer and the gyro must function [Chatfield and American Institute of Aeronautics and Astronautics., 1997]. Early INS used gyros and accelerometers mounted on a gimballed platform held steady by servomotors that respond to gyro inputs [Bletsos, 2004] (Figure 6.1). These gyros and accelerometers are isolated from the rotations of the vehicle so that they can be maintained in a specific orientation with respect to the earth or inertial space. The stabilized INS physically represents the inertial reference frame which simplifies the position and velocity computations.

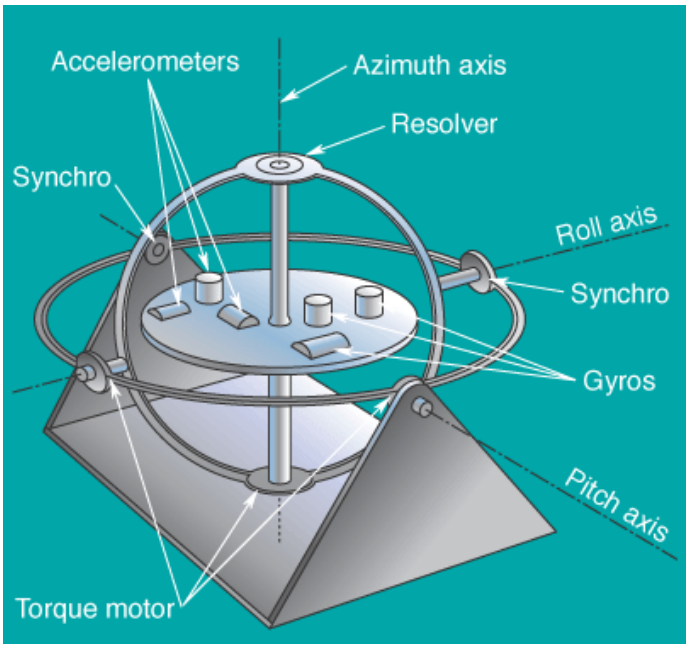

Figure 6.1: Gimballed Inertial Platform [Bletsos, 2004]

A Strapdown INS uses fixed gyros and accelerometers strapped down to the frame/circuitry of the equipment. The angular motion is continuously measured using the rate sensors, while the accelerometers follow the motion of the vehicle. The position and attitude information are integrated from the raw IMU measurements of acceleration and rate measurements. This integration is often termed the inertial mechanization [Kayton and Fried, 1997; Titterton and Weston, 2004]. Examples of strapdown INS are Micro Electro Mechanical Systems sensors (MEMS). In recent times they have become very widely used [Titterton and Weston, 2004]. MEMS can be found to be very small in size (sub-millimetre scale), low weight, low power consumption and can be considered as an inexpensive sensor [Osiander et al., 2006; Grewal et al., 2007]. MEMS accelerometers and gyros have various applications such as virtual reality, robotics, and machine control and monitoring, and are increasingly being used in navigation applications. However, they generally provide only short-term navigation capability due to large sensor errors that require continuous calibration. To estimate these sensor errors, GNSS measurements are usually used.

One of the most accurate and expensive types of Strapdown INS is the Ring Laser Gyro (RLG) INS (e.g. the Honeywell CIMU used in this research). One RLG is a triangle shaped device with a silicone body, three narrow tubes filled with a Helium-Neon Halogen mixture and a high voltage (about 1Kv) applied. In addition, Mirrors

in each corner are used to reflect the lasers around the unit's body. A cathode and two anodes are used to excite the gas and produce a light beam, which is split and forced to travel in opposite directions (Figure 6.2 (left)) [King, 1998]. Figure 6.2 (right) shows the FIN3110 instrument cluster, the heart of the system, which consists of three gyros and three accelerometers mounted in a mechanical frame designed to mitigate the effects of vibration, shock, thermal transients and other environmental features that can make life difficult for precision instruments [King, 1998].

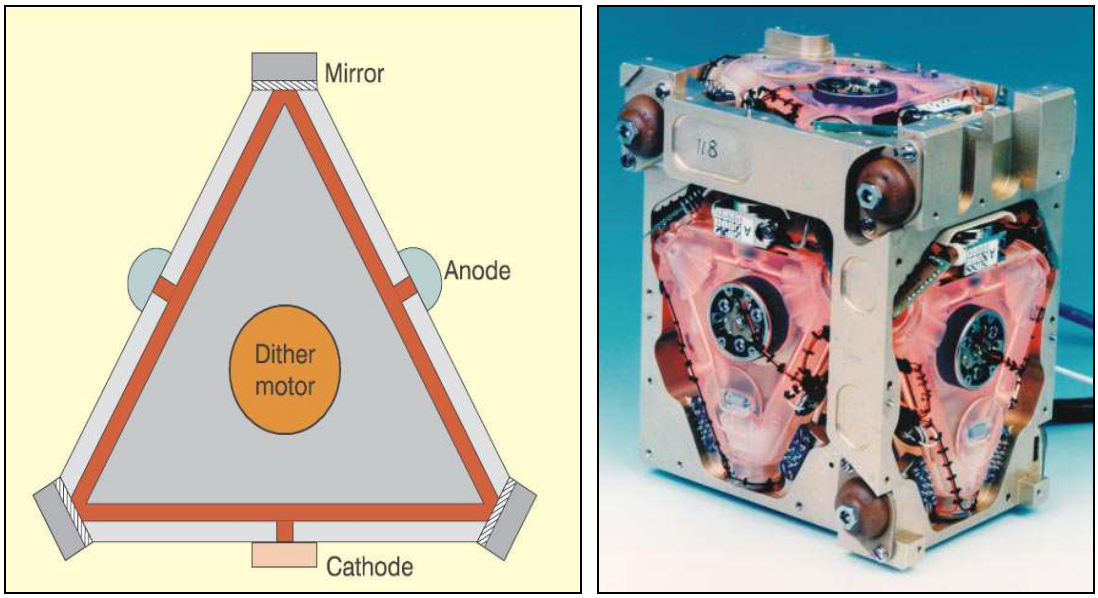

Figure 6.2: Ring Laser Gyro Schematic (left) and FIN3110 instrument cluster (right) [King, 1998]

When the IMU is stationary, the two beam pulses have the same frequency and come together at the same time [Chatfield and American Institute of Aeronautics and Astronautics., 1997]. As the unit is rotating the pulses of the split beam come together at slightly different times (because the distances travelled are slightly different) which results in a Frequency shift. The frequency of the beam can be measured and then used to determine the rotation rate of the gyro. The ring laser gyro INS combines high accuracy, low power requirements, small size and light weight with an instant alignment capability. In addition, because there are no moving parts involved, the ring laser gyros INS generally has a very high serviceability rate.

6.3 INS Drift

The problem with IMUs is that the error from sensors (noise, bias, scale factors, temperature sensitivity etc.) results in a drift of the position solution over time [Farrell et al., 2000]. The gyro bias appears as angular drift after integration and increases linearly over time. Furthermore, the errors in the accelerometers also increase linearly. After double integration, to obtain position, the sensor bias gives rise to a positional drift error raised to the power of 2. Although the error can be small, it increases rapidly when integrated twice over long periods of time [Groves, 2008]. The noise in the system is integrated along with the actual signal. This noise starts to accumulate and shows up as an ever increasing drift. This is not a serious problem if the IMU is used for a very short time (this time period is dependant on the quality of the IMU, although less than 1 minute is typical).

To overcome the INS drift, other sensors, such as odometers, speedometers, compasses or GNSS, can be integrated with the IMU to provide additional information for speed, heading and position. By using one or more of these sensors to augment the IMU, the performance of the system will be improved. GNSS can be used for real-time calibration of the INS using latitude and longitudinal coordinates. GNSS and INS are ideal for integration, as their error dynamics are totally different and uncorrelated [Kaplan and Hegarty, 2006]. GNSS/INS integration strategies are explained in section 6.5.

6.4 INS Alignment

The performance of an INS is governed by the accuracy of the initial alignment of the INS sensors. The alignment is the process of determining the orientation of the axes of an INS with respect to the reference/computational axis [Titterton and Weston, 2004]. It is also necessary to initialise the velocity and position as part of the alignment process. In an integrated system, position and velocity can be initialised using GNSS. Alignment of an INS is usually obtained in a static or, with aid of GNSS, a dynamic environment [Hofmann-Wellenhof et al., 2003]. In strapdown INS (SDINS), the alignment determines the transformation matrix relating a body frame (*b*-frame) to a navigation frame in the local level frame [Titterton and Weston, 2004].

Usually, this process is implemented using a Kalman filter that estimates the INS velocity and alignment errors.

6.4.1 Static Alignment

In static alignment, an INS is left stationary over a point (usually a point with known coordinates or on a point located in an open sky area if integrated with GNSS) for a period of time. For some high end IMU, static alignment is obtained in two steps: an initial coarse alignment followed by a fine alignment. A static INS is able to coarsely determine its own alignment by using directions that are defined by the physics of the earth (the direction of local gravity vector and the direction of the earth rotation axis) [Hofmann-Wellenhof et al., 2003]. In the coarse alignment, the time interval used for averaging is selected based on the noise of the sensor. The coarse estimates of the sensor biases are then used in the integration Kalman filter for the fine alignment. Because the system was static during the alignment process, the zero velocity and averaged GNSS position were applied in the fine alignment process. The raw inertial measurements are combined using Zero Velocity Update Points (ZUPT) with knowledge of the way that the inertial errors develop over time . This is usually achieved using a Kalman filter estimating the error states in the system.

6.4.2 Dynamic Alignment

For situations where a static alignment is impossible or impractical (such as in space or at sea), the alignment is performed using a dynamic alignment. This is usually achieved by integrating INS with another navigation sensor, usually with a GNSS, and using a Kalman filter [Hofmann-Wellenhof et al., 2003]. The dynamic alignment is also used after a static initialization to reduce the drift of the inertial sensor over time.

6.5 GNSS/INS Integration Strategies

GNSS/INS integration involves combining the outputs of GNSS and INS systems to obtain a single solution. The integration of GNSS and INS provides a survey system

that exhibits superior performance in comparison with either GNSS or INS alone. In addition, positioning availability can be improved because during GNSS outages (areas where the GNSS positions are unavailable) the navigation solution can be calculated by the INS data only. In such integration, GNSS can bound IMU time dependent errors and calibrate IMU errors, while, INS can bridge gaps in GNSS data. In general, there are four common approaches used for such integration: uncoupled, loosely coupled, tightly coupled and deep/ultra tightly coupled [Jekeli, 2000]. This section will focus on describing the loose coupled integration, since it was the more considered in this research. Similarly, the tight coupled integration will also be considered since it is widely used and researched.

A Kalman filter is the most commonly used method for integrating GNSS and INS measurements which makes use of the stochastic and dynamic properties of the GNSS and INS systems [Howell and Tang, 1994; Groves, 2008]. Other integration algorithms such as neural networks can be used (see, for example, Chiang et al. [2003] and El-Rabbany and El-Diasty [2004]). The use of Zero velocity measurements and a Kalman filter smoothing algorithm can significantly reduce the errors across GNSS outages [Hide and Moore, 2004]. However, smoothing is a post-processing algorithm that is used when all of the data are available.

6.5.1 Uncoupled Integration

In uncoupled integration, if GNSS data is available it is used to compute the system output and to initialize/update the INS. The INS output is then used in the absence of GNSS. This system suffers from large drift if the GNSS data is unavailable for a long period of time. More details can be found in [Jekeli, 2000].

6.5.2 Loosely Coupled Integration

The GNSS and INS sensors can be integrated using the loosely coupled integration algorithm where a navigation solution, position and velocity from a GNSS receiver is used to correct the INS errors [Farrell et al., 2000]. This algorithm is sometimes referred to as decentralised filtering since two Kalman filters are used: one to process

the GNSS measurements, and a second to perform the integration (Figure 6.3). This approach is generally used due to the simple implementation requirements and redundancy [Groves, 2008].

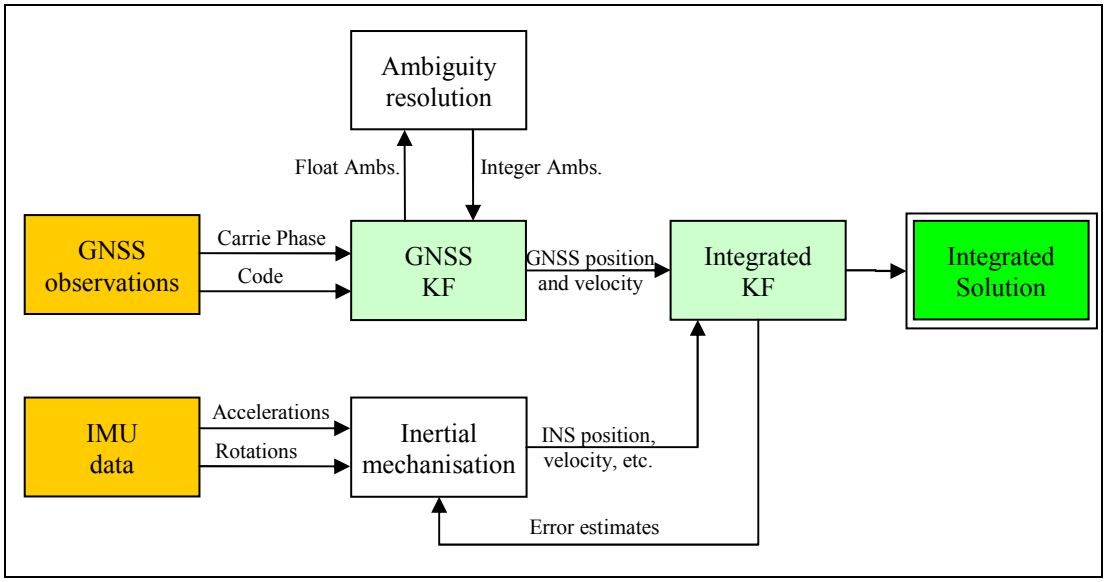

Figure 6.3: GNSS/INS loosely coupled integration flowchart

The IMU raw measurements of acceleration and rate, are converted using the strapdown navigation algorithms to estimates of position, velocity and attitude. This is often termed the inertial mechanization. Similarly, the GNSS measurements are processed to form the differenced GNSS measurements. The GNSS measurements are used to estimate position and velocity in a separate Kalman filter. The integration filter uses the difference between the position and velocity of the GNSS and INS solutions as measurements for an integration filter. The integration filter then estimates the error in the INS and feeds this back to the mechanization equations.

6.5.3 Tightly Coupled Integration

For applications where there is a restricted view of the sky such as in urban environments, it is clear that a significant improvement can be made by combining the GNSS and INS systems at the measurement level. Such integration is referred to as tightly coupled integration and uses a centralised filtering algorithm, and a single Kalman filter, to integrate the GNSS and INS measurement as shown in Figure 6.4.

In this sense, the GNSS raw data can continue to be used in the integrated solution even if the number of satellites drops below four [Cramer, 1997].

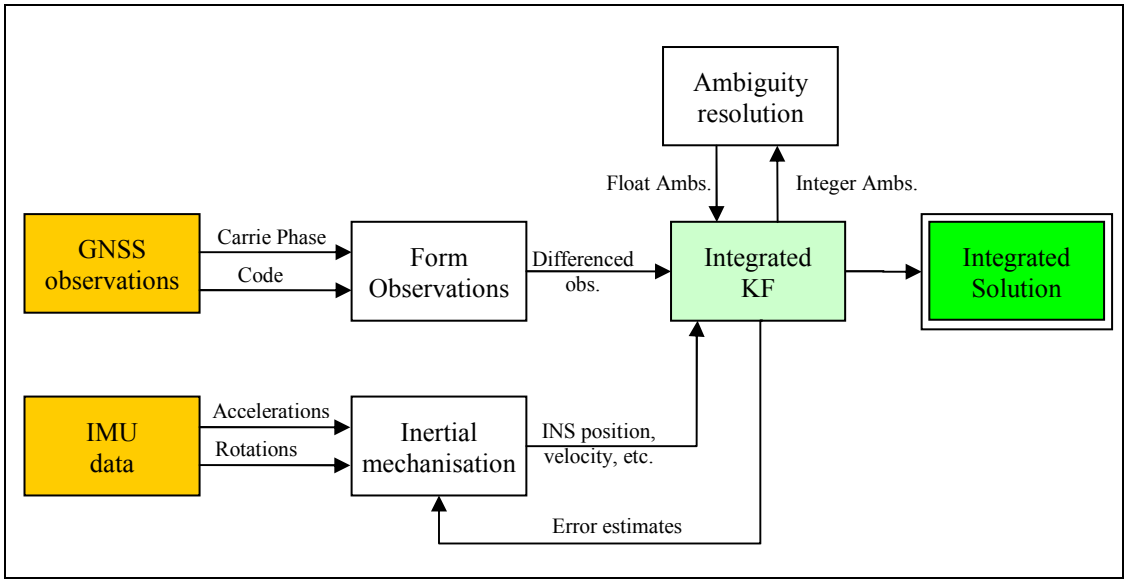

Figure 6.4: GNSS/INS tightly coupled integration flowchart

When using the tight coupled technique, the IMU raw data are converted to position, velocity and attitude measurements using the INS mechanization algorithms. The position and velocity measurements are then used to form predicted range measurements (corrected for the lever arm offset from the GNSS antenna to the INS) to each of the satellites [Farrell et al., 2000]. These ranges are then used with the differenced GNSS measurements to estimate the INS errors using a single integration filter. The errors estimated by the integration filter are fed back to the mechanization equations. The integration filter will also be used to estimate the carrier phase ambiguities if carrier phase measurements are being used.

6.5.4 Deep / Ultra Tightly Coupled Integration

The deep/ultra tightly coupled integration is done at the single correlation level, e.g. the INS measurements can be used to aid the carrier tracking loops in the GNSS receiver. The INS aiding can reduce the GNSS tracking loop bandwidth or reduce the integer ambiguity search volume with attitude determination systems to achieve optimal performance. More details about this type of integration can be found in [Groves, 2008].

6.6 Limitation of Previous Research

GNSS and INS integration has been researched for such a long time, and in so many ways, that it is difficult to summarize all the possible methods and results. In general, most of the previous researches have compared results achieved from a loosely coupled and tightly coupled integration. In addition, they have focussed on their studies on the accuracy of the integrated solution in the GPS outage, when using a GPS and a low cost MEMS INS system (see for example, Hide et al. [2006], Li et al. [2006] and El-Sheimy [2008]).

The major advantage of a loosely coupled system is its design simplicity relative to a tightly coupled system [Groves, 2008]. In addition, high quality position can only be chosen for updating, which ensures no GNSS position errors will affect the combined GNSS/INS position. Tightly coupled integration based on centralised Kalman filter is preferred [Gautier and Parkinson, 2003] and proved from previous researches (see, for example, [Hide and Moore, 2004]) to have several theoretic advantages over a loosely coupled system. The main advantage is that any number of GNSS measurements may be used in the filter to help bind INS error growth. The disadvantage to such a system is the complexity of the design and the ability to make such a system functional in practice.

Using a low cost inertial unit, motion sensor, integrated with DGPS and Doppler measurements, Salychev et al. [2000] reported meter-level accuracy for data outages of a few seconds. Centimetre-level accuracy over one second was reported in Farrell et al. [2000] using a real-time carrier phase DGPS aided inertial navigation system. Using GNSS/INS integration with the iMAR-FSAS IMU, Kennedy et al. [2006] achieved respectively about three decimetres and better than a decimetre in horizontal and vertical position accuracy over 100 seconds GPS outages. Similarly, using GPS tightly integrated with low cost IMU, Hide and Moore [2004] reported a maximum error of meter-level position accuracy over 180 second GPS outages with 3 satellites. In urban canyon environments, Hide et al. [2006] reported a sub-meter level accuracy for smoothed tightly integrated positions (post-processed positions) using a GPS and a low cost IMU.

Generally, GNSS and high precision IMU, such as navigation grade CIMU from Honeywell, are widely used for determining aircraft position and rotation angles for geo-referencing purposes of photogrammetry. In addition, previous research such as Hide et al. [2006] and Kennedy et al. [2006] used a GPS integrated with CIMU to provide a reference solution to compute the errors of the other sensors, i.e. errors of GPS integrated with low cost INS. In this research, GNSS and the high resolution INS will be used for the purpose of achieving a high level of positioning accuracy (few centimetres) in urban canyon environments, where GNSS outages of several minutes could occur. For such applications, position accuracy of only about 0.65m RMSE was achieved during a GPS outage of about 20 minutes in a preliminary GPS and INS integration conducted by Taha et al. [2006]. To achieve centimetre-level of accuracy, in such long outages, a Multiple Steps Integration Technique (MSIT) has been developed by the author as a methodology for GNSS/INS data collection and processing.

6.7 Multiple Steps Integration Technique (MSIT)

MSIT (illustrated in flowchart in Figure 6.5) involves both data collection and data processing. When collecting GPS and INS data, it is necessary to monitor the GPS availability. When GPS positions are available, it is possible to collect kinematic positions. However, when working in outages, a stop and go technique to initialize ZUPT must be employed.

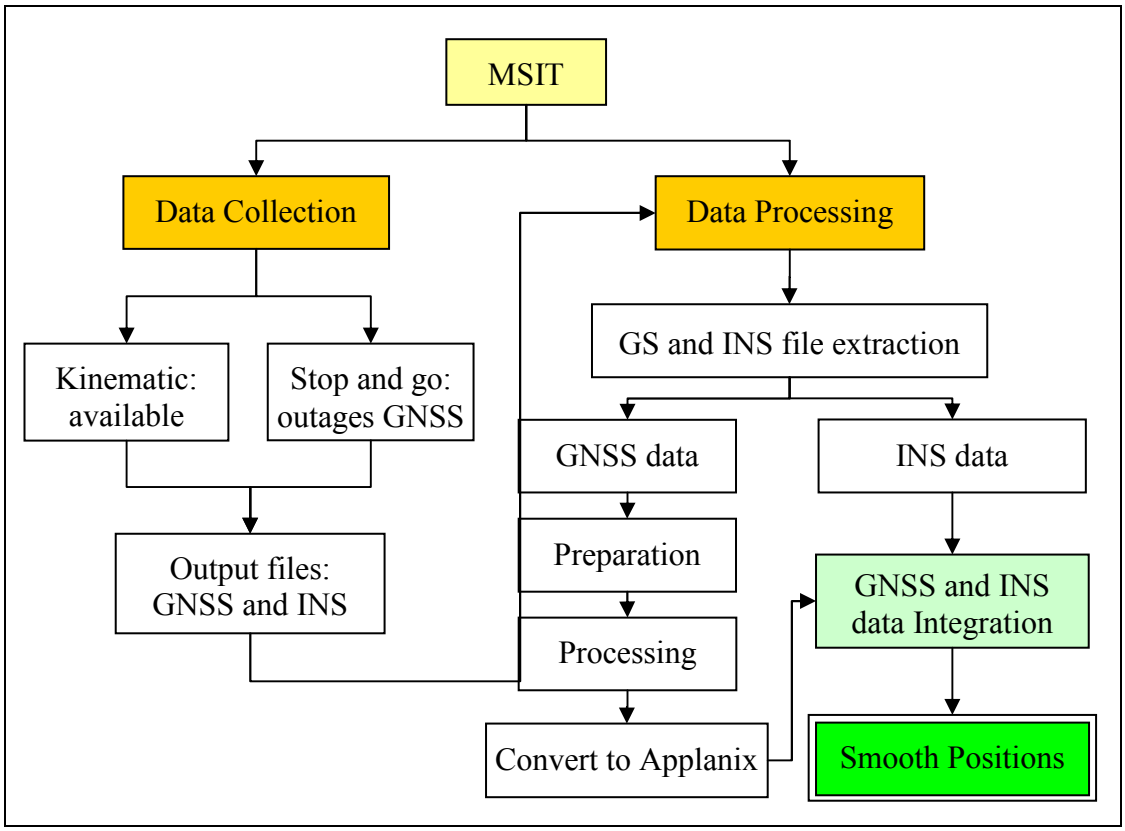

Figure 6.5: Multiple Steps Integration Technique flowchart

GNSS/INS data should be post-processed in multiple steps to produce integrated smoothed positions as follows:

- *Step 1*: GNSS and INS data preparation. Using the POSPac software, the GPS/INS file is extracted to produce a GPS observation file and a raw IMU data file. The GPS file is then converted to RINEX format using PosGPS. The RINEX observation file is modified by adding headers in specific location in this file to distinguish between epochs on which the equipment was either stopped or moving. LGO2Applanix Manager software has been developed by the author for this purpose Figure 6.6.

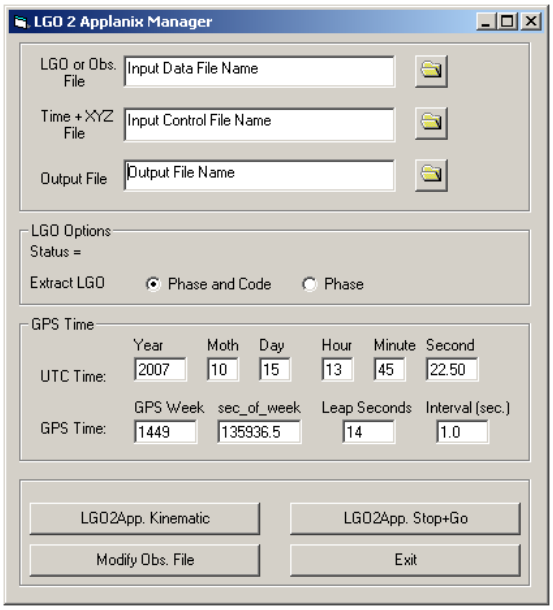

Figure 6.6: LGO2Applanix Manager menu

- *Step 2*: GPS data post processing. A Kalman filter processing for the GPS data can be carried out within PosGPS software (this technique will be called a 'one step technique' or OST). However in MSIT, the modified RINEX file is post processed using the LGO software.
- *Step 3*: The GPS Phase Solutions are now converted to a Binary Format. The phase and code, or the phase, solutions from LGO output can be converted to Applanix POSPac binary format using LGO2App software written by the author from either kinematic or stop and go files. However, only the phase solutions are required to be converted to Applanix format for MSIT.
- *Step 4*: GPS and INS data integration. GPS and INS data can be loosely coupled using Applanix POSPac software (version 4.2) to produce smoothed positions. This integration is mainly dependant on using the GPS positions calculated independently using different software, e.g. LGO. So the GPS KF part in the loose integration flowchart in Figure 6.3 is replaced with an independent GPS position. MSIT is also based on using ZUPT which assists in reducing the INS drift in the GPS outages.

Using this Multiple Steps Integration Technique (MSIT), a significant improvement has been noticed in the results when compared with the conventional loose integration (as in OST). More details about the results can be found in the following sections.

6.8 GNSS and INS Tests

Initially, three sets of GNSS and INS data were collected along the University of Nottingham's Campus trial route. Different strategies were used to process this data set to investigate any improvements made by using the MSIT.

6.8.1 GNSS/INS Data Collection

The GNSS/INS data were collected using an Applanix POSRS system fixed on a platform (Figure 6.7).

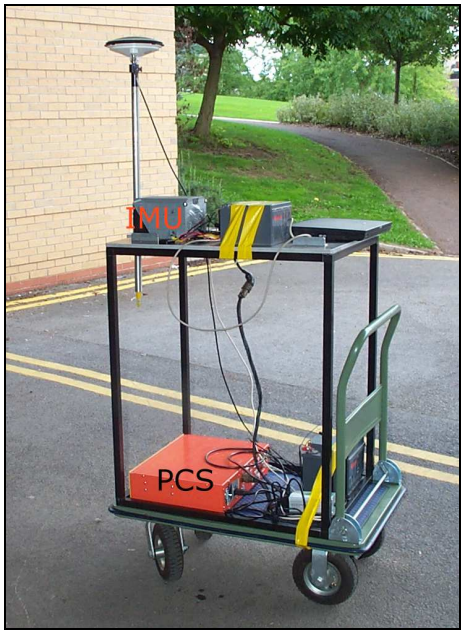

Figure 6.7: Applanix POSRS GPS and INS

The Applanix POSRS is a high performance GPS and INS integrated system that uses a Novatel OEM4 GPS receiver integrated with a high quality navigation grade Honeywell CIMU, which can cost the user over £100,000. The key performance specifications for the IMU are given in Table 6.1 [Hide et al., 2006].

Table 6.1: Honeywell CIMU specification

Error source	Accel (ms^{-2})	Gyro (°/s)
Bias	3×10^{-6}	$<1\times10^{-7}$
Noise	N/A	$<1\times10^{-7}$
Scale Factor	100 ppm	10 ppm
Saturation	±300	N/A

The lever arm between the GPS antenna and a reference point (typically on the ground) and between the INS and that reference point should be measured, either using a steel tape (as in this case) or total station.

Before moving the platform along the trial route and collecting the GPS and IMU data, it is necessary to collect GPS and IMU data in static mode, for about 20 minutes preferably in an open sky area. This data is required for initialization in order to define the INS alignment (static alignment). In the first data set, GNSS/INS data were collected on 7th September 2006 in GPS week 1391, along the trial route stopping for at least about 60 seconds on each of the testing points until closing on the STOP point. However in the second and third data sets, GNSS/INS data were collected on two different days, on 7th and 9th November 2007 (in GPS week 1452) at different times (the second set was in the morning while the third was in the afternoon) along the trial route stopping for at about 120 seconds on each of the testing points. The stopping time was noted down during the test and all the data was collected and stored in the POSRS system.

6.8.2 GNSS/INS Data Processing

GPS/INS data were post-processed using two different methods: the first processing we call the 'One Step Technique' (OST) and the second one is the MSIT. The only difference between the two techniques is in the post-processing of the GPS data. In the MSIT, the GPS data is post-processed following the strategy described previously in this chapter in section 6.7.

For both techniques OST and MSIT, the stored raw GPS and IMU data were extracted using Extract POS Data in Applanix POSPac software. The data extraction allows the detecting of potential data problems, such as gaps in the IMU data. According to [Grejner-Brzezinska and Toth, 2004]:

'*Continuity of IMU data is essential. An IMU data gap of more than one or two samples results in a sudden change in navigation accuracy that is inconsistent with the Kalman filter error model of inertial navigator errors. The inertial navigation*

solution becomes inconsistent with the aiding sensor data and measurement rejections can result. IMU data gaps are almost always caused by the IMU data acquisition system. If continuous measurement rejections appear to begin after a period of seemingly successful integration, then one or more IMU data gaps may be the cause.'

The collected IMU data had one gap of 0.01 second, eight gaps of an average of 0.005 and ten gaps an average of 0.005 second in the first, second and third datasets respectively. However, such gaps are negligible since the rotation and acceleration are unlikely to vary much in this time and this is very close to the IMU data rate.

In the OST, the GPS and INS data were post processed using the Applanix POSPac software (version 4.2). This software uses the loosely coupled GNSS and INS algorithms to produce smoothed positions. As mentioned before, the loosely coupled system uses the GPS calculated position to aid the INS; therefore RTK GPS positions are first calculated. Within POSPac this is performed using the PosGPS software. According to [Waypoint-Consulting-Inc., 2003]:

'*PosGPS is a full-featured kinematic and static GNSS post-processing package using Waypoint's proprietary GNSS processing engine*'.

PosGPS software allows loading configuration setting from Pre-loaded Profiles (e.g. Airborne, Low Cost, Tree Cover, etc. More information can be found in Waypoint-Consulting-Inc. [2003]). Since the data was collected in urban environments, the 'Tree Cover' profile was selected. Additionally, it provides several processing features allowing the user to choose the options best suited to the application.

In general, the default options were used; however, the elevation mask was modified to 10º and the datum to WGS84. Also the option to reject any GPS measurements worse than Quality 3 was implemented. In PosGPS, the quality number can be between 1 and 6 depending on the solution calculated. Table 6.2 summarizes the quality number description: colour, meaning and accuracies of these quality numbers (the accuracies given are only guidelines) [Waypoint-Consulting-Inc., 2003].

Table 6.2: PosGPS Quality Number Description

Quality	**Colour**	**Meaning**	**Accuracy** (m)
1 (Q1)	Green	Fixed Integer	0.00 – 0.15
2 (Q2)	Cyan	Converged Float or Noisy Fixed Integer	0.05 – 0.40
3 (Q3)	Blue	Converging Float	0.20 – 1.00
4 (Q4)	Purple	Converging Float	0.50 – 2.00
5 (Q5)	Magenta	DGPS	1.00 – 5.00
6 (Q6)	Red	DGPS	2.00 – 10.00
Unprocessed	Grey	Has not been processed	N/A

Forward and reverse GPS solutions can be combined to produce the final GPS position solution (therefore the described results are achieved using post processing only and cannot be recreated in real-time).

After post-processing the GPS data using PosGPS (as OST) or using the strategy described in MSIT, both the GPS and IMU data were post-processed using the POSProc part of POSPac. The automatic ZUPT technique was also used to detect when the IMU is static. ZUPTs are used to mitigate the IMU drift when stationary which results in an improved position solution. The lever arm between reference point and IMU and the reference point and GPS were stored in the Subsystems Setup. Besides, Kalman filter measurement rejections in the Inertial Integrated Navigation (IIN) setup were modified from 50 to 300. This is because the filter was terminated and there were no integrated solution. Other processing parameters were used as in the default values (for detail see [Applanix-Corporation, 2005]).

In total, seven tests were performed on the GPS/INS data (described in Table 6.3). The first three tests were carried out on the first GPS /INS data set using different processing techniques. Besides, the fourth and the fifth tests were performed on the second GPS /INS data set while the sixth and the seventh tests were performed on the third GPS /INS data set.

Table 6.3: GNSS/INS tests description

Test ID	Description	Test Time
Test1	Using OST with GNSS data of quality Q1 to Q3 – Data set 1	Mixed
Test2	Using OST with GNSS data of quality Q1 to Q2 – Data set 1	Mixed
Test3	Using MSIT with GNSS data of Phase solution – Data set 1	Mixed
Test4	Using OST with GNSS data of quality Q1 to Q2 – Data set 2	Morning
Test5	Using MSIT with GNSS data of Phase solution – Data set 2	Morning
Test6	Using OST with GNSS data of quality Q1 to Q2 – Data set 3	Afternoon
Test7	Using MSIT with GNSS data of Phase solution – Data set 3	Afternoon

6.8.3 GNSS/INS Results and Analysis

The following sections present and analyse the GPS /INS tests and results. The first test is analysed alone, then the other tests analysed as a pair to make the comparison between the OST and the MSIT easier. The analysis includes the availability of the GPS only solution and the availability and accuracy of the GPS/INS integrated solution. It is worth mentioning that the accuracy of the GPS only solution will not be analysed, since the GPS antenna was not perpendicular on the testing points and would therefore need to be corrected for tilt before accurate analysis could be made.

6.8.3.1 Test1: Results and Analysis

Following the processing strategy described previously, the GPS positioning results from the combined solution called ‘Test1’ are shown in Figure 6.8.

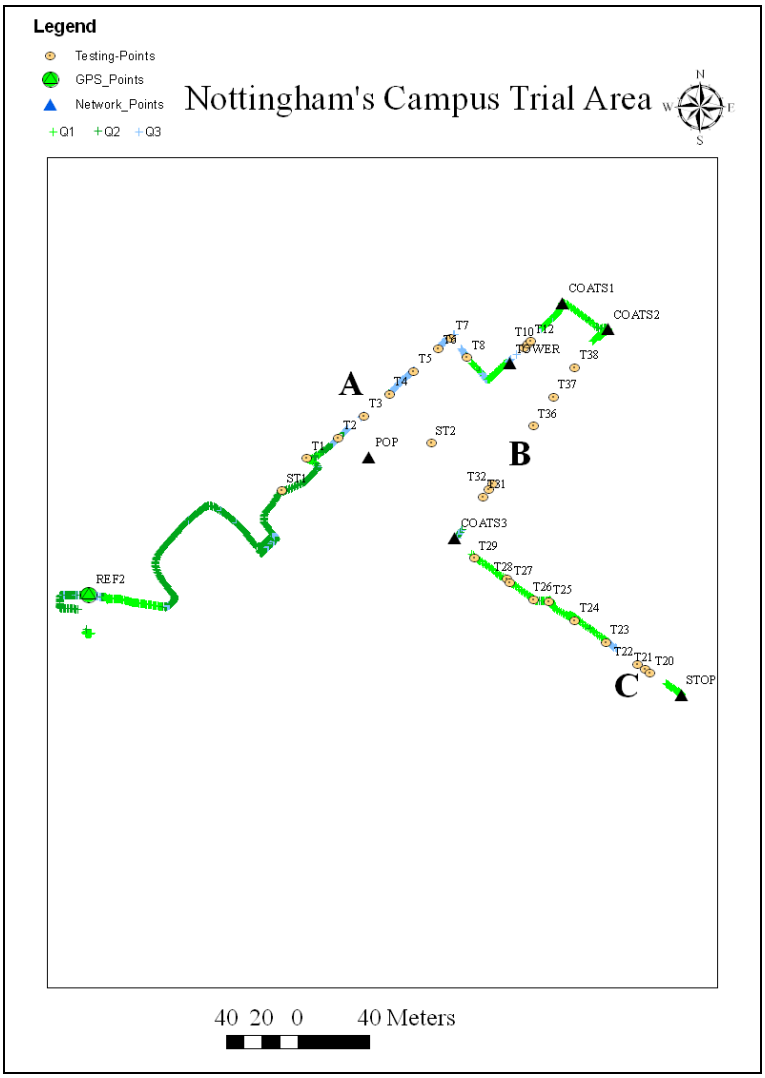

Figure 6.8: GPS only data processing results for Test1

From Figure 6.8, the different qualities (+Q1, +Q2 and +Q3) of GPS position solutions were calculated for the positions of the known points. Moreover, there are several areas with GPS outages, highlighted using the letters A, B and C. The length of time without any GPS positions yields a challenge when trying to solve for a position to centimetre level depending only on the IMU data.

The processing results from the GPS and INS combined solution data can be computed as a forward solution or a smoothed (forward and backward) solution. The forward solution can be calculated in real time. The main limitation of this solution is that large gaps occur where no GPS positions are available, resulting in a large drift away from the truth as the position is only computed from the INS measurements. As mentioned before, the INS errors grow very fast over time, therefore when the data is

post-processed using the forward and backward (smoothed) solutions, the INS errors during the GPS gaps are minimised. For this reason, the smoothed solution results will be discussed herein. The smoothed solution in Test1 shows that a maximum uncertainty of about 0.28m was estimated for the X, Y coordinates and of about 0.26m for the Z coordinate (Figure 6.9). These uncertainties and other peak uncertainties in Figure 6.9 occurred in the areas with GPS outages (e.g. the maximum uncertainty took place on area B in Figure 6.8).

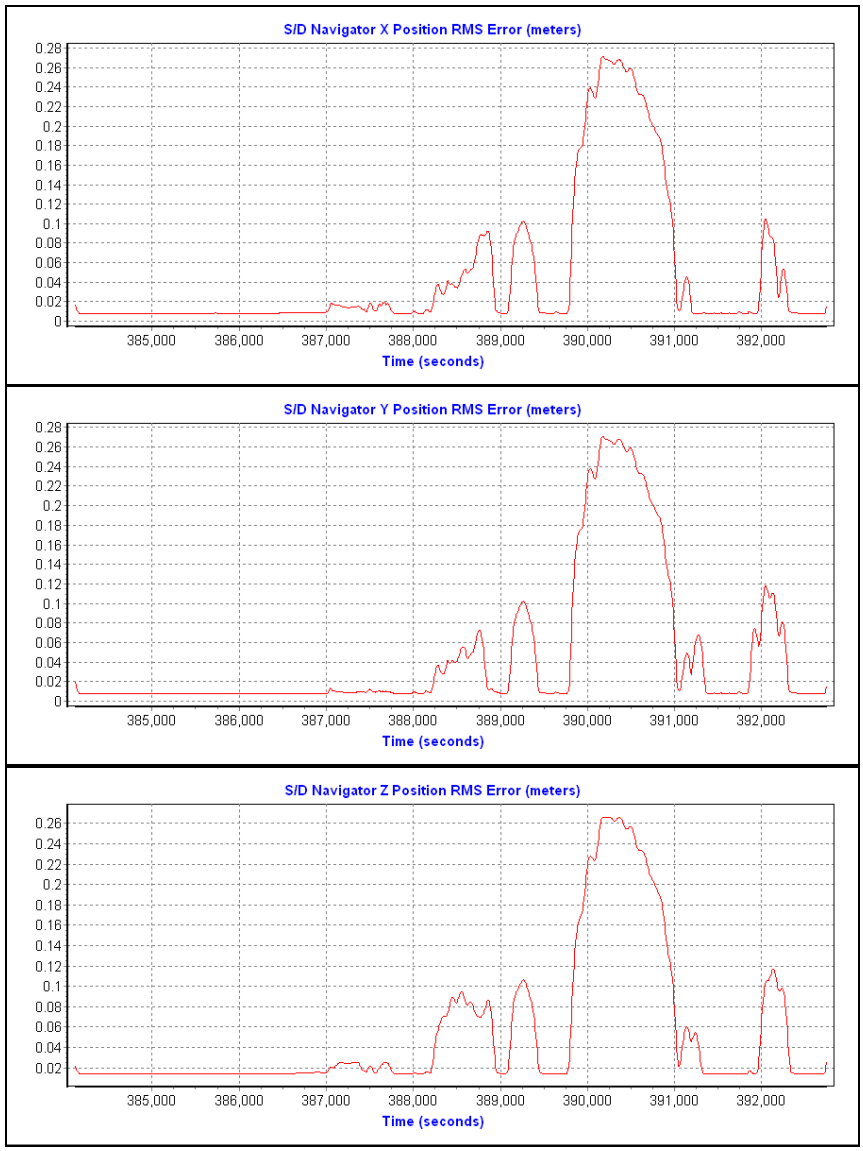

Figure 6.9: GPS position uncertainties X (top), Y (middle) and Z (bottom)

Integrated Inertial Navigation coordinates (WGS84 geographic coordinates) obtained from the smoothed solution were converted to National Grid (OSGB36) coordinates using Grid-InQuest version '6.0.8' software and are shown on an Ordnance Survey

MasterMap (Figure 6.10 left). The most difficult area in which to obtain GPS RTK positions was area B. Therefore in this area positions are reliant upon the measurements of the IMU only. A close up of this area is shown in (Figure 6.10 right).

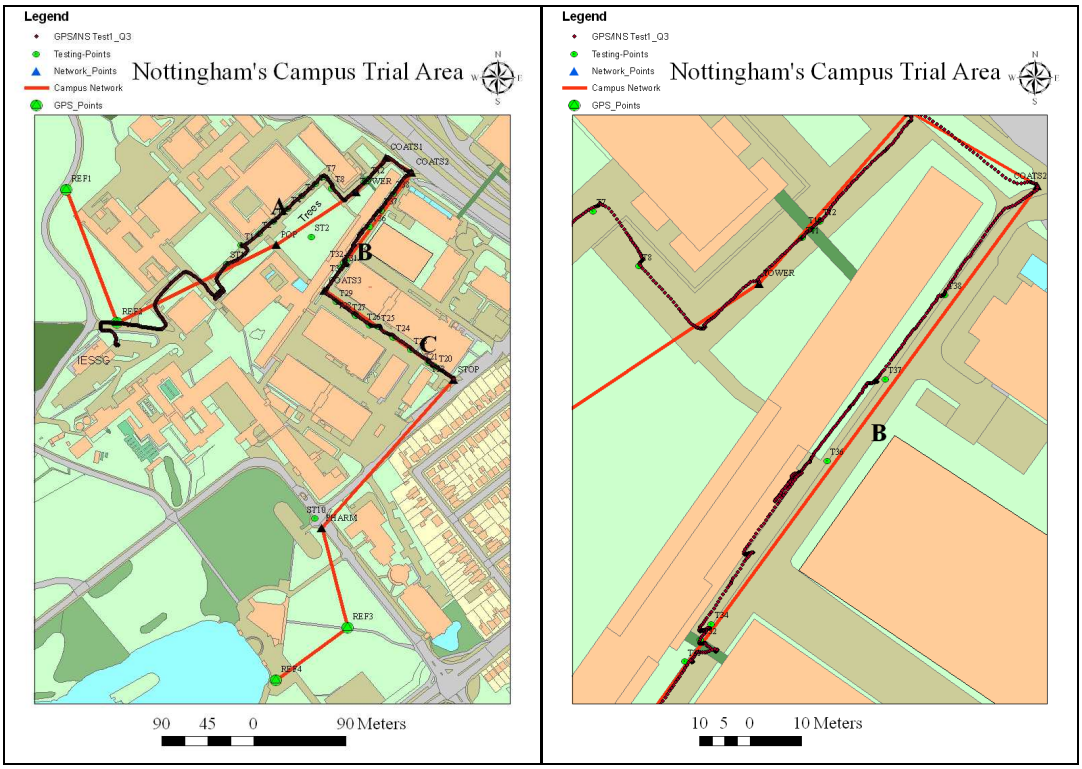

Figure 6.10: Test1: GPS and INS smoothed positions for the full route (left) and around area B (right) (Copyright © OS MasterMap)

From Figure 6.10, the GPS and INS integration solution fill the gaps in areas A, B, and C. This illustrates the advantages of the integration between the GPS and the INS which ensures high availability, in this case 100%, positioning along the trial route. However, the important factor about the position is to be accurate. For this purpose, the resultant grid coordinates were averaged for each of the testing points and compared with the 'truth' coordinates (Figure 6.11).

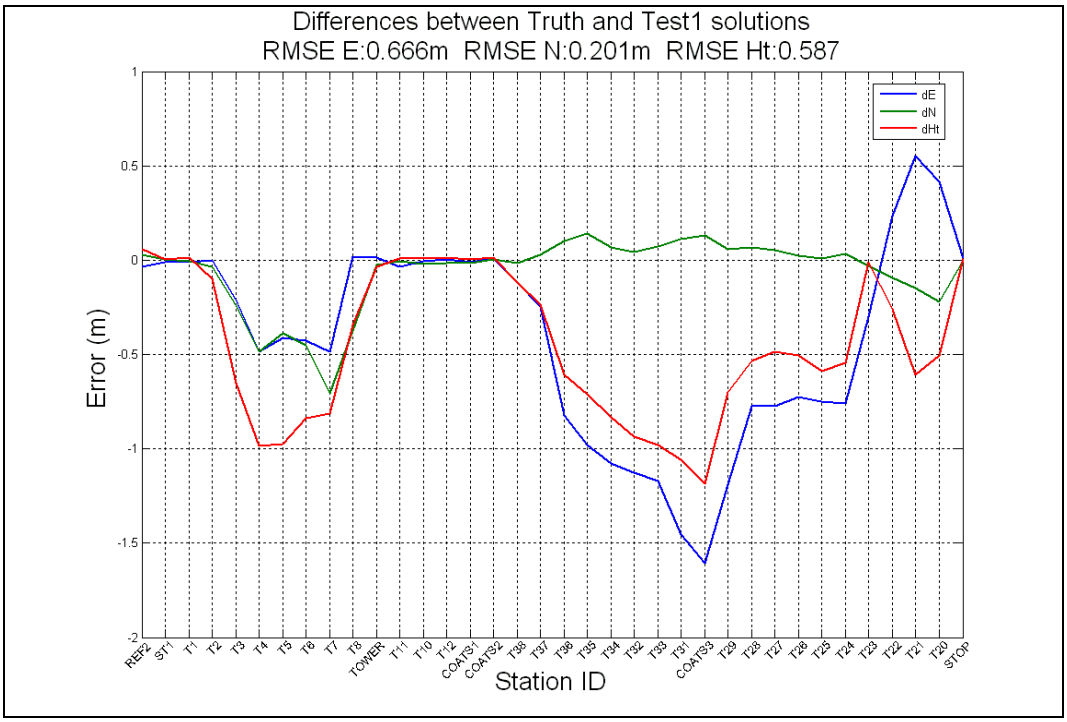

Figure 6.11: Test1: Differences between 'truth' and smoothed integrated coordinates for all points in Test1

From Figure 6.11, the points which have a small difference, when compared to the 'truth' coordinates, in the integrated solution are those which have a Q1 or Q2 GPS position available. The larger differences occurred at the points where there is no GPS available or the GPS position was only Q3. For further analysis, 6 points were considered and the differences between the 'truth' coordinates and the integrated coordinates as well as the GPS availability and quality are shown in Table 6.4.

Table 6.4: Differences between 'truth' coordinates and smoothed integrated coordinates for 6 points in Test1

'Truth' coordinates – Integrated coordinates				
Point ID	**dE** (m)	**dN** (m)	**dHt** (m)	**GPS Availability/Quality**
ST1	-0.009	0.004	0.006	Available GPS/+Q2
COATS2	0.009	0.004	0.016	Available GPS/Q1
COATS3	-1.607	0.129	-1.183	Available GPS/Q3
T7	-0.484	-0.703	-0.815	Available GPS/Q3
T36	-0.823	0.101	-0.609	570 sec. gap before point & 669 sec. after point
T10 (under bridge)	-0.007	-0.018	0.011	168 sec. before point & 171 sec. after point
Max. error/ Point ID	-1.607/ COATS3	-0.703/ T4	-1.183/ COATS3	Q1– Fixed Integer Q2– Stable Float Q3– Converging Float

From Table 6.4, it is clear that when a GPS solution with Q1 or Q2 is available, the integrated position is accurate to the centimetre level of accuracy, whereas the maximum error (1.607m in East, 0.703m in North and 1.183m in Ht) occurred for the points with a Q3 solution. Testing point T10 achieves high agreement between the GPS/INS integrated coordinates and the truth coordinates, even though it is located under the bridge. It is important to note that there was a GPS position with Q1 before and after T10 testing point. Furthermore, testing point T36, which is located approximately in the middle of a large GPS outage (about 20 minutes), was found to have better than a meter level of accuracy. This is because of the using of ZUPT technique which assists reducing the INS drift in the gap areas and hence increasing the final position accuracy.

6.8.3.2 Test2 & Test3: Results and Analysis

From the analysis in the previous section, it is clear that the GPS solution using Q3 reduces the position accuracy. For this reason, the same GPS and INS data in Test1 were post-processed twice, once using only Q1 and Q2 GPS positions and another one following the MSIT. The removal of Q3 positions as well as the use of the phase solution of the MSIT increased the GPS outages in Test2 (Figure 6.12 left) and Test3 in (Figure 6.12 right). For example, a large GPS outage occurred in the testing points from T2 to T8 (in area A in Figure 6.12) after the removal of Q3 positions and the use of phase solutions only (see Figure 6.12). Comparing Figure 6.12 left with Figure 6.12 right, it is clear that the number of epochs with no GPS increased (compare areas A and C in these two figures) when only using GPS phase solutions, otherwise referred to as Q1 and Q2 These outages could be due to the inability of the processor to solve the integer ambiguity to a high degree of confidence in these specific environments.

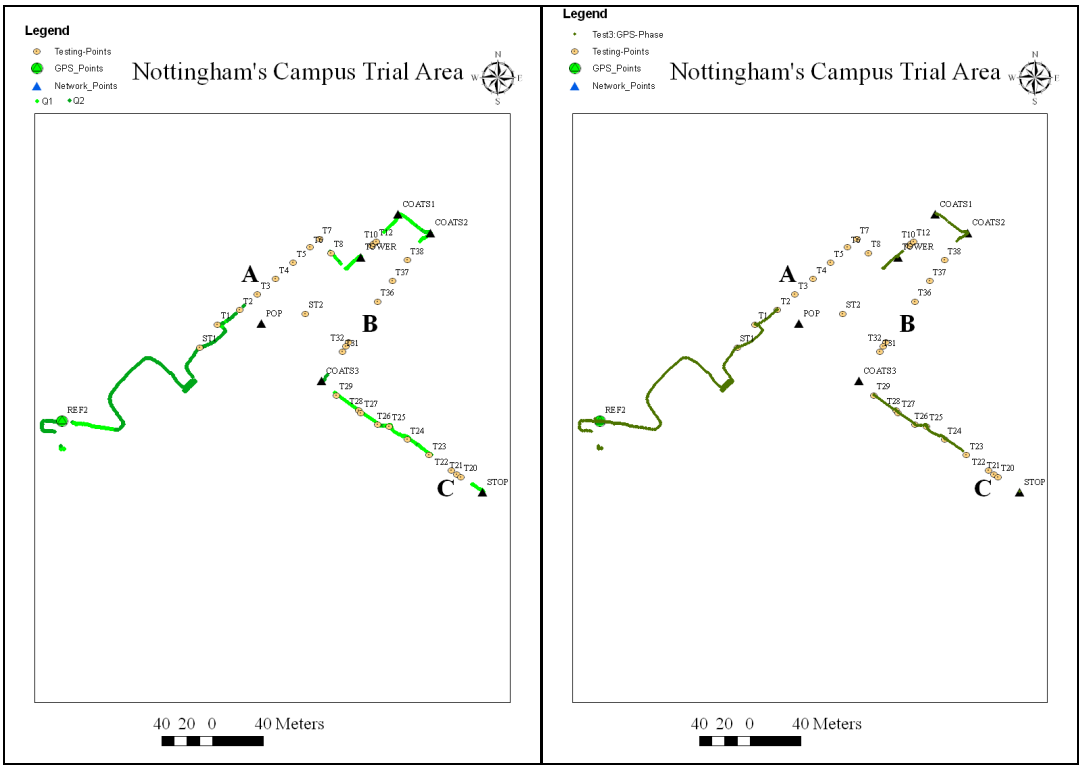

Figure 6.12: GPS data processing results for Test2 (left) and Test3 (right)

Similar maximum uncertainties to Test1 were estimated in the smoothed positions in Test2 (about 0.28m in X, Y and Z). However, the other peak uncertainties are increased in Test3 compared with Test2 due to larger GPS outages after removing the Q3 GPS positions. The maximum uncertainties of the smoothed positions in Test3 were found to be about 0.30m in X, Y and Z. Also, the other peak uncertainties were slightly higher in Test3 than those in previous tests, due to the larger GPS outages compared with previous tests. Similar to Test1, the results of GPS/INS integrated solution filled the gaps in the GPS only solution and ensured availability 100% of the time, in both Test2 and Test3. The resultant coordinates of Test2 and Test3 were converted to OSGB36 grid coordinates, averaged and compared with the 'truth' coordinates (Figure 6.13).

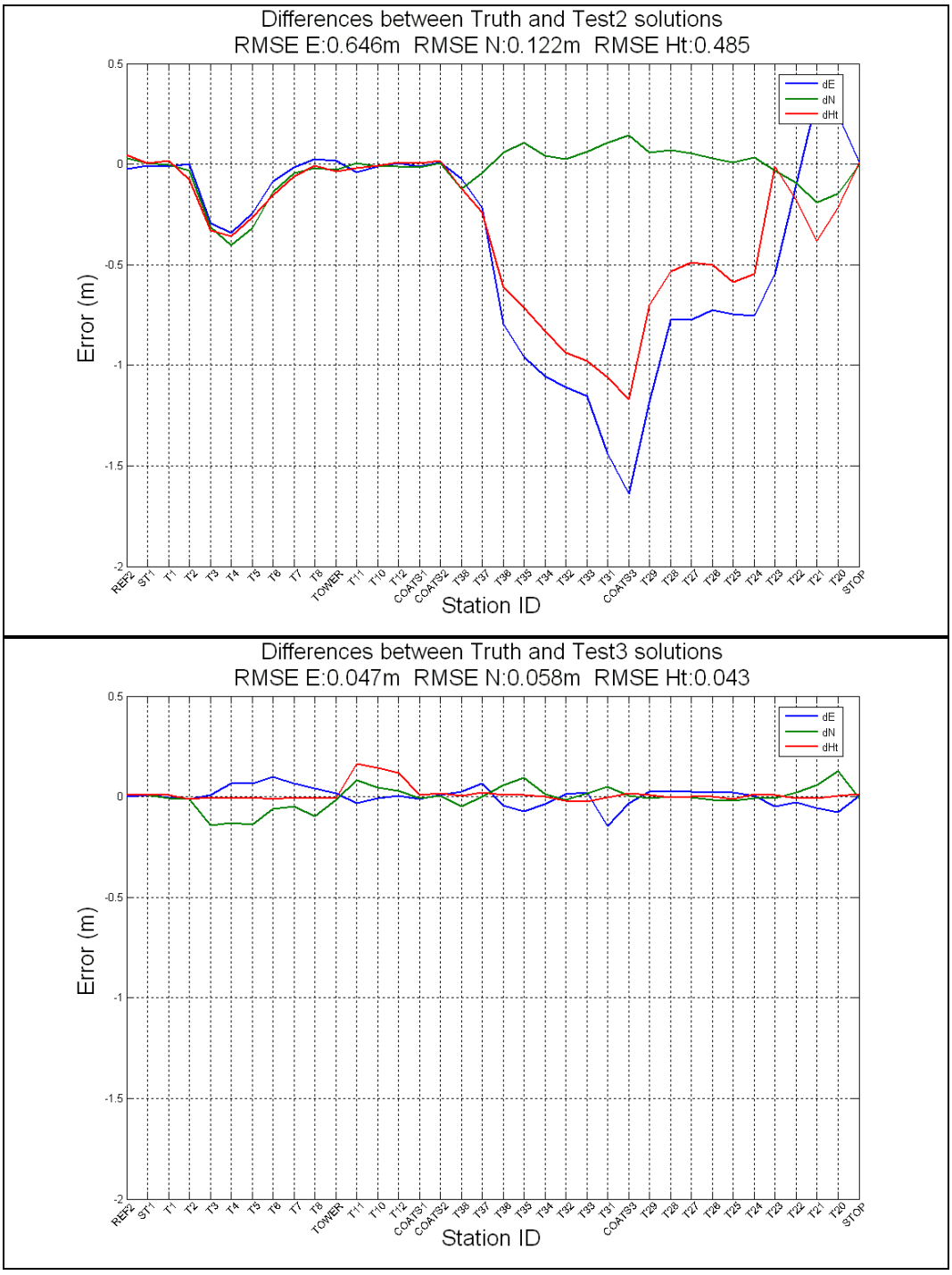

Figure 6.13: Differences between 'truth' and smoothed integrated coordinates for all points in Test2 (top) and Test3 (bottom)

As mentioned before, the points which are close to the 'truth' coordinates in the integrated solution are those which have a GPS position available. In addition in Figure 6.13 (top), the maximum errors were found on COATS3 testing point, equal to 1.640m and 1.170m in the E and Ht coordinates respectively, where a large GPS outage occurred before the point. Further, comparing the results of Test1 Figure 6.11 with the results from Figure 6.13 (top), position improvement can be seen around T4

and T5 points in Test2, which resulted in the more accurate coordinates and hence lower RMSE in E, N and Ht. This is due to the removal of the Q3 GPS positions which reduced the accuracy of the integrated positions in Test1. However, the accuracy achieved in Test2 is still not good enough to meet the accuracy requirements for this research. Therefore, another attempt was carried out to post-process the GPS/INS data based on Q1 GPS positions only. However, this attempt was not successful as the integration failed to calculate any positions. This was one of the reasons for developing the MSIT to overcome such limitations.

Comparing the results of Test3 (Figure 6.13 bottom) with the two previous tests shows a significant improvement in accuracy when using the MSIT. In general, RMSEs of 0.047m, 0.058m and 0.043m with maximum positions error of 0.148m, 0.142m and 0.166m were achieved in E, N and Ht respectively in Test3. As mentioned before in order to confirm this improvement, another two datasets were collected and post-processed: once using the OST with Q1 and Q2 GPS positions and once using the MSIT. The results of these tests are discussed and analysed in the next sub-sections.

6.8.3.3 Test4 & Test5: Results and Analysis

As mentioned before, Test4 and Test 5 were carried out during the morning. The GPS data in Test4 and Test5 were post-processed using the OST and MSIT respectively. The GPS positions of Q1 and Q2 for Test4 are shown in Figure 6.14 (left) and the GPS phase positions of Test5 are illustrated in Figure 6.14 (right).

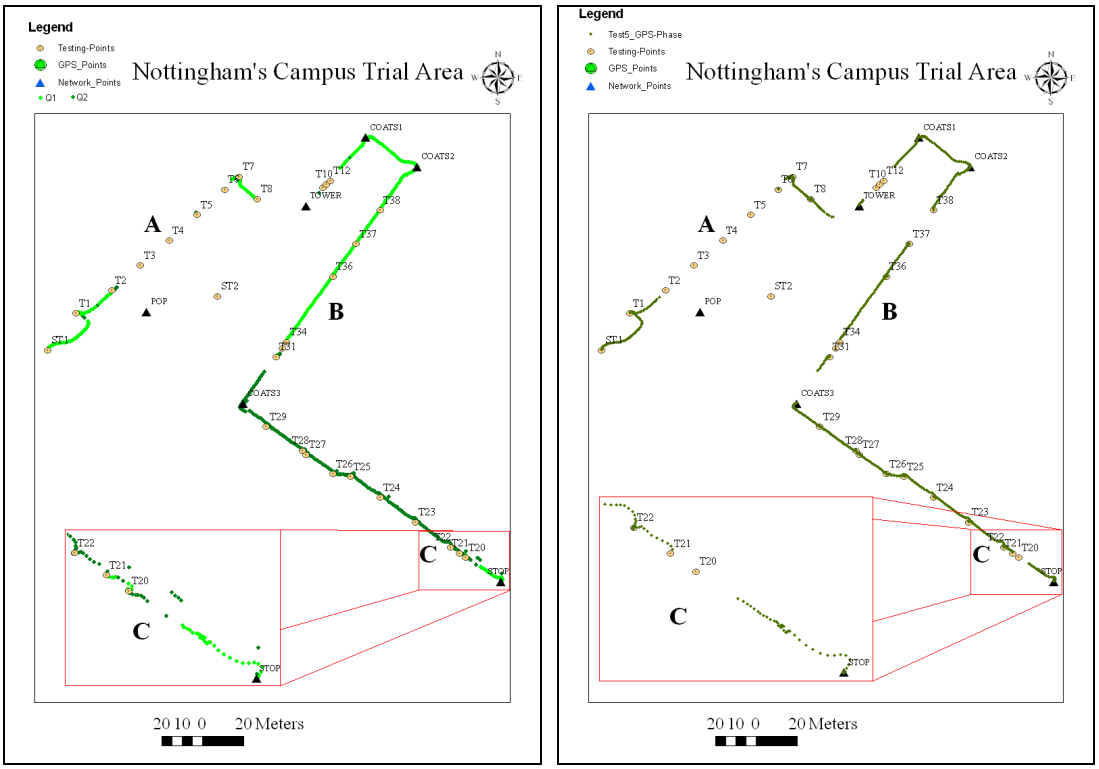

Figure 6.14: GPS only data processing results for Test4 (left) and Test5 (right)

From Figure 6.14, it can be seen that a large GPS outage occurred in area A while areas B and C were appropriately covered of GPS. However, the quality of the GNSS positions in area C were Q2, which, as shown in the zoomed area around point T20 in Figure 6.14 (left), has unsmoothed positions with missing epochs. This could be due to a multipath signals as there are high buildings to the north and south of point T20. These bad epochs were removed in Test5 Figure 6.14 (right) and a GPS outage found instead. Comparing Figure 6.14 left and right, more GPS outages were found in Test5 compared with Test4. As mentioned in the previous section, these outages could be due to inability of the processor to resolve the ambiguity with high confidence.

The maximum uncertainties, which mostly took place in area A, of the smoothed positions in Test4 were found to be about 0.24m in X, Y and about 0.26m in Z. Similarly, the maximum uncertainties of the smoothed positions in Test5 were found to be about 0.24m in X, Y and Z. Similar to the previous tests, the results of GPS/INS integrated solution showed that availability 100% of the time was achieved in both Test4 and Test5. The smoothed integrated GPS/INS positions of Test4 and

Test5 were converted to OSGB36 grid coordinates, averaged and compared with the 'truth' coordinates (Figure 6.15).

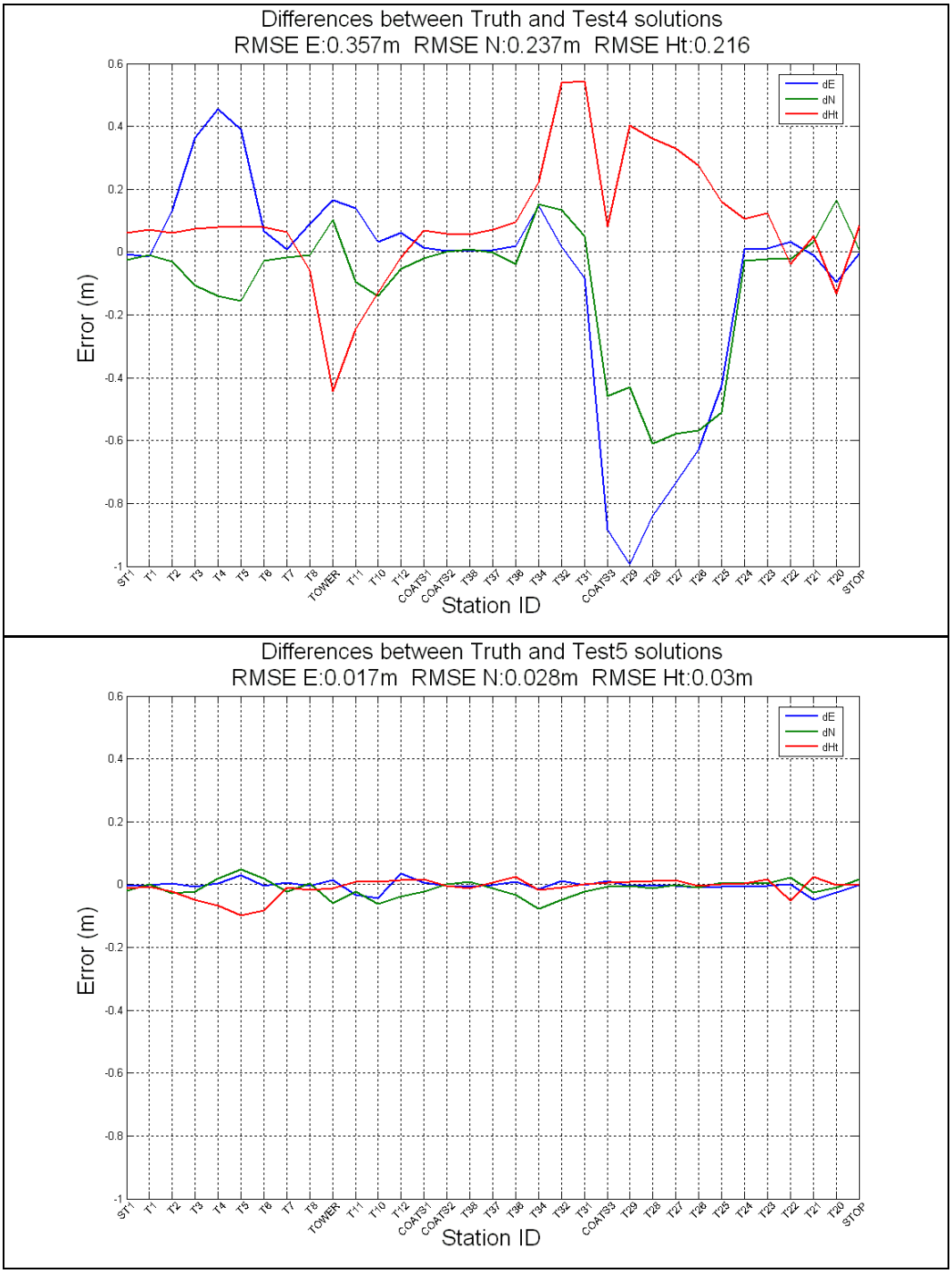

Figure 6.15: Differences between 'truth' and smoothed integrated coordinates for Test4 (top) and Test5 (bottom)

From Figure 6.15 (top), the large error in the integrated solution of Test4 was found in the area where GPS positions with Q2 are available, with a maximum error of up to 0.994m in the East coordinate of T29 testing point. From this, it is obvious that a

GPS position with Q2 is also unsuitable for high level of accuracy. RMSE of 0.017m, 0.028m and 0.03m with maximum positions error of 0.048m, 0.076m and 0.098m were achieved in E, N and Ht respectively in Test5. The results of Test5 not only confirm the accuracy achieved in Test3 using the MSIT, but also showed even better accuracy than Test3, due to the high availability of the GNSS positions in Test5 when compared with Test3. For additional confirmation of MSIT results, another dataset was post-processed and analysed in the next sub-section.

6.8.3.4 Test6 & Test7: Results and Analysis

As mentioned before, Test6 and Test7 were carried out during the afternoon to insure a different arrangement of the GPS constellation was available for positioning. Similar to the previous tests, the GPS data in Test6 and Test7 was post-processed using the OST and MSIT respectively. The GPS positions of Q1 and Q2 in Test6 are shown in Figure 6.16 (left) and the GPS phase positions for Test7 are illustrated in Figure 6.16 (right).

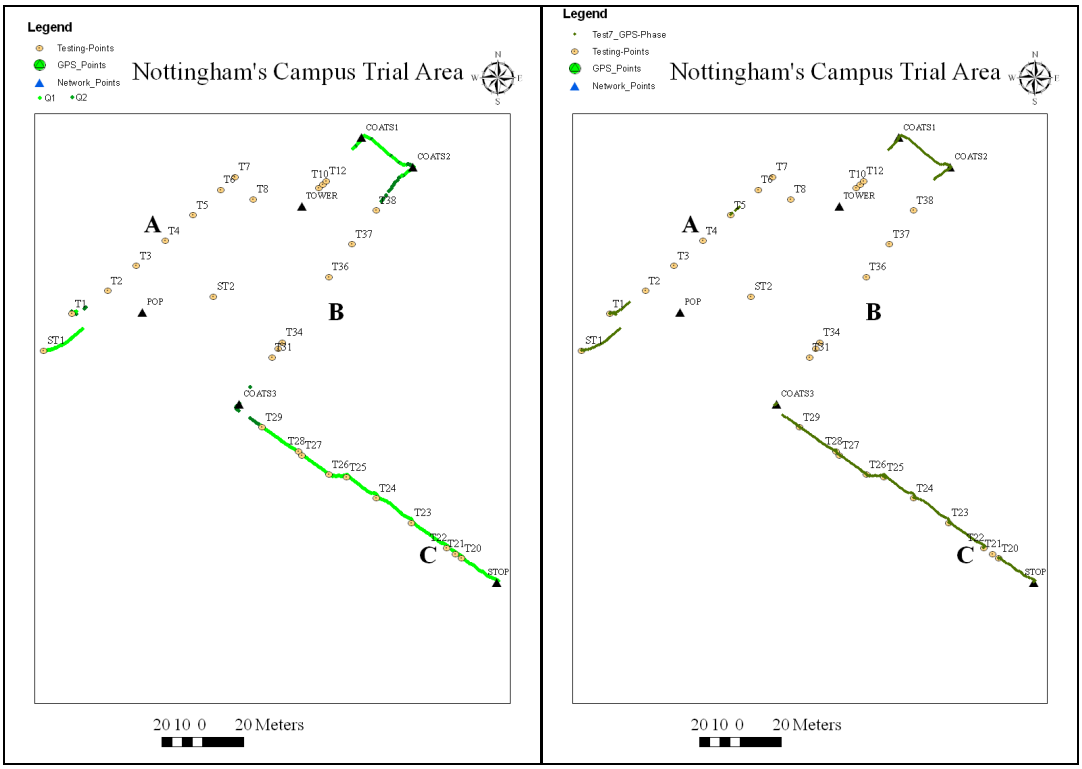

Figure 6.16: GPS only data processing results for Test6 (left) and Test7 (right)

Unlike the previous tests, there were very large GPS outages in area A and B while area C was appropriately covered. Furthermore, in Test6 most of the GPS epochs were Q1 (Figure 6.16 left). The location of the phase solutions in Test7 approximately match the location of the Q1 solutions in Test6. However, there are more epochs with phase solution around T1 and T5 testing points (Figure 6.16 right), although a small GPS outage took place around T21 testing point in Test7.

The maximum uncertainties, which mostly took place in areas A and B, of the smoothed positions in Test6 were found to be about 0.32m in X, Y and Z. Similarly, the maximum uncertainties of the smoothed positions in Test7 were found to be about 0.33m in X, Y and Z. Similar to the previous tests, the results of GPS/INS integrated solution showed that availability 100% of the time was achieved in both Test6 and Test7. The smoothed integrated GPS/INS positions of Test6 and Test7 were converted to OSGB36 grid coordinates, averaged and compared with the 'truth' coordinates (Figure 6.17 top and bottom).

Figure 6.17: Differences between 'truth' and smoothed integrated coordinates Test6 (top) and Test7 (bottom)

Although there were large GPS outages in Test6 which resulted in a maximum error of 0.372m in the North coordinate of the T5 testing point (Figure 6.17 top), this test can be considered the most accurate test that has been post-processed using OST. The reason for such accuracy is because most of the GPS epochs have a Q1 solution. However, the accuracy achieved in Test6 still does not meet the research requirements.

RMSEs of 0.057m, 0.035m and 0.016m, with maximum position error of 0.156m, 0.090m and 0.038m were achieved in E, N and Ht respectively in Test7. Additionally, comparing Figure 6.17 top with Figure 6.17 bottom, a significant improvement is clearly offered by the MSIT. This confirms the advantage of using the MSIT for GPS/INS data collection and processing.

6.9 Summary

This chapter introduced GNSS and INS integration and described a Multiple Steps Integration Technique (MSIT) which was developed by the author during this research, as a methodology for GNSS/INS data collection and processing to improve on an existing One Step Technique (OST). For MSIT, the GNSS/INS data processing is conducted in four steps to produce smoothly integrated positions. The key point of the data processing is the use of GNSS phase fixed positions calculated independently using a different software, i.e. LGO.

From the discussion and the analysis above, it is clear that high position accuracy can be achieved in urban canyons when GNSS positions are available, but it is necessary to monitor this availability so that kinematic techniques are replaced by stop and go techniques, when working in GNSS outages, in order to initialise ZUPT. This is the case for both OST and MSIT.

It was shown that the integrated positions obtained using OST are highly dependent on the GNSS position quality. If, for example, GNSS positions with Q1 are available, it is expected that a high level of accuracy will be achieved in the GNSS outage. However as the length of any GNSS outage increases, the integrated position accuracy based on OST will be reduced.

The MSIT was developed to offer higher positional accuracy, especially over large GNSS outage areas, and was demonstrated to do this in several tests based on GPS. For example, a maximum error of up to 1.640m in the East coordinate was verified in Test2 using the OST but when the same data was post-processed using the MSIT in Test3, the maximum error dropped to 0.148m in the East coordinate.

Unfortunately, such accuracy is still not enough to meet the research requirements, however MSIT could be used in the future when more satellites will be available, i.e. the four constellations as discussed in the previous chapter, to overcome the positioning difficulties under or near bridges with short outages.

To summarise, although GPS/INS offers 100% of the time position availability and, therefore, so should GNSS/INS, the current accuracy based on GPS is not good enough to meet the research requirements. Therefore, it is worth investigating other methods for a possible solution such as GNSS integrated with a total-station, as discussed in the next chapter.

Chapter 7: GNSS and Total Station Integration

7.1 Introduction

The previous chapters discussed different types of GNSS-based positioning techniques in difficult areas. Positioning using current and future GNSS satellites is not guaranteed 24 hours a day. Therefore in order to achieve 100% of the time positioning availability with centimetre-level accuracy, GNSS integrated with other systems could be the solution. GNSS integrated with INS was one of the suggested solutions which was shown in Chapter 6 to guarantee 100% of the time positioning availability. However, although the maximum position's accuracy was improved by the author from 1.6m to 0.17m when using the MSIT, such accuracy is still not good enough to meet the research requirements for the MTU project. So, GNSS integrated with a total-station will now be investigated, to see if this can overcome all previous limitations.

To maintain centimetre-level accuracy using a total-station and particularly when multiple setups are compulsory, several control points and numerous total station measurements (distances and angles) are required. This increases the effort and the time required to establish and complete the surveying. In recent years, a device that integrates a GNSS receiver/antenna with a total-station into one compact instrument, the Leica SmartStation, has been developed which, when coupled with a network RTK service, can provide the user with real time National Grid coordinates in a more efficient approach. Similarly, a SmartPole usually works together with a total-station and allows the user to survey using either the total-station or GNSS, depending on the environment. To make these systems even more efficient, a Continuous Updating Technique (CUPT) has been developed by the author as part of this research, to loosely couple GNSS RTK positions with angles and distances measured by a total-station.

The aim of this chapter is to present the results of various tests conducted through CUPT using three configurations on The University of Nottingham's Campus. The

first one is using a SmartStation. The second one is using a robotic total-station and an IntegratedPole equipped with a Leica 1200 dual frequency GPS receiver. The third one is using a robotic total-station and an IntegratedPole equipped with single frequency High Sensitivity GPS (HSGPS) receiver. Since the positioning in the first two technologies was based on the Leica SmartNet, the Network-RTK will be described herein.

7.2 Leica SmartStation Overview

According to Biasion et al. [2005] in 1993 Leica Geosystems registered a USA Patent for a "*Surveying system including an electro-optic total station and a portable receiving apparatus comprising a satellite position measuring system*". This has now been implemented in an instrument called Leica SmartStation.

Leica SmartStation comprises a TPS1200 total-station with an ATX1230 SmartAntenna (Figure 7.1). The SmartAntenna is a 12 channel dual frequency GPS RTK receiver with antenna that fits on and communicates with the total station [Leica-Geosystems-AG, 2006c].

Figure 7.1: Leica SmartStation

Typically, the GPS provides the user with a real time high accuracy position wherever it is available using either a network RTK service (i.e. SmartNet in the UK)

or a local base station. Then the user operates the total-station to measure angles and distances to objects that have to be surveyed in restricted areas. By using two of the GPS points together with the total station observations, the SmartStation can transform the coordinates of the measured points to grid coordinates (such as OSGB36). Hence, SmartStation eliminates the need for traversing to propagate control points into the survey area, by providing RTK GPS positioning of the total station [Cranenbroeck, 2005].

SmartStation uses Leica's SmartCheck algorithms to determines RTK position coordinates to centimetre level of accuracy within a few seconds, at ranges of up to 50km from a reference station [Leica-Geosystems-AG, 2006c]. The position coordinates for the RTK point are then updated continuously as long as SmartStation continues to receive GPS data (L1 and L2 phase and code observables) and corrections. This technique is used to ensure the highest possible RTK reliability for SmartStation RTK fixes. The horizontal accuracy of the RTK points is claimed to be 10mm+ 1ppm and the vertical accuracy 20mm + 1ppm [Leica-Geosystems-AG, 2006c].

The integration between GPS and Total Station, however, presents several issues to be considered which, as a result, can affect the accuracy of the SmartStation point. These issues include obstructions and multipath. Typically, the SmartStation is set up in an open environment to avoid obstructions and multipath. However, in urban canyons this may not always possible.

7.3 IntegratedPole/SmartPole Overview

An IntegratedPole is a pole with 360° prism and GNSS antenna (connected to a GNSS receiver) on the top, which usually works together with a total-station (Figure 7.2 left). One example of an IntegratedPole is the Leica SmartPole which uses the ATX1230 dual frequency Smart-Antenna (Figure 7.2 right), allows the user to survey using either GPS or total-station depending on the environment [Leica-Geosystems-AG, 2006b].

Figure 7.2: IntegratedPole (left) and Leica SmartPole (right)

7.4 Network-RTK Overview

A GNSS conventional RTK system involves one receiver on a local base station transmitting its raw observations, or observation corrections, to a rover receiver via some sort of data communication link (e.g., VHF or UHF radio, cellular telephone). One significant drawback of this approach is the limited distance between base and rover, arising from distance-dependent biases, namely orbit bias, ionosphere bias and troposphere bias [Rizos and Han, 2003].

To overcome this distance dependence, a network of GNSS reference stations spread over a wide geographic area can be used. If the measurement biases are appropriately modelled and corrected for, then positioning accuracy should be almost independent of the inter-receiver distance. To do this, a GNSS Network-RTK system computes models of ionospheric, tropospheric and orbit biases and provides network correction information to rover users. The basic principles of Network-RTK can be found in [Vollath et al., 2002; Rizos and Han, 2003; Leica-Geosystems-AG, 2005c]. Advantages of Network-RTK include significantly improved regional atmospheric models, fast and reliable positioning solutions, due to more robust integer ambiguity resolution approaches, and much improved mobility for the end-user receivers [Meng et al., 2007].

In the UK, the Ordnance Survey has established 100 GPS reference stations around the country [OS, 2008c]. These from the basis of a network RTK called OS Net which is used by the OS' surveyors around the country. As a service it is not available commercially, however through its partners, real-time and post-processed GPS services are provided to such users. Leica SmartNet (see Figure 7.3) and Trimble VRS Now are two examples of such services.

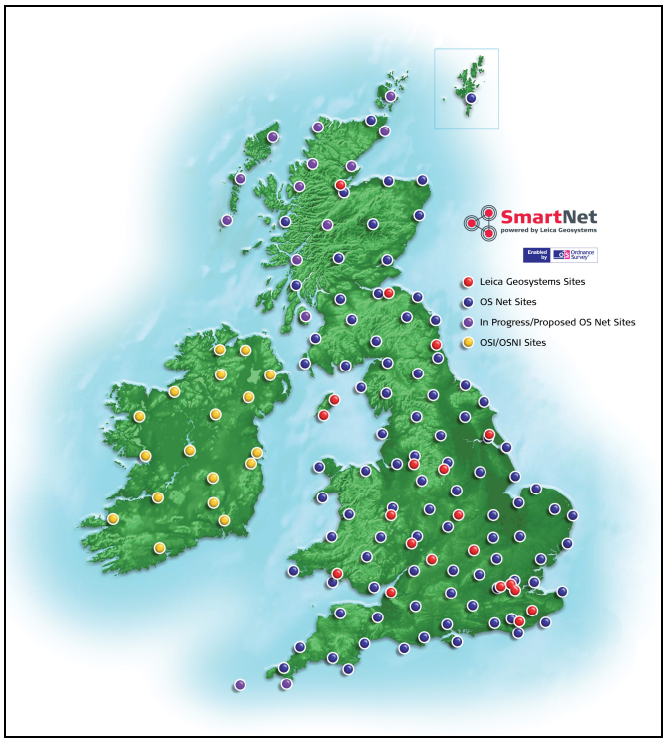

Figure 7.3: Ordnance Survey Network and Leica SmartNet [Leica-Geosystems-AG, 2008]

Leica has additional GPS+GLONASS receivers included in its SmartNet network in order to improve nationwide coverage and satellite availability [Leica-Geosystems-AG, 2006a]. It uses its SpiderNet software to implement the Network RTK architecture and ensures the highest possible RTK reliability for users of SmartStation/SmartPole as it involves ranges of about 50km from the reference stations.

Separately, the University of Nottingham and Leica Geosystems (U.K.) have jointly established the Nottingham/Leica GPS Network-RTK Test-bed. This network was designed to consist of 13 GPS reference stations (see Figure 7.4) and is the only GPS network facility in the UK established for purely scientific research purposes. It

covers an area of about 20,000 square kilometres, in the Midlands of the UK [Meng et al., 2006; Meng et al., 2007].

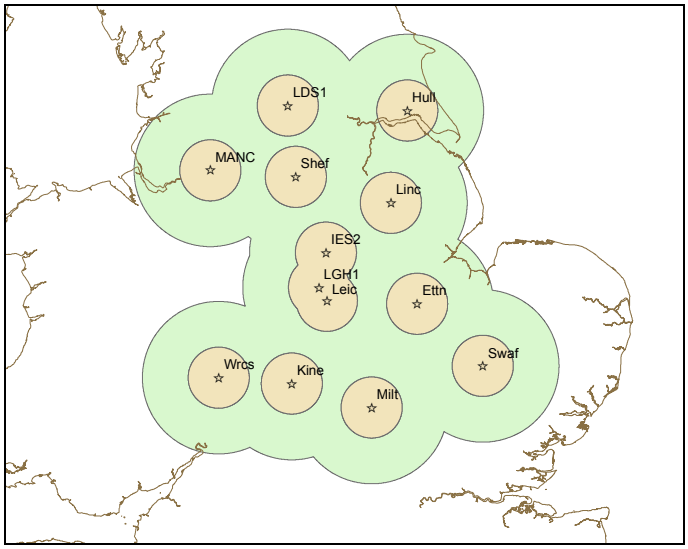

Figure 7.4: 50 km Coverage of the Nottingham/Leica GPS Network-RTK Test-Bed

7.5 Limitations of Previous Research

After the invention of the SmartStation, a few papers were published by Leica Geosystems to describe the combination of GPS and total-station instruments. See for example [Cranenbroeck, 2005; Hill, 2005; Leica-Geosystems-AG, 2006b; Leica-Geosystems-AG, 2006c]. The basic drive for such integration is that the GPS provides control points in real time while the total-station is employed to survey the required points, so, there is no need to carry out a conventional traversing to propagate control points.

Previous work by Hill [2005] showed that surveying using SmartStation was completed 38% faster than conventional traversing on a topographic survey, whilst maintaining an accuracy of better than 15mm in both horizontal and vertical components. Using the Leica SmartStation in urban areas, Parker [2006] reported an absolute accuracy of 15mm in 3D and showed the advantages of using this system over others. Similarly, Biasion et al. [2005] found that SmartStation was easy to use and the surveying speed was increased when compared with traditional surveying methods.

All set-up possibilities within the SmartStation, determined by Hill [2005], require having a minimum of two inter-visible RTK fixed control points to start the surveying. However, when positioning in urban canyons, it may be difficult to establish two inter-visible RTK fixed control points with good geometry. Furthermore, the current SmartStation does not support the updating of coordinates as new RTK points are available during multiple setups. Such RTK points, that could be available during the multiple setups, can be integrated with total-station observations to improve the overall accuracy of the integrated positions. Similar to the integration of GNSS/INS, GNSS/total-station integration hopes to provide a survey system that exhibits superior performance in comparison with either GNSS or total-station alone. Such integration could also be used for error detection and correction. To overcome the limitations of the SmartStation, a Continuous UPdating Technique (CUPT) has been developed by the author as part of this research to loosely couple RTK GPS positions with total-station observations (see Appendix 14 for more details on the steps involved in the least squares adjustment used in CUPT).

7.6 GPS and Total-Station Integration Methods

This section discusses the methods for integrating RTK GPS positions with total-station observations offered by CUPT. Such integration could be classified to three types: direct, indirect and network integrations. In the direct method, two visible RTK GPS points are integrated with multiple total-station measurements observed directly between these points, such as forward, backward, face left and face right observations. Similar to the direct method, in the indirect method two invisible RTK GPS points are integrated together with multiple total-station measurements observed indirectly by means of using one/or more total-station setups between these points. The network integration is used when three or more RTK GPS points as well as direct and indirect total-station observations are available. This provides redundant RTK GPS points which could assist in error detection and correction within the network.

7.6.1 GPS and Total-Station Integration: The Direct Method

As mentioned before in the direct method, two visible RTK GPS points are integrated together with multiple direct total-station observations. In order to evaluate the position's improvement after the direct integration, two tests were carried out. The first test used ST10 & STOP RTK GPS points while the second test used ST1 & ST2 RTK GPS points. Using the SmartStation, RTK GPS data with fixed solution was collected on each point for about 2 minutes. As mentioned before, the RTK GPS coordinates are continuously updated as long as the SmartStation continuous to receive the GPS data and the RTK corrections. Hence, the final RTK GPS position is the updated one. In addition, two rounds of direct total-station observations between these points were collected using the SmartStation on face left and on face right.

All of the previous data were integrated through CUPT. The output network geometry and error ellipses figure for the first test is illustrated in Figure 7.5 (left), and for the second test in Figure 7.5 (right).

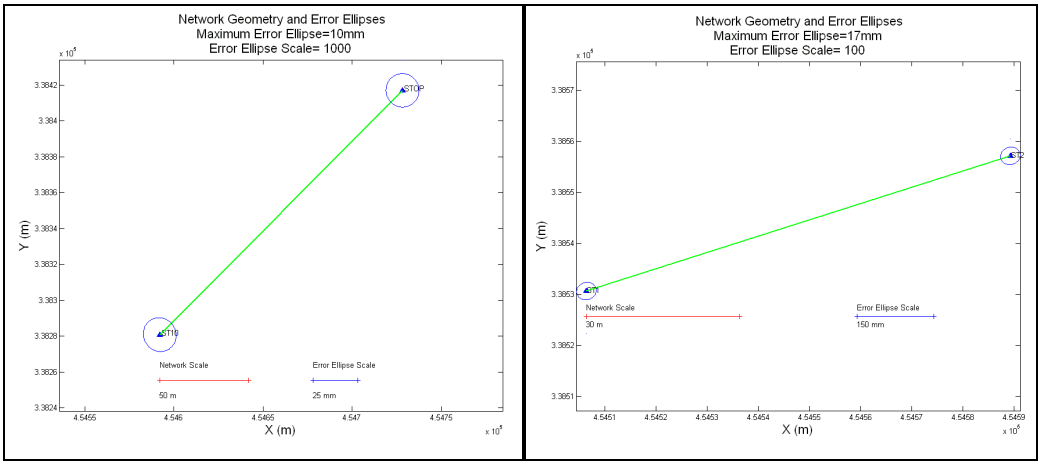

Figure 7.5: Direct method first test (left) and second test (right)

The results of integration show that maximum error ellipses of 0.010m and 0.017m were estimated for the first and the second tests respectively. For further analysis, the RTK GPS coordinates as well as the integrated coordinates were compared with 'truth' coordinates in Table 7.1.

Table 7.1: Differences between 'truth' coordinates and both RTK GPS and CUPT coordinates for the direct method

Station ID/ Test ID	dE (m)/ RTK	dE (m)/ CUPT	dN (m)/ RTK	dN (m)/ CUPT	dHt (m)/ RTK	dHt (m)/ CUPT
ST10/first test	0.001	0.005	-0.030	-0.024	-0.029	-0.008
STOP/ first test	-0.011	-0.015	0.004	-0.001	0.014	-0.007
ST1/ second test	-0.004	-0.002	-0.011	-0.010	0.007	0.005
ST2/ second test	0.001	-0.001	-0.009	-0.010	0.000	0.001

Table 7.1 shows that CUPT was successful in making a significant improvement in the height component in the first test. This is since the RTK GPS points (ST10 and STOP points) in the first test can be considered to have a low level of accuracy (such as 0.029m). So, the integration with the zenith angles improves the accuracy of the RTK GPS points. In case of RTK GPS points with a high level of accuracy (such as 0.007m), the results of integration show that CUPT maintains such high accuracy are contributes a small improvement, such as that in ST1.

The integration results show that CUPT could not improve the plan coordinates but it maintains their accuracies. This is because there are only two RTK GPS points used, which could not provide the integration with a redundancy to improve the plan coordinates but the inclusion of a slope distance in the direct method can be used as a scalar (slope distance can scale the RTK horizontal coordinates according to their weights).

7.6.2 GPS and Total-Station Integration: The Indirect Method

In the indirect method, two invisible RTK GPS points are integrated with the indirect total-station observations. Like the direct integration tests, in order to evaluate the position improvement after the indirect integration, two indirect tests were carried out. The first indirect test used three points: STOP & COATS2 RTK GPS points and COATS3 testing point. The second indirect test used four points: COATS2 & ST1 RTK GPS points and COAT1 and ST2 testing points. Using the SmartStation, RTK GPS data with fixed solution was collected on each of the RTK GPS points for about 2 minutes. Besides, two rounds of total station observations were collected between the RTK and the testing points using the SmartStation on face left and on face right.

All of the previous data were integrated using CUPT. The output network geometry and error ellipses figure of the first indirect test are illustrated in Figure 7.6 (left), and of the second indirect test in Figure 7.6 (right).

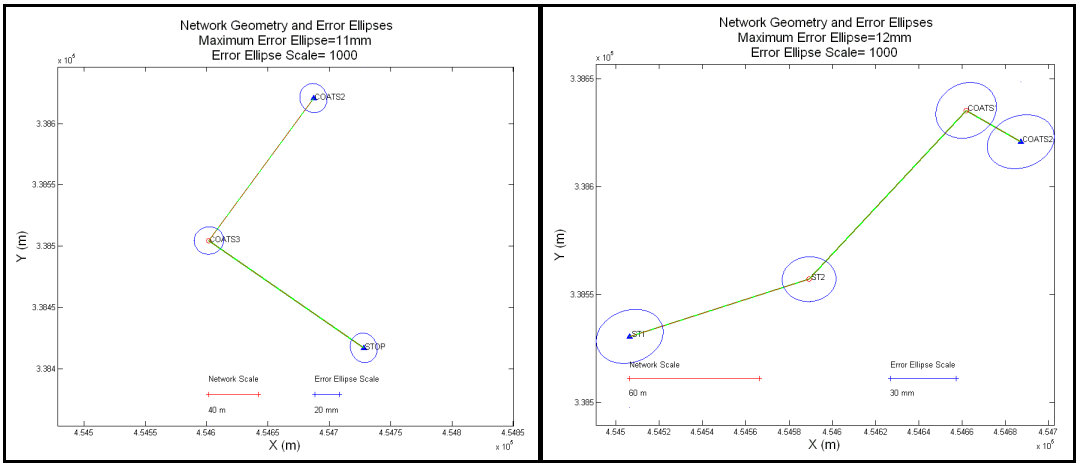

Figure 7.6: Indirect method first test (left) and second test (right)

The results of integration show that maximum error ellipses of 0.011m and 0.012m were estimated for the first and the second indirect tests respectively. For further analysis, the RTK GPS coordinates, as well as the integrated coordinates, were compared with 'truth' coordinates in Table 7.2.

Table 7.2: Differences between 'truth' coordinates and both RTK and CUPT coordinates for the indirect

Station ID/ Test No	dE(m)/ RTK	dE(m)/ CUPT	dN(m)/ RTK	dN(m)/ CUPT	dHt(m)/ RTK	dHt(m)/ CUPT
STOP/first indirect test	-0.011	-0.011	0.004	0.001	0.014	0.003
COATS3/ first indirect test	--	-0.006	--	0.004	--	0.003
COATS2/ first indirect test	-0.002	-0.003	-0.004	0.000	-0.006	0.005
COATS2/ second indirect test	-0.002	-0.003	-0.004	-0.005	-0.006	-0.004
COATS1/ second indirect test	--	-0.004	--	-0.009	--	0.001
ST2/ second indirect test	--	0.001	--	-0.008	--	0.002
ST1/ second indirect test	0.001	0.002	-0.009	-0.009	0.000	-0.002

Similar to the results achieved by the direct method, CUPT was successful in making a significant improvement in the height component for the RTK GPS points with a low level of accuracy (0.014m in this case). In the case of a high level of accuracy (such as that in the second indirect test), the integration results show that CUPT maintains such accuracy or contributes a small improvement such as that in COATS2 point.

Similar to the results achieved in the direct method, the integration results in the indirect method show that CUPT could not improve the plan coordinates but it maintains their accuracies. Again, this is because there are only two RTK GPS points used in the indirect tests which could not provide the integration with a redundancy to improve the plan coordinates.

7.6.3 GPS and Total-Station Integration: The Network Method

As mentioned before, the network integration is used when three or more RTK GPS points as well as direct and indirect total-station observations are available. This provides with redundant RTK GPS points which could assist in the error detection and correction within the network.

In order to evaluate the position improvement after the network integration, several tests using different techniques were carried out. These tests are discussed in great detail in the next three sections 7.7, 7.8 and 7.9.

7.7 SmartStation Tests

Preliminarily results of the SmartStation tests were published in [Taha et al., 2006]. The results achieved in those tests showed that SmartStation guarantees 100% of the time positioning availability in built-up areas. However, a maximum position error of about 0.05m was found in one point, even after multiple setups. Furthermore, there were several points where RTK GPS fixed was available but was not possible to be used in the SmartStation system.

The next sections discuss the data collection and results of 15 SmartStation tests (summarised in Table 7.3). In these tests, the SmartStation coordinates, RTK GPS coordinates and the integrated coordinates calculated by CUPT are compared with the 'truth' coordinates and analysed.

Table 7.3: Summary of SmartStation tests

SmartStation Tests					
Test No.	**Solution Type**	**No. of RTK Points**	**Observation Type**	**Location**	**Remarks**
Test1	SmartStation	2	Forwards	Nottingham	2 minutes
Test2	SmartStation	2	Backwards	Nottingham	2 minutes
Test3	CUPT	5	Forwards	Nottingham	2 minutes
Test4	CUPT	5	Backwards	Nottingham	2 minutes
Test5	CUPT	5	Combined	Nottingham	2 minutes
Test6	CUPT	3	Combined	Nottingham	2 minutes
Test7	CUPT	5	Combined	Nottingham	Morning 2 minutes
Test8	CUPT	3	Combined	Nottingham	Morning 2 minutes
Test9	CUPT	5	Combined	Nottingham	Morning 5 minutes
Test10	CUPT	3	Combined	Nottingham	Morning 5 minutes
Test11	CUPT	5	Combined	Nottingham	Afternoon 2 minutes
Test12	CUPT	3	Combined	Nottingham	Afternoon 2 minutes
Test13	CUPT	5	Combined	Nottingham	Afternoon 5 minutes
Test14	CUPT	3	Combined	Nottingham	Afternoon 5 minutes
Test15	CUPT	8	Combined	Ripley	2 minutes

The first six tests were conducted on the same data processed using different techniques. For example, Test1 and Test2 present the results of the SmartStation forwards and backward solutions respectively and Test3 to Test6 present the results of the integrated solution using CUPT. Test7 to Test14 present the results of the integrated solution using CUPT in four groups (e.g. Test7 and Test8 are one group) of data collected at different times at different days. Finally, Test15 was used for a comparison purpose, to evaluate the position uncertainties obtained by CUPT with different baselines length.

7.7.1 SmartStation Tests: Data Collection and Processing

In the first group of tests (Test1 to Test6) data were collected on 34 testing points located in a difficult area of the Campus trial route using the Leica SmartStation. The field work started by setting up the SmartStation on a point located with a reasonably open view of the sky (ST10 point used as a Reference Object -RO-). After a few seconds, a fix position was determined with RTK for this point. Another occupied point was then determined close to the area of interest on one of the Campus-

Network points (STOP point). From now on, any point determined using GPS data using the SmartStation will be called an occupied point.

From the STOP point, total-station observations were collected for the RO as well as for several testing points, (T20 to T29, forwards observations) and for a new SmartStation point (COATS3). Any point determined by total-station observations will be called a measured point. The next step was setting up the SmartStation on the COATS3 point. After several minutes on this point, it was not able to obtain a fixed position with RTK GPS. This is because this point was located in an obstructed area. However from this point, new total-station observations were collected for the testing points T20 to T29 (backward observations using different numbers), for new several testing points (T31 to T38, forwards observations) and for a new SmartStation point (COATS2). On COATS2 point, RTK GPS fixed solution was available after few seconds. Hence, now there were measured and occupied positions for this point with different names.

The data collection phase was continued for all testing points, collecting both forwards and backward total station observations as well as collecting any available RTK GPS positions. In total, 34 testing points were observed from 7 set ups. It is worth mentioning that it was possible to obtain a fix position with RTK on 5 of the SmartStation set ups. In addition, RTK data was collected for about 2 minutes at each of these points.

In the other four groups of tests (Test7 to Test14) it was possible to obtain a fix position with RTK GPS on 5 out of 6 setups. It is worth mentioning that the RTK GPS data were collected using SmartStation at different time intervals (e.g. 2 and 5 minutes) on different days. The total-station observations collected in the first group were used for other tests (Test7 to Test14).

As mentioned before, Test15 was used for a comparison purposes to evaluate the position uncertainties obtained by CUPT over different baseline lengths. Using the SmartStation, RTK GPS data were collected on 7 out of 8 points while total station observations were collected on all of the points. RTK GPS coordinates as well as total-station observations were stored in a file and post-processed using CUPT.

SmartStation provides real-time coordinates once the first two RTK GPS points are collected. However after that, it is not possible to update the coordinates if new RTK positions are made available. This was one of the main reasons for developing the CUPT, i.e. to make use of all available RTK GPS positions. As mentioned before, in order to process the data using the CUPT, an editing step to correct the point's number is required. Also, the RTK points and the total-station observations must be stored in a file in CUPT format. This can be done using the Total Station Observation Manager (TSOM) described in Appendix 1. Once the files have been prepared in CUPT format, CUPT can be run to integrate the RTK GPS positions with total-station observations through the network adjustment. As mentioned previously, the results of CUPT are a report and several figures. The results of the different tests will be discussed in the next sub-sections.

7.7.2 SmartStation Tests: Results and Analysis for Test1 to Test6

The results of real time SmartStation coordinates of the forwards and the backward observations compared with 'truth' coordinates are illustrated in Figure 7.7. It is worth reminding that the surveying was started from ST10 point moving towards T1 point.

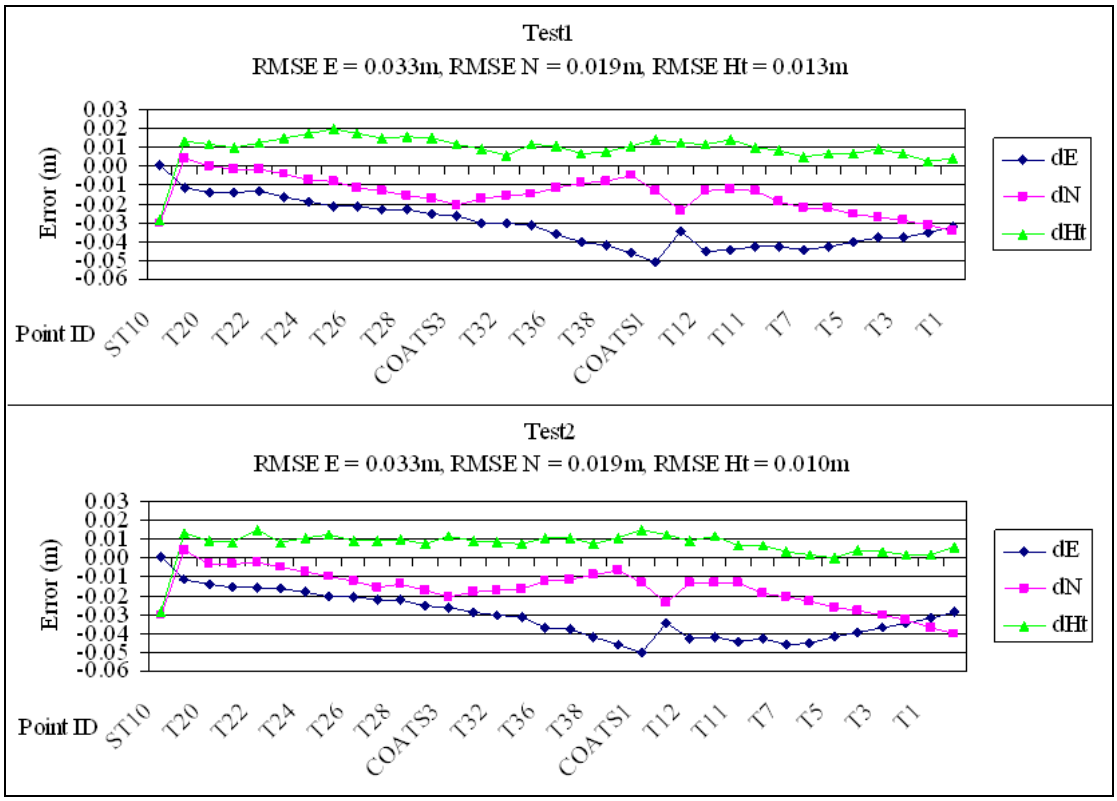

Figure 7.7: Differences between 'Truth' coordinates and SmartStation coordinates for Test1 (top) and Test2 (bottom)

In general, the previous tests showed 100% of the time positioning availability using the SmartStation. The errors calculated in Test1 and Test2 are approximately similar. In both tests, a maximum error of about 0.05m was found in East coordinate for COATS1 testing point. This error could be due to the multiple set-ups of the SmartStation which cause the errors to accumulate. However, the errors could have positive or negative sign which could appear, in some cases, to decrease as can be seen on the following points from T12 to T1.

As mentioned before, there were five RTK GPS points available during the data collection. Using CUPT, Test1 (forwards observations) and Test2 (backwards observations) were post-processed using all available RTK GPS points and the results are Test 3 and Test4 respectively (Figure 7.8).

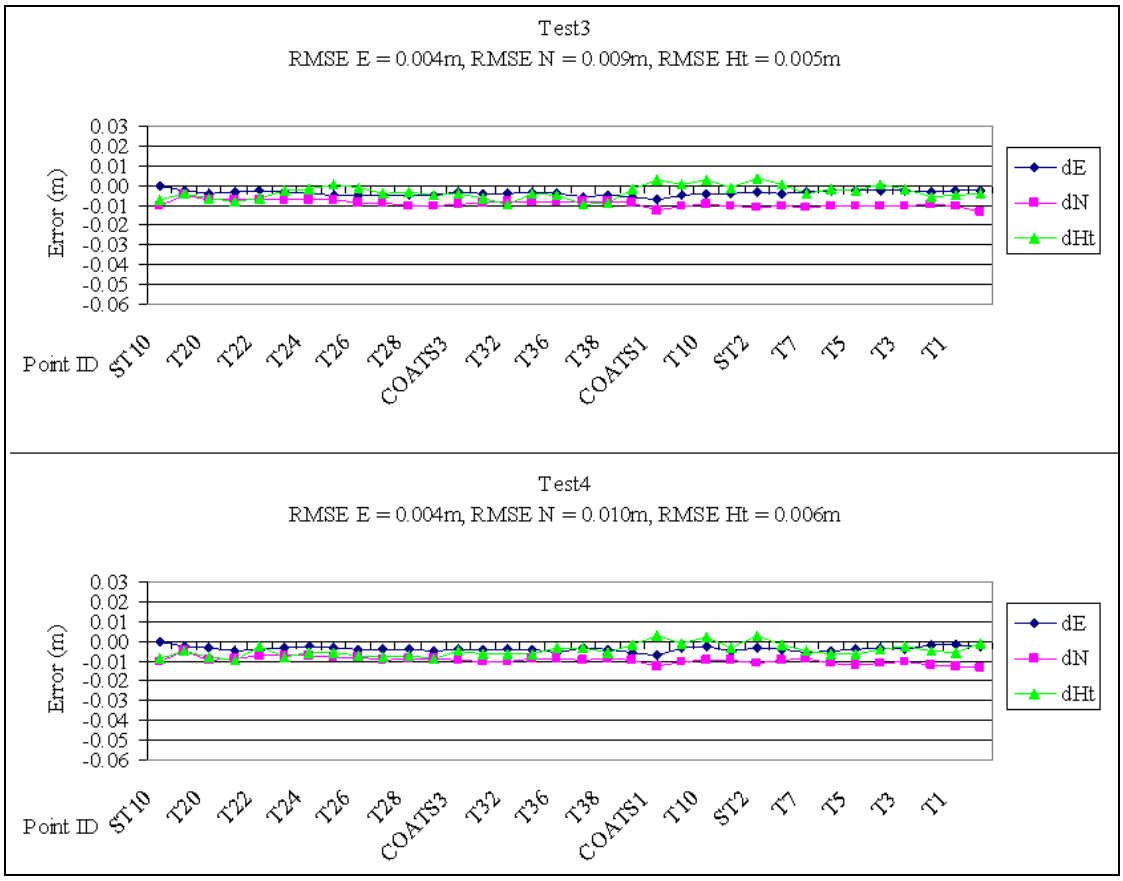

Figure 7.8: Differences between 'Truth' coordinates and CUPT coordinates for Test3 (top) and Test4 (bottom)

Comparing Figure 7.8 with Figure 7.7, it is very clear that the integrated solution from CUPT was very successful in improving the overall accuracy of the coordinates. The RMSE in Test3 and in Test4 are more or less similar, which suggests that if the total-station observations are collected with a high level of care, the overall position will not be affected by the total-station observations. Further tests were carried out using both the forwards and the backwards observations (called a combined solution) together with all available RTK GPS points (five points) in Test5 and with three RTK points in Test6. The results are illustrated in Figure 7.9.

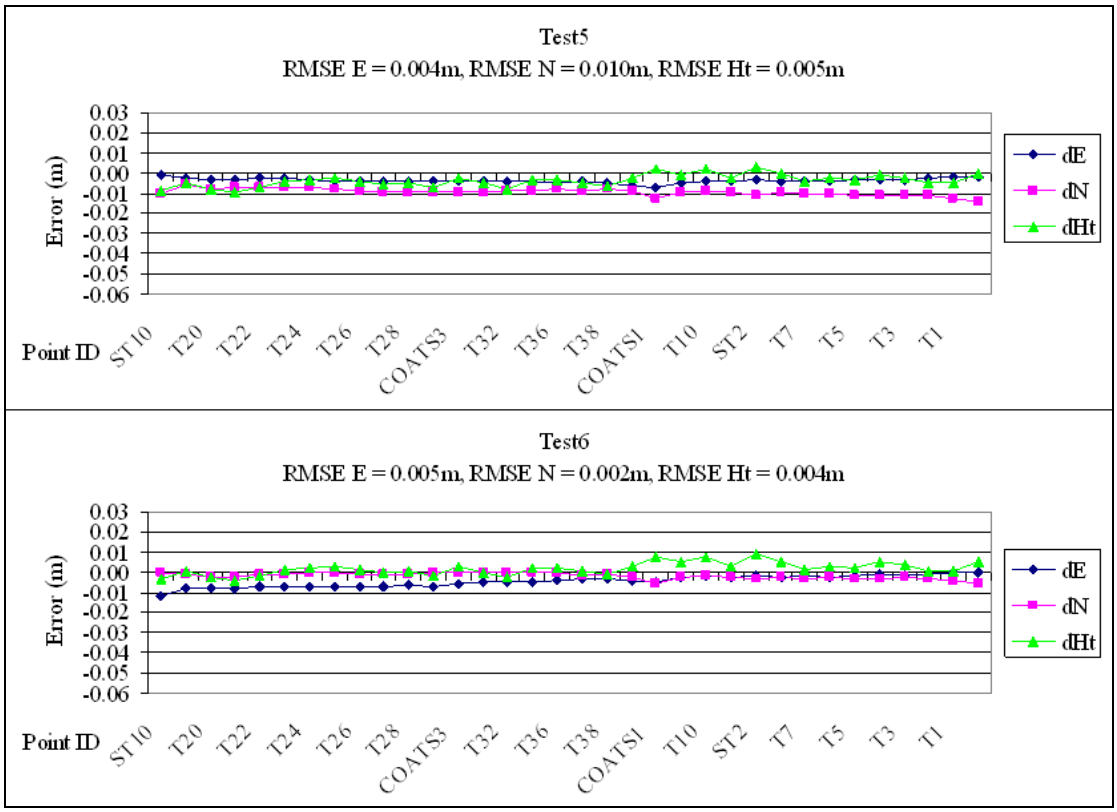

Figure 7.9: Differences between 'Truth' coordinates and CUPT coordinates for Test5 (top) and Test6 (bottom)

The RMSE of E, N and Ht for the combined solution in Test5 (Figure 7.9 top) are approximately equal to the RMSE in Test3 and Test4 confirming the high quality of the total-station observations both the forwards and backwards.

7.7.3 SmartStation Tests: Results and Analysis for Test7 to Test14

In order to confirm the improvement of the integrated solution over the SmartStation solution, the results of Test7 to Test14 are analysed in this section. As mentioned before, the RTK GPS data were collected using the SmartStation at different times (e.g. 2 and 5 minutes) on different days, whereas the total station observations collected in the first group were used in all tests. This is because, as discussed in the previous sub-section, if the total-station data were collected with a high level of care, then the overall accuracy is highly dependant on the accuracy of the RTK GPS points.

The combined total-station observations (forwards and backwards) together with all available RTK GPS points (five and three points were) used in Test7 and Test8

respectively. The integrated coordinates resultant from these tests as compared with 'truth' coordinates are illustrated in Figure 7.10.

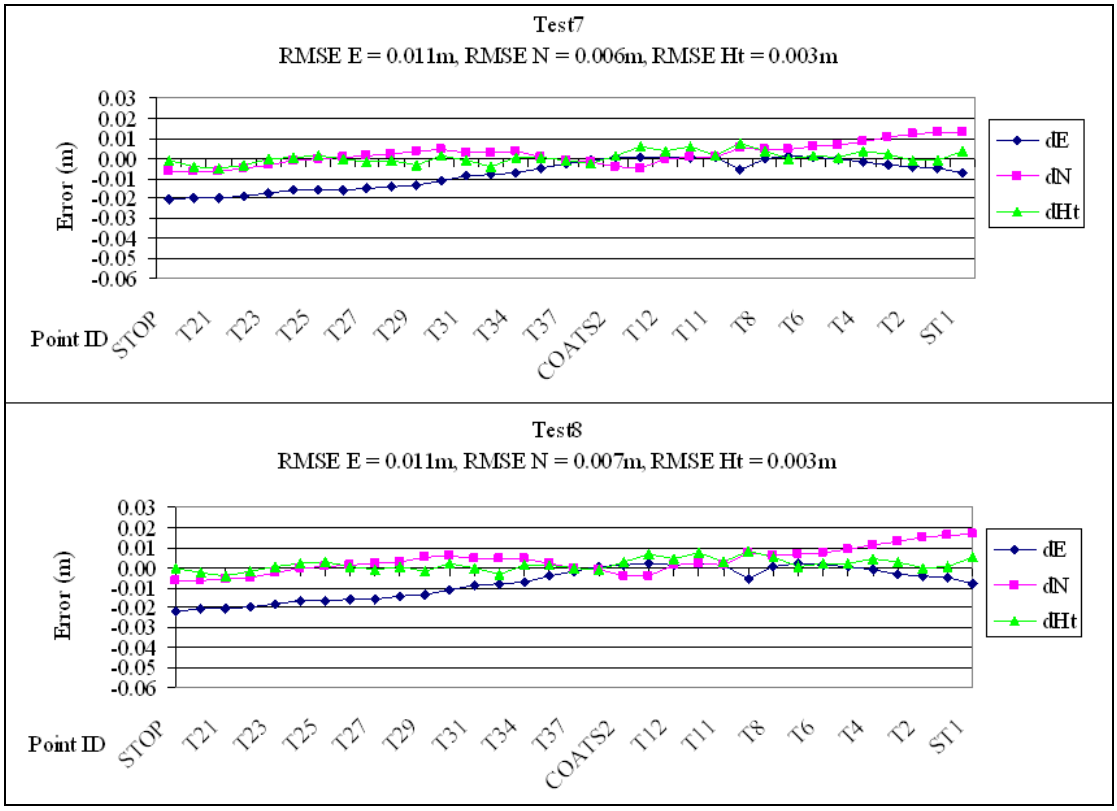

Figure 7.10: Differences between 'Truth' coordinates and CUPT coordinates for Test7 (top) and Test8 (bottom)

The RMSE in Test7 and Test8 are very similar. Comparing the results of Test7 and Test8 (Figure 7.10) with the results of Test5 and Test6 (Figure 7.9), the RMSE of the height coordinate in Test7 and in Test8 is lower than that in Test5 and Test6. However, the RMSE of East coordinate in Test7 and Test8 are slightly higher than those in Test5 and Test6. The maximum East error in Test7 and Test8 is about 0.02m at STOP point. This point was used in both tests and has an RTK fixed solution with about 0.020m error in the East coordinate. As a result of using this point, the integrated solution has approximately similar error. The level of improvement offered by CUPT is constrained by the level of confidence and therefore weight that is given to the GPS observations in the least squares computations. The following points have less error than the STOP points since their RTK GPS points were more precise. The results obtained from this test confirm that the integrated positions are much more accurate than the SmartStation positions (in Test1 and Test2). In

addition, it confirms again that the accuracy of the integrated solution is highly dependant on the accuracy of the RTK GPS points.

The results of Test9 to Test14 are compared with 'truth' coordinates and plotted in figures in Appendix 15. The results of these tests show that an overall RMSE of better than 0.01m was achieved in E, N and Ht and confirm the advantage of the integration of RTK points with total-station observations through the CUPT.

As discussed before, the accuracy of the integrated solution is highly dependant on the accuracy of the RTK GPS points. Therefore, the RMSE obtained from the integrated solution and the RMSE of the RTK GPS points for Test3 to Test14 are summarised in the Figure 7.11.

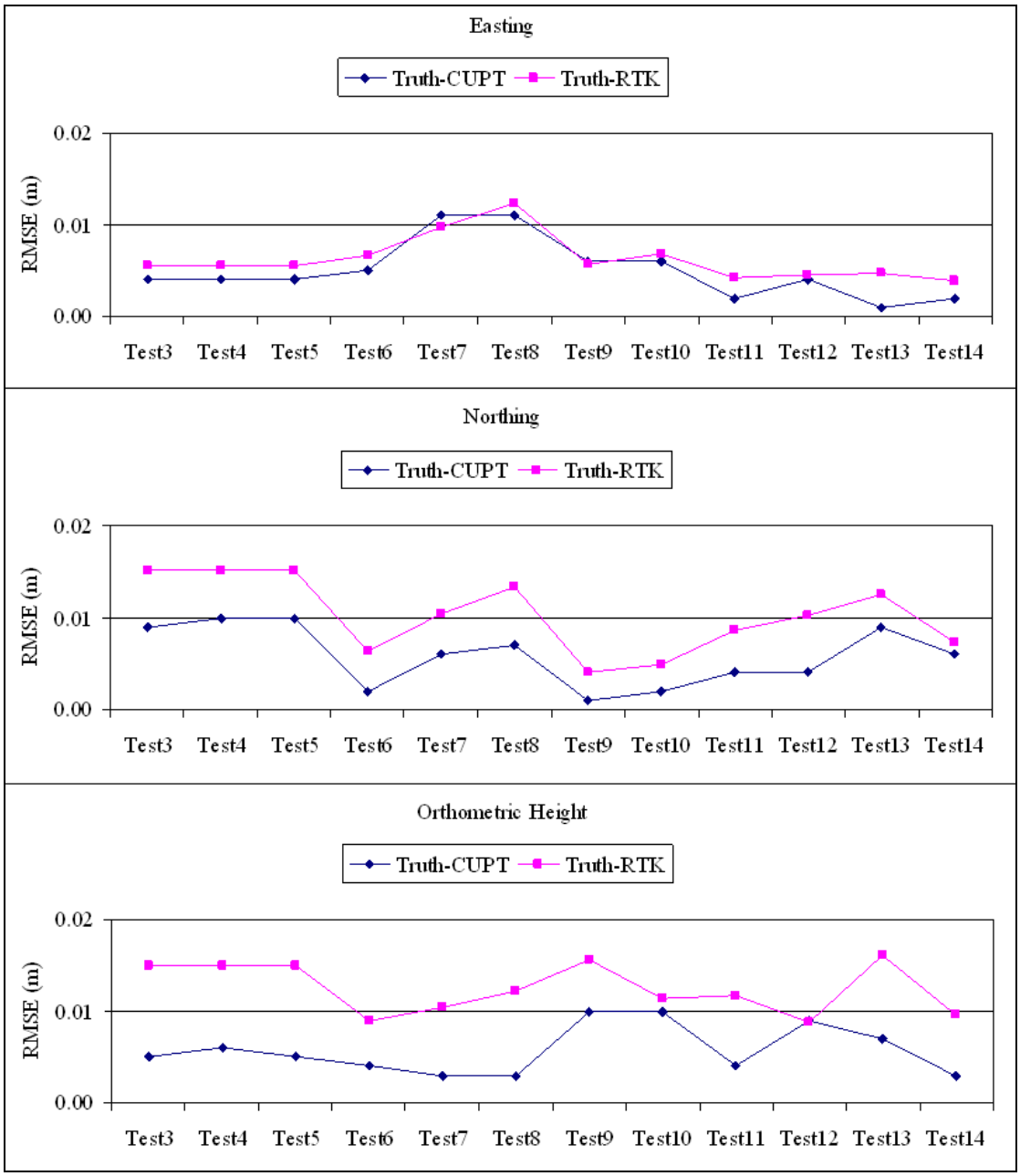

Figure 7.11: RMSE of CUPT solution compared with RMSE of RTK solution in East (top), North (middle) and Height (bottom)

From Figure 7.11, it is clear that, in most tests, the RMSE of the CUPT solution is less than the RMSE of the RTK solution. This means that the integrated solution not only provides a high of level of accuracy and availability for measured points, but also improves the coordinates of occupied points.

Overall from the discussion and the analysis above, the integration of the RTK GPS points with total-station observations through CUPT guarantees 100% of the time

positioning availability and assures a high level of accuracy (RMSE of better than 0.01m in most tests) for the integrated solution.

7.7.4 SmartStation Tests: Integrated Position Uncertainties

Centimetre-level of accuracy for the integrated positions was confirmed in the previous section. This section focuses on the uncertainties of the positions before (a priori STD) and after (a posteriori STD) the integration. Further for analysis the position uncertainties in Test7 (with baseline of about 2.3km between the Network-RTK reference station and the test site) and Test15 (with baseline of about 17.5km) were considered. It is worth reminding that the CUPT report includes the a priori STD for the RTK GPS positions and the a posteriori STD for the integrated positions, whereas the STD of the RTK GPS positions is usually available from the SmartStation. The position uncertainties estimated by different solutions in Test7 illustrated in Table 7.4.

Table 7.4: SmartStation and CUPT Uncertainties in Test7

Point ID	SmartStation (mm)			A-Priori STD (mm)			A-Posteriori STD (mm)		
	E	N	Ht	E	N	Ht	E	N	Ht
STOP	4.60	7.90	10.40	17.96	21.39	38.24	9.22	7.65	10.71
COATS2	4.10	5.60	9.40	18.05	21.47	38.29	6.12	6.73	10.69
COATS1	4.40	5.40	10.30	18.07	21.48	38.29	6.53	6.33	10.68
ST2	4.80	7.00	16.30	18.07	21.48	38.29	5.42	6.45	10.69
ST1	4.30	7.10	14.20	18.09	21.50	38.31	5.85	9.27	10.69
COATS3							6.07	6.96	10.70
T10							5.95	6.18	10.70
T1							5.58	8.74	10.71

The SmartStation STD is estimated from the variance covariance matrix in the SmartStation [Leica-Geosystems-AG, 2005a]. From Table 7.4, the STDs of the SmartStation positions are inconsistent for all points. For example the STD in the Ht component is varying from 9.40mm at COATS2 point to 16.30mm at ST2 point. As discussed before, the RTK GPS positions are affected by other uncertainties which should be taken into account, such as the nominal RTK position precision and the instrument position error. Adding these uncertainties to the estimated STD, the a

priori STD can be calculated. Fairly consistent a priori STD of about 18mm, 21mm and 38mm were estimated for the E, N and the Ht respectively. From the variance covariance matrix of the adjusted coordinates, the a posteriori STD of the integrated points can be estimated. Comparing the a posteriori with the a priori STD in Table 7.4, a noticeable improvement can be seen in E, N and Ht.

To confirm such improvement in the integrated position uncertainties, Test15 was considered. The position uncertainties estimated by different solutions in Test15 are illustrated in Table 7.5. It is worth reminding that the distance between the Network-RTK station and the middle of the Ripley testing area (baseline) is about 17.5 km.

Table 7.5: SmartStation and CUPT Uncertainties in Test15

Point ID	**SmartStation** (mm)			**A-Priori STD** (mm)			**A-Posteriori STD** (mm)		
	E	**N**	**Ht**	**E**	**N**	**Ht**	**E**	**N**	**Ht**
Ref001	9.70	12.10	28.30	25.10	28.59	49.77	13.82	12.40	19.43
Ref002	12.50	13.30	36.70	26.28	29.09	54.97	14.73	14.81	19.44
Ref003	1.60	5.30	4.50	23.24	26.47	41.20	10.68	12.71	19.38
Ref004	18.10	22.80	52.80	29.43	34.54	66.83	9.96	15.56	19.38
Ref006	10.80	19.60	31.10	25.51	32.46	51.39	12.53	13.82	19.38
Ref007	9.30	15.90	24.10	24.80	30.27	47.43	14.91	12.33	19.41
Ref008	16.70	19.30	34.90	28.43	32.20	53.73	12.09	13.64	19.43
Ref005							15.76	15.28	19.39

From Table 7.5, it is very clear that the STDs of the SmartStation solutions are inconsistent and varying, in Ht for example, from 4.5mm for Ref003 point to 52.8mm for Ref004 point. Also, the maximum a priori STD was found to be up to 66.83mm in Ht of Ref004 point. However, to some extent a consistent position uncertainty of about 19.4mm in Ht coordinate was estimated for the integrated solution in the a posteriori STD. Additionally, a significant improvement was found in the a posteriori STD compared with SmartStation and a priori STD.

Overall, the results of 15 tests confirm that the CUPT integration of SmartStation observations (RTK GPS positions and total-station measurements) not only guarantees 100% of the time availability, but also improves the overall accuracy. In most tests, RMSE of better that 0.01m was achieved for the integrated positions.

Similarly, the position uncertainties (a posteriori STD) of the integrated positions improve and become more consistent.

7.8 Robotic Total-Station and an IntegratedPole with Leica 1200 GPS Tests

With the Leica SmartPole it is not possible to collect RTK GPS positions and total-station observations simultaneously. Therefore, a Leica 1200 GPS system attached to a 360° prism were used to create an IntegratedPole.

Unlike the SmartStation, an IntegratedPole can provide several RTK GPS points (if located in a convenient place) when moving from one point to another. These numerous RTK points provide redundant positions that can be used in the integration with total-station observations within CUPT. The following sections discuss the data collection and processing as well as the results and analysis for a robotic total-station and an IntegratedPole with Leica 1200 GPS system.

7.8.1 IntegratedPole with Leica 1200 GPS Tests: Data Collection and Processing

Data were collected using the IntegratedPole along the trial route at the University of Nottingham's Campus. The most challenging environment on the campus, as far as GPS positioning is concerned, was utilised for this experiment so to best replicate worst case scenarios for positioning in urban environments. The campus network points STOP and COATS2 were used as the start and end points for this test. Both the start and end points of the test had a reasonable view of the sky so that RTK GPS positions would be available at the start and end of the network.

Angles and distances data were collected at 1 second intervals using a Leica TPS1200 series robotic total-station. Additionally, RTK GPS data with 1 second interval was collected using Leica's 1200 GPS and SmartNet corrections (the reference station used was RTCM-Ref 0112 which creates a baseline of about

47.7km between this point and the testing area). The robotic total-station was setup on the COATS3 point which has a clear line of sight to all points used during this test. A tripod, for the purposes of eliminating errors due to tilt of a pole, was setup over the STOP point with a 360˚ prism and GPS antenna fixed to the top.

After a few seconds a Network RTK position was available with the Leica 1200 GPS. Data from the GPS and the robotic total-station were recorded simultaneously as long as both GPS and total-station measurements were available. Data was collected on STOP point for a period of about 11 minutes. The start and end times for the collection period were noted. The tripod was then moved to the next point on the network, which is T20 and data was recorded here for a period of 5 minutes. No RTK fixed was possible during this time. On the next 2 points, data was also collected for a period of 5 minutes and again no RTK fixed was available, whereas on all of the subsequent points data was only collected for 2 minutes. This is because from previous experience of this area it is not always possible to obtain RTK GPS positions on the points T20, T21 and T22 and, because of the narrow road between buildings multipath is high. The IntegratedPole was located longer on these points to improve the RTK GPS position. After collecting data on all testing points between STOP and COATS2 the tripod was returned to points T20, T21 and T22 and data was collected for 5 minutes again on each point. On this occasion an RTK fixed was possible and these results have been included in the processing. All the other points used in the test are either in more open areas or are points where no RTK fix is possible.

RTK GPS positions were, therefore, available at 12 of the 19 testing points utilised. Total-station observations were taken to all of the 19 points. The 7 points where a RTK GPS position was not possible were the points T31 – T38. These points are located in a very narrow urban canyon with a very restricted view of the sky. This makes getting positions from GPS extremely difficult. All the other points used in this test have more open views of the sky and have a greater chance of having line of sight to more than 5 well distributed satellites.

7.8.2 IntegratedPole with Leica 1200 GPS Tests: Results and Analysis

As discussed in the data collection sub-section, it was not possible to log RTK GPS data and total-station observations simultaneously using the Leica SmartPole. Therefore, RTK GPS data and total-station observations were collected using two separate instruments. Using two devices could cause differences between the RTK GPS positions and total-station positions in kinematic mode while the two systems are logging observations simultaneously. There are three issues concerned with these differences: total-station internal time, total-station time increments and measurement time. The total-station time depends on its internal clock. Hence, there could be an offset between total-station time and GPS time. The time offset in the SmartPole test was found to be about 4 seconds. This offset could be eliminated by updating the total-station time when it connects to a GPS receiver.

The second issue is the total-station time increment. After analysis the total-station observation's time, it was found that the time increment between the sequence epochs was not constant. For example, a time increment of 1.00 second was found between the points SP0212 and SP0213, then it was found to be equal to 1.08 second between the following points SP0213 and SP0214. The third issue is the measurement time. When the operator presses the measurement button, the total-station will directly measure and record the observations. The time of this measurement could include a fraction of seconds' i.e. time at point SP0212 is 11:09:28.14 (hh:mm:ss.ss). As a result of these issues, there was an offset between the RTK GPS position and total-station position, i.e. an offset of 0.228m between the GPS point RTK0683 and the total-station point SP0213 (Figure 7.12).

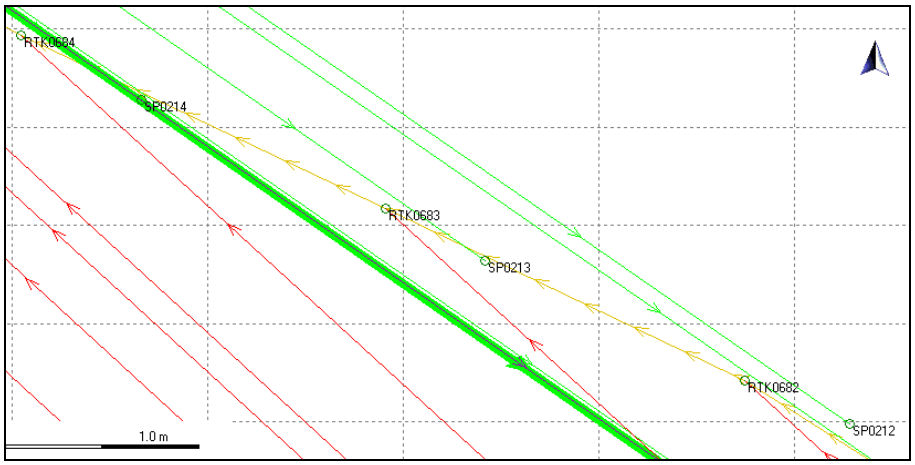

Figure 7.12: Timing differences between RTK GPS position and total-station position when using an IntegratedPole with Leica 1200 GPS

The second and third issues require the manufacturer to resolve. For this research, in order to have a synchronised position for a specific point, a stop & go technique was used. The names of RTK GPS points can be recorded as well as the names of total-station points for any testing point. For instance, names of STOP point were from RTK0001 to RTK0678. In order to use the RTK GPS positions within CUPT, the coordinates for all available points (12 points measured depending on Leica SmartNet) were averaged. Some of these points were found to have a large magnitude of scattering around the mean, i.e. 0.156m for the point T24 in plan coordinates (Figure 7.13).

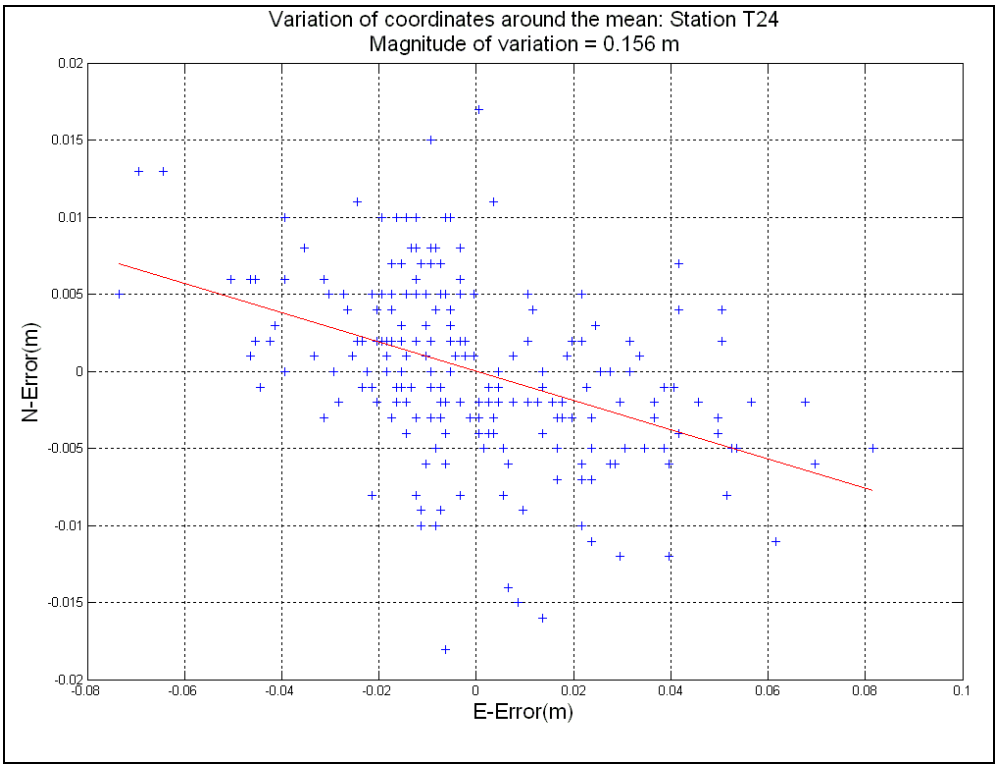

Figure 7.13: Scattering of plan coordinates around the mean for point T24 when using an IntegratedPole with Leica 1200 GPS

For further analysis and assessments of the Network RTK positions in built-up areas, STOP and T21 testing points were considered. STOP point is located at an intersection and had a fairly open sky view and T21 had a limited sky view due to the buildings on both sides of the road. The STD generated by the real-time processor of the Leica 1200 GPS along with the variation of the coordinates around the mean, in E, N and Ht directions for STOP point are demonstrated in Figure 7.14.

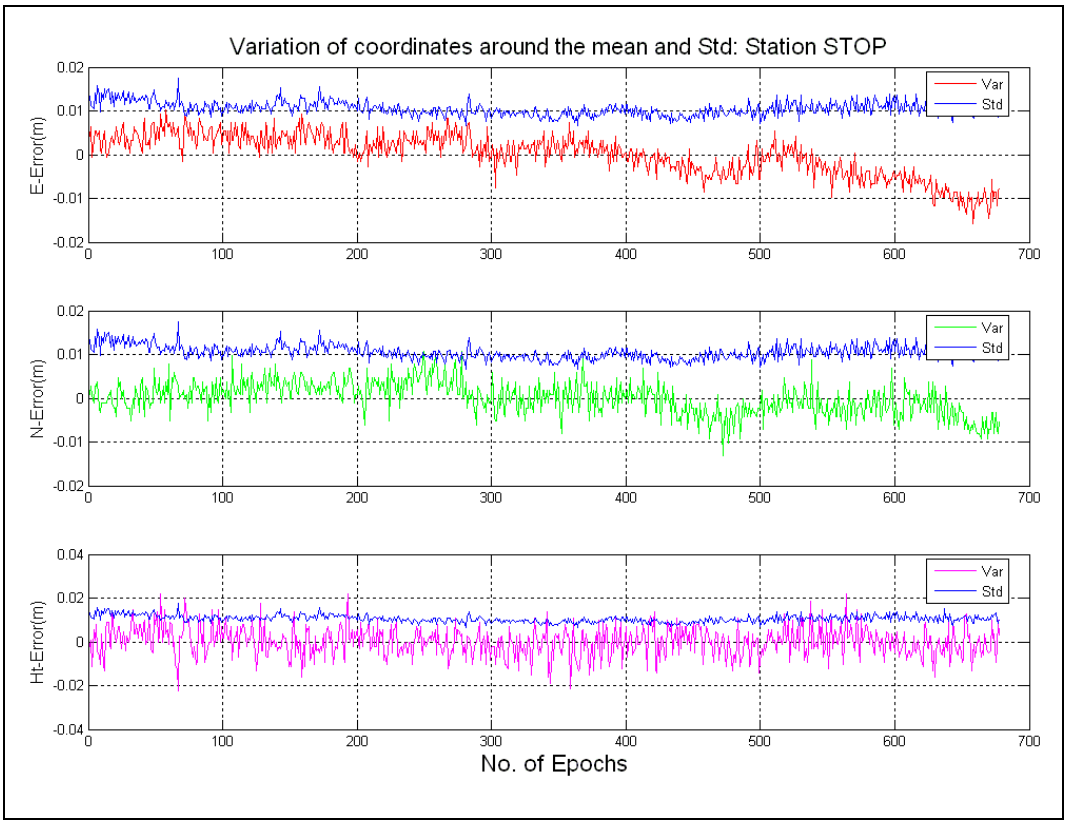

Figure 7.14: Standard deviation and variation of coordinates around the mean in E, N and Ht for STOP point when using an IntegratedPole with Leica 1200 GPS

From Figure 7.14, the variation from the mean in the Ht is centred around zero with no cyclic patterns evident. However, in the E and N some cyclic patterns are evident especially in the latter half of the observation session. Similar to STOP point, the STD along with the variation of the coordinates around the mean of point T21 in E, N and Ht directions are demonstrated in Figure 7.15.

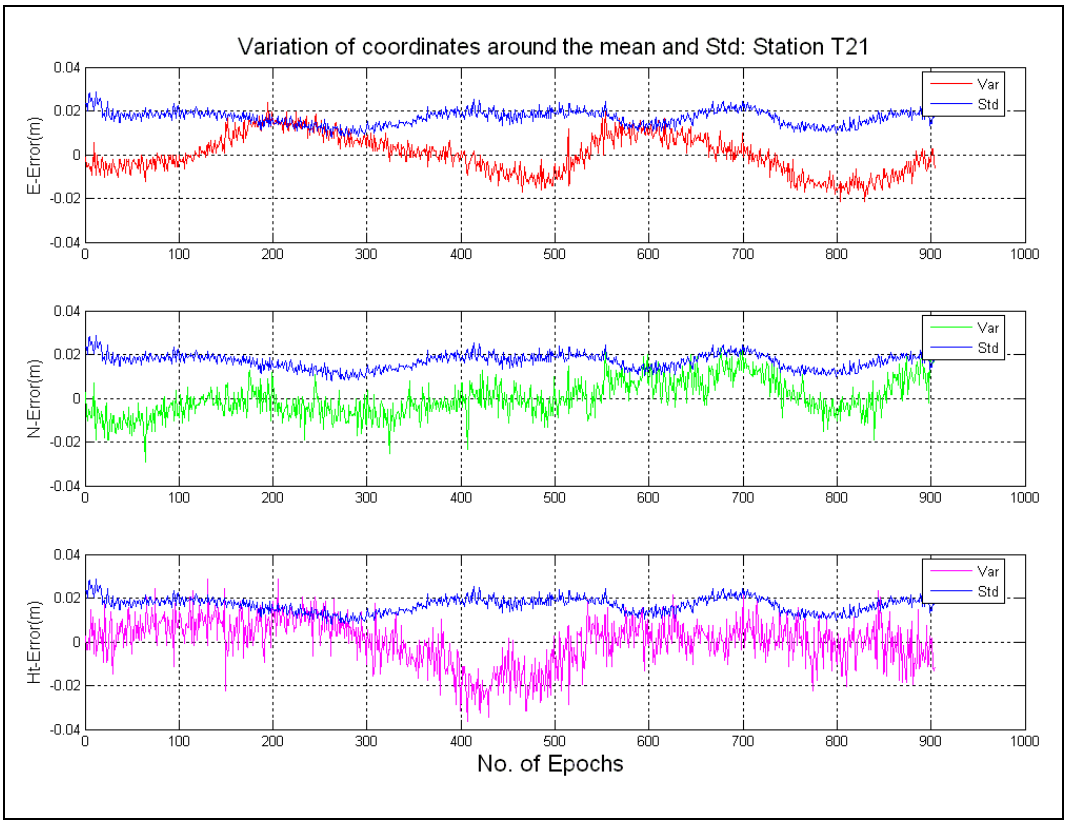

Figure 7.15: Standard deviation and variation of coordinates around the mean in E, N and Ht for T21 point when using an IntegratedPole with Leica 1200 GPS

Figure 7.15 for T21 point compared with Figure 7.14 for STOP point show clearly a cyclic pattern in the variation of the coordinates from the mean as well in the STD of the RTK GPS processing computation. GPS signal multipath due to the surrounding buildings at T21 could be the main source of error for this location. Apart from the cyclic pattern the height variation from the mean is also very noisy with high frequency variations evident. The large baseline of 47.7km between the reference station, which was used in the SmartNet, and the testing area could also introduce some errors. The effect of the large baseline could cause high position uncertainties to be estimated by the software as shown in Figure 7.15.

The magnitude of the variation around the mean for STOP point was found to be about half that for point T21. Further, after fitting RTK GPS positions in lines for all testing points between STOP and COATS3 points, the direction of the fitted lines were found to be parallel to the direction of the buildings in the more open areas. These fitting lines gradually move towards being perpendicular to the buildings the closer to the buildings that the points were (Figure 7.16).

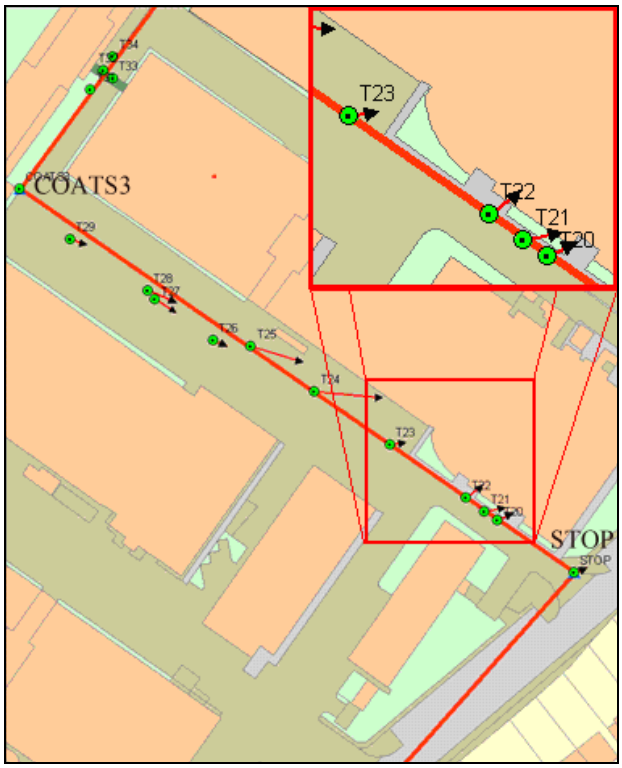

Figure 7.16: Direction of fitting lines for RTK GPS positions when using an IntegratedPole with Leica 1200 GPS (© OS MasterMap)

A reason for the direction of the errors could be from the satellites geometry. As the positions get closer to the buildings, multipath becomes more of an issue, and this most likely causes the positional errors to be perpendicular to the buildings.

Comparing the average of the RTK GPS coordinates with the truth coordinates, an RMSE of better than 0.018m was demonstrated with a maximum error of 0.032m in plan coordinates and 0.032m in height (Figure 7.17).

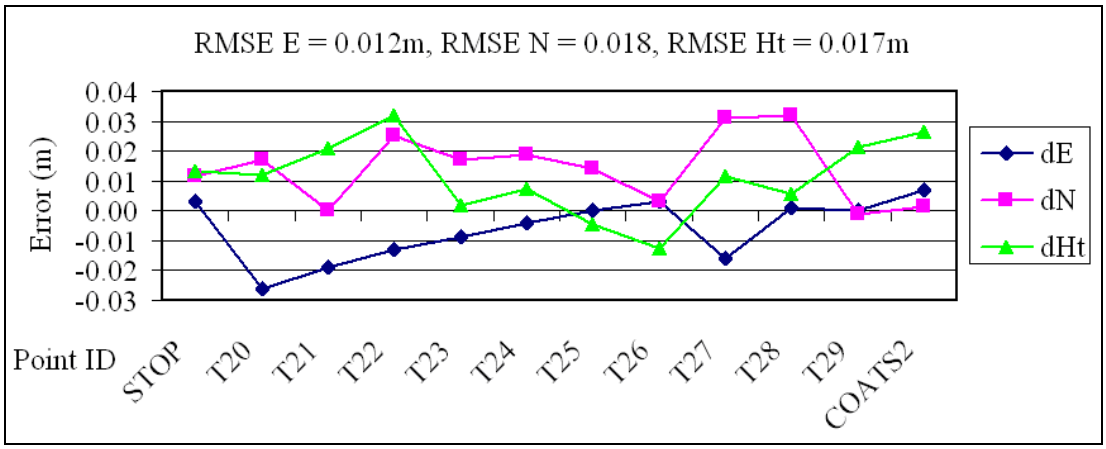

Figure 7.17: Differences between 'Truth' coordinates and average RTK GPS coordinates when using an IntegratedPole with Leica 1200 GPS

All available RTK GPS points together with robotic total-station observations (average observations for all testing points including those points with unavailable GPS position) were integrated using CUPT. Integration results showed that the maximum error ellipse was found to be 0.06m for the CUPT coordinates. Besides, when the CUPT coordinates are compared with the truth coordinates, an RMSE of better than 0.017m was achieved with a maximum error of 0.029m in plan coordinates and 0.023m in height (Figure 7.18).

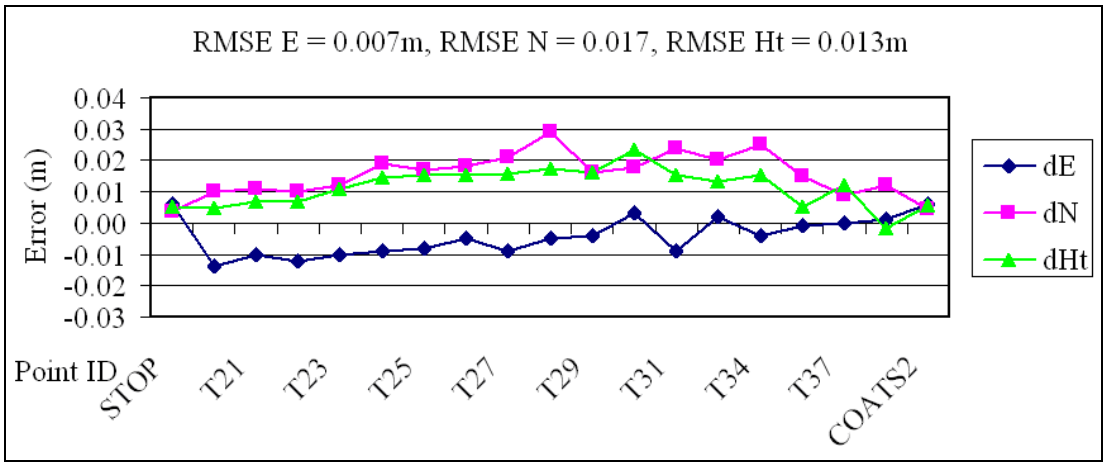

Figure 7.18: Differences between 'Truth' coordinates and CUPT solution using all RTK GPS points for IntegratedPole with Leica 1200 GPS test

Comparing the RTK GPS positions with the CUPT positions, a noticeable position improvement for the CUPT coordinates was found in several points i.e. Easting in T20 and the Height in T22. As mentioned before, the level of improvement offered by CUPT is constrained by the level of confidence and therefore weight that is given to the GPS observations in the least squares computations. Confidence limits of about 0.02m for plan coordinates and about 0.04m for height components were used in the CUPT processing.

Using RTK GPS positioning only, centimetre level positions were available for 12 out of the 19 points surveyed. This is because points T31 – T38 lie along a very narrow single lane urban canyon making satellite visibility to four or more satellites difficult to maintain. However, using the CUPT technique centimetre level positions were obtainable for all 19 points.

More position improvement with less maximum error for the CUPT coordinates was achieved after eliminating seven RTK GPS points with high STD (only five RTK points were used in the solution). More RTK points will provide greater redundancy which could help for error detection and correction. However, the quality of the RTK points is a major issue which as a result can reduce the overall accuracy for the combined positions. RMSE values of better than 0.012m with a maximum error of 0.023m for plan coordinates and 0.022m for the height were verified for the combined coordinates (Figure 7.19).

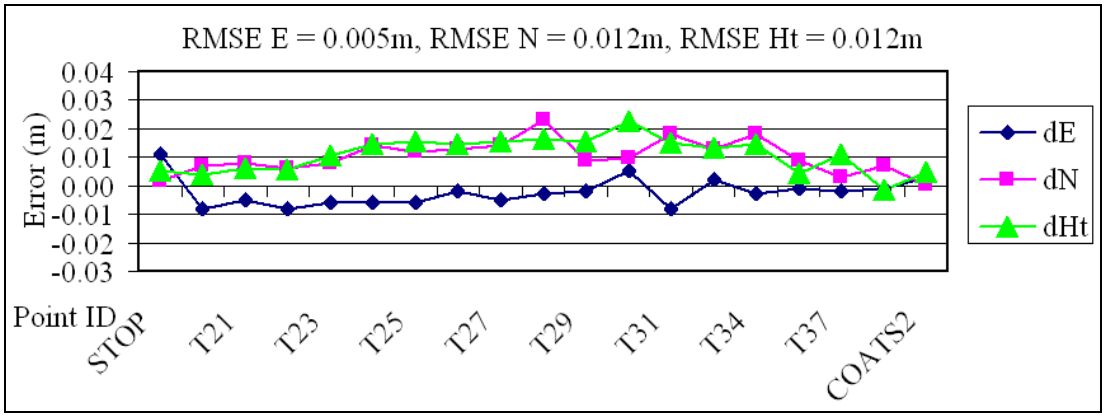

Figure 7.19: Differences between 'Truth' coordinates and CUPT solution using five RTK GPS points for IntegratedPole with Leica 1200 GPS test

Using three RTK points, an RMSE value of better than 0.012m in with a maximum error of 0.024m was calculated in plan and an RMSE value of 0.024m with a maximum of 0.034m was calculated for the heights (Figure 7.20).

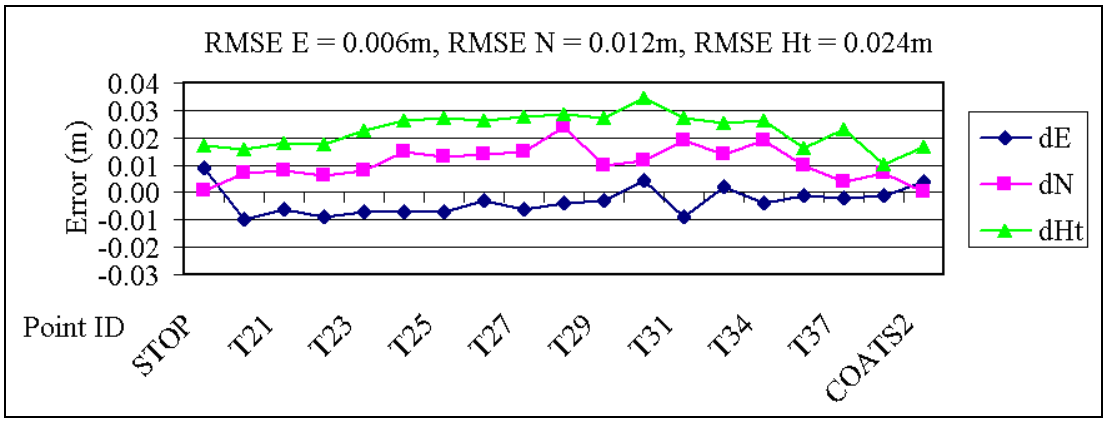

Figure 7.20: Differences between 'Truth' coordinates and CUPT solution using three RTK GPS points for IntegratedPole with Leica 1200 GPS test

These results indicate the high accuracy for the integrated positions. Also, they show the changes of the accuracy of the CUPT solution according to the changes in the number of RTK GPS points and their accuracies. More RTK points provide redundancy, which could help for error detection and correction. However, the quality of the RTK GPS points is a major issue. When using RTK GPS positions with high STD, the overall accuracy of the combined solutions could be reduced. As an example, an RMSE of 0.017m was obtained when using 12 RTK GPS points on the IntegratedPole with Leica 1200 test. This RMSE drooped to 0.012m after removing points with high STD and using only five RTK GPS points.

7.9 Robotic Total-Station and an IntegratedPole with High Sensitivity GPS Tests

HSGPS has the ability to track GPS signals that are much weaker than normal GPS receivers. This means that the availability of GPS positions is increased; the downside of this is that the quality of these measurements can be decreased [Hide et al., 2006].

An example of a single frequency HSGPS receiver is the SuperSense GPS receiver which has been utilised in this research and is based on the U-Blox's high performance ANTARIS 4 technology. The advantages of using this piece of hardware are that it is very cheap (e.g. cost of about £150) and has very low power consumption. In addition, it includes a more accurate time base (TCXO) and additional software, providing up to 10dB additional sensitivity, which allows these receivers to be used in challenging environments [u-blox-AG, 2007].

7.9.1 IntegratedPole with HSGPS Tests: Data Collection and Processing

In addition to GPS data being collected using the IntegratedPole with a Leica 1200, measurements were recorded along the same area of the campus network using an IntegratedPole with a Ublox HSGPS receiver. The Ublox receiver was connected to a Thales L1 GPS antenna and then attached to a tripod. To obtain an integer ambiguity fixed, the receiver was initialised over STOP point for 10 minutes. The tripod was

then moved along the campus network stopping at each testing point for several minutes as done previously. Data were recorded from both the Total-station and the GPS receiver at 1 second intervals.

In order to post-process the HSGPS data, the Ublox binary file was firstly converted to RINEX format using teqc software (version 25 June 2007). The RINEX file was then modified, using special software developed by the author, by adding headers to specify the static and the kinematic epochs. The modified RINEX file was then post-processed using Leica Geo Office. A permanent dual frequency GPS receiver, recording at 1 second intervals was used as the reference station, creating a baseline of approximately 350 metres. Unfortunately, only the starting point resolved with phase solution. This is because every time the ambiguity fixed was lost; a new initialisation has to be done. To overcome this, the RINEX file was modified by adding headers to specify the start point epochs as static and the rest of the file as kinematic. Using this technique, it was possible to have phase solution for the starting point as well as for several epochs located in fairly open view of the sky.

The tests using HSGPS were performed on three separate days. On all three occasions data was collected first on STOP for a period of 10 minutes. During the first trial, data was collected on all other points for a period of 2 minutes except for points T20, T21 T22 where data was collected for 5 minutes as in the IntegratedPole with Leica 1200 GPS test and also for 6 minutes on COATS which is the last station on the network. Only 15 of the testing points on this part of the network were utilised in this test due to some of the points being obstructed. Using the above technique to post-process the HSGPS data, phase solutions were achieved on five of the 15 points.

On the second day a similar test was performed using HSGPS using the same method as in the first test as described above. On this occasion, it was possible to collect HSGPS data on all testing points. However, a phase solution was only achieved on the first point (STOP point) when the HSGPS data was post-processed using the previous technique. This was possibly due to the way the satellites were distributed at this specific time.

The test performed on the third day was done at a time that, from previous experience, was known to have more satellites available for data collection. On this

occasion it was decided to stay on each point for a period of 2 minutes but to stay on points T23, T26, and T36 for a period of greater than 6 minutes. This time period was decided as that is the amount of time required to obtain a phase solution in static mode when using the Ublox HSGPS receiver and processing with LGO. These points are regarded as points with a fairly open view of the sky compared with the point immediately before them on the network. It was hoped that by collecting a greater amount of data at these selected points that Phase solutions could be recovered if it had been lost. Data were collected on the point COATS2 for a period of 10 minutes. A phase solution was available on 11 of the 19 points utilised in this survey when the HSGPS data was post-processed in the technique described previously. The eight points that were not available as a phase solution were in the areas that had the most limited view of the sky.

It was noticed that when the GPS was in an area with a reasonable view of the sky the strength of the satellite signals used in the solution were all greater than 35dB, i.e. each of Satellite Vehicle (SV) 30 and SV 5 has signal strength of 53dB (see Figure 7.21). The lowest signal being used is 38dB on SV 7. In Figure 7.21**,** satellites green in colour are used in the solution , cyan in colour are available for use in the solution but are not used, blue in colour have a satellite signal but are not available for use and red in colour have no signal available.

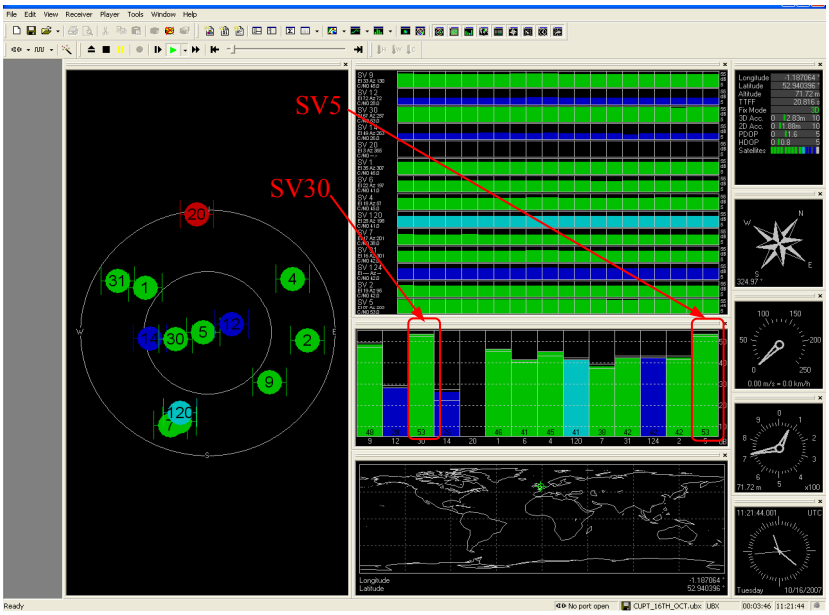

Figure 7.21: Ublox monitoring interface shows high signal strength in HSGPS test

In an area with a more restricted view of the sky, satellites had much weaker signal strengths of 35dB or below, i.e. SV 24 has signal strength of 32dB (see Figure 7.22), could be used in the position solution.

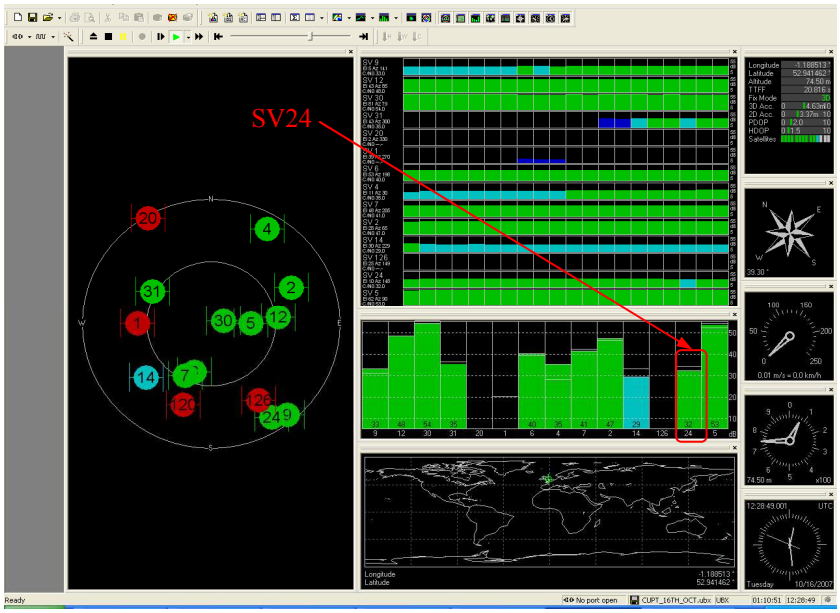

Figure 7.22: Ublox monitoring interface shows low signal strength in HSGPS test

These lower signals have either propagated through buildings or are reflected signals and probably degrade the position. This could be a contributing factor to why a phase position is not achieved in areas with a more restricted view of the sky.

7.9.2 IntegratedPole with HSGPS Tests: Results and Analysis

As mentioned in the data collection and processing section, since HSGPS is a single frequency receiver a special technique was used to collect and post-process the HSGPS data. The output Cartesian coordinates from LGO, from the third day of observations, were converted to OSGB36 grid coordinates and superimposed on the OS MasterMap (Figure 7.23).

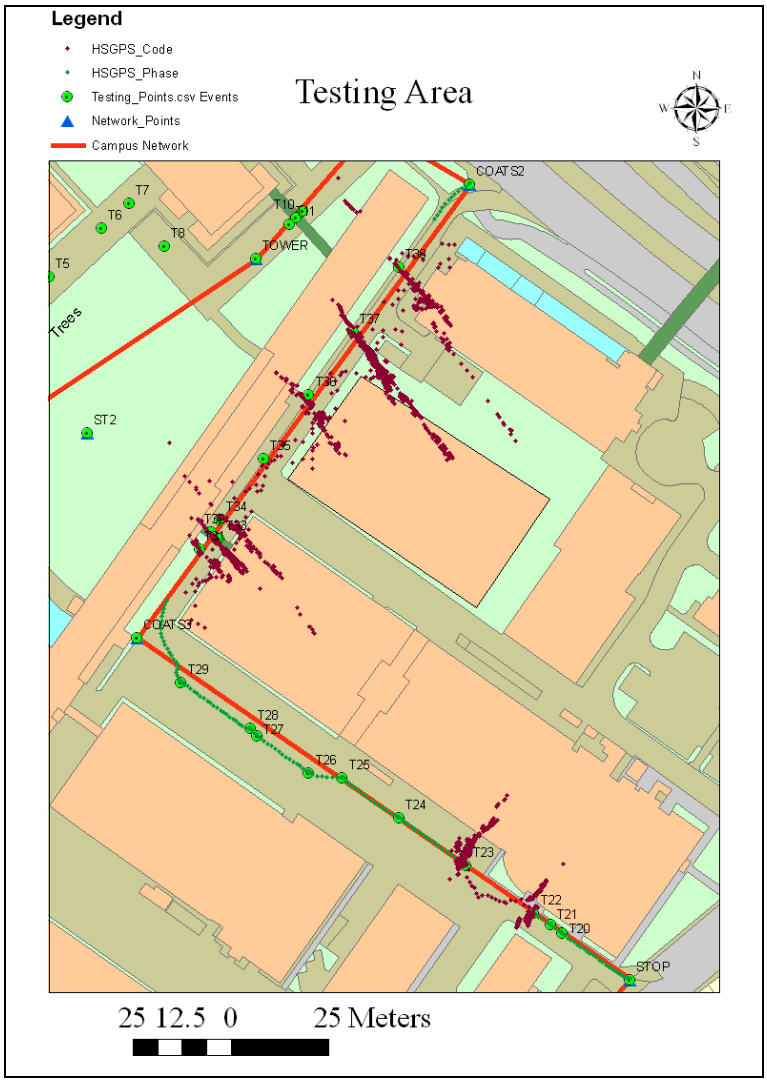

Figure 7.23: HSGPS phase and code solutions (Copyright © OS MasterMap)

From Figure 7.23, several testing points, 11 out of 19 points, were calculated with phase solution. For further analysis on the quality of the phase solution of the HSGPS in a built-up area, T21 point show only a small scattering around the mean i.e. 0.042m (Figure 7.24). The magnitude of the scattering around the mean of this point is less than that in the previous test using the Leica 1200 GPS. The reason could be due to post-processing the HSGPS data using the IESSG as a base station with a short baseline, about 0.5km between IESSG and the testing area.

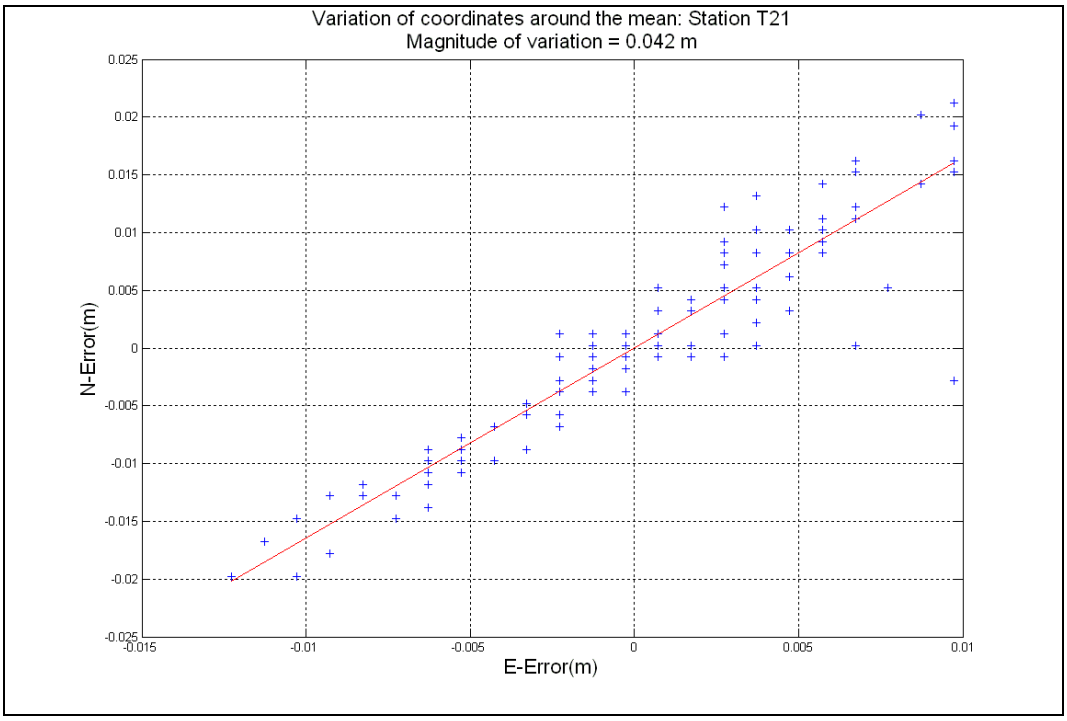

Figure 7.24: Scattering of plan coordinates around the mean for point T21

Furthermore the HSGPS coordinates with phase solution were compared with truth coordinates. RMSE of better than 0.022m was achieved for the phase HSGPS positions with a maximum error of 0.049m for plan coordinates and 0.052m for height at T23 testing point (Figure 7.25).

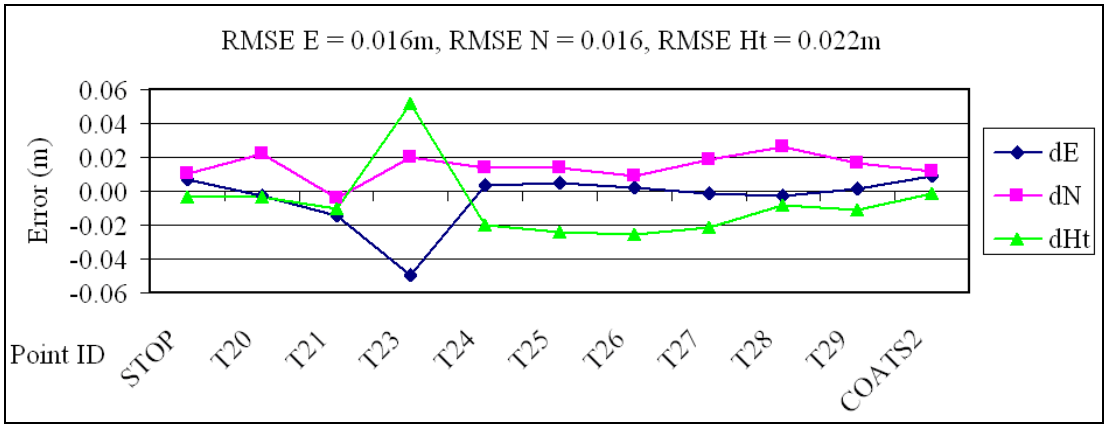

Figure 7.25: Differences between 'Truth' coordinates and HSGPS phase solution coordinates in the IntegratedPole with HSGPS test

When the phase HSGPS positions were combined with total-station observations using CUPT, an RMSE of better than 0.017m with a maximum error of 0.029m for plan and 0.020m for the heights was achieved (Figure 7.26).

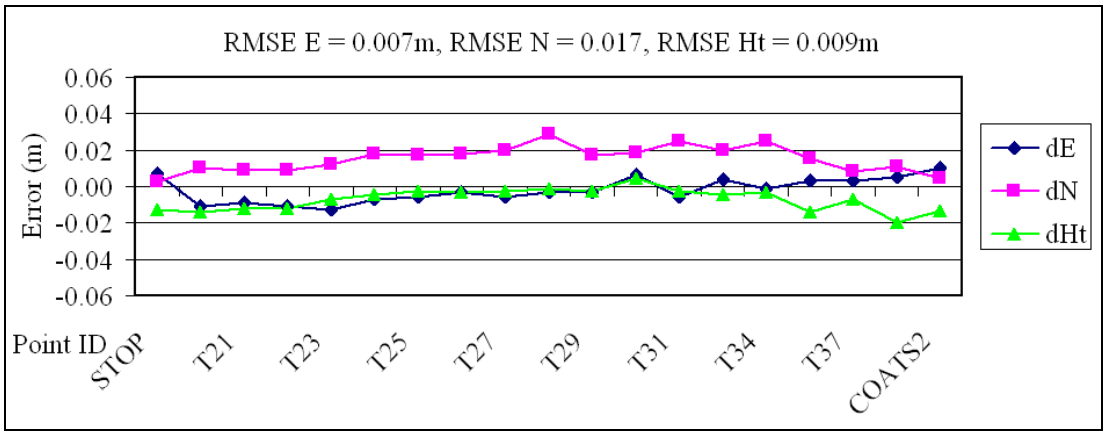

Figure 7.26: Differences between 'Truth' coordinates and CUPT solution using all available points with phase solution in the IntegratedPole with HSGPS test

A noticeable improvement can be seen for the CUPT solution in Figure 7.26 compared with HSGPS phase solution coordinates Figure 7.25 especially at point T23. The previous combination was repeated using five points and three points of HSGPS phase solution (Figure 7.27). The results of the integrated positions show that RMSE of better than 0.02m and 0.021m were achieved when five and three points with phase solution were utilised respectively.

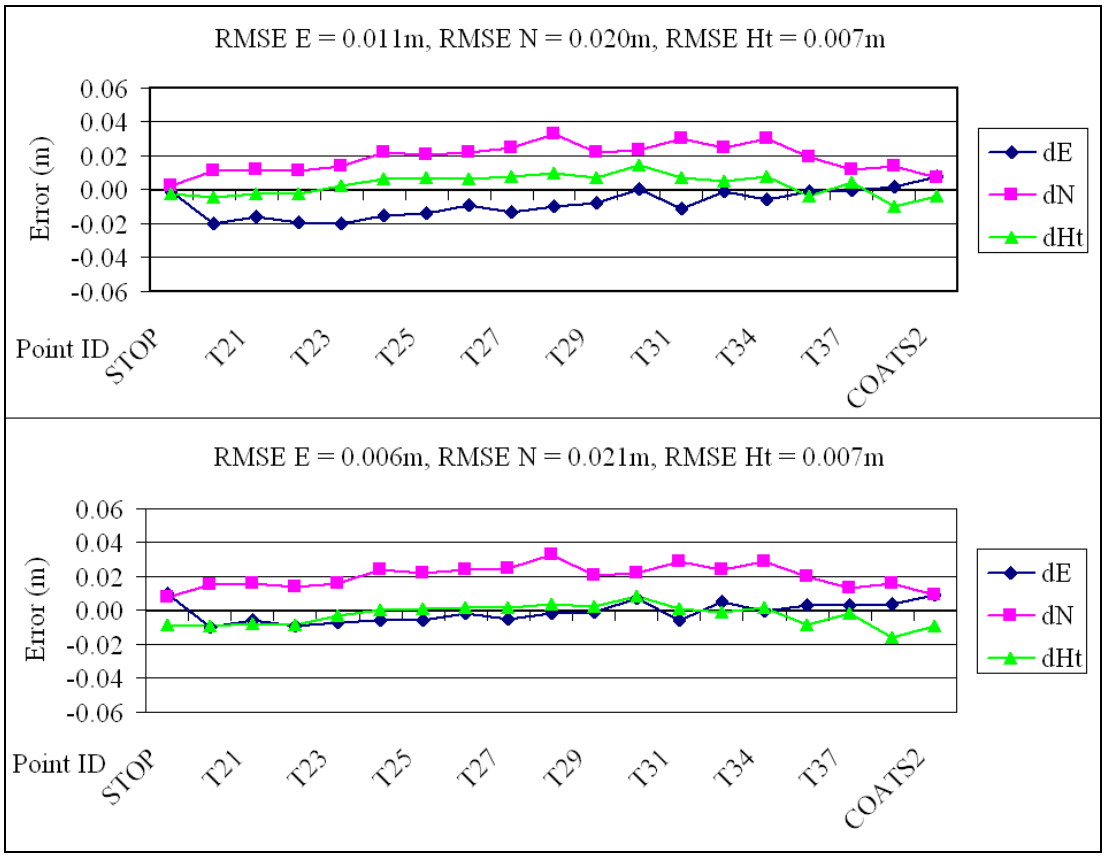

Figure 7.27: Differences between 'Truth' coordinates and CUPT solution using five points (top) and three points (bottom) with phase solution in the IntegratedPole with HSGPS test

Overall, high positions accuracy, better than 0.021m, were obtained for the integrated points of total-station observation with HSGPS phase solution points. However when HSGPS was utilised, a planning for the best observation time with high number of satellites is essential. In addition, stopping for few minutes in a fairly open area can be an advantage for ambiguity recovery.

7.10 Summary

This chapter introduced the Continuous UPdating Technique (CUPT) developed by the author for integrating loosely coupled RTK GPS positions with total station observations (distances and angles). The integration of these observations being performed through a combination of stochastic and functional least squares models.

This Chapter also presented the results of various tests conducted using CUPT in three configurations. The first one used the Leica SmartStation along the trial route

on The University of Nottingham's Campus, as well as in Ripley. The results of 15 tests confirmed that the integration between SmartStation observations (RTK GPS positions and total-station measurements) not only guarantees 100% of the time availability, but also improves the overall accuracy of the integrated positions. In most tests, RMSE of better that 0.01m was achieved for the integrated positions. However, the integration results also showed that the quality of the RTK GPS points is a major issue that affects the overall accuracy of the integrated positions.

The second combination used an IntegratedPole equipped with a dual frequency Leica 1200 GPS receiver. The combination of total-station observations (obtained from a robotic total-station) with different number of RTK GPS points through CUPT was analysed. Since there were position differences between the RTK GPS and total-station positions in kinematic mode, position synchronisation was obtained by collecting simultaneous data in stop & go mode. It was concluded that, RTK GPS positioning in built-up areas can suffer from a large amount of scattering of the RTK GPS coordinate around the mean, which could be due to multipath errors from the surrounding environment, i.e. buildings and trees. In addition, the large baseline of 47.7km between the reference station, which was used in the SmartNet Network RTK, and the testing area could also introduce some errors. When fitting RTK GPS positions in lines, it was found that the direction of the fitting lines were parallel to the direction of the buildings in more open environments and perpendicular to the buildings in environments with a more restricted view of the sky. This effect is likely to be due the satellite geometry and GPS signal multipath of the buildings.

The combination of total-station observations with different number of RTK GPS points through CUPT was also investigated. For example, 12, five or three RTK GPS points were used in the IntegratedPole with Leica 1200 GPS tests. More RTK GPS points provide redundancy which can help error detection and correction. However, the quality of the RTK GPS points remains a major issue.

The third configuration used an IntegratedPole equipped with a single frequency High Sensitivity GPS (HSGPS) receiver. When HSGPS is utilised, a planning for the best observation time with high number of satellites was found to be necessary before the data collection. In addition, stopping for few minutes in a fairly open area

could be an advantage for ambiguity recovery. RMSE of better than 0.022m was achieved for the phase HSGPS positions, and RMSE of better than 0.017m was achieved for the integrated coordinates, although this was based on the use of a short baseline.

Finally based on the results of the different tests, it was shown that CUPT was able to maintain centimetre level of accuracy for the integrated points as well as to improve the uncertainties of the integrated positions. Additionally, it showed improvement for the integrated positions when compared with RTK GPS, especially for heights. However, the level of improvement offered by CUPT is constrained by quality of the RTK GPS positions.

Chapter 8: Conclusions and Recommendations

8.1 Conclusions

In the UK there is a massive network of buried pipes and cables - a combination of water, sewage, gas, electricity and drainage - where the exact positions of many of them are either unknown or very inaccurate (up to several metres in error). This means that locating them in order to carry out maintenance is a difficult task. Hence, pipes and cables must be located accurately to ensure that streetworks projects are carried out quickly, efficiently and safely.

The aim of this thesis was to research various means of improving the position accuracy and availability for positioning underground utilities in built-up areas through a GNSS based system, integrated with other systems such as INS and total-stations. The reliability and accuracy of the overall positioning system was an underpinning issue, with a need for positioning in urban canyons with an accuracy down to the centimetre level.

This thesis has presented research on the development and testing of various GNSS-based positioning techniques that could be used to position pipes and cables in difficult environments such as urban canyons. This includes several novel approaches, developed by the author during the research, to overcome the limitations of current positioning techniques. The following is a summary of the main conclusions resulting from this research.

A new testing facility was established at The University of Nottingham that encompasses different obstruction levels, comparable to those which could be found in city centres. This include a network of stations and testing points a long a trial route on the University of Nottingham's Campus, which were coordinated to a few millimetres and acted as 'truth' for all tests.

The results of testing the use of current GNSS satellite constellation's (GPS and GLONASS) along the Campus trial route proved that a GPS and GLONASS solution can improve the availability of phase fixed solutions, by increasing the number of satellites compared with a GPS-only solution. However, there were still large areas of degraded positioning accuracy. Therefore, a new GIS tool called the Urban Canyon GNSS Simulation (UCGS) was developed by the author to simulate current and future GNSS satellite constellations within a 3D city model (either TIN or raster). Critical to this was the process developed by the author for the addition of buildings to a bare-earth TIN, in a hierarchical way, to accurately represent the obstructions seen in the real world in any simulation.

Using the UCGS tool, two simulations were carried out in two different environments using two different datasets as 3D models. When, different GNSS simulations were carried out using a 3D model of the University of Nottingham Campus (Campus simulation), these simulations gave evidence that using more than one GNSS constellation will significantly increase the availability of GNSS positions in urban environments. However, although the minimum number of satellites available when using a combination of GPS, GLONASS, Galileo and COMPASS was found to be equal to eight and nine satellites (in the Morning and the Afternoon simulations respectively), a PDOP value of less than 6 was still not guaranteed all of the time. As a result, position availability using the criteria of five or more satellites with PDOP value of 6 or less for centimetre level accuracy, is not guaranteed 100% of the time as the distribution of these satellites may still restrict the times of day when a centimetre level position is available.

To overcome the limitations of using GNSS alone, a GNSS/INS combined system was developed and tested. A Multi Step Integration Technique (MSIT) was developed by the author as a methodology for the GNSS/INS data collection and processing. MSIT is based on the integration of GNSS/INS data collected in stop & go mode (stopping for few minutes during GNSS outages and moving when the GNSS position is available), with the GNSS data being post-processed independently, i.e. using LGO, to produce phase fixed positions.

Based on the results of different tests, it was clear that position availability 100% of the time can be guaranteed in all environments by using GNSS integrated with INS. Also, it was found that high position accuracy to a centimetre level, was achieved in all tests along the trail route, when GPS positions with phase solution were available. When compared to the use of Applanix POSRS standard solution, it was found that the MSIT offers higher positional accuracy, especially over large GPS outage areas where accuracy is normally reduced. For example, a maximum error of about 1.65m in the East coordinate was found in one test when using Applanix POSRS but when the same data post-processed using the MSIT this was reduced to 0.15m. Such accuracy is clearly still not sufficient to meet the requirement of centimetre level positioning, although the MSIT could be used in the future when more satellite constellations will be available, i.e. the four GNSS constellations, to overcome the positioning difficulties under or near bridges with short outages.

Following the development and testing of a GPS integrated with INS, the use of GNSS integrated with a total-station was integrated as another alternative for positioning buried assets in any environment. A new software called Continuous Updating Technique (CUPT) was developed by the author to combine RTK GNSS positions with total station observations (distances and angles). A loosely coupled integration of these observations is performed through building an appropriate stochastic and a functional least squares model. Three integration approaches (direct, indirect and network integration) were tested for a GPS/total-station integration through CUPT. In the direct method, two RTK GPS points are integrated with multi total station observations being observed directly between them. in the indirect method two invisible RTK GPS points are integrated together with multiple total-station measurements observed indirectly by means of using one/or more total-station setups between these points. The network integration is used when three or more RTK GPS points as well as direct and indirect total-station observations are available. This provides redundant RTK GPS points which could assist in error detection and correction within the network.

The results of direct and indirect integrations showed that CUPT was successful in making a significant improvement in the height component for RTK GPS points with low accuracy, while maintaining plan coordinate accuracy. For example, a height

accuracy of -0.029m was improved to -0.008m after the direct integration, and a height accuracy of 0.014m was improved to 0.003m after the indirect integration.

To test the GNSS/total-station network integrated solution, three configurations were tested. The first one used the Leica SmartStation along the trial route on The University of Nottingham's Campus. The results of 15 tests confirmed that the integration between SmartStation observations (RTK GPS positions and total-station measurements) using CUPT not only guarantees availability 100% of the time, but also improves the overall accuracy of the integrated positions. In all tests, an RMSE of better that 0.011m was achieved for the integrated positions. However, the integration results showed that the quality of the RTK GPS points is a major issue that affects the overall accuracy of the integrated positions.

The second configuration used a robotic total station and an IntegratedPole equipped with a Leica 1200 dual frequency GPS receiver receiving network RTK corrections as part of SmartNet. Since there were position differences between the RTK GPS and total-station positions in kinematic mode, position synchronisation was obtained by collecting simultaneous data in stop & go mode. Using RTK GPS positioning only, it was found that centimetre level positions were only available for some of the points. For example 12 points, located in fairly open areas, out of a total of 19 points were available as some points lie in the obstructed urban canyon making satellite visibility to four or more satellites difficult to maintain. However, when using the CUPT technique, it was verified that centimetre level positions were obtainable for ALL required points with RMSE of 0.012m to 0.017m typical. The combination of total-station observations with different numbers of RTK GPS points (i.e. 12, five or even three) through CUPT was also investigated and based on the analysis of these combinations, it was found that more RTK GPS points provide redundancy which can help in error detection and correction. However, the quality of the RTK GPS points is still a major issue.

The third configuration used an IntegratedPole equipped with a single frequency High Sensitivity GPS (HSGPS) receiver. The results of different HSGPS data collections showed the differences in the availability according to the observation time and hence indicated the need for planning before the data collection when using

HSGPS. In addition, stopping for few minutes in a fairly open area is an advantage for ambiguity recovery. An RMSE of better than 0.022m was achieved for the phase HSGPS positions, and an RMSE of better than 0.017m was achieved for the integrated coordinates. Similarly, the results of the integrated positions showed that RMSEs of better than 0.02m and 0.021m were achieved when 5 and 3 HSGPS points with phase solution were utilised respectively.

To summarise the conclusions with regards to positioning buried utilities in urban canyons:

- Using more than one GNSS constellation will significantly increase the availability of GNSS positions in urban environments. However, the simulation using the UCGS tool developed by the author shows that the position availability using the criteria of five or more satellites with a PDOP value of 6 or less for centimetre level is not guaranteed 100% of the time, even when using a GNSS based around four constellations.
- Considering the results of the combined GNSS/INS system, the position availability was guaranteed 100% of the time in all environments. However, the accuracy is not enough to meet the research requirement.
- The best results were offered when using GNSS integrated with a total-station through the CUPT developed by the author with position availability to a centimetre level of accuracy guaranteed 100% of the time in all environments. This meets the research requirement and paves the way for such techniques to be widely used in the future with a SmartStation or the total-station and IntegratedPole.

8.2 Recommendations

Even though the UCGS software shows the number of satellites, and their geometry that might be available in the near future, it does not take the effects of multipath into account, which will affect the quality of the GNSS positions. Furthremore, it does not consider signals that pass through vegetation. These could be added to improve the reliability of the simulation.

The ideas behind UCGS could also be taken forward in terms of multipath detection. For example, if a receiver was to contain a 3D city model it could use this to compare simulated satellites with tracked satellites and reject any observations that are from satellites that should not be visible.

The GNSS/INS integration could be improved by using the tightly coupled integration. So I highly recommend the development of KinPos software, which is available at the IESSG, to perform such integration and enhance the noisy GNSS data that could be collected in built-up areas.

The concept used for the CUPT software could be further developed to support real time applications and could be taken by Leica, for example, and embedded in future updates of SmartStation and SmartPole.

More trials with HSGPS would be useful for further analysis as they are such cheap devices. Also, HSGPS and total station could be subject to tightly coupled integration by using the total station observations to accelerate the integer ambiguity fixing of HSGPS.

References

ANON (2007) Radical Change in the Air for GLONASS. *GPS World.*

APPLANIX-CORPORATION (2005) POS RS User Guide. Canada.

ARNOTT, D. & KEDDIE, A. (1992) Data Capture – The standards and procedures utilised within Northumbrian Water Group. *Association for Geographic Information (AGI) conference.* Birmingham, In Proceedings of the Association for Geographic Information (AGI) conference. 24-26 November 1992.

BECK, A., COHN, A. G., SANDERSON, M., RAMAGE, S., TAGG, C., FU, G., BENNETT, B. & STELL, J. (2008) UK Utility Data Integration: Overcoming Schematic Heterogeneity. *in the proceedings of GeoInformatics 2008, 11-13th of June 2008.* Potsdam, Germany.

BECK, A. R., FU, G., COHN, A. G., BENNETT, B. & STELL, J. G. (2007) A framework for utility data integration in the UK. IN RUMOR, M., COORS, V., FENDEL, E. M. & ZLATANOVA, S. (Eds.) *Urban and Regional Data Management - UDMS 2007 Annual.* London, Taylor & Francis.

BIASION, A., CINA, A., PESENTI, M. & RINAUDO, F. (2005) An Integrated GPS and Total Station Instrument for Cultural Heritage Surveying: The Leica SmartStation Example. *The International Committee for Documentation of Cultural Heritage (CIPA) 2005 XX International Symposium. volume XXXVI-5/C34 1, pp. 113-118.* Torino, Italy. http://cipa.icomos.org/index.php?id=39/Accessed_on_15/04/2008.

BIGF (2008) British Isles GPS archive Facility : Frequently asked questions. http://www.bigf.ac.uk/faq.htm/Accessed_on_15/01/2008.

BINGLEY, R. (2004) Computation of the BIGF Scientific Station ETRS89 Coordinates. IESSG, The University of Nottingham. Available from BIGF http://www.bigf.ac.uk/papers/Report_041117.pdf/Accessed_on_15/03/2008.

BLETSOS, N. A. (2004) Launch Vehicle Guidance, Navigation, and Control. *Crosslink.* CA, The Aerospace Corporation. Volume 5, Number 1 (Winter 2004). http://www.aero.org/publications/crosslink/winter2004/06.html/Accessed_on_10/03/2008.

BLOM (2008) BLOM Aerofilms Limited. http://www.blomasa.com/aerofilms/en/Accessed_on_24/02/2008.

BOSSLER, J. D. (1984) Standards and specifications for geodetic surveys. *Silver Spring: Maryland, National Geodetic Survey, National Oceanic and Atmospheric Administration, 29 p.*

BOSSLER, J. D. (2002) *Manual of geospatial science and technology,* London ; New York, Taylor & Francis.

BOULIANNE, M., SANTERRE, R., GAGNON, P. & NOLETTE, C. (1996) Floating lines and cones for use as a GPS mission planning aid. *Photogrammetric Engineering & Remote Sensing,* 62 (3)**,** 311–315.

BOWYER, A. (1981) Computing Dirichlet tessellations. *The Computer Journal* 24**,** pp. 162-166.

BROOKES, A. D. (1996) Enhancement to the Horizontal Network Adjustment Program - HORNET. *IESSG.* Nottingham, The University of Nottingham. MSc Thesis.

BROOKS, K. R. (2004) REGIONAL LANDSCAPE INVENTORY and ANALYSIS. Washington State University, http://www.spokane.wsu.edu/gis/Classes/LA467/x834.htm/27/01/2008.

BURKE, R. (2003) *Getting to know ArcObjects : programming ArcGIS with VBA,* Redlands, Calif., ESRI Press.

BURTON, T. & NEILL, L. (2007) Use of Low-Level LiDAR Systems for Commercial Large Scale Survey Applications. *Proceedings of the 2007 Annual Conference of the Remote Sensing & Photogrammetry Society (RSPSoc2007): Challenges for earth observation -scientific, technical and commercial. 11 - 14 September 2007.* Newcastle University, Newcastle upon Tyne. http://www.ceg.ncl.ac.uk/rspsoc2007/papers/93.pdf?Accessed_on_15/04/2008.

CAMPBELL, N. & WU, X. (2004) Robust Estimation: Towards Automated Image Orientation. *The 12th Australasian Remote Sensing and Photogrammetry Conference Proceedings. 18-22 October.* Western Australia. http://www.cmis.csiro.au/rsm/research/pdf/campbell_n_12arspc_robustestimation.pdf/_Accessed_on_20/02/2008.

CHANG, K.-T. (2008) *Programming Arcobjects with Vba a Task-Oriented Approach Second (2nd Edition)* Boca Raton, Florida, Taylor & Francis Group, LLC.

CHATFIELD, A. B. & AMERICAN INSTITUTE OF AERONAUTICS AND ASTRONAUTICS. (1997) *Fundamentals of high accuracy inertial navigation,* Reston, VA., American Institute of Aeronautics and Astronautics, Inc.

CHEN, D. & LACHAPELLE, G. (1995) A comparison of the FASF and least-squares search algorithms for on-the-fly ambiguity resolution. *Navigation: Journal of The Institute of Navigation,* Vol. 42**,** pp. 371-390.

CHIANG, K.-W., NOURELDIN, A. & EL-SHEIMY, N. (2003) Multisensor integration using neuron computing for land-vehicle navigation. *GPS Solutions,* 6**,** pp. 209–218.

COSTELLO, S. B., CHAPMAN, D. N., ROGERS, C. D. F. & METJE, N. (2007) Underground asset location and condition assessment technologies. *Tunnelling and Underground Space Technology,* 22**,** 524-542.

COUNSELMAN, C. C. & GOUREVITCH, S. A. (1981) Miniature interferometer terminals for earth surveying: ambiguity and multipath with Global Positioning System. *IEEE Transactions on Geoscience and Remote Sensing,* Vol. GE-19**,** pp. 244-252.

CRAMER, M. (1997) GPS/INS Integration. in Fritsch/Hobbie (eds), Photogrammetric Week 1997, Stuttgart, Germany, pp. 1-10, http://www.ifp.uni-stuttgart.de/publications/phowo97/cramer.pdf/Accessed_on_22/03/2008.

CRANENBROECK, J. V. (2005) A New Total Station Tracking GPS Satellites in a Network RTK Infrastructure Perspective. *TS 8 – GNSS II, From Pharaohs to Geoinformatics: FIG Working Week 2005 and GSDI-8.* Cairo, Egypt.

CROSIER, S., BOOTH, B. & MITCHELL, A. (2002) *Getting started with ArcGIS : GIS by ESRI,* Redlands, CA, Environmental Systems Research Institute.

CSR/TSGC (2007) ICESat / GLAS. http://www.csr.utexas.edu/glas/Accessed_on_21/03/2008.

CUMBERBATCH, S. (2005) What lies beneath? *Surveyor, SVY0505.* www.surveyormagazine.com.

DAGHAY, S., MOINS, M., BRUYNINX, C., ROLAIN, Y. & ROOSBEEK, F. (2005) Impact of the Combined GPS + Galileo Satellite Geometry on Positioning Precision. *Proc. EUREF symposium.* Vienna, Austria. June 1-4, 2005 http://www.epncb.oma.be/_newsmails/papers/eurefsymposium2005/impact_of_the_combined_gps_galileo_satellite_geometry_on_positioning_precision.pdf/Accessed_on_20/05/2008.

DAVIES, P. (2000) *Great Britain's Ordnance Survey National GPS Network*, Cambridge Journals Online, Volume 53, pp. 397-402.

DAVIS, B. E. (2001) *GIS : a visual approach,* Albany, Delmar Thomson Learning.

DAVIS, R. E. (1981) *Surveying theory and practice,* New York, McGraw-Hill.

DE MERS, M. N. (1997) *Fundamentals of geographic information systems,* New York, Wiley.

DFT (2006) Traffic Management Act, Parts 3-4 and New Roads and Street Works Act s.74., http://www.dft.gov.uk/stellent/groups/dft_roads/documents/page/dft_roads_610568-07.hcsp/20/07/2006.

DUGGAL, S. K. (2004) *SURVEYING : VOLUME II,* New Delhi, TATA MCGRAW HILL PUBLIHSERS.

EASA, S., CHAN, Y. & AMERICAN SOCIETY OF CIVIL ENGINEERS. GEOGRAPHIC INFORMATION SYSTEMS COMMITTEE. (2000) *Urban planning and development applications of GIS,* Reston, Va., American Society of Civil Engineers.

EBNER, H. (1976) Self-calibrating block adjustment. *Proceeding of Congress of the International Society for Photogrammetry.* Helsinki, Finland, Bildmessung und Luftbildwesen, vol. 44, June 1, 1976, pp. 128-139.

EL-RABBANY, A. (2006) *Introduction to GPS : the Global Positioning System,* Boston, MA, Artech House.

EL-RABBANY, A. & EL-DIASTY, M. (2004) An Efficient Neural Network Model for De-noising of MEMS-Based Inertial Data. *THE JOURNAL OF NAVIGATION,* 57**,** pp. 407–415.

EL-SHEIMY, N. (2008) The Potential of Partial IMUs for Land Vehicle Navigation. *Inside GNSS,* 3**,** pp. 16-25.

ESA (2002) European Space Agency: GALILEO Mission High Level Definition. http://ec.europa.eu/dgs/energy_transport/galileo/doc/galileo_hld_v3_23_09_02.pdf/Accessed_on_08/04/2008.

ESA (2006) European Space Agency: The First Galileo Satellites: Galileo In-Orbit Validation Element (GIOVE), BR-251. Noordwijk, The Netherlands, http://www.esa.int/esapub/br/br251/br251.pdf/Accessed_on_10/01/2008.

ESRI (1996) *Environmental Systems Research Institute: Working with the ArcView Spatial Analyst*, http://www.sli.unimelb.edu.au/gisweb/GISModule/GISTheory.htm/Accessed_on_11/01/2008.

ESRI (2006a) *Environmental Systems Research Institute: ArcGIS 9: What is ArcGIS 9.2?,* Redlands, CA, ESRI, http://webhelp.esri.com/arcgisdesktop/9.2/index.cfm?TopicName=welcome/Accessed_on_10/01/2008.

ESRI (2006b) Environmental Systems Research Institute: Geodatabase Extension Object Model Terrain. http://edndoc.esri.com/arcobjects/9.2/ComponentHelp/esriGeoDatabaseExtensions/GeoDatabaseExtensionsObjectModel.pdf/Accessed_on_08/04/2008.

EUROPEAN-SPACE-AGENCY (2008) Galileo Open Service Signal In Space Interface Control Document (OS SIS ICD) Draft 1. European Space Agency / European GNSS Supervisory Authority.

FALCONE, M., ERHARD, P. & HEIN, G. W. (2006) Galileo. IN KAPLAN, E. D. & HEGARTY, C. J. (Eds.) *Understanding GPS : principles and applications, 2nd ed.* Boston, Mass, Artech House.

FARRELL, J. & BARTH, M. (1999) *The global positioning system and inertial navigation,* New York, McGraw-Hill.

FARRELL, J. A., GIVARGIS., T. & BARTH, M. (2000) Real-time Differential Carrier Phase GPS-Aided INS. *Institute of Electrical and Electronics Engineers (IEEE) Transactions on Control Systems Technology,* Vol. 8 pp. 709-721.

FREI, E. & BEUTLER, G. (1990) Rapid static positioning based on the fast ambiguity resolution approach "FARA": theory and first results. *Manuscripta Geodaetica,* Vol. 15**,** pp. 325-356.

GAUTIER, J. D. & PARKINSON, B. W. (2003) Using the GPS/INS Generalized Evaluation Tool (GIGET) for the Comparison of Loosely Coupled, Tightly Coupled and Ultra-Tightly Coupled Integrated Navigation Systems. *Proceedings of the ION 59th Annual Meeting and CIGTF 22nd Guidance Test Symposium.* New Mexico June 23 - 25, 2003, pp. 65-76.

GERMROTH, M. & CARSTENSEN, L. (2005) GIS and satellite visibility: Viewsheds from space. *Proc. 2005 Environmental Systems Research Institute (ESRI) International User Conference, CD-ROM.* San Diego, CA, July 25–29, 2005.

GHILANI, C. D. & WOLF, P. R. (2006) *Adjustment computations : spatial data analysis,* Hoboken, N.J., Wiley.

GIS.COM (2007) What is GIS? , http://www.gis.com/whatisgis/index.html/Accessed_on_01/02/2008.

GOPI, S. (2005c) *Global Positioning System: Principles and Applications,* New Delhi, Tata McGraw-Hill Pub. Co. Limited.

GPS-WORLD (2007) New Beidou Satellite. *GPS World: System Design & Test.* http://sidt.gpsworld.com/gpssidt/article/articleDetail.jsp?id=422958/Accessed_on_27/04/2007.

GREAVES, M. & FANE, C. (2003) The British EUREF GB 2001 GPS Campaign. Ponta Delgada, Report on the Symposium of the IAG Subcommission for the European Reference Frame (EUREF) held in Ponta Delgada, 5-8 June 2002, ISSN 1436-3445, pp 168-184.

GREJNER-BRZEZINSKA, D. A. & TOTH, C. (2004) High-Accuracy Direct Aerial Platform Orientation with Tightly Coupled GPS/INS System. Final Report. Columbus, OH, The Ohio Department of Transportation and the U.S. Department of Transportation, Federal Highway Administration. http://www2.dot.state.oh.us/research/2004/Aerial/14661-FR.pdf/Accessed_on_21/03/2008.

GRELIER, T., DANTEPAL, J., DELATOUR, A., GHION, A. & RIES, L. (2007) Initial Observations and Analysis of Compass ME O Satellite Signals. *Inside GNSS, May/June 2007, pp. 39-43.*

GREWAL, M. S., WEILL, L. R. & ANDREWS, A. P. (2007) *Global postioning systems, inertial navigation, and integration* Hoboken, N.J., Wiley-Interscience.

GROVES, P. G. (2008) *Principles of GNSS, Inertial, and Multisensor Integrated Navigation Systems,* Boston ; London Artech House.

GRUBER, M. & LADSTÄDLER, R. (2006) Geometric Issues of the digital large format aerial camera UltraCamD. *International Calibration and Orientation Workshop, EuroCOW 2006.* Castelldefels, Spain, EuroSDR Commission I and ISPRS Working Group 1/3.

GRUBER, M., PERKO, R. & PONTICELLI, M. (2004) The all Digital Photogrammetry Workflow: Redundancy and Robustness. *Geo-Imagery Bridging Continents* Istanbul, Turkey XXth ISPRS Congress, Commission I papers, Vol. XXXV, part B1.

HABIB, A. F., GHANMA, M. S. & TAITA, M. (2004) Integration of LiDAR and photogrammetry for close range applications. *Geo-Imagery Bridging Continents, Commission 5.* Istanbul, Turkey, International Archives of XXth International Society for Photogrammetry and Remote Sensing (ISPRS) Congress, 12-23 July 2004, pp. 170-176

HAINES, E. (1994) Point in Polygon Strategies. IN HECKBERT, P. S. (Ed.) *Graphics Gems IV*. Boston, Academic Press, p. 24-46

HATCH, R. (1990) Instantaneous ambiguity resolution. *Proc. of the International Symposium on Kinematic System in Geodesy, Surveying and Remote Sensing, KIS90, September 10-13, 1990.* Banff, Canada, pp. 299-308.

HEIN, G. W., ÁVILA-RODRÍGUEZ, J.-Á., WALLNER, S., PANY, T., EISSFELLER, B. & HARTL, P. (2007) Envisioning a Future: GNSS System of Systems, Part 1. *Inside GNSS, January/February 2007, pp. 58-67.*

HIDE, C. & MOORE, T. (2004) Low cost sensors high quality integration. *Proceedings of NAV/AIS04, Location and Timing Applications, CD-ROM.* London, pp. 40.1-4.10

HIDE, C., MOORE, T., HILL, C. & PARK, D. (2006) Low Cost, High Accuracy Positioning in Urban Environments. *Journal of Navigation,* 59**,** pp 365-380.

HILL, C. (2005) Leica SmartStation – The Integration of GPS & Total Station Technologies. Heerbrugg, Switzerland.

HOFMANN-WELLENHOF, B., LEGAT, K. & WIESER, M. (2003) *Navigation : principles of positioning and guidance,* Wien ; London, Springer.

HOWELL, G. & TANG, W. (1994) A universal GPS/INS Kalman filter design. *Proceedings of ION GPS 1994, The 9th Technical Meeting of the Satellite Division of the Institute of Navigation.* Salt Lake City, Utah, pp. 443–451.

ICA (2002) Russian Space Agency Information-analytical centre: Glonass interface control document v5.0. Moscow, Russia, Coordination Scientific Information Centre.

IGS (2006) The International GNSS Service. http://igscb.jpl.nasa.gov/Accessed_on_03/04/2006.

IRVINE, W. & MACLENNAN, F. (2006) *Surveying for Construction. 5th ed.*, Maidenhead : McGraw-Hill Education.

ITRC (2003) Irrigation Training and Research Centre : Report No. R03-010

JAVAD (2008) The TRIUMPH® Chip... with 216 channels. http://www.javad.com/jgnss/Accessed_on_25/07/2008.

JEKELI, C. (2000) *Inertial navigation systems with geodetic applications,* New York, Walter de Gruyter.

JEONG, H. S., ARBOLEDA, C. A., ABRAHAM, D. M., HALPIN, D. W. & BERNOLD, L. E. (2002) Imaging and Locating Buried Utilities. West Lafayette, IN, Joint Transportation Research Program: Purdue University. October 2002, Final Report FHWA/IN/FTRP-2003/12.

KAPLAN, E. D. (1996) *Understanding GPS : principles and applications,* Boston, Artech House.

KAPLAN, E. D. & HEGARTY, C. J. (2006) *Understanding GPS : principles and applications. -2nd ed.,* Boston, Mass, Artech House.

KAVANAGH, B. F. (2006) *Surveying : principles and applications,* Upper Saddle River, NJ, Prentice Hall.

KAYTON, M. & FRIED, W. R. (1997) *Avionics navigation systems,* New York, J. Wiley.

KENNEDY, M. (2002) *The global positioning system and GIS : an introduction,* London ; New York, Taylor & Francis.

KENNEDY, S., HAMILTON, J. & MARTELL, H. (2006) GPS/INS Integration with the iMAR-FSAS IMU. *Proceedings of the conference: Shaping the Change, XXIII International Federation of Surveyors (FIG) Congress.* Munich, Germany, October 8-13, 2006, pp. 1-15.

KIM, D. & LANGLEY, R. B. (1999) An optimized least-squares technique for improving ambiguity resolution performance and computational efficiency. *Proceedings of ION GPS'99, 14-17 September, 1999. pp. 1579-1588.* Nashville, Tennessee.

KIM, D. & LANGLEY, R. B. (2000) GPS Ambiguity Resolution and Validation: Methodologies, Trends and Issues. *Proceedings of the 7th GNSS Workshop - International Symposium on GPS/GNSS, 30 November-2 December, 2000. pp. 213-221.* Seoul, Korea.

KING, A. D. (1998) Inertial Navigation – Forty Years of Evolution. *GEC REVIEW,* VOL. 13**,** pp. 140-149.

KLEUSBERG, A. & LANGLEY, R. B. (1990) The Limitations of GPS. *GPS World***,** pp. 50-52.

KRUCK, E. (2006) Simultaneous Calibration of Digital Aerial Survey Cameras. *Proceeding of the International Calibration and Orientation Workshop, European Spatial Data Research (EuroSDR) Commission I and International Society for Photogrammetry and Remote Sensing (ISPRS) Working Group 1/3, 25 - 27 January 2006, CD-ROM.* Castelldefels, Spain.

LEE, I. S., CHANG, H.-C. & GE, L. (2005) GPS Campaigns for Validation of InSAR Derived DEMs. *Journal of Global Positioning Systems,* Vol.4**,** 82-87.

LEICA-GEOSYSTEMS-AG (1999) GPS Surveying - System 500: Technical Specifications. Heerbrugg, Switzerland.

LEICA-GEOSYSTEMS-AG (2005a) Format manager Application V. 3.0 Help.

LEICA-GEOSYSTEMS-AG (2005b) Leica Geo Office Help.

LEICA-GEOSYSTEMS-AG (2005c) Leica Geosystems Networked Reference Stations. Heerbrugg, Switzerland.

LEICA-GEOSYSTEMS-AG (2005d) Surveying with SmartStation: An introduction to RTK. Heerbrugg, Switzerland.

LEICA-GEOSYSTEMS-AG (2006a) Leica SmartNet: Commercial RTK Network Solution for Great Britain. Heerbrugg, Switzerland.

LEICA-GEOSYSTEMS-AG (2006b) Leica SmartPole: Measure non-stop with setup On-the-Fly. Heerbrugg, Switzerland.

LEICA-GEOSYSTEMS-AG (2006c) Leica SmartStation: Total Station with integrated GPS. Heerbrugg, Switzerland.

LEICA-GEOSYSTEMS-AG (2006d) Leica TPS1200 Series: Technical Data. Heerbrugg, Switzerland.

LEICA-GEOSYSTEMS-AG (2007a) Leica GPS1200 Series Technical Data. Heerbrugg, Switzerland.

LEICA-GEOSYSTEMS-AG (2007b) Leica Photogrammetry Suite. http://gi.leica-geosystems.com/LGISub1x11x0.aspx/Accessed_on_25/02/2008.

LEICA-GEOSYSTEMS-AG (2008) Leica SmartNet http://smartnet.leica-geosystems.co.uk/spiderweb/weblink/information2.htm/Accessed_on_25/05/2008 .

LEICK, A. (2004) *GPS satellite surveying,* Hoboken, NJ, John Wiley.

LI, Y., WANG, J., RIZOS, C., MUMFORD, P. & DING, W. (2006) Low-cost tightly coupled GPS/INS integration based on a nonlinear Kalman filter design. *in: Proceeding of the U.S. Institute of Navigation National Tech. Meeting, 18-20 January. pp. 958-966.* Monterey, California.

LI, Z., ZHU, Q. & GOLD, C. (2005) *Digital terrain modeling : principles and methodology,* Boca Raton ; New York, CRC Press.

LOHANI, B. (2001) Airborne altimetric LiDAR for topographic data collection: Issues and application. *Proc. of International conference MapIndia-2001, 7-9 February 2001.* New Delhi, http://www.gisdevelopment.net/application/urban/products/urbanp0003.htm/Accessed_on_18/05/2008.

LOHANI, B. (2008) Airborne Altimetric LiDAR: Principle, Data Collection, Processing and Applications. http://home.iitk.ac.in/~blohani/LiDAR_Tutorial/Airborne_AltimetricLidar_Tutorial.htm/Accessed_on_04/04/2008.

LONGLEY, P. (2005) *Geographical information systems and science,* Chichester, Wiley.

MAGELLAN-PROFESSIONAL (2008) Support: Almanac. Magellan Navigation, Inc. http://pro.magellangps.com/en/support/almanac.asp/Accessed_on_31/03/2008.

MCMAHON, W., EVANS, M., BURTWELL, M. H. & PARKER, J. (2005) The real costs of street works to the utility industry and society. UKWIR 05/WM/12/8, 2005.

MENG, X., DODSON, A., MOORE, T. & ROBERTS, G. (2007) Ubiquitous Positioning – Anyone, Anything: Anytime, Anywhere. *GPS World.*

MENG, X., DODSON, A. H., MOORE, T., HILL, C. & ROBERTS, G. W. (2006) Development of the Nottingham RTK GPS Testbed. *In: European Navigation Conference, ENC 2006, 8-10 May 2006, CD-ROM.* Manchester, UK.

METJE, N., ATKINS, P. R., BRENNAN, M. J., CHAPMAN, D. N., LIM, H. M., MACHELL, J., MUGGLETON, J. M., PENNOCK, S., RATCLIFFE, J., REDFERN, M. A., ROGERS, C. D. F., SAUL, A. J., SHAN, Q., SWINGLER, S. & THOMAS, A. M. (2007) Mapping the Underworld – State-of-the-Art Review. *Tunneling and Underground Space Technology,* 22**,** pp. 568-586.

MIKHAIL, E. M., BETHEL, J. S. & MCGLONE, J. C. (2001) *Introduction to modern photogrammetry,* New York Chichester, Wiley.

MOORE, T. (2006) Satellite Positioning Beyond 2010: Simulation and Implementation. Nottingham, The University of Nottingham. Mapping Technologies Workshop, 14 September 2006.

MTU (2006) Mapping The Underworld: The Accuracy of Geophysical Utility Mapping http://www.mappingtheunderworld.ac.uk/qupdate1.html/Accessed_on_30/05/2008.

MTU (2008) Mapping The Underworld. http://www.mappingtheunderworld.ac.uk/Accessed_on_25/07/2008.

NAVIGATION-CENTER (2008a) Definition of a Yuma Almanac. Navigation Center: The Navigation Center of Excellence. http://www.navcen.uscg.gov/GPS/gpsyuma.htm/Accessed_on_02/04/2008.

NAVIGATION-CENTER (2008b) GPS Almanacs, NANUS, and Ops Advisories (Including Archives). Navigation Center: The Navigation Center of Excellence. http://www.navcen.uscg.gov/gps/almanacs.htm/Accessed_on_31/03/2008.

NETTWORK (2002) Trenchless Technology Network: Underground Mapping, Pipeline Location Technology and Condition Assessment. Birmingham, The University of Birmingham, Infrastructure Engineering and Management Research Centre. March 2002. http://www.ttn.bham.ac.uk/Final%20Reports/Pipe%20Location%20and%20Assessment.pdf/Accessed_on_15/07/2008.

NUAG (2006) Capturing, recording, storing and sharing underground asset information: A review of current practice and future requirements, UKWIR 06/WM/12/13, http://www.nuag.co.uk/outputs/public_NUAG_report_final.pdf/Accessed_on_10/04/2008.

OS (2008a) Ordnance Survey: Antenna phase centre offsets. http://www.ordnancesurvey.co.uk/oswebsite/gps/osnetfreeservices/furtherinfo/antenna.html/Accessed_on_21/01/2008.

OS (2008b) Ordnance Survey: Great Britain's national mapping agency. http://www.ordnancesurvey.co.uk/oswebsite/products/Accessed_on_30/01/2008.

OS (2008c) Ordnance Survey: OS Net® frequently asked questions. http://www.ordnancesurvey.co.uk/oswebsite/gps/commercialservices/faqs.html/Accessed_on_25/05/2008.

OSIANDER, R., DARRIN, M. A. G. & CHAMPION, J. (2006) *MEMS and Microstructures in aerospace applications,* Boca Raton, Taylor & Francis.

PARKER, J. (2006) Minimising Street Works Disruption: Buried Asset Data Collection and Exchange Field Trials. . UKWIR Report 06/WM/12/9, 2006.

PIERCE, F. J. & CLAY, D. (2007) *GIS applications in agriculture,* Boca Raton, CRC Press.

PROAKIS, J. G. (2001) *Digital communications,* Boston, McGraw-Hill.

QUEST (2007) Quest Geo Solutions Limited: Grid InQuest: 3D Datum Transformations for Great Britain and Ireland. http://www.qgsl.com/?product=gridinquest/Accessed_on_10/11/2007.

REVNIVYKH, S. (2005) GLONASS Status, Performance and Perspectives. *Proceedings ION GNSS 2005, 13-16 September 2005. CD-ROM.* Long Beach, CA.

RIZOS, C. (1999) Principles and Practice of GPS Surveying. The Satellite Navigation & Positioning Laboratory (SNAPlab) within the School of Surveying & Spatial Information Systems, at the University of New South Wales, Australia.

RIZOS, C. & HAN, S. (2003) Reference Station Network Based RTK Systems - Concepts and Progress. *Wuhan University Journal of Nature Sciences,* 8**,** pp. 566-574.

RIZOS, C., HIGGINS, M. & HEWITSON, S. (2005) New GNSS Developments and their Impact on Survey Service Providers and Surveyors. *Proceedings of SSC2005 Spatial Intelligence, Innovation and Praxis: The national biennial Conference of the Spatial Sciences Institute.* Melbourne, Spatial Sciences Institute, pp. 1100-1113.

RODDY, D. & EBRARY INC. (2006) Satellite communications. 4th ed. New York, McGraw-Hill.

SALYCHEV, O. S., VORONOV, V. V., CANNON, M. E., NAYAK, R. & LACHAPELLE, G. (2000) Low Cost INS/GPS Integration: Concepts and Testing. *In: Proceedings of the Institute of Navigation (ION) National Technical Meeting 2000, September 19-22, 2000. pp. 98–105.* Anaheim, CA.

SANG HOON, L., SANG HOON, L., SANGHO, B. & SHUM, C. K. (2005) Multi-temporal, multi-resolution data fusion for Antarctica DEM determination using InSAR and altimetry. *Proceeding of International Geoscience and Remote Sensing Symposium (IGARSS) '05. Institute of Electrical and Electronics Engineers (IEEE),* Volume 4**,** pp. 2827-2829.

SANTERRE, R. (1991) Impact of GPS satellite sky distribution. *Manuscripta Geodaetica,* 16**,** pp. 28-53.

SCHENK, T. F. (1999) *Digital photogrammetry,* Laurelville, OH, TerraScience.

SCHOFIELD, W. (2001) *Engineering surveying : theory and examination problems for students,* Oxford, Butterworth-Heinemann.

SEEBER, G. (2003) *Satellite geodesy,* Berlin ; New York, Walter de Gruyter.

SHAMSI, U. M. (2005) *GIS applications for water, wastewater, and stormwater systems,* Boca Raton, Taylor & Francis.

SINGH, V. P. & FIORENTINO, M. (1996) *Geographical information systems in hydrology,* Boston, Kluwer Academic Publishers.

SINODEFENCE (2007) Chinese Defence Today: Compass Satellite Navigation Experimental System (BeiDou 1). http://www.sinodefence.com/strategic/spacecraft/beidou1.asp/Accessed_on_20/04/2008.

SMITH, M. J., KOKKAS, N. & QTAISHAT, K. S. (2007) Investigation into Self-Calibration methods for the Vexcel UltraCam D Digital Aerial Camera. *In: International Society for Photogrammetry and Remote Sensing (ISPRS) Hannover Workshop, High Resolution Earth Imaging for Geospatial Information, 29 May - 1 June. CD-ROM.* Hannover, Germany.

SOYCAN, M. (2006) A Cost Effective GPS Leveling Method Versus Conventional Leveling Methods For Typical Surveying Applications. *GIS Development Asia Pacific,* Volume 10, Issue 8 Aug 2006**,** pp. 30-32.

SPENCER, J. (2003) *Global Positioning System : a field guide for the social sciences,* Malden, MA, Blackwell Pub.

STANFORDS (2007) LiDAR. http://www.stanfords.co.uk/business-mapping/lidar/Accessed_on_21/03/2008.

STRANG, G. & BORRE, K. (1997) *Linear algebra, geodesy, and GPS,* Wellesley, MA, Wellesley-Cambridge Press.

TAHA, A., MENG, X., ROBERTS, G. W., HIDE, C. & MONTILLET, J.-P. (2006) Using SmartStation and GPS integrated with INS to Map Underground Pipes and Cables. *Proceedings of Institute of Navigation (ION) GNSS 2006, 26-29 September 2006.* Fort Worth Convention Center, Fort Worth, Texas. CD-ROM.

TAHA, A., OGUNDIPE, O., HANCOCK, C., ROBERTS, G. & MENG, X. (2007) Kinematic Positioning Through Continuous Updating Technique. *Proceedings of the Royal Institute of Navigation's Nav'07 Conference, 30 October – 1 November 2007.* Church House, Westminster, London. CD-ROM.

TAYLOR, G., LI, J., KIDNER, D., BRUNSDON, C. & WARE, M. (2007) Modelling and prediction of GPS availability with digital photogrammetry and LiDAR. *International Journal of Geographical Information Science,* 21**,** 1 - 20.

TEUNISSEN, P. J. G. (1994) A New Method for Fast Carrier Phase Ambiguity Estimation. *Proceedings Institute of Electrical and Electronics Engineers (IEEE) Position, Location and Navigation Symposium PLANS'94, 11-15 April 1994. pp. 562–573.* Las Vegas, NV, USA.

TITTERTON, D. H. & WESTON, J. L. (2004) *Strapdown inertial navigation technology,* London, U.K., Institution of Electrical Engineers.

TRIMBLE (2008) Trimble Navigation Limited: Trimble's Planning Software. http://www.trimble.com/planningsoftware.shtml/Accessed_on_05/02/2008.

U-BLOX-AG (2007) *GPS Modules - System Integration Manual (SIM) (incl. Reference Design). GPS.G4-MS4-05007-A1,* Thalwil, Switzerland. , u-blox AG.

VAN SICKLE, J. (2001) *GPS for Land Surveyors. Second edition,* New York CRC Press.

VERBREE, E., TIBERIUS, C. & VOSSELMAN, G. (2004) Combined GPS-Galileo positioning for Location Based Services in urban environment. *Proceedings of the 2nd symposium on location based services & telecartography, 28 – 29 January 2004.* Vienna, Institute for Cartography and Geo-Media Techniques. pp. 99-107.

VERHAGEN, S. (2006) Visualization of GNSS-related design parameters; Manual for the Matlab user interface VISUAL. (not published, distributed with the software). Delft, The Netherlands, Delft Institute of Earth Observation and Space Systems, Delft University of Technology.

VOLLATH, U., LANDAU, H. & CHEN, X. (2002) Network RTK – Concept and Performance. *In: Proceedings of the International Symposium on GPS/GNSS, 6–8 November 2002.* Wuhan, China. , www.gpsnet.dk/showimg.php?ID=371/Accessed_on_13/05/2008.

WAGNER, C. (2000) GPS Vis. http://dclapp.home.znet.com/GPS/GPS_VIS/Accessed_on_05/02/2008.

WALKER, R. & SANG, J. (1997) Mission planning for high precision RTK GPS surveying using accurate digital terrain information. *In Proceedings of Institute of Navigation (ION) GPS 1997 Conference, 14-16 January 1997, pp. 367-376.* Kansas City, Missouri, USA.

WATSON, D. F. (1981) Computing the n-dimensional Delaunay tessellation with application to Voronoi polytopes. *The Computer Journal* 24**,** pp. 167-172.

WAYPOINT-CONSULTING-INC. (2003) *Guide to Using PosGPS: Reference Manual. PUBS-MAN-000016, Revision 3, dated November 5, 2003,* Canada, Aplanix Corporation / Waypoint Consulting.

WISE, S. (2002) *GIS basics,* London ; New York, Taylor & Francis.

WOLF, P. R. & DEWITT, B. A. (2000) *Elements of photogrammetry : with applications in GIS,* Boston, McGraw-Hill.

WOLF, P. R. & GHILANI, C. D. (2006) *Elementary surveying : an introduction to geomatics,* Upper Saddle River, N.J., Prentice Hall.

ZARCHAN, P. & MUSOFF, H. (2005) *Fundamentals of Kalman filtering : a practical approach,* Reston, Va., American Institute of Aeronautics and Astronautics.

Appendices

Appendix 1: Establishment of Testing Facilities

A1.1 Introduction

As the research work for this thesis was focussed on integrated GNSS based positioning, a series of testing points were required in order to serve as ground 'truth' for the accuracy assessment of different techniques. This was achieved on the Nottingham Campus trial route by building three networks: a GPS network, a vertical network and a horizontal network. The observations from these various networks were then processed and adjusted to produce the 'truth' coordinates.

This chapter starts by describing the network design and planning, and shows the distribution of the testing points along the trial route. Then, it discusses the three networks (GPS, Vertical and Horizontal) that were used to establish the 'truth' coordinates. For each of the networks, the instrument used and the methodology followed are illustrated in the data collection section. Subsequently, the software and the strategy utilised to process the different observations are discussed in the data processing section. Next, the results achieved from the processing stage are analysed. After that, the software and the adjustment strategy used to adjust different networks are discussed in the data adjustment section. Finally, the adjusted network coordinates were validated with those obtained from the GPS network and compared with those from the vertical and horizontal networks sections.

A1.2 Network Design and Planning

Reconnaissance was carried out in order to define a trial area (route) at The University of Nottingham that is comparable to what can be found in urban canyons. This trial route needed to be encompass different obstruction levels and so the area shown in Figure A1.1 was selected. This has open areas (A, F), streets with different

widths (B and C), streets with buildings of different heights (i.e. D), streets with bridges between buildings (C and D) and a street with buildings and trees (E).

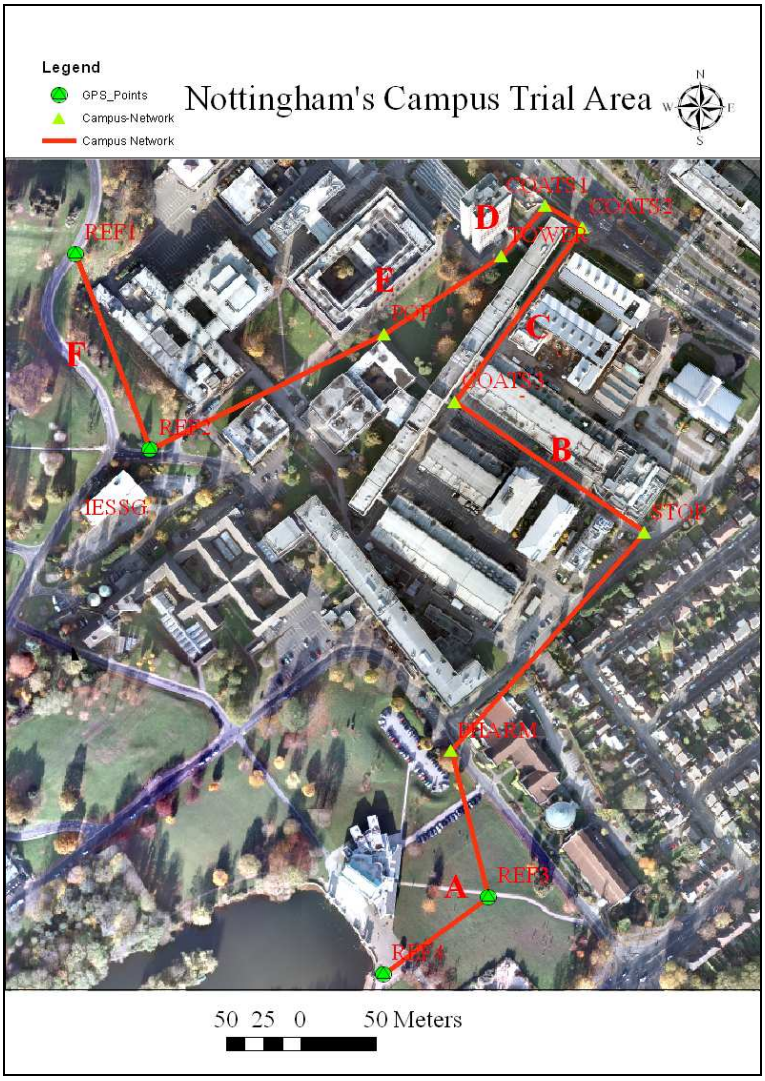

Figure A1.1: An aerial photograph for the trial area on the University Campus (Copyright © BlomAerofilms Ltd.)

Along the trial route a network of 11 points, fixed using survey nails, were distributed close to the testing points, with an accumulated distance of 1,160.86m. This network is called Campus-Network in this thesis. Intervisibility between sequential points was made possible with careful planning. The Campus-Network was planned to comprise of 4 GPS points labelled REF1-REF4 (GPS network), located in nearly open sky areas (A and F in Figure A1.1) and another 7 points located close to the trial route labelled POP, COATS1, etc.. These points, situated along the trial route, are located in restricted sky areas (close to buildings and trees). Hence, in order to achieve high levels of accuracy for the points located in the

restricted areas, two separate networks (vertical network using precise levelling and horizontal networks using a high specification total-station) were established. The Campus-Network points are superimposed on the Ordnance Surveying (OS) Mastermap in Figure A1.2.

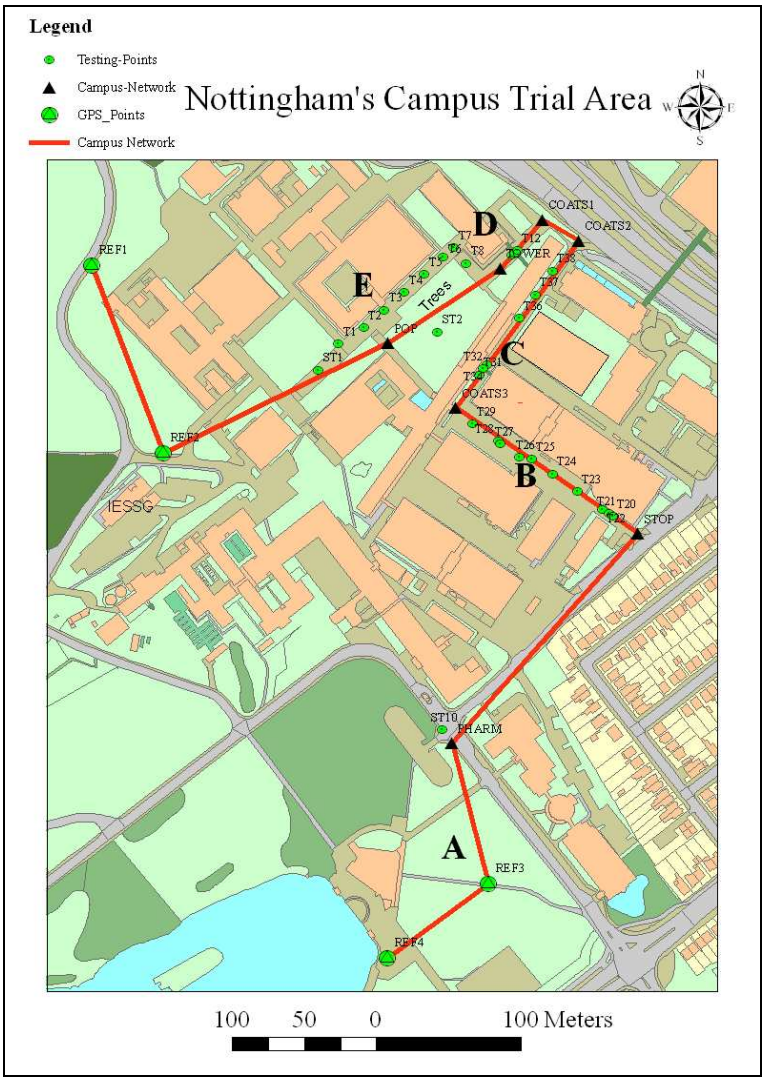

Figure A1.2: The trial route on the University Campus superimposed on an OS MasterMap (Copyright © OS MasterMap)

Another network of 30 points was designed to be distributed in the most difficult areas along the trial route. These were named Testing-Points and labelled T1-T38 (Figure A). Similar to the points located in the restricted sky areas in Campus-Network, two separate networks (vertical and horizontal) were required to determine accurate coordinates for the Testing-Points. In total, therefore, there were 41 points established to serve as testing points with 'truth' coordinates.

A1.3 GPS Network

In the Campus-Network, the GPS network consists of 4 points distributed in reasonably open areas. Intervisibility between each of two GPS points was considered. Additionally, two permanent reference stations, IESSG (IESG) and OS's Nottingham (NOTT), were used. This is to provide redundant observations for the adjustment. When redundant observations are available, a strategy has to be chosen so as to get a unique and optimal solution. After carrying out a least squares adjustment, the best possible solution based on the available observations is achieved. Having determined a solution, it is important to be able to assess the quality of this solution, and therefore necessary to quantify the quality. The quality of a network can be assessed in terms of precision and reliability. This means that the quality control will have to include some sort of statistical testing, in order to eliminate outliers. The effectiveness of the testing will depend on the reliability of the network. The more reliable a network is, the higher the probability that outliers will be detected by the testing.

A1.3.1 Data Collection

Static GPS data were collected at the four points in the Campus-Network using a Leica dual frequency SR530 GPS receiver with Leica choke ring antenna (AT503). The manufacturer's horizontal specifications for this receiver are ± (3mm + 0.5ppm RMS) with static (phase) and long observations using choke-ring antenna and ± (5mm + 0.5ppm RMS) with static and rapid static (phase) with standard antenna [Leica-Geosystems-AG, 1999]. The precision of the height are two times of the horizontal one [Leica-Geosystems-AG, 1999].

The methodology of the data collection was as follows:

- *GPS observables*: Raw static GPS data was collected for about 30 minutes to about 1 hour with an elevation angle cut-off of 0° and an epoch interval of 1 second on each of the four GPS network points.
- *Number of sessions*: Data was collected in two sessions on two different days (24^{th} and 25^{th} March 2006 in the GPS week of 1367) at different times on each of the four GPS network points.

- *Height measurement*: In order to minimise vertical errors at GPS points, the vertical antenna height was measured twice per session using the Leica GPS Height Hook.
- *Reference Stations*: In order to have redundant observations for the adjustment, data from two reference stations (IESG and NOTT) were used. The IESG station is a scientific station in the British Isles GPS archive Facility (BIGF), and is located on the IESSG building. This station collects GPS data every 30 seconds interval [BIGF, 2008]. The average length of the GPS baselines from IESG to each of the four GPS network points was 233m. The NOTT station is an Ordnance Survey active station which collects GPS data every 15 seconds interval [Davies, 2000]. The average length of the GPS baselines from NOTT to each of the four GPS network points was 2,540m.

A1.3.2 Data Processing

GPS data was post-processed using Leica Geo Office (LGO) software version 3.0. This software allows processing and management of static and kinematic GPS data with an option to use precise orbital data (ephemeris). In general, the GPS data processing strategy involves several steps as follows:

- *Import Data*: GPS rover data was imported from Leica DBX file using all available sampling rates (1 sec. interval). Moreover, GPS reference stations data (IESG and NOTT) were imported from RINEX files using all available sampling rates (30 sec. for IESG station and 15 sec. for NOTT station).
- *Orbital Data*: The final precise ephemeris data, downloaded from the International GNSS Service (IGS) website [IGS, 2006], was used.
- *Reference Station Coordinates*: For NOTT station, precise Cartesian coordinates, in the European Terrestrial Reference System 1989 (ETRS89) at epoch 1989.0 (e1989.0), are included in the active station RINEX observation data file header. Furthermore, precise Cartesian coordinates in ETRS89 e1989.0 for IESG station can be found in [Greaves and Fane, 2003] and [Bingley, 2004]. The known coordinates of NOTT and IESG reference stations were used in the processing with STD of 0.00m for X, Y and Z.

- *Antenna Phase Centre*: The antenna offsets are applied as corrections during the baseline processing. The antennas within LGO can be modified for phase centre offsets (horizontal and vertical). For example, NOTT and IESG reference stations use Ashtech antennas (ASH700936E SNOW and ASH700936D_M SNOW respectively) which were modified to phase centre offset (vertical) L1 equal to 0.11m and phase centre offset (vertical) L2 equal to 0.128m [OS, 2008a]. However, Leica AT503 choke ring antenna has different offsets which are defined automatically when importing the data by LGO.
- *Processing Parameters*: The processing computation parameters can be selected before starting computation. System default settings are available for all parameters; however, they can be changed individually. For example, the cut-off angle was modified from 15°, as in the defaults, to 10° to allow for more satellites in view to be available in the processing. Hence, the more satellites are, the better geometry is and the better PDOP is. The 10° was chosen because it has been tested and used by most IGS analysis centres, such as CODE (the Center for Orbit Determination in Europe) and was used in [Greaves and Fane, 2003]. On the other hand, other processing parameters were used the same as in the LGO defaults. For instance, solution type is automatic (options available: Phase, Code or Float), Tropospheric model is Hopfield and Ionospheric model is automatic (options available: Computed model, Klobuchar model, Standard, Global/Regional model or No model).

A1.3.3 Processing Results and Analysis

After the GPS data has been post-processed using LGO, the results can be viewed using the Results View. This includes point results, GPS-processing report, GPS-processing analysis tool and other results. As two reference stations were utilised for post-processing, and there were four GPS points, this makes eight baselines calculated per day. The processing results (point results) show a phase solution with ambiguity fixed was achieved for all GPS points. The coordinate's variation around mean was calculated for each of the GPS points and illustrated in Figure A1.3.

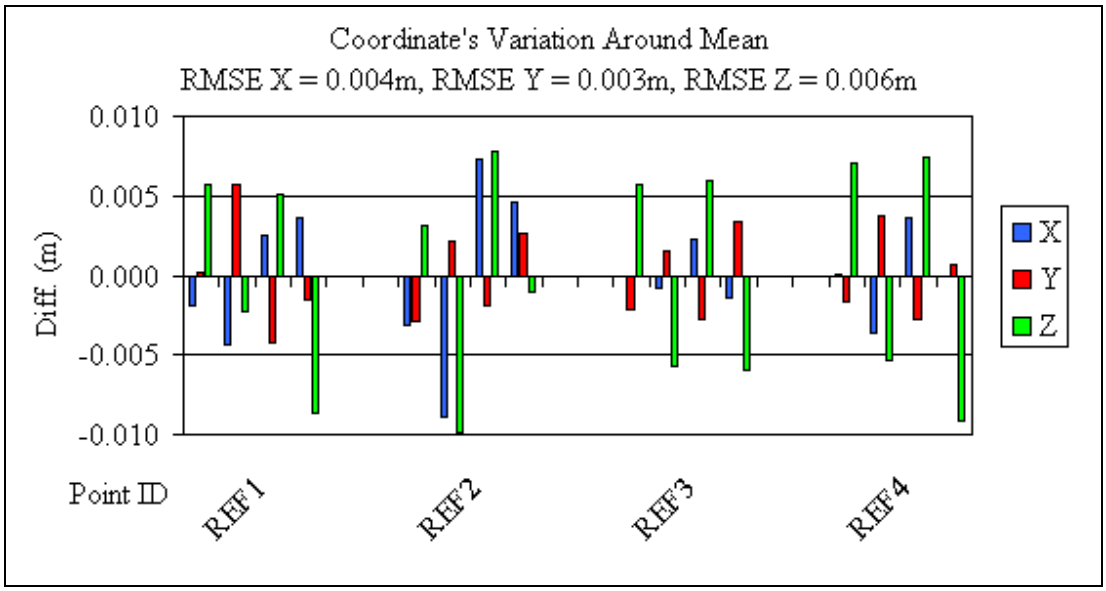

Figure A1.3: Coordinate variation around the mean of the four GPS points

From Figure , it can be seen that the differences around the mean were found in most points to be less than ±0.005m for X and Y coordinates with RMSE of 0.004m and 0.003m in X and Y respectively. However, the differences of Z coordinate found to be two times higher than that of the X and Y coordinates. The maximum difference of the Z coordinate is about -0.010m with an overall RMSE of 0.006m.

Using the expected precision of 5mm + 0.5ppm, uncertainties of about 0.006m and 0.012m were estimated for the horizontal and vertical coordinates respectively. Thus, the above differences (RMSE of 0.004m, 0.003m and 0.006m in X, Y and Z respectively) were within the estimated uncertainties of static survey with GPS and hence all of the resultant coordinates were used in the adjustment.

A1.3.4 Network Adjustment

GPS network adjustment was carried out using LEICA Geo Office software version 3.0, and the computation was performed using the 'MOVE3 3.3.1' Adjustment kernel within LGO. In general, several steps were necessary to perform the GPS network adjustment as follows:

- *Reference station coordinates*: Unlike the reference stations coordinates in post-processing stage, the coordinates of the reference stations (IESG and NOTT) should be weighted. This is to allow treating control points as

weighted fixed according to standard deviations in the adjustment. Standard deviation of 0.008m for plan coordinates and 0.020m for height was used as this is the claimed standard error of OS Active stations [OS, 2008b].

- *General adjustment parameters*: The general adjustment parameters should be defined to be taken into account during the adjustment. These parameters include: Control, Standard Dev., Centring/Height, Known Stations, Test Criteria and Coordinate System. Some parameters that are defined include Rover/Target Centring (0.001m) and Height (0.002m) and treat control points as weighted fixed according to standard deviations (Weighted Constrained Adjustment).
- *Pre-analysis adjustment*: Before running the adjustment, pre-analysis can be run for checking the network prior to the adjustment. Quality control checks as well as mathematical checks on the data are carried out. Depending on the type of network, the type of observations included and the contents of the report, some or all of the following will appear in the Pre-analysis Report: Project Information, General Information, Configuration Defects (report on unknowns which cannot be solved (singularities)) and Check of Input Data. Configuration Defects and Check of Input Data did not appear in the report for GPS points, as there were not any abnormal observations within the four GPS network.
- *Compute Network*: The network computation performs the adjustment computation. The network adjustment report, first adjustment report, shows that there are estimated errors for observations with rejected W-Test and T-Test. To overcome this, the option *Apply only if fail F-test*, under *Test Criteria* under *Sigma a posteriori*, was selected. The new network adjustment report (Appendix 3: GPS Network - Second Adjustment Report) shows that there were not any estimated errors for observations with rejected W-Test and T-Test.

A1.3.5Network Adjustment Results and Analysis

The adjusted geographic coordinates were converted to National Grid (OSGB36) coordinates (Easting, Northing and Orthometric Height) using Grid-InQuest (version 6.0.8) software [Quest, 2007] and are shown in Table A1.1.

Table A1.1: The National Grid (OSGB36) coordinates and their standard deviation for the four GPS points

Point Id	**Coordinates** (m)			**Standard Deviation** (m)		
	E	**N**	**Ht**	**E**	**N**	**Ht**
REF1	454348.848	338603.134	43.141	0.006	0.006	0.015
REF2	454398.461	338472.766	37.589	0.006	0.006	0.015
REF3	454624.113	338173.719	25.382	0.006	0.006	0.014
REF4	454553.763	338122.106	25.391	0.006	0.006	0.014

As can be seen from Table A1.1, the GPS coordinates have small standard deviations, less than 0.006m for plan coordinates and less than 0.015m for height. In order to further validate the GPS coordinates, a Leica total-station and digital level were employed. Using the Leica total-station, slope distances and vertical angles were observed between the GPS points. The measured slope distance was reduced to horizontal distance using the vertical angle. Then the horizontal distance was reduced to mean sea level and to the projection using local scale factor to produce a grid distance. This grid distance was then compared with the calculated distance between adjacent GPS points as shown in Table A1.2.

Table A1.2: Calculated horizontal distance based on GPS compared to measured grid distance based on total-station for the four GPS points

Baseline	**Calculated Distance** (m)	**Measured Distance** (m)	**Differences** (m)
REF1-REF2	139.489	139.486	0.003
REF3-REF4	87.253	87.251	0.002

From Table A1.2, the differences between the calculated horizontal distances and the measured grid distances of the GPS points are 0.003m and 0.002m. There are several reasons for these differences such as GPS and total-station centring errors,

instrument errors and other errors. However, the above differences indicate that there are no gross errors in the GPS plan coordinates.

Using the Wild NA 2000 automated digital level, a levelling closed-loop (levelling circuit) between two OS Bench Marks and REF1 and REF2 GPS points was carried out, and the results are in Table A1.3.

Table A1.3: Orthometric height based on GPS compared to Orthometric height based on levelling for two of the four GPS points

Station .ID	**GPS Ortho. Ht.** (m)	**Levelling Ortho. Ht.** (m)	**Ortho. Ht. Difference** (m)
REF1	43.141	43.140	0.001
REF2	37.589	37.586	0.003

Another levelling closed-loop was carried out from REF2 to REF3 and REF4 and the results are shown in Table A1.4.

Table A1.4: Orthometric height based on GPS compared to Orthometric height based on levelling for another two of the four GPS points

Station .ID	**GPS Ortho. Ht.** (m)	**Levelling Ortho. Ht.** (m)	**Ortho. Ht. Difference** (m)
REF3	25.382	25.382	0.000
REF4	25.391	25.393	-0.002

From Table A1.3 and Table A1.4, the differences between the GPS Orthometric heights and the levelled Orthometric heights were found to be less than ±0.003m, indicating that there are not any gross errors in the GPS Orthometric heights.

The GPS grid coordinates and Orthometric heights (and their standard deviations) were then used as control in the next sections, for adjusting the horizontal and the vertical networks of the Campus-Network and the Testing-Points.

A1.4 Vertical Network

Vertical control networks are a series of points on which precise heights, or elevations, have been established. As part of a vertical control network, the benchmark's elevation is known relative to a vertical reference datum.

Depending on accuracy requirements, vertical surveys can be run by differential levelling, trigonometric levelling (i.e. using total-stations) or satellite positioning systems (i.e. GPS levelling). The most accurate and widely applied method is precise differential levelling [Schofield, 2001; Duggal, 2004; Wolf and Ghilani, 2006; Soycan, 2006]. With this method, the height of one point is determined relative to the known height of another point using high specifications levelling instruments, such as digital level and bar-coded invar level staff. In addition, observations are usually taken under certain procedures and weather conditions.

There were three vertical networks observed in this research: OSBM-Network, Campus-Network and Testing-Points. The OSBM-Network was carried out as a gross error check for the GPS Orthometric heights and the adjusted Orthometric heights from the Campus-Network to serve as vertical control for the Testing-Points. The adjusted Orthometric heights from the Campus-Network and from the Testing-Points will then be considered as the ‘truth’ coordinates.

A1.4.1 Data Collection

The Wild NA2000 automated digital level with a bar-coded invar level staff was employed in the data collection (Figure A1.4). According to Schofield [2001], the standard deviation for a 1-km double-run levelling, at ranges below 50m, for digital levelling is ± 1.5mm.

Figure A1.4: The author working with the Wild NA2000 automated digital level (left) and a colleague holding the bar-coded invar level staff (right)

Before the data collection started, it was necessary to conduct a Two-Peg-Test in order to define the magnitude of the collimation error which will be applied to the levelling observations. More information about this test can be found in surveying books (i.e. [Schofield, 2001; Kavanagh, 2006; Wolf and Ghilani, 2006]. This test was conducted near the IESSG building by taking levelling readings and measuring horizontal distances between the instrument and the bar-coded staff. A collimation error of -0.0055 mm per metre was found in the Wild NA200 digital level.

In order to determine the misclosure error of the levelling, levelling closed-loops were carried out between the 'truth' points. Besides, approximate horizontal distances were measured between the digital level and Back-Sight (BS), Intermediate-Sight (IS) or Fore-Sight (FS) points using the digital level.

Levelling closed-loops were carried out for three vertical networks: OSBM-Network, the Campus-Network and the Testing-Points. In the OSBM-Network, a levelling closed-loop between two of OSBMs (OSBM41 and OSBM42) and two of the GPS points (REF1 and REF2) were carried out. This loop was performed as follows: OSBM42 → REF1→ OSBM41→ REF1→ OSBM42→ REF2→ OSBM42. Between the sequential points, there were several turning points (TPs) used which are not illustrated in the loop. Furthermore, horizontal distances measured by the digital level were noted together with the BSs and FSs in field levelling sheets.

In the Campus-Network levelling, closed-loops were carried out between every sequential station of the Campus Network, starting from GPS/Total-Station point to another GPS/Total-Station point and back to the starting point. For example, a

closed-loop REF1→ REF2→ REF1 and another closed-loop REF2→ POP→ REF2. Between the sequence points, there were several TPs used which are not illustrated in the loop. Furthermore, horizontal distances measured by the digital level were noted together with the BSs and FSs in field levelling sheets. In total, there were 11 levelling closed-loops used in the Campus-Network.

For the Testing-Points, levelling closed-loops between the Campus Network points and all Testing-Points located between these points were carried out. For example, a closed-loop TOWER→ T8→ T7…T1→ ST1→ POP→ ST1→ T1→ T2…T8→ TOWER. Between the sequential points, there were several TPs used which are not illustrated in the loop. Furthermore, horizontal distances measured by the digital level were recorded together with the BSs, ISs and FSs in the field levelling sheets. In total, there were 4 levelling closed-loops used for the Testing-Points.

A1.4.2 Data Processing

Levelling data were transferred from the field levelling sheets to Microsoft Excel software. An Excel sheet was used for every levelling closed-loop. In addition, one Excel sheet was used for the differences in heights (Dhs) of the Campus-Network and their misclosure, another for the Dhs of the Testing-Points and their misclosure and one for the two-peg test.

In the three vertical networks (OSBM-Network, Campus Network and Testing-Points), the processing strategy for processing the levelling data was as follows:

- *Collimation Error Determination*: Collimation error was calculated using the two-peg test observations.
- *Apply Collimation Error*: The BSs, ISs and FSs observations were corrected for the collimation error.
- *Calculate Reduced Level (RL)*: RLs were calculated from the adjusted BS, IS and FS using height of plane collimation concept.
- *Misclosure Error Determination*: By closing the levelling survey to the start point, makes it possible to determine the discrepancy (misclosure) in the measurement by subtracting the last calculated RL from the first one.

- *Misclosure Error Distribution*: Misclosure errors were distributed (as corrections) between levelling points by allocating the error in proportion to the distance levelled.
- *Adjusted RL Calculation*: The adjusted RL can be calculated simply by adding the calculated RL to the correction.

A1.4.3 Processing Results and Analysis

The misclosure error for the OSBM-Network was found to be equal to 0.003m. Furthermore, the misclosure errors for the Campus-Network loops were found to be varying between 0.002m to -0.003m while, the misclosure errors for the Testing-Points loops were found to be varying between 0.002m to -0.003m (Figure A1.5).

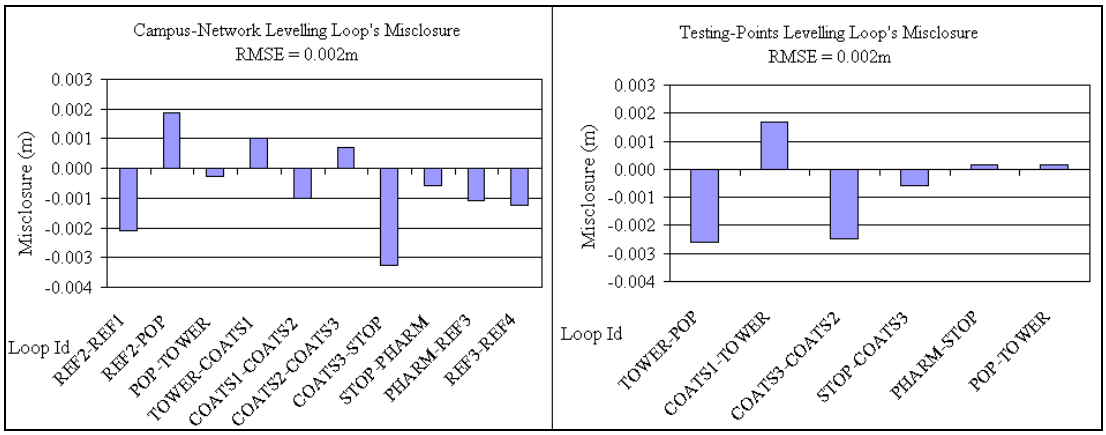

Figure A1.5: Misclosure error for the Campus Network's loops (left) and Testing Points (right)

According to Schofield (2001), a common criterion used to assess the misclosure (E) is:

$$E = m\sqrt{K}$$

where K = distance levelled or length of loop in kilometres, m = a constant in millimetres and E = the allowable misclosure in millimetres. For a levelling loop, the value of m can be 4mm, 5mm, 6mm, 8mm or 12mm for first order class I, first order class II, second order class I, second order class II or third order respectively [Bossler, 1984; Wolf and Ghilani, 2006]. Using the previous formula used for assessing the misclosure, the constant m for Campus-Network and Testing-Points were found to vary from 0.3mm to 6.0mm which indicate that all loops were better

than the second order class I specifications. According to Kavanagh [2006], for most engineering works, benchmarks are established at third order specifications.

A1.4.4 Network Adjustment

The vertical networks (OSBM-Network, Campus Network and Testing-Points) were adjusted using VERNET software; a software developed by the IESSG for adjustment and analysis of vertical networks. VERNET performs a least squares adjustment of a vertical network. It requires the preparation of a control file that includes: approximate heights, height differences, absolute heights of the control points and their standard errors and other information. Complete explanation about VERNET control file can be found in Appendix 4 (VERNET Manual).

The following strategy was followed to adjust the different vertical networks:

- *Approximate heights*: The adjusted RLs, calculated from different loops in previous section, were used as approximate heights. The number of points for the OSBM-Network, Campus-Network and Testing-Points were 4, 11 and 39 respectively.
- *Difference in height*: From the adjusted RLs, the differences in height (Dhs) between sequential points were calculated. The number of observations (Dhs) of the OSBM-Network, Campus-Network and Testing-Points were 6, 10 and 76 respectively.
- *Vertical control points*: For the OSBM-Network, the Orthometric heights for the OS BMs (2 BMs) with standard error of 0.000m were used as vertical control points. For the Campus-Network, the Orthometric heights for the GPS points (4 GPS Points) and their standard errors were used as vertical control points. The output heights from the adjustment of the Campus-Network points (only 7 points were used) and their standard errors were used as vertical control points for the Testing-Points.
- *Adjustment parameters*: Standard deviation for the height differences and for the control points can be included in the control file. This allows VERNET to take them into account in the computations.

- *Compute Network*: The network computation performs the adjustment computation. After successfully carrying out the network adjustment, there were two files resultant from the adjustment; vertical coordinates file and report file. The vertical coordinates file includes the adjustment results such as point number, adjusted coordinates, RMSE and point Id. The report file includes all information about observations (as in the control file), adjustment results and statistics about network reliability analysis.

A1.4.5 Adjustment Results and Analysis

In the adjustment report, the results of the OSBM-Network showed a sigma zero of 0.36mm ± 0.13mm with an a-posteriori RMSE of better than 0.3mm estimated for the adjusted heights (Appendix 5: OSBM Network – Vertical Adjustment Network). Besides, from the network reliability analysis, a maximum value of the residuals/sigma (RES/SIGMA) for the spirit levels was found equal to 1.61. The lower the RES/SIGMA is, the more reliable the results are, as clarified by VERNET, with a flag * for RES/SIGMA > 2.0, a flag ** for RES/SIGMA > 2.5 and a flag *** for RES/SIGMA > 3.0. Furthermore, a maximum RATIO (a-posteriori RMSE / a-priori RMSE) was found equal to 0.71. Similar to the RES/SIGMA, the lower the RATIO is, the more reliable the results are, as clarified by VERNET, with a flag @ for a RATIO > 0.9. Hence, based on the network reliability analysis, the adjustment results were found to be within the tolerances specified in VERNET.

The adjustment results of the Campus-Network showed sigma zero of 0.16mm ± 0.06mm with an a-posteriori RMSE of 1.1mm estimated for the adjusted heights. Besides from the network reliability analysis, maximum values of RES/SIGMA were found equal to 1.11 and 1.58 for the spirit levels and the height respectively. Furthermore, RATIOs of 1.0 (with a flag) @ and 0.51 were calculated, for the spirit levels and the height respectively.

The adjustment results of the Testing-Points showed a sigma zero of 0.83mm ± 0.09mm with an a-posteriori RMSE of better than 1.1mm estimated for the adjusted heights. Besides from the network reliability analysis, maximum values of the

RES/SIGMA were found equal to 3.46 (with a flag ***) and 1.87, for the spirit levels and the height respectively. Additionally, there were another two flags ** and two other flags * appearing in the report. Furthermore, RATIO between 0.63 and 0.68 were calculated in the spirit levels and RATIO between 0.71 and 0.91 were calculated in the heights.

Although there were some flags appearing in the network reliability analysis in the Campus-Network and Testing-Points vertical network adjustment, a high level of precision could be considered to have been achieved for the heights of these vertical networks. Hence, the Orthometric heights of Campus-Network and the Testing-Points and their RMSE given in Appendix 6 (Truth Coordinates) were used as part of the 'truth' coordinates for all tests.

A1.5 Horizontal Network

A horizontal network is a network of stations of known geographic or grid positions referenced to a common horizontal datum. These stations are established to the degree of accuracy needed for the purpose of the survey. Usually, horizontal controls are established with conventional survey methods by measuring horizontal angles and horizontal distances using a total-station instrument.

There were two horizontal networks carried out to establish the horizontal coordinates of the 'truth' points: Campus-Network and Testing-Points. The horizontal grid coordinates of the GPS points were used as horizontal controls for the Campus-Network. Besides, the adjusted horizontal grid coordinates of the Campus-Network were used as horizontal controls for the Testing-Points. The adjusted horizontal grid coordinates from the Campus-Network and from the Testing-Points will be considered as the 'truth' coordinates. For the horizontal network, the following section will discuss: the data collection, data processing, processing results and analysis, network adjustment and network adjustment results and analysis.

A1.5.1 Data Collection

Two total-stations were employed in the data collection: a Leica TCR1201 and a Leica TCA2003 (robotic total-station). These instruments are considered to have a high level of manufacturer specifications. as shown in Table A1.5 [Leica-Geosystems-AG, 2005b; Leica-Geosystems-AG, 2006d].

Table A1.5: Leica TCR1201 and Leica TCA2003 manufacturer specifications

Total-Station	Angle Precision: Hz/V	Compensator Setting Precision	Distance Measurement Precision: Standard / Tracking	Laser Plummet Precision
Leica TCR1201	1"	0.5"	2mm+2ppm / 5mm+2ppm	1mm at 1.5m
Leica TCA2003	0.5"	0.3"	1mm+1ppm / 5mm+2ppm	1mm at 1.5m

Although the above instruments have a high level of manufacturer specifications, there are a number of errors that can be inherent in the surveying equipment. Verification of EDM equipment is concerned with the determination of instrument errors. These can then be used to monitor the performance of the instrument. So, before starting observations, it is necessary to conduct some tests to make sure that the instrument functions properly. For example, Laser/Optical plummet test, Collimation in Azimuth, Spire test (vertical axis test) and Additive Constant (more information about these tests can be found in [Schofield, 2001]). Laser plummet test was carried out for the above instruments and the results showed that the laser plummet errors were within the size of the manufacturer tolerance (within 1mm). Besides, the results of the Collimation in Azimuth and the Spire test showed that there are not any errors found in the TCA2003 and TCR1201 total-stations (Appendix 7). In general, the collimation and vertical axis errors can be eliminated by observing face left and face right horizontal and vertical angles.

In order to determine the additive constant (zero error correction) for the Leica TCR1201 and TCA2003 total-station instruments with particular prisms, a zero error test was carried out near the IESSG building (points A, B and C) (Figure A1.6). More information about the zero error test can be found in [Schofield, 2001; Kavanagh, 2006; Wolf and Ghilani, 2006].

Figure A1.6: The author conducting the Zero Error Test using the Leica TCR1201 total-station

Constant errors of -2mm and 0mm were found in prisms 5 and 6 respectively, when used with the Leica TCR1201 total-station (Appendix 7). However, a constant error of 0mm was found for the prisms 1, 2 and 3 when used with the Leica TCA2003 total-station (Appendix 7). Hence, a correction of 2mm was applied for all future distances measured using prism 5 and the Leica TCR1201 total-station.

For the horizontal network, field data collection was carried out in two stages. The first stage was the data collection of the Campus Network using the Leica TCR1201 total station together with prisms (5 and 6) attached to tripods. Data collection started by setting one prism on REF1 point (GPS point), the total-station on REF2 point (GPS point) and another prism on POP point (first point of the Campus Network). Total-station observations including horizontal angles, vertical angles and slope distances were measured between these points and stored with point numbers in the memory card of the instrument. In addition, point numbers, prism types and instrument height and the target height, measured using a steel tape, were noted in a special sheet. Since it was not possible to collect multiple total-station observations for a point under the same point name, data was collected for the particular point using different point names. Two rounds of measurements were observed with both face left and face right between the points. The total-station was then moved to POP point, the prism on REF1 point was moved to REF2 point and the prism on POP point was moved to TOWER point (second point of the Campus Network). Similar to the previous data collection, two rounds observations were collected between points. Following the same procedure, the total-station and prisms continued to be

moved on all of Campus points closing on REF3 and REF4 points (GPS points). In all, there were 9 total-station setups in this stage.

The second stage was the data collection of the Testing-Points which consists of 31 points fixed (using surveying nails) along the most difficult area within the trial route. The Leica TCA2003 total-station together with prisms (1, 2 and 3) attached to tripods were employed in this stage. Data collection started by setting one prism on REF2 point, the total-station on ST1 point (new testing point), another prism on T1 point (new testing point) and another prism on ST2 point (new testing point). Total-station observations of two rounds (with face left and face right) were collected between these points and stored in the memory card of the instrument. In addition, point numbers, prism types, instrument height and the target height were noted in special sheet.

The prism on T1 point was then moved to T2 point (new testing point) while the total-station and the prisms on REF2 and ST2 were left on the same points. Similar to the previous data collection, two rounds of observations were collected between these points. After that, the prism of T2 continued to be moved to new testing points (from T3 to T8) and data collection continued with the same technique.

The total-station then moved to ST2 point, the prism on REF2 moved to ST1, the prism on ST2 moved to TOWER point and the prism on T8 returned to T1 point. Again, two rounds of observations were collected between these points and all of the testing points from T1 point to T8 point.

The total-station and the prisms continued to be moved along all testing points fixed along the trial route. In general, each of the testing points were observed two rounds (with face left and face right) from one station with two reference objects and another two rounds from a different station with two reference objects. In all, there were 6 total-station setups on this stage.

A1.5.2 Data Processing

The survey data was transferred from the total-station to a computer and saved in Leica TPS and/or GSI format. Since multiple total-station observations were collected for each of the network points (Campus-Network and Testing-Points) using different IDs, control files were prepared to include information about all total-station setups. The first two lines in the control file start with '%' and could include any desired information about the network or the control file. After that for each total-station setup, a line with '*' refers to a new total-station setup being started. The next line includes information about reference station such as point ID and instrument height. The following lines include information about targets being observed from the total-station setup. This information includes the target new ID, target height, prism's constant error correction and target IDs as in the total-station file. An example of control a file for the total station data collection can be found in Appendix 8.

The total-station observations were then pre-analysed using Total Station Observations Manager (TSOM – a software developed by the author) (Figure A1.7).

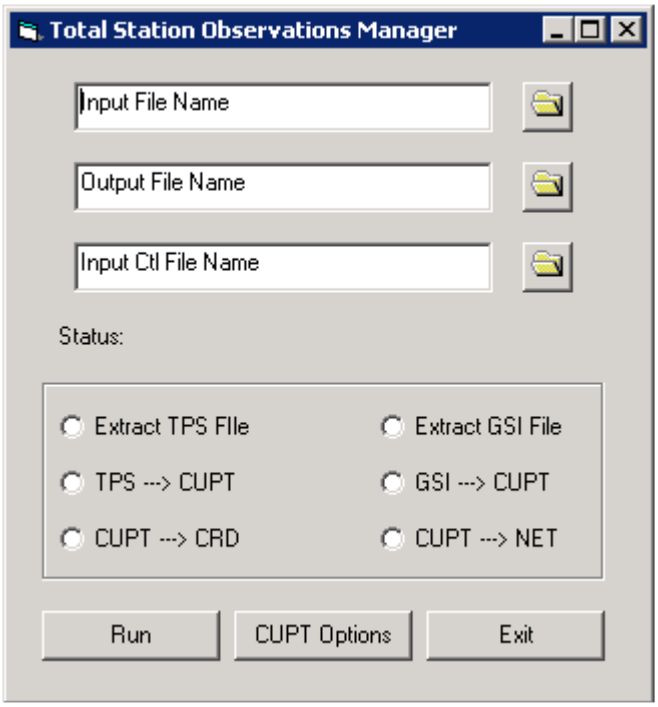

Figure A1.7: Total Station Observations Manager software

TSOM software can perform the following:

- *Extract TPS file and Extract GSI file*: extract coordinates and total-station observations in two separate files (total-station observations file and coordinates file).
- *TPS → CUPT and GSI → CUPT*: convert total-station file from TPS/GSI format to CUPT format based on the set-up information in the control file. Converting total-station observations to CUPT format make it possible to process these observations using CUPT software. This software was developed by the author and can perform a 3d network adjustment using least squares. Generally, CUPT format is a special format suggested by the author for total-station observations. The file with CUPT format can be divided into three parts: headers, control points and observations. The headers include total-station instrument and human errors and can be determined using *CUPT Options* (Figure A1.8). Some of manufacturer specifications for the TCR1201 and TCA2003 total stations (as shown in Table A1.5) are stored within TSOM.

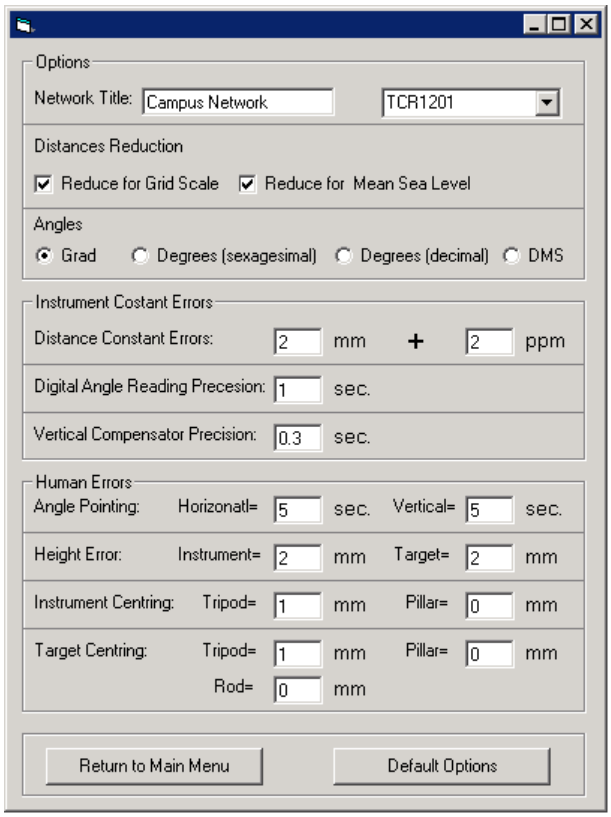

Figure A1.8: CUPT Options

- The second part of the CUPT file includes information about the control points such as the coordinates of the control points (E, N and Ht), standard deviation, fixed coordinates (i.e. XYZ means use E, N and Ht as control points) and control points ID (i.e. RTK or CTRL). The major part -the last part- of the CUPT file includes stations set-up information (i.e. station ID and hi) and total-station observations made from each set-up.
- *CUPT → CRD*: calculate coordinates (CRD) for total station observations from CUPT file. Scale factor could be taken into account in the calculation depends on the headers of CUPT. The output coordinates from this option can be similar to those calculated by the total-station.
- *CUPT → NET*: convert CUPT file to network (NET) files. Mainly, there are three outputs from this option: HORNET files, network reduction sheet files, and calculated coordinates file (similar to the file obtained from *CUPT → CRD* option). HORNET files are used in HORNET software for horizontal network adjustment and include a control file (HORCTL.CTL), horizontal angle observations file (angles.dat), distance observations file (dists.dat), position observations file (points.dat) and approximate coordinates for all points (Approx.pos). More detail about HORNET can be found in [Brookes, 1996]. The network reduction sheet files include 'Net_Sheet.txt' file and 'ErrorsSummary.txt' file. The 'Net_Sheet.txt' file contains horizontal angles reduction, vertical angles reduction and distances reduction while the 'ErrorsSummary.txt' file summaries the different errors of the reductions (see Appendix 9: Example of Network Reduction Sheet Files).

A1.5.3 Processing Results and Analysis

Using TSOM, the Campus-Network file was converted to CUPT format (Appendix 10: Example of CUPT File). Then the CUPT file was converted to NET files. Considering the 'ErrorsSummary.txt' file, the RMSE for the differences between the maximum and minimum measured distances were found to be equal to 0.61mm, with maximum differences of 1.0mm. However, the RMSE for the differences of the maximum and minimum reduced horizontal angles in two rounds were found to be equal to 3.66 seconds, with maximum differences of about 8 seconds (Figure A1.9

left). Furthermore, the RMSE for the differences of the maximum and minimum reduced vertical angles in two rounds were found to be equal to 4.34 seconds, with maximum differences of about 8 seconds (Figure A1.9 right).

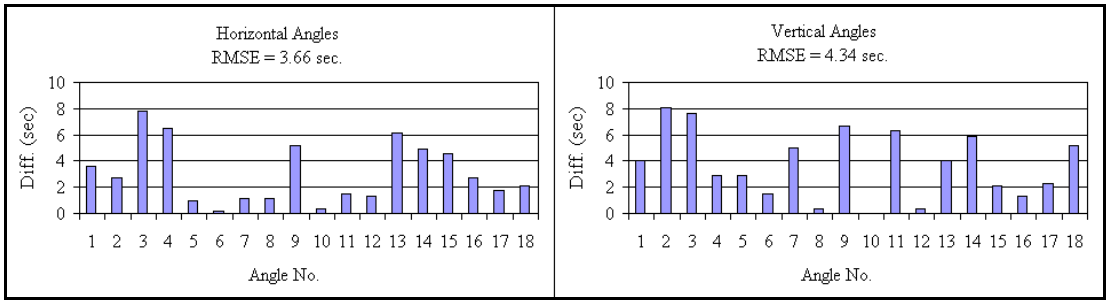

Figure A1.9: Differences of the reduced horizontal angles in two rounds (left) and differences of the reduced vertical angles in two rounds (right)

Similar to the Campus-Network, using TSOM the Testing-Points file was converted to CUPT format. Then the CUPT files were converted to NET files. After Analysing the 'ErrorsSummary.txt' file, the RMSE for the differences between the maximum and minimum measured distances were found to be equal to 0.3 mm, with maximum differences of 1 mm. However, the RMSE for the differences of the maximum and minimum reduced horizontal angles in two rounds were found to be equal to 2.46 seconds, with maximum differences of about 10 seconds (Figure A1.10 left). Furthermore, the RMSE for the differences of the maximum and minimum reduced vertical angles in two rounds were found to be equal to 1.25 seconds, with maximum differences of about 8 seconds (Figure A1.10 right).

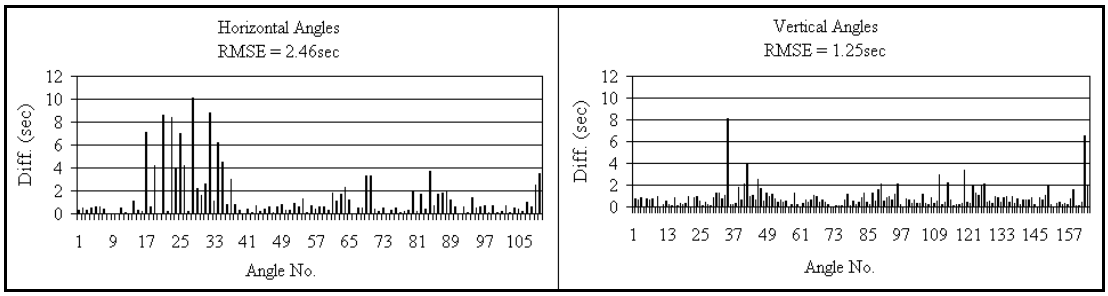

Figure A1.10: Differences of the reduced horizontal angles in two rounds (left) and differences of the reduced vertical angles in two rounds (right)

The differences in the measured distances in both Campus-Network and Testing-Points were found to be within the instrument's claimed precision (see Table A1.5). However, the differences in the horizontal and vertical angles of the Campus-

Network and the Testing-Points were not, which could be due to a combination of different uncertainties such as digital angle precision, instrument and target centring errors and pointing errors.

Overall, the total-station observations can be considered to be free of gross errors and suitable for use in the adjustment.

A1.5.4 Network Adjustment

Horizontal networks were adjusted twice, using CUPT and using HORNET, for comparison purposes. As mentioned in the Data Processing section, CUPT performs a 3D network adjustment, whereas HORNET software was developed by the IESSG for adjustment and analysis of horizontal networks.

In general, the following strategy was followed for horizontal network adjustment:

- *Observation files*: CUPT and HORNET observation files were produced from the total-station observation file using TSOM.
- *Control points*: The adjusted Orthometric heights and their standard deviations obtained from the vertical network adjustment were used as vertical controls in both the Campus-Network and the Testing-Points using CUPT. Further, the horizontal grid coordinates of the GPS points and their standard deviations were utilised as horizontal controls in the Campus-Network using CUPT and HORNET. The adjusted horizontal grid coordinates of the Campus-Network and their standard deviations were utilised as horizontal controls in the Testing-Points using CUPT and HORNET.
- *Adjustment parameters*: Instrument uncertainties and human uncertainties can be included in CUPT headers. These uncertainties are used in CUPT to build a stochastic model for the least squares adjustment. Also, CUPT allows defining alpha (the significance level used to compute the confidence level; the confidence level equals 100 * (1 - alpha) %) to be used in X^2 test. Besides, the instrument uncertainties and human uncertainties can be included as headers in each of HORNET observation files.

- *Compute Network*: The network computation performs the adjustment computation. After successfully carrying out the network adjustment using CUPT, there were a plot of several graphs and a report. The output graphs show the network geometry, observation residuals (each graph shows residuals plot, histogram plot and normal probability plot) and RMSE for coordinates (each graph shows similar plots to that on observation residuals). The adjustment report shows the adjustment results (such as redundancies, X^2 test results, etc), observed coordinates with their a-priori standard errors and adjustment coordinates with their a-posteriori standard errors and their absolute positional error ellipses. In addition, it shows adjustment observations (such as distances and angles) with their residuals and their standard errors. After successfully carrying out the network adjustment using HORNET, there were two main files resultant from the adjustment: horizontal coordinates file and a report. The horizontal coordinates file includes the adjustment results such as point number, adjusted coordinates, RMSE and point Id. The report includes all information about observations (as in the control file), adjustment results and statistics about network reliability analysis.

A1.5.5 Network Adjustment Results and Analysis

After successfully running CUPT to adjust the Campus-Network, the adjustment results show that X^2 test was passed with 95% confidence with a maximum error ellipse of 3mm for the adjusted coordinates. One of the output figures from CUPT is the network geometry and error ellipses figure of the adjusted points (Figure A1.11). It is worth mentioning that all coordinates used in the adjustments are in the National Grid OSGB36 coordinate system.

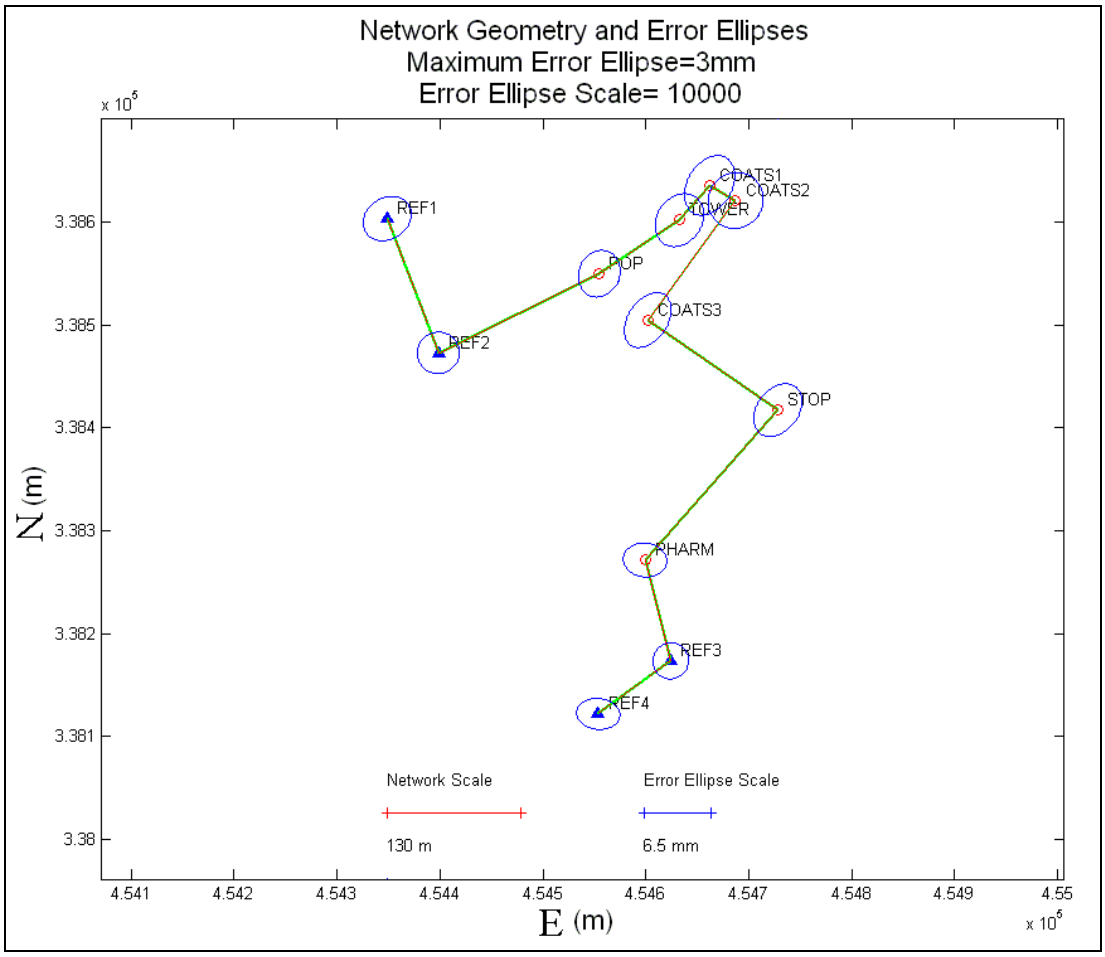

Figure A1.11: Campus-Network network geometry and error ellipse output from CUPT

Other output figures from CUPT include: horizontal angles residuals, vertical angles residuals, distances residuals, Northing residuals, Easting residuals and Orthometric heights residuals which are plotted in figures show the residuals, histogram plot and normal probability plot. For example, Figure A1.12 shows horizontal angles residuals in different plots.

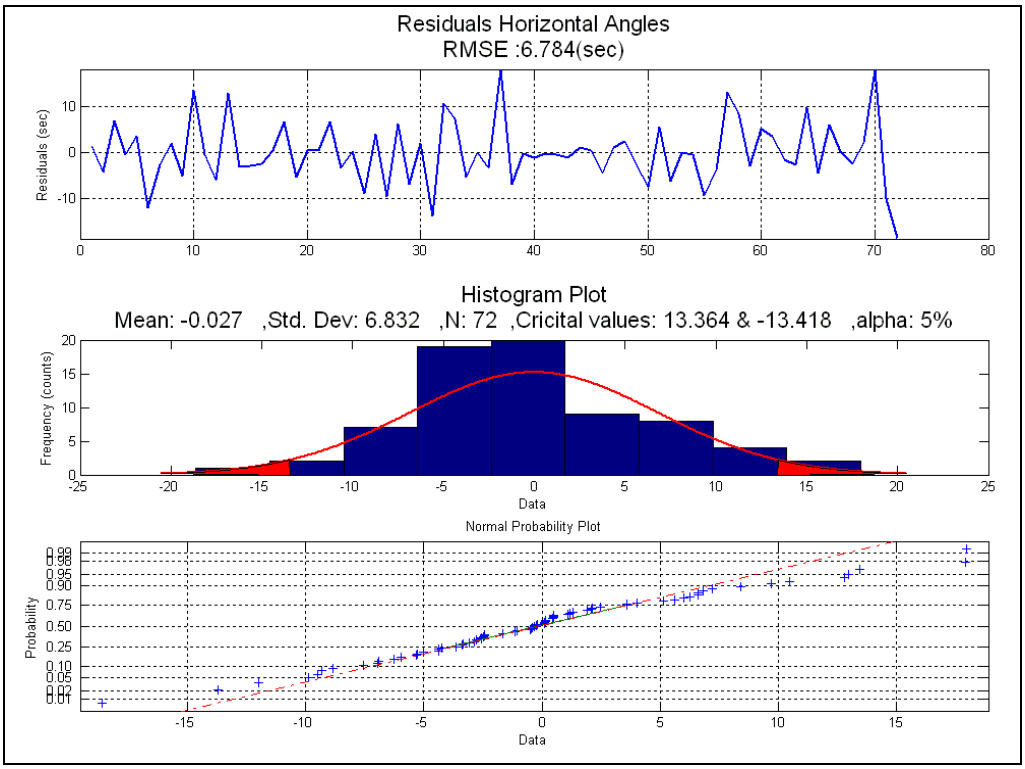

Figure A1.12: Horizontal angle residuals plot (top), histogram plot (middle) and normal probability plot (bottom) for the Campus Network

In general, most of the residuals of the total-station observations (distances and angles) were found to be located within the normal distribution in the histogram plot. However, few observations were found to be located within the tails (at alpha of 5%). Furthermore, most of the residuals were found to be located close to the normal probability plot line. The residual of the output adjusted coordinates (E, N and Ht) were found within the normal distribution in the histogram plot. Besides, the residuals were found to be located close to the normal probability plot line. These results indicate the high quality of the observations as well as for the adjusted coordinates.

For comparison purposes, Campus-Network was adjusted using HORNET software. The results of HORNET adjustment showed maximum error ellipses of 4.8mm with sigma zero of 0.82mm ± 0.72mm (Appendix 11: Example of HORNET Adjustment Report) for the adjusted coordinates. Besides from the network reliability analysis, maximum values of RES/SIGMA were found equal to 1.49, 1.78 and 2.06 for the observed angles, observed distances and observed positions respectively. Furthermore, maximum RATIOs of 0.67, 0.87 and 0.90 were calculated for the observed angles, observed distances and observed positions respectively.

The output horizontal coordinates (E, N) from CUPT were compared with the horizontal coordinates calculated from HORNET. Additionally, the Orthometric heights computed from CUPT were also compared with 'truth' heights achieved from the Vertical-Network (Figure A1.13).

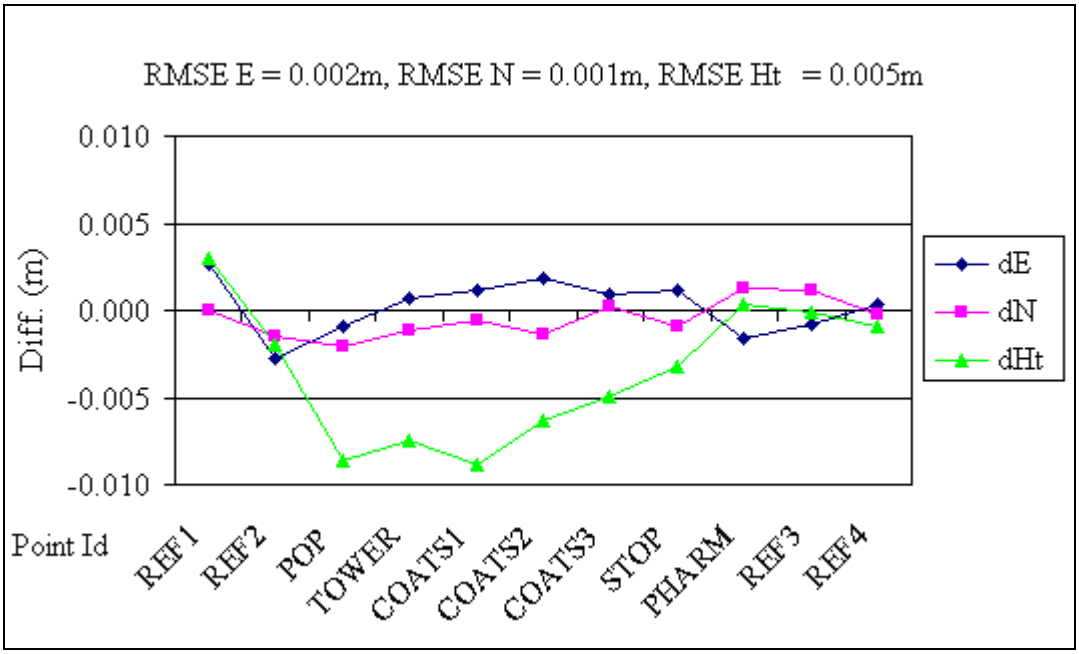

Figure A1.13: Campus-Network, differences between CUPT horizontal coordinates and HORNET horizontal coordinates and between CUPT heights and 'truth' heights

The RMSEs were found to be equal to 0.002m, 0.001m and 0.005m for the differences in Easting, Northing and Orthometric heights respectively. The differences in Easting and Northing coordinates could be due to the use of different uncertainties in CUPT and HORNET. In CUPT, various uncertainties were used in the horizontal angles and in the distances. However, fixed uncertainties for all horizontal angles and for all distances were used within HORNET. Another reason could be the adjustment of a combined network (3d network in CUPT) rather than a horizontal network (2D network in HORNET). Within 3d adjustment, the vertical angles can affect the height coordinate which as a result can affect the slope distances. The differences in the Orthometric heights could be due to the use of trigonometric levelling technique for measuring the heights differences which is less accurate than the use of precise levelling techniques [Duggal, 2004].

Overall, it was decided that the adjusted horizontal coordinates of Campus-Network output from CUPT software were suitable for use as 'truth' coordinates for all tests.

Similar to the first adjustment, the second adjustment was carried out for the Testing-Points using CUPT in the first instance and using HORNET in the second instance. The East and North coordinates of the Campus-Network were utilised as horizontal controls while the Orthometric heights obtained from Vertical-Network were used as vertical controls. The results of CUPT adjustment show that X^2 test was fail with 95% confidence with a maximum error ellipse of 2mm for the adjusted coordinates (Figure A1.14).

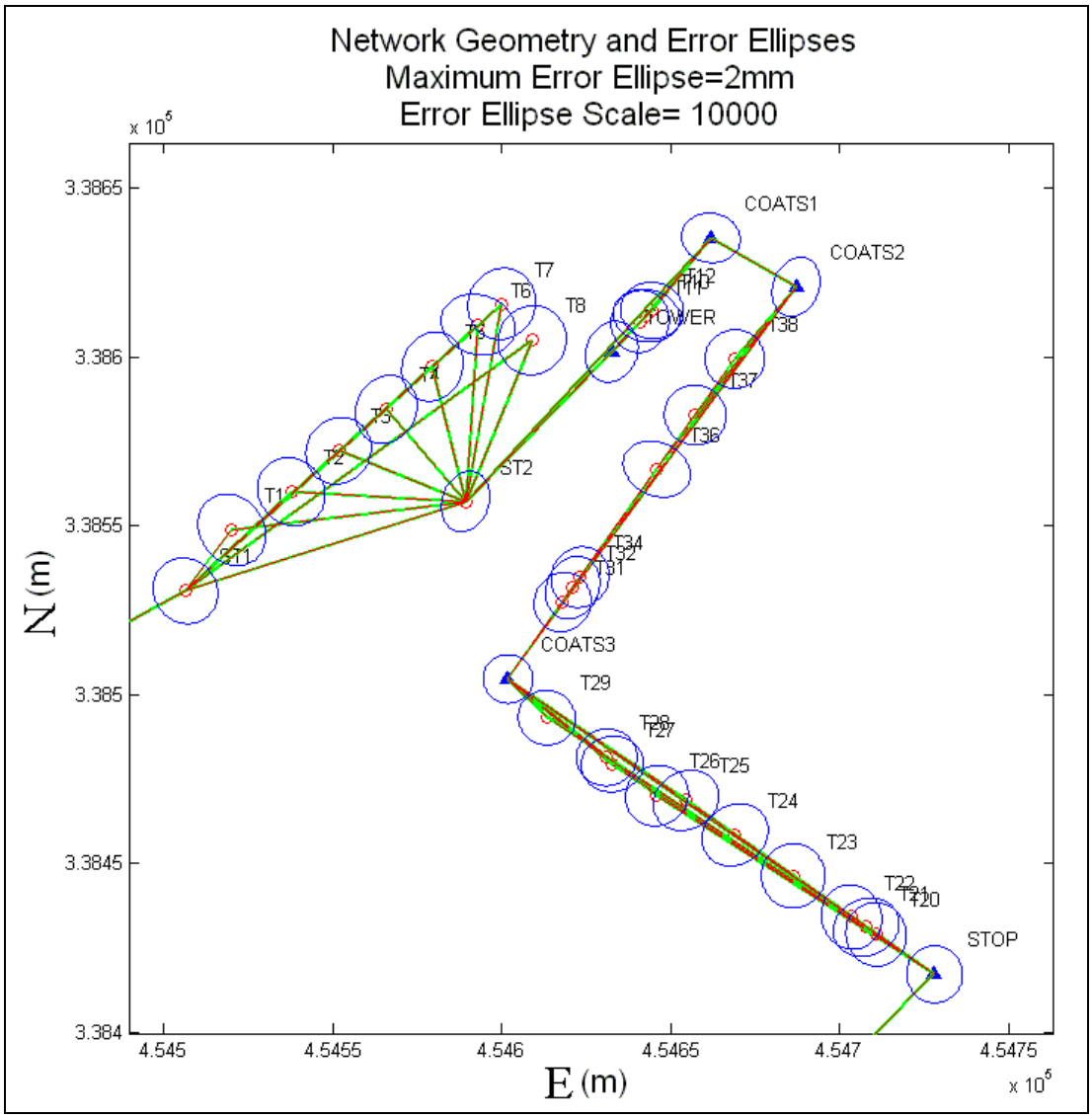

Figure A1.14: Testing-Points network geometry and error ellipse output from CUPT

The fail of X^2 test puts forward the importance the analysis of adjustment's observation residuals. Horizontal angles residuals, vertical angles residuals, distances residuals, RMSE Northing, RMSE Easting and RMSE Orthometric heights were plotted in different figures. These figures show the residuals, histogram plot and normal probability plot for the residuals or the RMSE. For example, Figure A1.15 shows horizontal angles residuals in different plots.

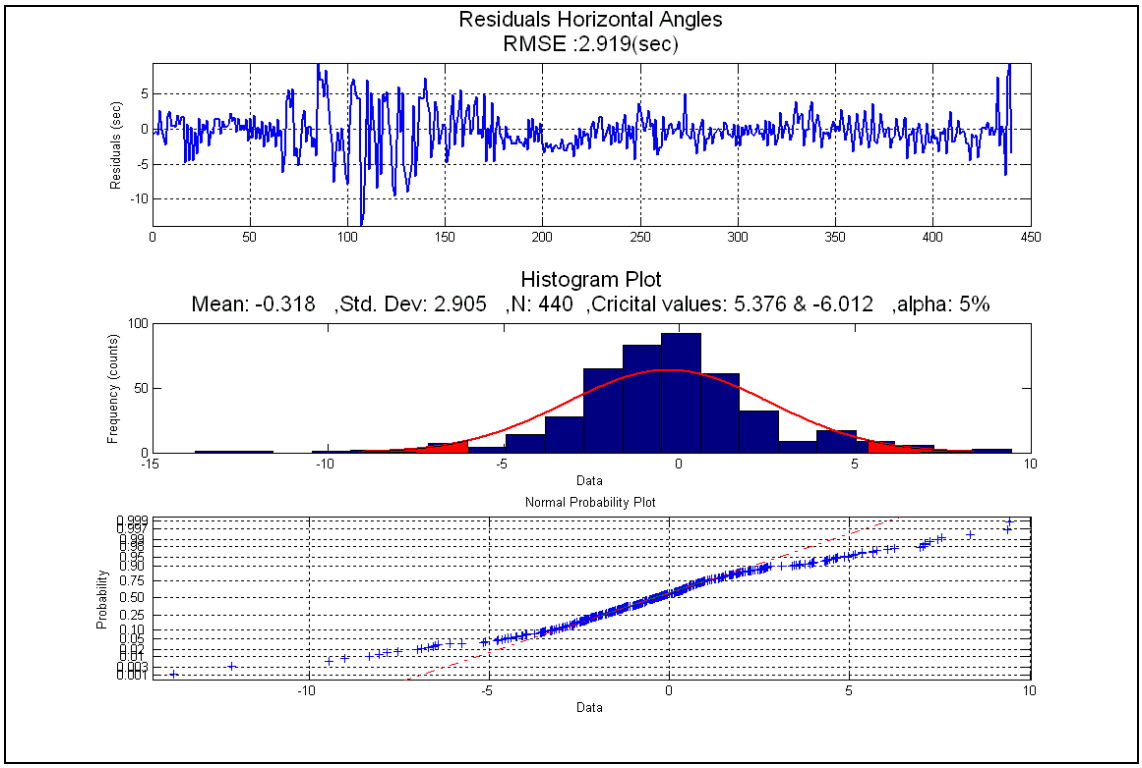

Figure A1.15: Horizontal angles residuals plot (top), histogram plot (middle) and normal probability plot (bottom) for the Testing-Points

From Figure A1.15, some of the residuals of the horizontal angles were found outside the normal distribution and hence these residuals were found away from the normal probability line. Similar outliers were found in the distances residuals as well as in the vertical angles residuals. More to the point, RMSE of 0.001m, 0.001m and 0.000m were estimated for the E, N and Ht respectively. In addition, the RMSE Easting of the GPS point REF4 was found outside the normal distribution and hence it was found away from the normal probability line (Figure A1.16). The RMSE Northing of the GPS point REF2 was found outside the normal distribution and hence the residuals were found away from the normal probability line (Figure A1.17). These outliers could be the reason that caused the X^2 test to fail.

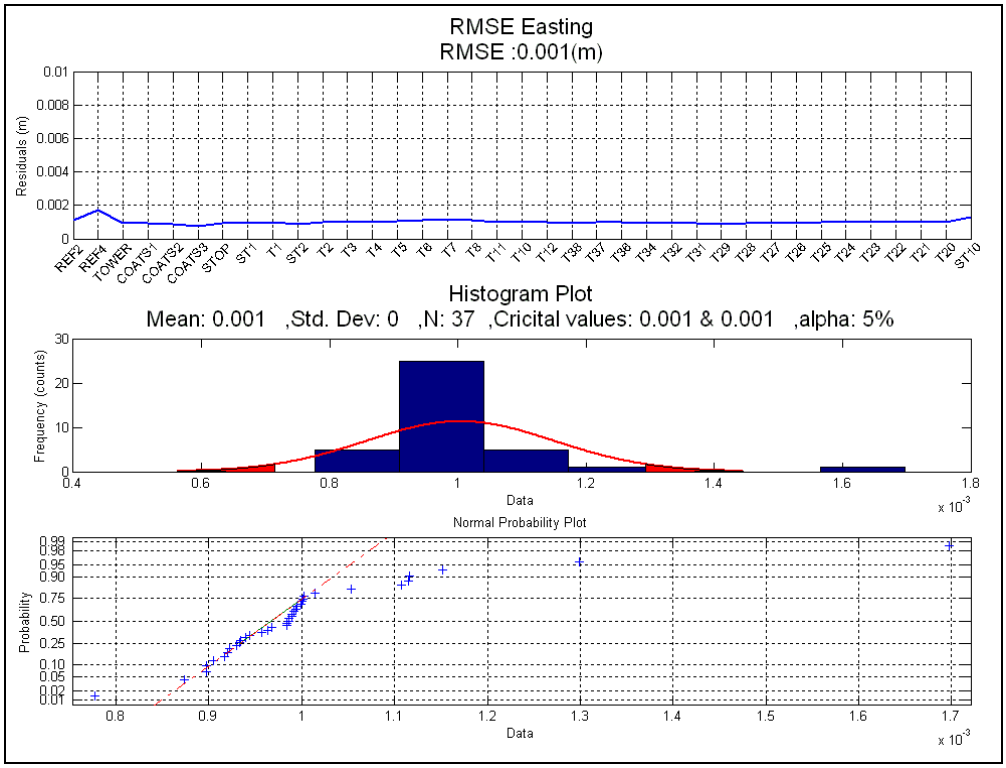

Figure A1.16: Easting RMSE plot (top), histogram plot (middle) and normal probability plot (bottom) for the Testing-Points

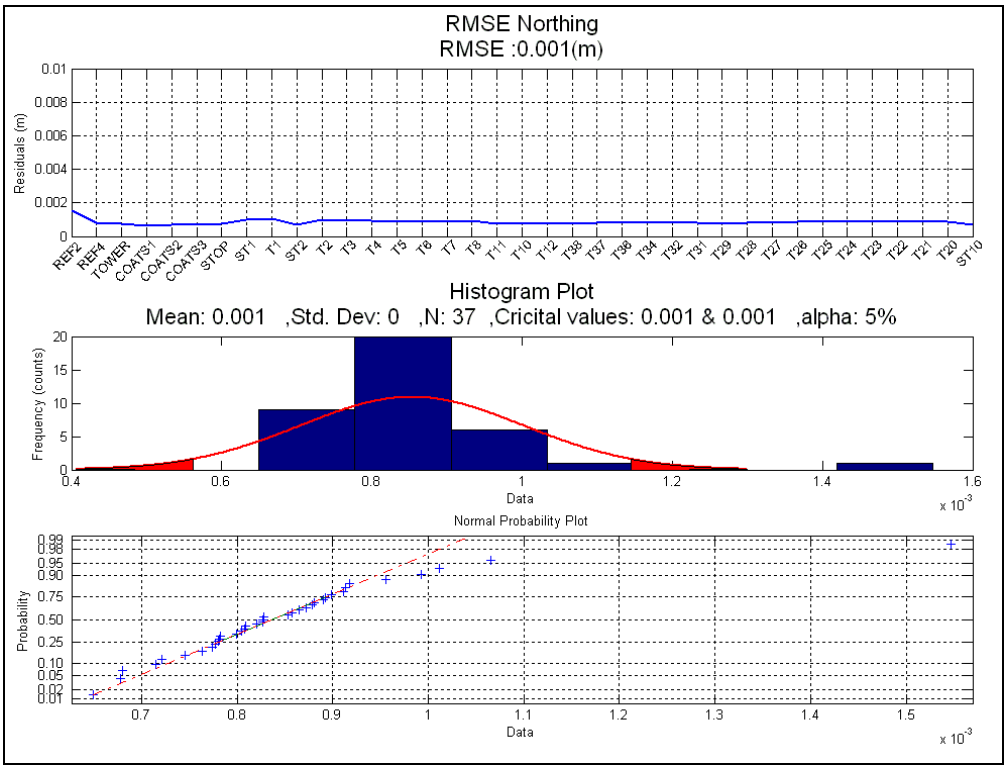

Figure A1.17: Northing RMSE plot (top), histogram plot (middle) and normal probability plot (bottom) for the Testing-Points

Unlike the RMSE of the Easting and Northing, the RMSE of the Orthometric heights were found within the normal distribution and hence close to the normal probability plot line (Figure A1.18).

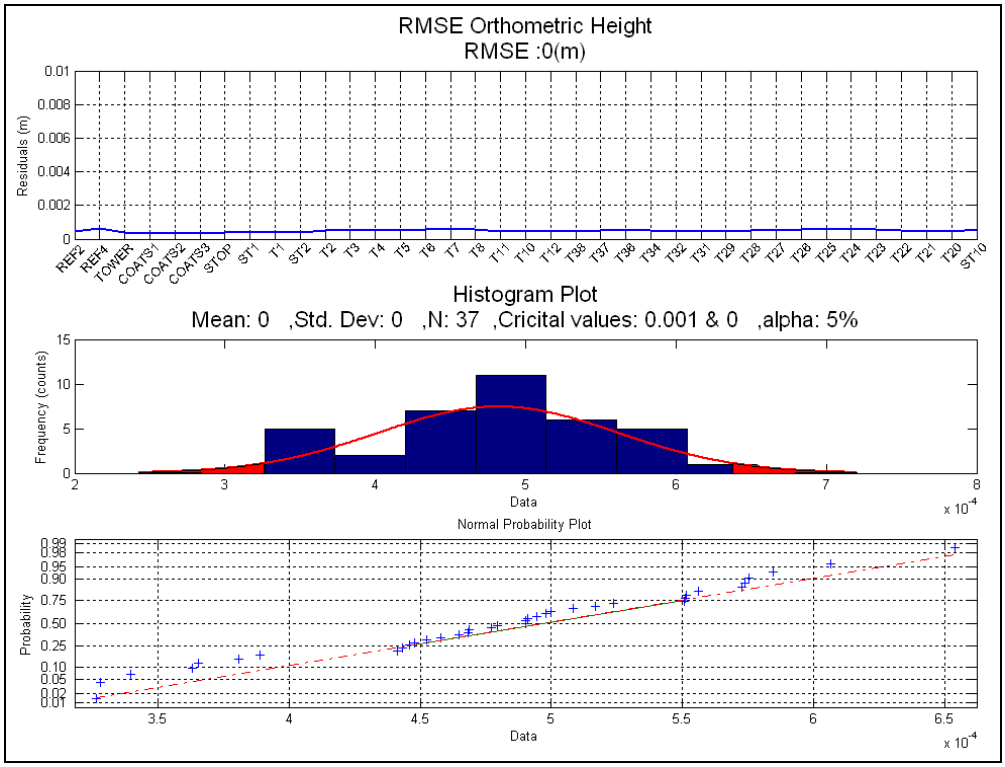

Figure A1.18: Orthometric heights RMSE plot (top), histogram plot (middle) and normal probability plot (bottom) for the Testing-Points

For comparison purposes, Testing-Points were adjusted using HORNET software. The results of HORNET adjustment showed a maximum error ellipse of 1.3mm with sigma zero of 0.43mm ± 0.02mm for the adjusted coordinates. Besides from the network reliability analysis, a maximum value of RES/SIGMA was found equal to 2.73 with a flag ** for the observed angles. Also, there were 4 observations with flags ***, 3 observations with flags ** and 8 observations with flags * in the RES/SIGMA of the observed distances. In addition, there were two positions with flags *** and one position with a flag ** in the observed positions. Furthermore, maximum RATIOs of 0.72, 0.94 and 0.91 were calculated for the observed angles, observed distances and observed positions respectively.

The resultant horizontal coordinates (E, N) from CUPT were compared with the coordinates calculated from HORNET (Figure A1.19). Additionally, the Orthometric

heights computed from CUPT were also compared with 'truth' heights achieved from levelling network (Figure A1.19).

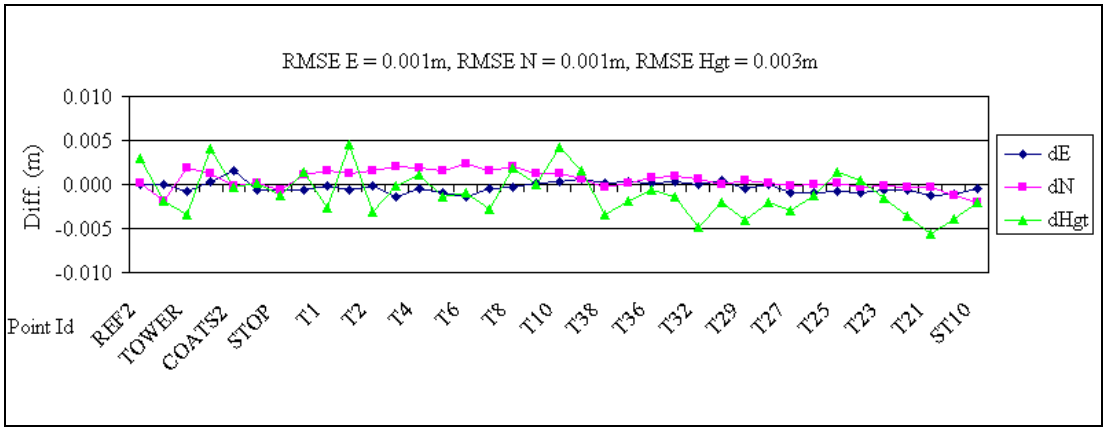

Figure A1.19: Differences between CUPT horizontal coordinates and HORNET horizontal coordinates and between CUPT heights and 'truth' heights for the Testing-Points

The RMSEs were found to be equal to 0.001m, 0.001m and 0.003m for the differences in E, N and Ht respectively. These differences could be due to similar reasons that are found in the Campus-Network adjustments.

Based on these results, the adjusted horizontal coordinates of the Testing-Points from CUPT software were considered to be suitable for use as 'truth' coordinates for all tests.

A1.6 Summary

This Appendix started by describing the network design and planning for a trial route at The University of Nottingham. This route includes different obstruction levels: for example open areas, streets with bridges and buildings in different heights and street with buildings and trees. In total, there were 41 points established, distributed mainly on the most difficult area of the trial route, to serve as testing points with ground 'truth' coordinates.

Three networks (GPS, Vertical and Horizontal networks) were used to establish the ground 'truth' coordinates. For each of the networks, the instrument used and the methodology followed in the data collection were described. For example, dual

frequency GPS receivers were employed in the GPS data collection. Data were collected in two days for about 30 minutes to 1 hour on each the GPS points. The Wild NA2000 digital level was utilised for vertical network data collection using closed loop level technique, and high specification total-stations were used in the data collection in the horizontal network.

Subsequently, the software and strategy utilised to process the different observations were discussed in the data processing. Next, the results achieved from the processing stage were analysed. The software and the adjustment strategy, used to adjust different networks, were discussed in the data adjustment sections. LGO software was used to post-process and adjust the GPS network and the adjusted results were used as 'truth' coordinates for both horizontal and vertical networks. The vertical network was then adjusted using VERNET. The horizontal network was pre-analysed using the author developed TSOM software, adjusted using the author developed CUPT software, and HORNET for comparison purposes.

Overall, a high level of precision was estimated for the vertical network, with 0.16mm ± 0.06mm and 0.83mm ± 0.09mm, and an a-posteriori RMSE of 1.1mm, estimated for the adjusted heights of the Campus-Network and the Testing-Points respectively. On the other hand, the adjusted horizontal coordinates output from CUPT software had a maximum error ellipse of 3mm and 2mm for the Campus-Network and for the Testing-Points respectively.

Through a combination of the three networks, a set of 'truth' coordinates were established for use in the tests on integrated GNSS based positioning.

Appendix 2: Collection of Photos for the Trial Area at the University of Nottingham's Campus

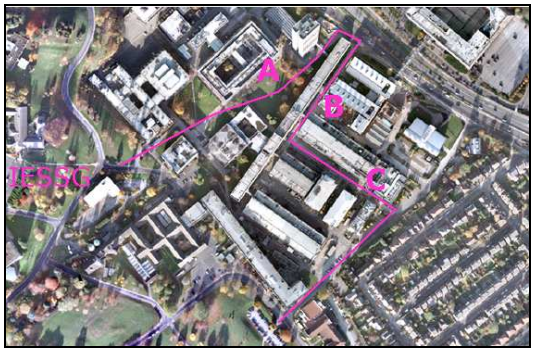

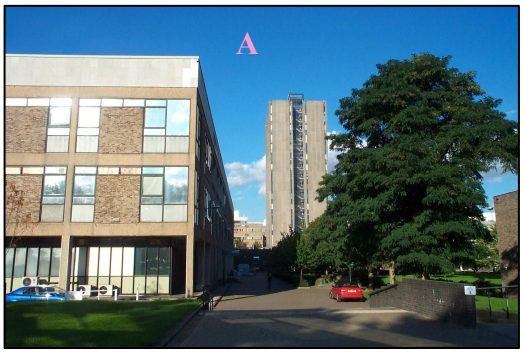

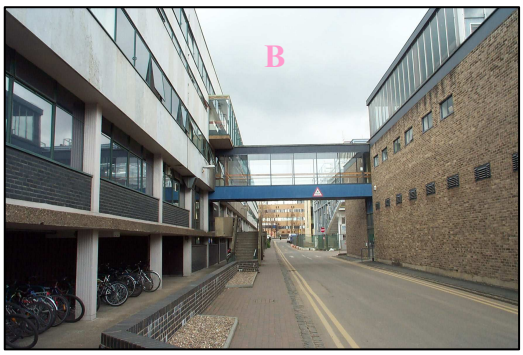

Appendix 3: GPS Network – Second Adjustment Report

Network Adjustment

www.MOVE3.com

Created: 12/18/2007 21:16:19

Project Information

Project name:	24+25-03-06_BIGF_SP3-Adjustment
Date created:	11/18/2007 14:32:16
Time zone:	0h 00'
Coordinate system name:	WGS 1984
Application software:	LEICA Geo Office 3.0
Processing kernel:	MOVE3 3.3.1

General Information

Adjustment

Type:	Weighted constrained
Dimension:	3D
Coordinate system:	WGS 1984
Height mode:	Ellipsoidal
Number of iterations:	1
Maximum coord correction in last iteration:	0.0000 m ✔ (tolerance is met)

Stations

Number of (partly) known stations:	2
Number of unknown stations:	4
Total:	6

Observations

GPS coordinate differences:	48 (16 baselines)

Known coordinates:	6
Total:	54

Unknowns

Coordinates:	18
Total:	18

Degrees of freedom:	36

Testing

Alfa (multi dimensional):	0.5096	
Alfa 0 (one dimensional):	5.0 %	
Beta:	80.0 %	
Sigma a-priori (GPS):	10.0	
Critical value W-test:	1.96	
Critical value T-test (2-dimensional):	2.42	
Critical value T-test (3-dimensional):	1.89	
Critical value F-test:	0.98	
F-test:	0.43	✔ (accepted)

Results based on a-posteriori variance factor

Adjustment Results

Coordinates

Station		Coordinate	Corr	Sd	
IESG	Latitude	52° 56' 26.47595" N	-0.0022 m	0.0057 m	fixed
	Longitude	1° 11' 32.22846" W	0.0024 m	0.0057 m	fixed
	Height	98.4376 m	-0.0058 m	0.0142 m	fixed
NOTT	Latitude	52° 57' 43.88785" N	0.0022 m	0.0057 m	fixed
	Longitude	1° 11' 50.91575" W	-0.0024 m	0.0057 m	fixed
	Height	93.8187 m	0.0058 m	0.0142 m	fixed
REF1	Latitude	52° 56' 31.54665" N	0.0000 m	0.0060 m	
	Longitude	1° 11' 33.71394" W	0.0000 m	0.0058 m	
	Height	91.6761 m	0.0000 m	0.0146 m	
REF2	Latitude	52° 56' 27.31013" N	0.0000 m	0.0059 m	
	Longitude	1° 11' 31.13527" W	0.0000 m	0.0058 m	
	Height	86.1205 m	0.0000 m	0.0145 m	

REF3	Latitude	52° 56' 17.55129" N	0.0000 m	0.0058 m
	Longitude	1° 11' 19.23053" W	0.0000 m	0.0058 m
	Height	73.9004 m	0.0000 m	0.0144 m
REF4	Latitude	52° 56' 15.90678" N	0.0000 m	0.0059 m
	Longitude	1° 11' 23.02960" W	0.0000 m	0.0057 m
	Height	73.9123 m	0.0000 m	0.0144 m

Observations and Residuals

	Station	Target	Adj obs	Resid	Resid (ENH)	Sd
DX	IESG	REF4	249.4621 m	-0.0019 m	0.0007 m	0.0019 m
DY			166.6456 m	0.0007 m	0.0016 m	0.0010 m
DZ			-216.4754 m	0.0001 m	-0.0010 m	0.0027 m
DX	IESG	REF4	249.4621 m	0.0016 m	-0.0004 m	0.0019 m
DY			166.6456 m	-0.0004 m	-0.0010 m	0.0010 m
DZ			-216.4754 m	0.0006 m	0.0014 m	0.0027 m
DX	IESG	REF3	210.3696 m	-0.0015 m	0.0002 m	0.0021 m
DY			238.4245 m	0.0003 m	0.0011 m	0.0011 m
DZ			-185.8468 m	-0.0002 m	-0.0011 m	0.0025 m
DX	IESG	REF3	210.3696 m	0.0008 m	-0.0003 m	0.0021 m
DY			238.4245 m	-0.0003 m	-0.0006 m	0.0011 m
DZ			-185.8468 m	0.0000 m	0.0005 m	0.0025 m
DX	IESG	REF2	-27.5704 m	-0.0020 m	-0.0004 m	0.0026 m
DY			20.9935 m	-0.0004 m	0.0012 m	0.0013 m
DZ			5.7111 m	-0.0007 m	-0.0018 m	0.0029 m
DX	IESG	REF2	-27.5704 m	0.0085 m	0.0009 m	0.0026 m
DY			20.9935 m	0.0007 m	-0.0044 m	0.0013 m
DZ			5.7111 m	0.0039 m	0.0082 m	0.0029 m
DX	IESG	REF1	-129.7141 m	-0.0026 m	0.0024 m	0.0024 m
DY			-25.0468 m	0.0025 m	0.0024 m	0.0014 m
DZ			89.0670 m	0.0006 m	-0.0011 m	0.0035 m
DX	IESG	REF1	-129.7141 m	0.0020 m	-0.0019 m	0.0024 m
DY			-25.0468 m	-0.0020 m	-0.0016 m	0.0014 m
DZ			89.0670 m	0.0000 m	0.0012 m	0.0035 m
DX	NOTT	REF4	2169.0493 m	-0.0023 m	0.0012 m	0.0023 m
DY			475.5832 m	0.0012 m	0.0017 m	0.0013 m
DZ			-1654.5751 m	-0.0003 m	-0.0016 m	0.0032 m

DX	NOTT	REF4	2169.0493 m	0.0014 m	-0.0017 m	0.0023 m
DY			475.5832 m	-0.0018 m	-0.0036 m	0.0013 m
DZ			-1654.5751 m	-0.0041 m	-0.0024 m	0.0032 m
DX	NOTT	REF3	2129.9568 m	0.0010 m	-0.0009 m	0.0025 m
DY			547.3621 m	-0.0009 m	-0.0007 m	0.0014 m
DZ			-1623.9466 m	0.0003 m	0.0008 m	0.0031 m
DX	NOTT	REF3	2129.9568 m	0.0004 m	0.0010 m	0.0025 m
DY			547.3621 m	0.0010 m	-0.0003 m	0.0014 m
DZ			-1623.9466 m	0.0000 m	0.0002 m	0.0031 m
DX	NOTT	REF2	1892.0169 m	-0.0044 m	-0.0003 m	0.0028 m
DY			329.9311 m	-0.0002 m	0.0024 m	0.0014 m
DZ			-1432.3887 m	-0.0018 m	-0.0041 m	0.0032 m
DX	NOTT	REF2	1892.0169 m	0.0091 m	0.0005 m	0.0028 m
DY			329.9311 m	0.0003 m	-0.0031 m	0.0014 m
DZ			-1432.3887 m	0.0070 m	0.0111 m	0.0032 m
DX	NOTT	REF1	1789.8732 m	-0.0016 m	0.0030 m	0.0027 m
DY			283.8907 m	0.0031 m	0.0039 m	0.0015 m
DZ			-1349.0327 m	0.0044 m	0.0025 m	0.0039 m
DX	NOTT	REF1	1789.8732 m	0.0064 m	-0.0040 m	0.0027 m
DY			283.8907 m	-0.0041 m	-0.0064 m	0.0015 m
DZ			-1349.0327 m	-0.0020 m	0.0023 m	0.0039 m

GPS Baseline Vector Residuals

	Station	Target	Adj vector (m)	Resid (m)	Resid [ppm)
DV	IESG	REF4	369.9509	0.0020	5.5
DV	IESG	REF4	369.9509	0.0018	4.8
DV	IESG	REF3	368.2942	0.0016	4.2
DV	IESG	REF3	368.2942	0.0008	2.2
DV	IESG	REF2	35.1208	0.0022	62.0
DV	IESG	REF2	35.1208	0.0094	267.1
DV	IESG	REF1	159.3299	0.0036	22.7
DV	IESG	REF1	159.3299	0.0028	17.5
DV	NOTT	REF4	2769.2189	0.0026	0.9
DV	NOTT	REF4	2769.2189	0.0046	1.7
DV	NOTT	REF3	2733.7746	0.0014	0.5
DV	NOTT	REF3	2733.7746	0.0010	0.4

DV	NOTT	REF2	2395.8965	0.0048	2.0
DV	NOTT	REF2	2395.8965	0.0115	4.8
DV	NOTT	REF1	2259.2320	0.0056	2.5
DV	NOTT	REF1	2259.2320	0.0079	3.5

Absolute Error Ellipses (2D - 39.4% 1D - 68.3%)

Station	A (m)	B (m)	A/B	Phi	Sd Hgt (m)
IESG	0.0057	0.0057	1.0	5°	0.0142
NOTT	0.0057	0.0057	1.0	5°	0.0142
REF1	0.0060	0.0058	1.0	11°	0.0146
REF2	0.0059	0.0058	1.0	-3°	0.0145
REF3	0.0058	0.0058	1.0	2°	0.0144
REF4	0.0059	0.0057	1.0	7°	0.0144

Testing and Estimated Errors

Coordinate Tests

Station		MDB	BNR	W-Test	T-Test
IESG	Latitude	0.0320 m	2.9	0.39	0.17
	Longitude	0.0318 m	2.8	-0.42	
	Height	0.0797 m	2.8	0.41	
NOTT	Latitude	0.0320 m	2.9	-0.39	0.17
	Longitude	0.0318 m	2.8	0.42	
	Height	0.0797 m	2.8	-0.41	

Observation Tests

	Station	Target	MDB	Red	BNR	W-Test	T-Test
DX	IESG	REF4	0.0092 m	63	2.1	-0.82	0.31
DY			0.0060 m	64	2.1	0.39	
DZ			0.0136 m	65	2.0	0.50	
DX	IESG	REF4	0.0089 m	55	2.5	0.78	0.28
DY			0.0058 m	55	2.6	-0.33	
DZ			0.0130 m	56	2.5	-0.19	
DX	IESG	REF3	0.0099 m	65	2.1	-0.61	0.13
DY			0.0068 m	68	2.0	0.10	

DZ			0.0113 m	56	2.5	0.37	
DX	IESG	REF3	0.0096 m	56	2.4	0.38	0.07
DY			0.0063 m	53	2.7	-0.22	
DZ			0.0115 m	63	2.2	-0.19	
DX	IESG	REF2	0.0113 m	48	2.8	-0.78	0.25
DY			0.0070 m	46	3.0	-0.20	
DZ			0.0128 m	51	2.7	0.27	
DX	IESG	REF2	0.0140 m	82	1.5	1.48	0.85
DY			0.0093 m	83	1.3	0.23	
DZ			0.0148 m	76	1.6	-0.67	
DX	IESG	REF1	0.0124 m	70	2.0	-0.82	0.73
DY			0.0082 m	69	2.0	1.13	
DZ			0.0178 m	65	2.2	0.28	
DX	IESG	REF1	0.0119 m	57	2.3	0.56	0.54
DY			0.0078 m	59	2.4	-1.05	
DZ			0.0182 m	65	2.0	-0.34	
DX	NOTT	REF4	0.0122 m	69	1.8	-0.60	0.24
DY			0.0079 m	71	1.8	0.50	
DZ			0.0177 m	74	1.7	0.31	
DX	NOTT	REF4	0.0134 m	77	1.5	0.68	0.41
DY			0.0085 m	77	1.5	-0.61	
DZ			0.0199 m	81	1.3	-0.79	
DX	NOTT	REF3	0.0140 m	79	1.5	0.19	0.05
DY			0.0096 m	80	1.4	-0.30	
DZ			0.0156 m	71	1.8	-0.16	
DX	NOTT	REF3	0.0132 m	73	1.6	0.12	0.07
DY			0.0085 m	72	1.7	0.44	
DZ			0.0164 m	77	1.6	-0.11	
DX	NOTT	REF2	0.0127 m	63	2.1	-1.19	0.54
DY			0.0077 m	60	2.3	0.03	
DZ			0.0147 m	63	2.1	0.35	
DX	NOTT	REF2	0.0160 m	85	1.4	0.91	0.56
DY			0.0107 m	85	1.2	0.00	
DZ			0.0169 m	78	1.5	0.00	
DX	NOTT	REF1	0.0141 m	72	1.8	-0.83	0.73
DY			0.0094 m	72	1.8	0.99	
DZ			0.0200 m	71	1.9	0.75	

DX	NOTT	REF1	0.0161 m	78	1.4	1.25	1.15
DY			0.0104 m	79	1.5	-1.12	
DZ			0.0253 m	83	1.2	-0.87	

Redundancy:

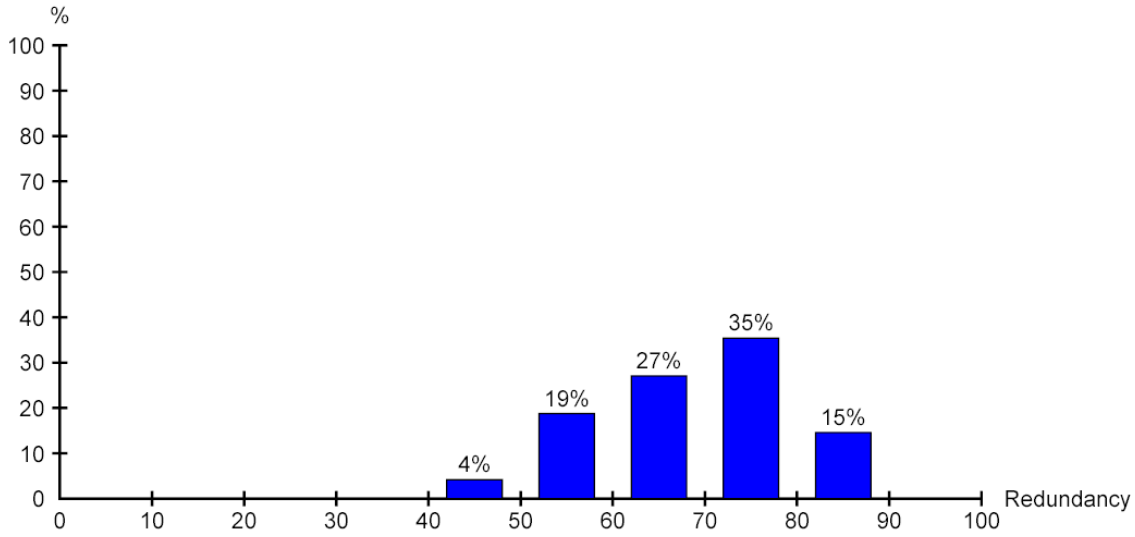

W-Test:

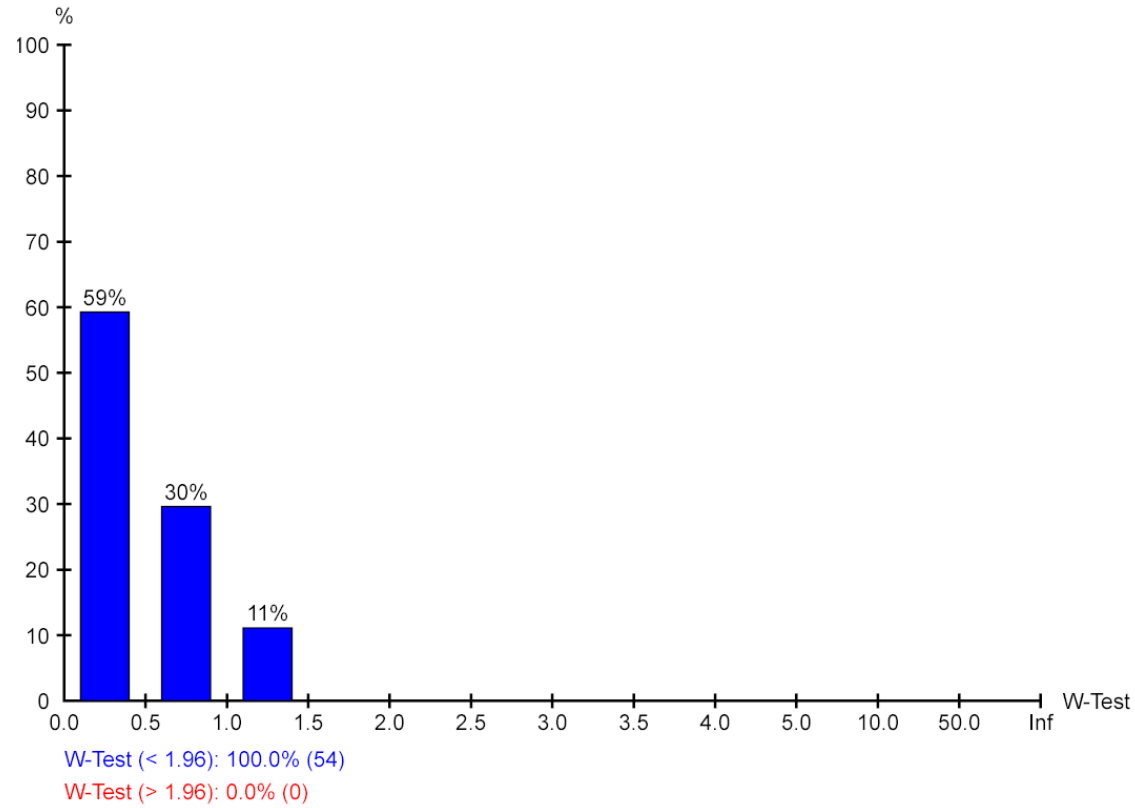

T-Test (3-dimensional):

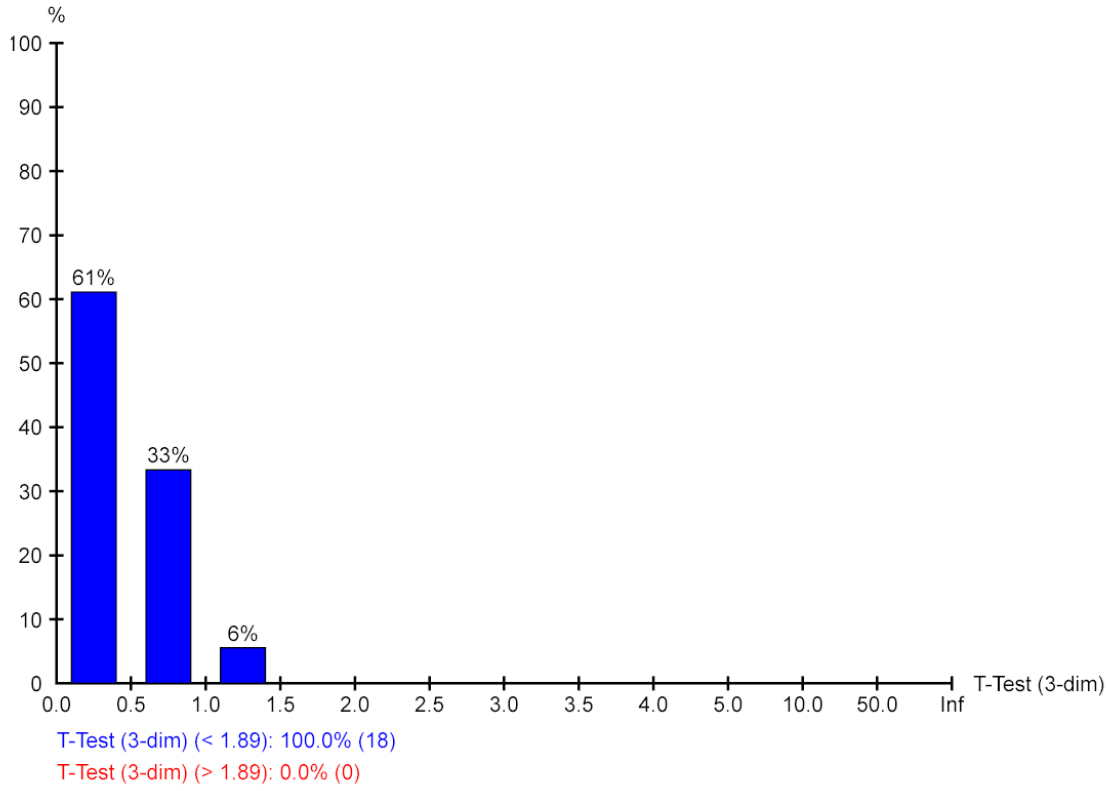

Appendix 4: VERNET Manual

Program: vernet

Purpose: adjustment and analysis of vertical networks

Description :

important all standard errors in millimetres

This program performs a full least squares variation of coordinates adjustment of a vertical network. The program will deal with vertical angles (or zenith angles), spirit levelled height differences and absolute heights. The reference heights are always taken as the top of the permanent or temporary monuments. The coordinates from the horizontal adjustment are used to compute the distances for trigonometric heighting. The coefficient of refraction is fixed at 0.07 if the parameter ifref is set to 0 or can be treated as unknown if ifref is set to 1.

The estimated a priori standard error of an observed trigonometric height difference is computed from :

$$\text{sigma} = \text{sqrt}(d/500)*\text{sigma500}$$

where sigma500 is the estimated a priori sigma for a trig. Height difference on a line 500 metres long and d is the length of the line.

The program will deal with three cases for trigonometric heighting:

case 1 : instrument and target heights constant.

case 2 : target height constant but instrument height varies.

case 3 : instrument and target heights vary.

the vertical angles can be input as elevations and depressions

(ifvorz = 0) or as zenith angles (ifvorz = 1)

Input specifications:

1. Number of stations, observed vertical (or zenith) angles (nov), spirit levelled height differences (nol) and absolute heights (noh, at least one), (4(i3,1x))
2. The network name and data set information (10a8).
3. ifout and ifline (2(i1,1x)) ifout = 1 if the adjusted station heights and standard errors are printed out for use in the comparison program concomp and ifout = 0 if not. ifline = 1 if the standard error of a selected number of height differences is printed out for use in concomp and ifline = 0 if not.

4. if(nov.ne.0)case, ifvorz, ifref (3(i1,1x))

5. if(nov.ne.0) for each station input the station number, adjusted northing and easting, approximate height and station name (i2,2x,3(f10.3,1x),3a8) if(nov.eq.0) for each station input the station number, approximate height and station name (i2,2x,f10.3,1x,3a8) if nov = 0 omit 6,7 and 8

6. if case = 1 read inst. height and target height(2(f5.3,1x)) if case = 2 read target height (f5.3).

7. estimated a priori sigma for a 500 metre trigonometric levelled line (mm). (f4.1)

8. trigonometric levelling data for each observed vertical angle input: ifvorz = 0 (vertical angle has a '+' or '-' sign 'is').

****

case = 1 fr, to, is, deg, min, sec (2(i2,2x),a1,1x,i3,1x,i2,1x,f4.1)

case = 2 fr, to, is, deg, min, sec, instht (2(i2,2x),a1,1x,i3,1x,i2,1x,f4.1,1x,f6.3)

case = 3 fr, to, is, deg, min, sec, instht, targht (2(i2,2x),a1,1x,i3,1x,i2,1x,f4.1,2(1x,f6.3)) ifvorz = 1

****

case = 1 fr, to, deg, min, sec 2(i2,2x),i3,1x,i2,1x,f4.1)

case = 2 fr, to, deg, min, sec, instht 2(i2,2x),i3,1x,i2,1x,f4.1,1x,f6.3)

case = 3 fr, to, deg, min, sec, instht, targht 2(i2,2x),i3,1x,i2,1x,f4.1,2(1x,f6.3)) 9. spirit levelling data (omit if nol = 0) fr, to, height diff., estimated s.e.(mm). (2(i2,2x),f9.4,1x,f4.1)

10. Absolute height data (must have at least one of these) station, height, estimated s.e.(mm).(set se to 0.0 to fix ht) (i2,2x,f9.4,1x,f4.1) if ifline = 0 omit 11 and 12

11. number of lines for which the standard error of the height difference is required in concomp (i2)

12. for each of these lines read in stations "from" and "to" (i2,1x,i2)

Appendix 5: OSBM Network – Vertical Adjustment Report

```
**********************************************************************************************
*   UNIVERSITY OF NOTTINGHAM                INSTITUTE OF ENGINEERING SURVEYING          *
*                                                  AND SPACE GEODESY                    *
*                ENGINEERING NETWORK ADJUSTMENT PROGRAM                                 *
*                ---------------------------------------                                *
*            (CONTROL NETWORK FOR MONITORING VERTICAL DEformatIONS)                     *
*   NETWORK : OSBM-Network                                                              *
*   -------                                                                             *
*                    NUMBER OF STATIONS :  4                                            *
*                    ------------------                                                 *
*                    NUMBER OF OBSERVATIONS :                                           *
*                    ----------------------                                             *
*              ZENITH OR VERTICAL ANGLES       :  0                                     *
*              SPIRIT LEVELLED HEIGHT DIFFERENCES :  6                                  *
*              ABSOLUTE HEIGHTS            :  2                                         *
*                  PROGRAM RUN ON  13/ 1/2008  AT  22:13:52                             *
**********************************************************************************************
```

APPROXIMATE STATION HEIGHTS (METRES)

STATION	HEIGHT	
1	42.200	OSBM41
2	40.730	OSBM42
3	43.130	REF1
4	37.580	REF2

SPIRIT LEVELLING

OBSERVATIONS NO.	FROM	TO	OBSERVED DELTA H (M)	COMPUTED DELTA H (M)	O-C (MM)	ESTIMATED PRE-RMSE (MM)
1	2	3	2.4098	2.4000	9.8	1.0
2	3	1	-.9405	-.9300	-10.5	1.0
3	1	3	.9401	.9300	10.1	1.0
4	3	2	-2.4095	-2.4000	-9.5	1.0
5	2	4	-3.1437	-3.1500	6.3	1.0
6	4	2	3.1437	3.1500	-6.3	1.0

HEIGHT OBSERVATIONS

NO.	STATION	OBSERVED HEIGHT (M)	COMPUTED HEIGHT (M)	O-C (MM)	ESTIMATED PRE-RMSE (MM)

7	1	42.2000	42.2000	.0	FIXED STATION
8	2	40.7300	40.7300	.0	FIXED STATION

RESULTS OF ADJUSTMENT

STATION	CORRECTION (M)	ADJ. HEIGHT (M)	POST-RMSE (MM)	
1	.0000	42.2000	.0	OSBM41
2	.0000	40.7300	.0	OSBM42
3	.0100	43.1400	.2	REF1
4	.0063	37.5863	.3	REF2

SIGMA ZERO = .36 +/- .13

NETWORK RELIABILITY ANALYSIS

* : RESID/SIGMA > 2.0
** : RESID/SIGMA > 2.5
*** : RESID/SIGMA > 3.0

@ : POST/PRE-RMSE > 0.9

SPIRIT LEVELS

OBS. NO.	FROM	TO	RESIDUAL (MM)	SIGMA (MM)	RES/SIGMA	POST-RMSE (MM)	PRE-RMSE (MM)	RATIO
1	2	3	.2	.3	.54	.2	.4	.50
2	3	1	.5	.3	1.61	.2	.4	.50
3	1	3	-.1	.3	.42	.2	.4	.50
4	3	2	-.5	.3	1.50	.2	.4	.50
5	2	4	.0	.3	.14	.3	.4	.71
6	4	2	.0	.3	.14	.3	.4	.71

HEIGHTS

OBS. NO.	AT	RESIDUAL (MM)	SIGMA (MM)	RES/SIGMA	POST-RMSE (MM)	PRE-RMSE (MM)	RATIO
7	1	THE HEIGHT OF THIS STATION IS FIXED					
8	2	THE HEIGHT OF THIS STATION IS FIXED					

****

PROGRAM RUN SUCCESSFULLY COMPLETED

****

Appendix 6: 'Truth' Coordinates

Truth' Coordinates						
Point Id	Easting (m)	Northing (m)	Ht. (m)	RMSE E (m)	RMSE N (m)	RMSE Ht. (m)
REF4	454553.763	338122.106	25.393	0.006	0.006	0.001
REF3	454624.113	338173.719	25.382	0.006	0.006	0.001
PHARM	454599.102	338271.604	26.241	0.002	0.002	0.001
ST10	454592.064	338280.797	26.211	0.001	0.001	0.001
STOP	454728.129	338417.135	25.831	0.003	0.002	0.001
T20	454710.854	338428.945	25.756	0.001	0.001	0.001
T21	454707.861	338431.064	25.765	0.001	0.001	0.001
T22	454703.546	338434.098	25.764	0.001	0.001	0.001
T23	454686.287	338446.295	25.797	0.001	0.001	0.001
T24	454669.076	338458.427	25.938	0.001	0.001	0.001
T25	454654.556	338468.650	26.032	0.001	0.001	0.001
T26	454645.943	338470.049	26.058	0.001	0.001	0.001
T27	454632.752	338479.402	26.027	0.001	0.001	0.001
T28	454631.089	338481.385	25.997	0.001	0.001	0.001
T29	454613.352	338493.138	25.982	0.001	0.001	0.001
COATS3	454601.880	338504.616	26.051	0.003	0.002	0.001
T31	454618.012	338527.372	26.165	0.001	0.001	0.001
T32	454621.018	338531.643	26.152	0.001	0.001	0.001
T34	454623.215	338534.775	26.172	0.001	0.001	0.001
T36	454645.930	338566.783	26.431	0.001	0.001	0.001
T37	454657.291	338582.826	26.592	0.001	0.001	0.001
T38	454669.020	338599.395	27.057	0.001	0.001	0.001
COATS2	454687.121	338620.778	27.739	0.003	0.002	0.001
COATS1	454661.891	338635.285	28.195	0.003	0.002	0.001
T12	454644.498	338613.802	28.406	0.001	0.001	0.001
T10	454642.827	338612.261	28.394	0.001	0.001	0.001
T11	454640.966	338610.531	28.432	0.001	0.001	0.001
TOWER	454632.574	338601.606	28.410	0.003	0.002	0.001

ST2	454589.297	338557.189	27.455	0.001	0.001	0.001
POP	454554.673	338549.600	28.157	0.002	0.002	0.001
T8	454609.030	338604.970	28.454	0.001	0.001	0.001
T7	454600.004	338615.762	28.118	0.001	0.001	0.001
T6	454593.035	338609.582	28.076	0.001	0.001	0.001
T5	454579.495	338597.197	28.264	0.001	0.001	0.001
T4	454565.820	338584.485	28.483	0.001	0.001	0.001
T3	454551.715	338572.250	28.612	0.001	0.001	0.001
T2	454537.713	338560.102	28.585	0.001	0.001	0.001
T1	454520.133	338548.802	28.818	0.001	0.001	0.001
ST1	454506.388	338530.703	29.837	0.001	0.001	0.001
REF2	454398.461	338472.766	37.586	0.006	0.006	0.001
REF1	454348.848	338603.134	43.142	0.006	0.006	0.001
			RMSE	**0.002**	**0.002**	**0.001**

Appendix 7: Total-Station Calibration

(a) Zero Error Test

Zero Error Test **Instrument: Leica TCR 1201** **Prism: Leica prism no. 5**

Distance	**Measure 1** (m)	**Measure 2** (m)	**Measure 3** (m)	**Measure 4** (m)	**Mean** (m)
A to B	19.251	19.251	19.251	19.251	19.251
B to C	20.136	20.136	20.136	20.136	20.136
A to C	39.385	39.385	39.385	39.385	39.385

Calculations: e=AC-AB-BC e=39.385-20.136-19.251 e=-0.002m

Correction = 0.002m

Zero Error Test **Instrument: Leica TCR 1201** **Prism: Leica prism no. 6**

Distance	**Measure 1** (m)	**Measure 2** (m)	**Measure 3** (m)	**Measure 4** (m)	**Mean** (m)
A to B	19.252	19.252	19.252	19.252	19.252
B to C	20.136	20.136	20.136	20.136	20.136
A to C	39.388	39.388	39.388	39.388	39.388

Calculations: e=AC-AB-BC e=39.388-20.136-19.252 e=0.000m

Correction = 0.000m

Zero Error Test **Instrument: Leica TCA 2003** **Prism: Leica prism no. 1**

Distance	**Measure 1** (m)	**Measure 2** (m)	**Measure 3** (m)	**Measure 4** (m)	**Mean** (m)
A to B	20.206	20.206	20.206	20.206	20.206
B to C	20.235	20.235	20.235	20.235	20.235
A to C	40.441	40.441	40.441	40.441	40.441

Calculations: e=AC-AB-BC e=40.441-20.235-20.206 e=0.000m

Correction = 0.000m

Zero Error Test **Instrument: Leica TCA 2003** **Prism: Leica prism no. 2**

Distance	**Measure 1** (m)	**Measure 2** (m)	**Measure 3** (m)	**Measure 4** (m)	**Mean** (m)
A to B	20.206	20.206	20.206	20.206	20.206
B to C	20.235	20.235	20.235	20.235	20.235
A to C	40.441	40.441	40.441	40.441	40.441

Calculations: e=AC-AB-BC e=40.441-20.235-20.206 e=0.000m

Correction = 0.000m

Zero Error Test **Instrument: Leica TCA 2003 Prism: Leica prism no. 3**

Distance	**Measure 1** (m)	**Measure 2** (m)	**Measure 3** (m)	**Measure 4** (m)	**Mean** (m)
A to B	20.207	20.207	20.207	20.207	20.207
B to C	20.235	20.235	20.235	20.235	20.235
A to C	40.442	40.442	40.442	40.442	40.442

Calculations: e=AC-AB-BC e=40.441-20.235-20.206 e=0.000m

Correction = 0.000m

(b) Collimation in Azimuth

Instrument	**Face left Reading** (m)	**Face left Reading** (m)	**Difference** (m)	**Distance to Staff** (m)
Leica TCR 1201	4.54	4.54	0	4.388
Leica TCA 2003	3.98	3.98	0	4.388

(c) Vertical Circle Index

Instrument	**Face left Reading** (m)	**Face left Reading** (m)	**Difference** (m)	**Distance to Staff** (m)
Leica TCR 1201	4.74	4.74	0	5.134
Leica TCA 2003	2.65	2.65	0	5.526

Appendix 8: Example of Control File - Total-Station Data Collection

%Station_ID	hi				
%Target_ID	ht	Prism_Constant	Round1FL	Round1FR	Round2FL	Round2FR
*						
ST1	1.65					
REF2	1.86	0	1	6	9	10
T1	1.602	0	2	5	8	11
ST2	1.765	0	3	4	7	12
*						
ST1	1.65					
REF2	1.86	0	13	18	21	22
T2	1.606	0	14	17	20	23
ST2	1.765	0	15	16	19	24
*						
ST2	1.767					
ST1	1.646	0	97	102	105	106
T8	1.582	0	98	101	104	107
TOWER	1.656	0	99	100	103	108
*						
etc.						

Appendix 9: Example of Network Reduction Sheet Files

(a) Example of Net_Sheet.txt file

TPS Station

Stn.ID App Height hi

REF2 37.586 1.734

HORIZONTAL ANGLES REDUCTION SHEET

STATION TO FL FR MEAN REDUCED

REF1 017 05 49.63 197 06 11.66 017 06 00.65
POP 101 44 12.84 281 44 29.36 101 44 21.10 084 38 20.46
REF1 017 05 52.55 197 06 05.18 017 05 58.87 275 21 37.77

REF1 050 08 00.96 230 08 12.30 050 08 06.63
POP 134 46 21.90 314 46 39.40 134 46 30.65 084 38 24.02
REF1 050 08 09.38 230 08 12.95 050 08 11.17 275 21 40.52

MEAN REDUCED HZ: AT: REF2 FROM: REF1 TO: POP 084 38 22.24

Angle: Min= 084 38 20.46 Max= 084 38 24.02 Difference= 000 00 03.57

MEAN REDUCED HZ: AT: REF2 FROM: POP TO: REF1 275 21 39.14

Angle: Min= 275 21 37.77 Max= 275 21 40.52 Difference= 000 00 02.75

VERTICAL ANGLES REDUCTION SHEET

STATION TO FL FR REDUCED MEAN

REF1 087 43 02.06 272 16 48.22 087 43 06.92
REF1 087 43 01.09 272 16 49.51 087 43 05.79
REF1 087 42 57.85 272 16 50.81 087 43 03.52
REF1 087 43 12.43 272 16 57.29 087 43 07.57 087 43 05.95

Angle: Min= 087 43 03.52 Max= 087 43 07.57 Difference= 000 00 04.05

POP 093 15 14.22 266 44 32.82 093 15 20.70
POP 093 15 23.94 266 44 26.34 093 15 28.80 093 15 24.75

Angle: Min= 093 15 20.70 Max= 093 15 28.80 Difference= 000 00 08.10

SLOPE DISTANCES REDUCTION SHEET

STATION TO: REF1 Height = 43.142

STATION TO MEASURE MEASURE MEASURE MEASURE MEAN

REF1 139.648 139.648 139.648 139.648

	139.648	139.648	139.648	139.648	139.648

GRID SCALE (GScale) = 0.99964
HORIZONTAL DISTANCE (Hd=MSD*cos V) = 139.5373
MSL CORRECTION (MSLcorr=Hd*H/R) = 0.0009
REDUCED DISTANCE (RD=Hd-MSLcorr) = 139.5364
SCALE CORRECTION(SCLcorr=(1-GScale)*RD)= 0.0506
GRID DISTANCE (GD=RD-SCLcorr) = 139.4858

SLOPE DISTANCES REDUCTION SHEET

STATION TO: POP Height = 28.16

STATION TO	MEASURE	MEASURE	MEASURE	MEASURE	MEAN
POP	174.435	174.436	174.436	174.436	174.436

GRID SCALE (GScale) = 0.99964
HORIZONTAL DISTANCE (Hd=MSD*cos V) = 174.154
MSL CORRECTION (MSLcorr=Hd*H/R) = 0.0009
REDUCED DISTANCE (RD=Hd-MSLcorr) = 174.1531
SCALE CORRECTION(SCLcorr=(1-GScale)*RD)= 0.0631
GRID DISTANCE (GD=RD-SCLcorr) = 174.09

TPS Station
.
.
.
etc.

(b) Example of ErrorsSummary.txt file

Horizontal Angles Error

At	From	To	Differences (sec)
REF2	REF1	POP	03.56
REF2	POP	REF1	02.75
POP	REF2	TOWER	07.77
POP	TOWER	REF2	06.48
TOWER	POP	COATS1	00.98
TOWER	COATS1	POP	00.16
COATS1	TOWER	COATS2	01.15
COATS1	COATS2	TOWER	01.14
COATS2	COATS3	COATS1	05.18
COATS2	COATS1	COATS3	00.32
COATS3	STOP	COATS2	01.47
COATS3	COATS2	STOP	01.31
STOP	PHARM	COATS3	06.16
STOP	COATS3	PHARM	04.87
PHARM	REF3	STOP	04.53
PHARM	STOP	REF3	02.75
REF3	REF4	PHARM	01.78
REF3	PHARM	REF4	02.10

RMSE= 03.66

Vertical Angles Error

At	To	Differences (sec)
REF2	REF1	04.05
REF2	POP	08.10
POP	REF2	07.61
POP	TOWER	02.92
TOWER	POP	02.91
TOWER	COATS1	01.45
COATS1	TOWER	05.02
COATS1	COATS2	00.32
COATS2	COATS3	06.64
COATS2	COATS1	00.00
COATS3	STOP	06.32
COATS3	COATS2	00.32
STOP	PHARM	04.05
STOP	COATS3	05.84
PHARM	REF3	02.11
PHARM	STOP	01.30
REF3	REF4	02.27
REF3	PHARM	05.19

RMSE= 04.34

Slope Distances Error

At	To	Differences (mm)
REF2	REF1	00.000
REF2	POP	01.000
POP	REF2	01.000
POP	TOWER	01.000
TOWER	POP	00.000
TOWER	COATS1	01.000
COATS1	TOWER	00.000
COATS1	COATS2	00.000
COATS2	COATS3	00.000
COATS2	COATS1	00.000
COATS3	STOP	01.000
COATS3	COATS2	00.000
STOP	PHARM	00.000
STOP	COATS3	00.000
PHARM	REF3	00.000
PHARM	STOP	00.000
REF3	REF4	01.000
REF3	PHARM	01.000

RMSE= 00.61

Appendix 10: Example of CUPT File

```
Testing Points
% Reduce Distance to Grid Scale (i.e. GScale=1) and/or Mean Sea Level (i.e. MSL=0)
 1          1
% Total Station Constant Errors= amm + bppm
1          1
% Total Station Constant Errors= Reading error=Re + Vertical Compensator Error=Le (Sec.)
0.5        0.3
% Pointing Errors(HPe & VPe in sec.)...i.e. one face H=10 + V=5... two faces H=4 + V=2
5          5
% Inistrument Centring Error (Icet + Icep in mm)...i.e. Leica TPS 1200 has...1.0mm for laser plummet
at 1.5m (deviation from plumb line)
1          0
% Target Centring Error (Tripod=Tcet + Pillar=Tcep + Rod=Tcer in mm)
1          0          0
% Height Error (Instrument=Ihe + Target=The in mm)
2          2
%Control points
REF2          454398.4610     338472.7660    37.5860  0.0030  0.0027  0.0011    XYZ     CTRL
REF4          454553.7630     338122.1060    25.3930  0.0030  0.0019  0.0011    XYZ     CTRL
TOWER         454632.5740     338601.6060    28.4100  0.0027  0.0023  0.0011    XYZ     CTRL
COATS1        454661.8910     338635.2850    28.1950  0.0030  0.0024  0.0011    XYZ     CTRL
COATS2        454687.1210     338620.7780    27.7390  0.0029  0.0024  0.0011    XYZ     CTRL
COATS3        454601.8800     338504.6160    26.0510  0.0027  0.0023  0.0011    XYZ     CTRL
STOP          454728.1290     338417.1350    25.8310  0.0026  0.0023  0.0011    XYZ     CTRL
*
ST1        1.65
REF2        359  59  57.90       122.798       086  17  00.80        1.860        0.0000
T1          155  26  25.20        22.759       092  40  37.40        1.602        0.0000
ST2         190  30  37.10        87.099       091  29  33.60        1.765        0.0000
*
ST1        1.65
REF2        180  00  09.60       122.798       273  42  58.90        1.860        0.0000
T1          335  26  37.10        22.759       267  19  25.30        1.602        0.0000
ST2         010  30  45.90        87.100       268  30  28.70        1.765        0.0000
*
ST2        1.767
ST1         000  00  01.80        87.098       088  30  26.50        1.646        0.0000
T8          130  09  24.90        51.720       089  05  39.80        1.582        0.0000
TOWER       151  58  07.20        62.044       089  12  45.50        1.656        0.0000
*
etc.
```

Appendix 11: Example of HORNET Adjustment Report

```
*****************************************************************************************************
*                                                                                                   *
*   UNIVERSITY OF NOTTINGHAM                    INSTITUTE OF ENGINEERING SURVEYING                  *
*                                                AND SPACE GEODESY                                  *
*                                                                                                   *
*****************************************************************************************************
*                                                                                                   *
*                  H   H  OOO   RRRR   N   N  EEEEE  TTTTT                                          *
*                  H   H O   O R   R  NN  N  E        T                                             *
*                  HHHHH O   O RRRR   N N N  EEEE     T                                             *
*                  H   H O   O R   R  N  NN  E        T                                             *
*                  H   H  OOO   R   R  N   N  EEEEE    T                                            *
*                                                                                                   *
*                   HORIZONTAL NETWORK ADJUSTMENT PROGRAM                                           *
*                                                                                                   *
*****************************************************************************************************
*                                                                                                   *
*   NETWORK :                    'Campus Network'                                                   *
*                                                                                                   *
*   NUMBER OF STATIONS   :  11                                                                      *
*                                                                                                   *
*   NUMBER OF DATASETS   :  3                                                                       *
*                                                                                                   *
* NUMBER OF OBSERVATIONS   :  44                                                                    *
*                                                                                                   *
*          ANGLES   :  18                                                                           *
*                                                                                                   *
*        DISTANCES   :  18                                                                          *
*                                                                                                   *
*      ORIENTATIONS   :  0                                                                          *
*                                                                                                   *
*        POSITIONS   :  8                                                                           *
*                                                                                                   *
*  THEODOLITE POINTINGS   :  0 IN   0 ROUNDS                                                        *
*                                                                                                   *
*      PROGRAM MODE    :  2  Real Data, Standard Output.                                            *
*                                                                                                   *
*                   Program started at 12:30:16  on  29-12-2007                                     *
*                                                                                                   *
*                   Program HORNET Version 10.01 c IESSG April 2003                                 *
*                                                                                                   *
*                                                                                                   *
*****************************************************************************************************
```

APPROXIMATE COORDINATES (metres)

STATION	EASTING	NORTHING	
1	454348.848	338603.134	REF1
2	454398.461	338472.766	REF2
3	454624.113	338173.719	REF3
4	454553.763	338122.106	REF4
5	454554.729	338549.646	POP
6	454632.653	338601.676	TOWER
7	454661.979	338635.370	COATS1
8	454687.218	338620.860	COATS2
9	454601.945	338504.654	COATS3
10	454728.242	338417.140	STOP
11	454599.170	338271.554	PHARM

ANGULAR OBSERVATIONS FROM D:\HorCamp\angles.dat

NO.	AT	FROM	TO	CLOCKWISE ANGLES OBSERVED deg	min	sec	COMPUTED deg	min	sec	O-C secs	SE secs
1	2	1	5	84	38	22.24	84	38	19.80	2.44	10.00
2	2	5	1	275	21	39.14	275	21	40.20	-1.06	10.00
3	5	2	6	172	27	49.21	172	27	53.77	-4.56	10.00
4	5	6	2	187	32	9.17	187	32	6.23	2.94	10.00
5	6	5	7	164	45	59.60	164	45	58.34	1.26	10.00
6	6	7	5	195	13	58.87	195	14	1.66	-2.79	10.00
7	7	6	8	258	51	39.09	258	51	34.81	4.28	10.00
8	7	8	6	101	8	24.96	101	8	25.19	-.23	10.00
9	8	9	7	83	37	28.81	83	37	23.56	5.25	10.00
10	8	7	9	276	22	29.08	276	22	36.44	-7.36	10.00
11	9	10	8	271	33	8.11	271	33	9.38	-1.27	10.00
12	9	8	10	88	26	52.13	88	26	50.62	1.51	10.00
13	10	11	9	83	9	34.38	83	9	35.12	-.74	10.00
14	10	9	11	276	50	31.61	276	50	24.88	6.73	10.00
15	11	3	10	235	53	27.08	235	51	43.34	103.74	10.00
16	11	10	3	124	6	24.74	124	8	16.66	-111.92	10.00
17	3	4	11	111	56	22.05	111	57	47.42	-85.37	10.00
18	3	11	4	248	3	40.22	248	2	12.58	87.64	10.00

HORIZONTAL DISTANCE OBSERVATIONS (metres) FROM D:\HorCamp\dists.dat

DISTANCE STANDARD ERRORS : 2.0 mm + 2.0 ppm

NO.	FROM	TO	OBSERVED	COMPUTED	O-C(mm)	SE (mm)
19	2	1	139.4858	139.4893	-3.5	2.3
20	2	5	174.0900	174.1557	-65.7	2.3
21	5	2	174.0883	174.1557	-67.4	2.3
22	5	6	93.6613	93.6978	-36.5	2.2
23	6	5	93.6657	93.6978	-32.1	2.2
24	6	7	44.6497	44.6688	-19.1	2.1
25	7	6	44.6525	44.6688	-16.3	2.1
26	7	8	29.1014	29.1127	-11.3	2.1
27	8	9	144.0813	144.1365	-55.2	2.3
28	8	7	29.1026	29.1127	-10.1	2.1
29	9	10	153.5959	153.6543	-58.4	2.3
30	9	8	144.0840	144.1365	-52.5	2.3
31	10	11	194.4923	194.5633	-71.0	2.4
32	10	9	153.5935	153.6543	-60.8	2.3
33	11	3	101.0255	100.9646	60.9	2.2
34	11	10	194.4915	194.5633	-71.8	2.4
35	3	4	87.2509	87.2526	-1.7	2.2
36	3	11	101.0253	100.9646	60.7	2.2

POSITION OBSERVATIONS (metres) FROM D:\HorCamp\points.dat

NO.	STATION	OBSERVED EAST/NORTH	COMPUTED EAST/NORTH	O-C(mm) EAST/NORTH	SE (mm) EAST/NORTH
38		E 454348.8480	454348.8480	.0	3.1
37	1	N 338603.1340	338603.1340	.0	3.1
40		E 454398.4610	454398.4610	.0	3.0
39	2	N 338472.7660	338472.7660	.0	2.7
42		E 454624.1130	454624.1130	.0	2.8
41	3	N 338173.7190	338173.7190	.0	2.1
44		E 454553.7630	454553.7630	.0	3.0
43	4	N 338122.1060	338122.1060	.0	1.9

RESULTS OF ADJUSTMENT (metres)

	APPROXIMATE COORDINATES		CORRECTIONS (UNKNOWNS)		FINAL ADJUSTED COORDINATES		
STATION	EASTING	NORTHING	DELTA E	DELTA N	EASTING	NORTHING	
1	454348.8480	338603.1340	.0033	-.0010	454348.8513	338603.1330	REF1
2	454398.4610	338472.7660	-.0022	-.0005	454398.4588	338472.7655	REF2
3	454624.1130	338173.7190	-.0022	.0018	454624.1108	338173.7208	REF3
4	454553.7630	338122.1060	.0017	-.0008	454553.7647	338122.1052	REF4
5	454554.7290	338549.6460	-.0551	-.0439	454554.6739	338549.6021	POP
6	454632.6530	338601.6760	-.0797	-.0689	454632.5733	338601.6071	TOWER
7	454661.9790	338635.3700	-.0891	-.0844	454661.8899	338635.2856	COATS1
8	454687.2180	338620.8600	-.0988	-.0806	454687.1192	338620.7794	COATS2
9	454601.9450	338504.6540	-.0659	-.0382	454601.8791	338504.6158	COATS3
10	454728.2420	338417.1400	-.1141	-.0041	454728.1279	338417.1359	STOP
11	454599.1700	338271.5540	-.0664	.0487	454599.1036	338271.6027	PHARM

NETWORK RELIABILITY ANALYSIS

* : RESIDUAL/SIGMA > 2.0
** : RESIDUAL/SIGMA > 2.5
*** : RESIDUAL/SIGMA > 3.0

@ : A POSTERIORI/A PRIORI STANDARD ERROR > 0.9

OBSERVED ANGLES

OBS.	STATIONS			RESIDUAL	SIGMA	RESIDUAL/	STANDARD ERRORS (secs)	
NO.	AT	FROM	TO	sec	sec	SIGMA	A PRIORI	A POSTERIORI	RATIO
1	2	1	5	8.74	6.80	1.29	8.17	4.52	.55
2	2	5	1	-10.12	6.80	1.49	8.17	4.52	.55
3	5	2	6	1.73	6.15	.28	8.17	5.37	.66
4	5	6	2	-.11	6.15	.02	8.17	5.37	.66
5	6	5	7	-2.86	6.28	.46	8.17	5.23	.64
6	6	7	5	4.39	6.28	.70	8.17	5.23	.64
7	7	6	8	-7.68	6.44	1.19	8.17	5.02	.61
8	7	8	6	3.63	6.44	.56	8.17	5.02	.61
9	8	9	7	7.48	6.49	1.15	8.17	4.96	.61
10	8	7	9	-5.37	6.49	.83	8.17	4.96	.61
11	9	10	8	.00	6.07	.00	8.17	5.47	.67
12	9	8	10	-.24	6.07	.04	8.17	5.47	.67
13	10	11	9	.66	6.44	.10	8.17	5.02	.61
14	10	9	11	-6.65	6.44	1.03	8.17	5.02	.61
15	11	3	10	-1.11	6.27	.18	8.17	5.23	.64
16	11	10	3	9.29	6.27	1.48	8.17	5.23	.64
17	3	4	11	-7.44	6.62	1.12	8.17	4.78	.59
18	3	11	4	5.17	6.62	.78	8.17	4.78	.59

MIN RESIDUAL -10.12
MAX RESIDUAL 9.29

MEAN RESIDUAL 5.37
S.D. RESIDUAL 8.31

RESIDUALS ARE NORMALLY DISTRIBUTED (AT 95% REJECTION LEVEL)

OBSERVED DISTANCES

OBS.	STATIONS		RESIDUAL	SIGMA	RESIDUAL/	STANDARD ERRORS (mm)	
NO.	FROM	TO	mm	mm	SIGMA	A PRIORI	A POSTERIORI	RATIO
19	2	1	1.1	.9	1.25	1.9	1.6	.87
20	2	5	-.8	1.4	.62	1.9	1.4	.70
21	5	2	.9	1.4	.63	1.9	1.4	.70
22	5	6	2.1	1.3	1.69	1.8	1.3	.70
23	6	5	-2.3	1.3	1.78	1.8	1.3	.70

24	6	7	1.2	1.2	1.02	1.7	1.2	.70
25	7	6	-1.6	1.2	1.29	1.7	1.2	.70
26	7	8	1.0	1.2	.80	1.7	1.2	.70
27	8	9	1.6	1.3	1.19	1.9	1.3	.70
28	8	7	-.2	1.2	.20	1.7	1.2	.70
29	9	10	-.7	1.3	.54	1.9	1.3	.70
30	9	8	-1.1	1.3	.84	1.9	1.3	.70
31	10	11	-.2	1.4	.14	2.0	1.4	.70
32	10	9	1.7	1.3	1.25	1.9	1.3	.70
33	11	3	.4	1.3	.29	1.8	1.3	.70
34	11	10	.6	1.4	.44	2.0	1.4	.70
35	3	4	.1	.9	.10	1.8	1.5	.85
36	3	11	.6	1.3	.45	1.8	1.3	.70

MIN RESIDUAL -2.3
MAX RESIDUAL 2.1

MEAN RESIDUAL .3
S.D. RESIDUAL 1.4

RESIDUALS ARE NORMALLY DISTRIBUTED (AT 95% REJECTION LEVEL)

OBSERVED POSITIONS

OBS. NO.	STATION	RESIDUAL (mm) EAST/NORTH	SIGMA (mm) EAST/NORTH	RESID/SIGMA EAST/NORTH	STANDARD ERRORS (mm) A PRIORI EAST/NORTH	A POSTERIORI EAST/NORTH	RATIO EAST/NORTH
		-1.0	1.2	.86	2.5	2.2	.89
37	1	3.3	1.6	2.06 *	2.5	2.0	.78
		-.6	1.2	.52	2.5	2.2	.88
39	2	-2.0	1.3	1.49	2.2	1.8	.80
		2.4	1.4	1.73	2.3	1.8	.80
41	3	-1.7	.8	1.99	1.7	1.5	.87
		-1.3	1.5	.89	2.5	2.0	.80
43	4	1.1	.7	1.61	1.6	1.4	.90

SIGMA ZERO SQUARED : .67

SIGMA ZERO : .82 (WITH RMS ERROR : .12)

SIGMA ZERO NOT SIGNIFICANTLY DIFFERENT FROM UNITY

ADJUSTED COORDINATES AND THEIR A POSTERIORI RMS ERRORS

STATION	ADJUSTED COORDINATES (m) EASTING	NORTHING	ABSOLUTE POSITIONAL ERROR ELLIPSES RMS ERRORS (mm) MAXIMUM RMS EASTING	MINIMUM RMS NORTHING	BEARING OF ERROR (mm)	MAJOR AXIS (deg)
1	454348.8513	338603.1330	2.2	2.0	2.3	1.9	64
2	454398.4588	338472.7655	2.2	1.8	2.2	1.8	88
3	454624.1108	338173.7208	1.8	1.5	1.8	1.5	98
4	454553.7647	338122.1052	2.0	1.4	2.0	1.4	99
5	454554.6739	338549.6021	2.7	3.0	3.2	2.4	328
6	454632.5733	338601.6071	3.4	3.6	4.1	2.6	318
7	454661.8899	338635.2856	4.0	3.7	4.7	2.7	131
8	454687.1192	338620.7794	3.9	3.9	4.8	2.7	316
9	454601.8791	338504.6158	3.9	3.6	4.5	2.8	130
10	454728.1279	338417.1359	4.0	3.2	4.5	2.6	123
11	454599.1036	338271.6027	2.9	1.9	2.9	1.9	92

ADJUSTED DISTANCES AND BEARINGS AND THEIR A POSTERIORI RMS ERRORS

LINE	DISTANCE	RMSE	RELATIVE ERROR ELLIPSES BEARING	RMSE

	metres	mm	deg	min	sec	secs	MAXIMUM RMS ERROR (mm)	MINIMUM RMS ERROR (mm)	BEARING OF MAJOR AXIS (deg)
1 TO 2	139.4869	1.6	159	10	1.74	4.07	2.8	1.6	72
1 TO 3	510.0614	2.5	147	20	22.32	1.17	2.9	2.4	70
1 TO 4	522.8550	2.5	156	55	35.17	1.18	3.0	2.4	83
1 TO 5	212.6700	2.9	104	34	43.18	3.35	3.5	2.8	2
1 TO 6	283.7262	3.4	90	18	29.33	2.98	4.3	3.2	334
1 TO 7	314.6856	3.9	84	8	8.30	2.88	4.8	3.4	321
1 TO 8	338.7280	3.9	87	0	49.51	2.78	5.0	3.4	325
1 TO 9	271.5304	4.4	111	16	25.00	2.83	4.6	3.5	317
1 TO 10	422.4283	4.5	116	7	23.91	1.70	4.6	3.4	126
1 TO 11	415.3776	2.9	142	57	10.91	1.66	3.5	2.7	81
2 TO 3	374.6285	2.5	142	57	45.59	1.41	2.8	2.3	93
2 TO 4	383.5135	2.4	156	6	41.94	1.49	2.9	2.2	96
2 TO 5	174.0892	1.4	63	48	32.73	3.77	3.2	1.3	330
2 TO 6	267.2261	1.9	61	10	27.97	3.28	4.3	1.8	325
2 TO 7	309.5299	2.2	58	19	41.05	3.17	4.8	2.1	319
2 TO 8	324.3964	2.3	62	51	10.77	3.12	5.0	2.1	323
2 TO 9	205.8987	3.4	81	6	4.39	4.05	4.7	2.5	315
2 TO 10	334.3297	4.3	99	34	41.02	2.07	4.6	3.0	126
2 TO 11	284.1211	3.0	135	4	25.87	2.09	3.4	2.5	95
3 TO 4	87.2510	1.5	233	43	51.79	4.76	2.0	1.5	133
3 TO 5	382.2410	3.1	349	32	1.31	1.65	3.3	2.8	125
3 TO 6	427.9700	3.3	1	7	58.90	1.83	4.2	2.9	125
3 TO 7	463.1084	3.3	4	40	45.26	1.98	4.8	2.9	121
3 TO 8	451.4770	3.4	8	1	20.75	2.03	4.8	2.9	127
3 TO 9	331.6410	3.4	356	9	22.59	2.37	4.2	2.8	122
3 TO 10	264.7083	2.3	23	8	17.44	3.26	4.2	2.2	121
3 TO 11	101.0259	1.3	345	40	6.47	4.55	2.2	1.3	75
4 TO 5	427.4978	3.3	0	7	18.68	1.64	3.7	2.9	130
4 TO 6	485.9350	3.5	9	20	.29	1.80	4.6	3.0	130
4 TO 7	524.4475	3.4	11	53	52.73	1.92	5.2	3.0	125
4 TO 8	516.1971	3.5	14	58	17.77	1.98	5.3	3.0	129
4 TO 9	385.5248	3.6	7	10	9.61	2.47	5.0	3.0	126
4 TO 10	342.7034	2.5	30	34	59.09	3.01	5.0	2.5	121
4 TO 11	156.2214	1.9	16	52	16.44	4.33	3.3	1.9	102
5 TO 6	93.6634	1.3	56	16	23.67	4.81	2.2	1.2	320
5 TO 7	137.2477	1.7	51	22	9.40	4.60	3.1	1.7	133
5 TO 8	150.3595	1.9	61	44	45.54	4.59	3.4	1.8	322
5 TO 9	65.2081	3.6	133	37	16.49	7.06	3.6	2.2	126
5 TO 10	218.2511	3.7	127	22	7.81	2.96	3.7	3.0	106
5 TO 11	281.5273	3.0	170	55	11.35	2.50	3.5	3.0	102
6 TO 7	44.6509	1.2	41	2	20.41	5.99	1.3	1.2	103
6 TO 8	57.8173	1.4	70	38	2.05	6.50	1.8	1.4	327
6 TO 9	101.7322	1.9	197	33	38.52	6.65	3.3	1.8	121
6 TO 10	207.7505	3.1	152	36	58.38	3.45	3.7	2.8	95
6 TO 11	331.6973	3.2	185	47	28.53	2.45	4.0	3.1	117
7 TO 8	29.1024	1.2	119	53	51.82	6.13	1.2	.9	121
7 TO 9	143.7912	1.5	204	40	1.95	5.38	3.8	1.4	119
7 TO 10	227.9841	3.1	163	6	35.49	3.50	4.1	2.7	100
7 TO 11	369.0628	3.2	189	47	42.04	2.54	4.6	3.0	116
8 TO 9	144.0829	1.3	216	16	15.53	5.26	3.7	1.3	129
8 TO 10	207.7315	3.1	168	36	51.69	3.60	3.9	2.8	110
8 TO 11	360.0988	3.2	194	8	51.40	2.58	4.7	2.9	124
9 TO 10	153.5952	1.3	124	43	7.42	3.77	2.8	1.3	32
9 TO 11	233.0296	3.3	180	40	56.78	2.89	3.6	2.8	316
10 TO 11	194.4921	1.4	221	33	32.37	3.80	3.6	1.4	135

ADJUSTED ANGLES AND THEIR A POSTERIORI RMS ERRORS

CLOCKWISE ANGLES						RMSE
AT	FROM	TO	deg	min	sec	secs
2	1	5	84	38	30.99	4.52
2	5	1	275	21	29.01	4.52
5	2	6	172	27	50.94	5.37
5	6	2	187	32	9.06	5.37
6	5	7	164	45	56.74	5.23
6	7	5	195	14	3.26	5.23
7	6	8	258	51	31.41	5.02
7	8	6	101	8	28.59	5.02

8	9	7	83	37	36.29	4.96
8	7	9	276	22	23.71	4.96
9	10	8	271	33	8.11	5.47
9	8	10	88	26	51.89	5.47
10	11	9	83	9	35.04	5.02
10	9	11	276	50	24.96	5.02
11	3	10	235	53	25.90	5.23
11	10	3	124	6	34.10	5.23
3	4	11	111	56	14.67	4.78
3	11	4	248	3	45.33	4.78

****

End of Program - Mode 2 Completed

****

Appendix 12: Urban Canyon GNSS Simulation (UCGS) Tool

This tool was developed by the author in the Microsoft Visual Basic for Applications (VBA) version 6.3 editor embedded with ArcView/ArcScene. ArcScene was chosen for this purpose because it provides 3D visualization techniques which enhance the data checking and interpretation of 3D models. Within ArcScene, the building of UCGS tool was started by creating a new toolbar (UCGS Tool), and adding a programmed ArcMap command 'Add Buildings to TIN' to this toolbar. The next step was creating a new User Interface Button (UIButton) -UCGS button-, adding it to the toolbar and changing the button image. These tasks were performed within Customize menu from Tools in ArcScene's pop up menu (Figure A12.1).

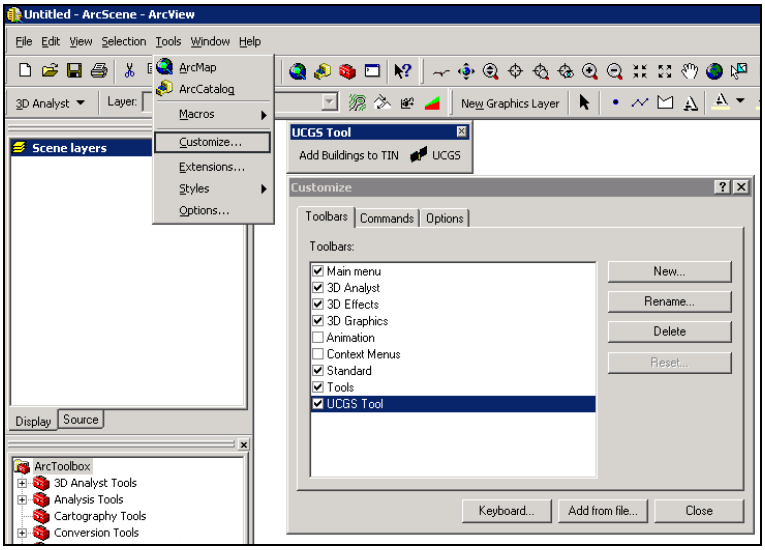

Figure A12.1: Customisation of ArcScene for the UCGS tool

As with any UIButton, clicking the UCGS button loads and displays the UCGS user form (Figure A12.2). The UCGS user form is the interface which controls the input and output options.

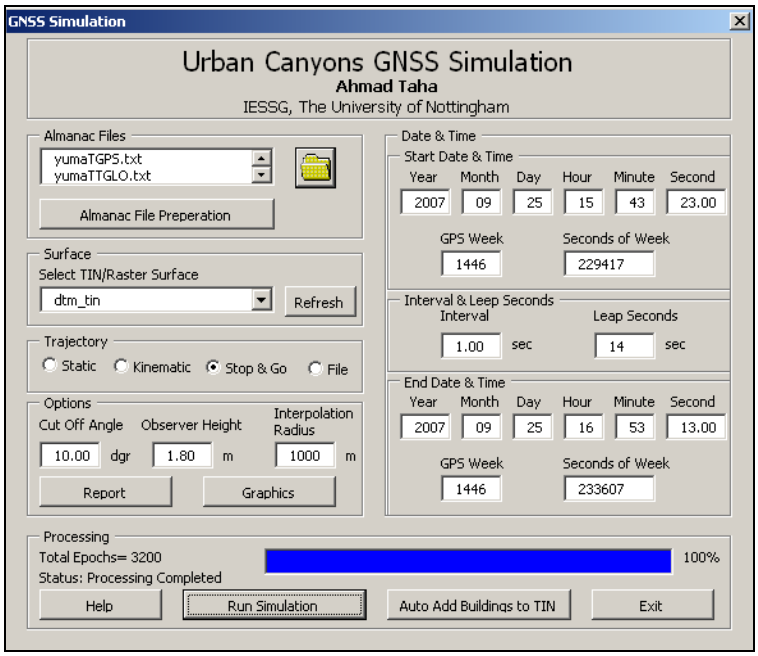

Figure A12.2: The developed UCGS user form

From Figure A12.2, it can be seen that the UCGS user form is divided into six major frames. These are defined and described below:

1. *Almanac files frame*: This frame contains two options: load almanac files and 'Almanac File Preparation'. Multiple almanac files can be browsed from any particular location and loaded to be used in UCGS. These files must be in Yuma format (see Appendix 13: Example of almanac file in Yuma format). The GPS Almanac file in Yuma format (either Current or archives from 1996-current) can be obtained over the internet from [Navigation-Center, 2008b]. Alternatively, the latest GPS or GPS+GLONASS almanac files can be downloaded as a combined file from the Magellan Support FTP site [Magellan-Professional, 2008]. These files are stored in Ashtech Binary file format, but Ashtech Evaluate, i.e. Version 6.01, software can be used to read the Almanac file in the Ashtech Binary format and save it as an ASCII file in Yuma format. The output almanac file contains information about all of the GPS and GLONASS satellites. It is important to notice the satellites health within the Almanac file. Satellites with health of 0 mean that the satellite is fully working, but satellite with health of 1 means bad (unreliable) satellite. Using the option 'Almanac File Preparation' within UCGS, it is possible to separate GPS satellites from GLONASS satellites. In addition,

it can interpolate the location of the bad satellites based on the nominal orbit parameters. GPS and GLONASS aside, there are no available almanacs for other GNSS constellations i.e. Galileo and COMPASS. However, for these constellations, almanacs in Yuma format can be generated based on their nominal values using the 'Almanac File Preparation' option, assuming that the orbital nominal values for a GNSS constellation are available and have been loaded using the 'Constellation Builder' form.

2. *Surface frame*: The surfaces, either TIN (Triangulated Irregular Network) or Raster, are loaded automatically when the UCGS form is initialised. All layers within ArcView's table of contents are filtered and any layer with type TIN and/or Raster layer are added to Combo-Surface in the Surface frame. In case of different TIN/Raster layers are found, a user can select one layer in order to be used as a working surface. Otherwise, the first TIN/Raster layer will be selected by default as the working surface.

3. *Trajectory frame*: In order to be capable to simulate different scenarios, four trajectory options are available: Static, Kinematic, Stop & Go and File. Firstly, the Static option provides three static options: One Point, Grid Points and Polyline (Figure A12.3). These options provide flexibility for a desired static scenario to be simulated.

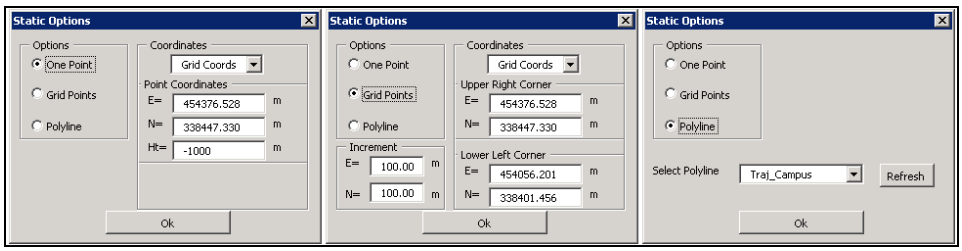

Figure A12.3: Static Options: One Point (left), Grid Points (middle) and Polyline (right)

In addition, the height coordinate in the One Point option can be either specified in the 'Ht' text box or is interpolated automatically from the surface, in the case that the default 'Ht' value (i.e. -1000 m) is detected. Similarly, the heights along a selected polyline in the Polyline option will

be interpolated automatically from the surface. All polyline layers will be automatically initialized in Combo-Polyline of Static Options when opening the UCGS tool.

Secondly, two options are available in the Kinematic Option menu: Time Interval and Distance Interval (Figure A12.4). One of these options, together with Speed (observer speed), are used for interpolation of the trajectory polyline into equal segments. Similar to the Static Option menu, all polyline layers are automatically initialized in Combo-Polyline of Kinematic Options when opening the UCGS tool.

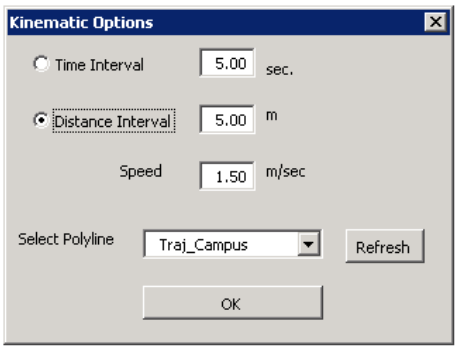

Figure A12.4: Kinematic Option Menu

Thirdly, two options are available in the Stop & Go Option menu: Speed between points and Jump from one point to another (Figure A12.5). The 'Speed between points' option assumes that a time between points is to be calculated after completing the time on the point. Whereas, 'Jump from one point to another' assumes a continuous time for the new point after completing the time on the point. All polyline layers will be automatically initialized in Combo-Polyline of the Stop & Go Options when opening the UCGS tool.

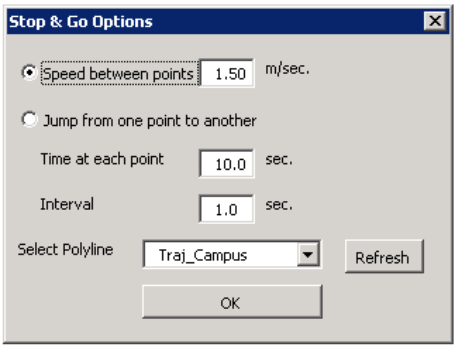

Figure A12.5: Stop & Go Option Menu

The last option in the trajectory frame is the File option. In this case, ASCII file can be created to perform the simulation for desired times and locations. This file must be in text delimited format and include the following in each row: Point Id, East, North, Height, GPS seconds of week and GPS week. Similar to the Static One Point option, if the point's height is -1000, the height will be interpolated from the surface.

4. *Options frame*: Within the option frame, it is possible to define the Cut-Off-Angle (10 degrees by default), Observer height (1.80 m by default) and Interpolation Radius (1000 m by default). The interpolation radius is important in two ways: satellite interpolation and visibility radius. Since the 3D model should be in a rectangular grid coordinate system, such as British National Grid in UCGS, the satellite's coordinates must be in the same system. Therefore, it is necessary to interpolate the satellite location to be within the transformation limits of the country, e.g. within the UK as determined by Grid InQuest software. On the other hand, the satellite visibility is performed along a line of sight between the interpolated satellite and the observer. The longer the interpolation radius is, the more coverage of the 3D model is, but the more time for checking the visibility.

   Another option in the Options frame is the Report option which allows the user to control of the output data in report files (Figure A12.6).

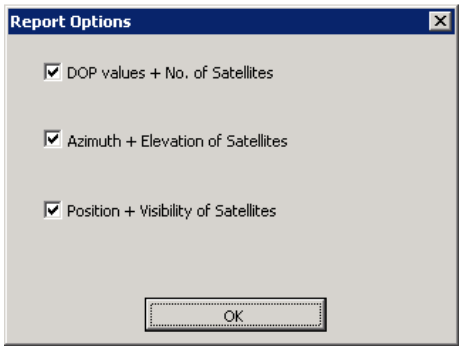

Figure A12.6: Report Options menu

   Separately, the Graphics option enables different graphics to be visualised, printed or saved. These graphics include Variation of Number

of satellites, DOP values, Azimuth of satellites, Elevation of satellites, Azimuth versus Elevation and Sky plot.

5. *Date & Time frame*: Start and end date and time of the simulation can be specified as either UTC time (year, month, day, hour, minute and seconds) or GPS time (GPS week and GPS seconds of week). Interval and Leap seconds are also specified at this stage.

6. *Processing frame*: the Help option provides instructions about the different frames within UCGS. When the 'Run Simulation' button is clicked, the program will run the satellite visibility simulation within the 3D model using the trajectory scenario. The output results are several graphs (which are explained in the Options Frame) and reports. 'Auto Add Buildings to TIN' option is used to categorise the buildings level, to add them to a new field ('Level' field) in the buildings layer's attributes and to add buildings to a TIN. The simulation and 'Auto Add Buildings to TIN' algorithms are discussed in more detail in the next section on UCGS tool algorithms.

Appendix 13: Example of Almanac File in Yuma Format

GPS**** Week 1446 almanac for PRN-01 **********
ID: 001
Health: 000
Eccentricity: 6.920337677e-003
Time of Applicability(s): 4.055040000e+005
Orbital Inclination(rad): 9.911517630e-001
Rate of Right Ascen(r/s): -7.428880871e-009
SQRT(A) (m^1/2): 5.153372070e+003
Right Ascen at TOA(rad): 8.611639313e-002
Argument of Perigee(rad): -1.810511534e+000
Mean Anom(rad): -6.373300686e-001
Af0(s): 1.554489136e-004
Af1(s/s): 0.000000000e+000
week: 1446

GPS**** Week 1446 almanac for PRN-02 **********
ID: 002
Health: 000
Eccentricity: 8.664131165e-003
Time of Applicability(s): 4.055040000e+005
Orbital Inclination(rad): 9.452401974e-001
Rate of Right Ascen(r/s): -8.263201338e-009
SQRT(A) (m^1/2): 5.153579102e+003
Right Ascen at TOA(rad): -2.067155209e+000
Argument of Perigee(rad): 2.398507792e+000
Mean Anom(rad): 1.894657272e-001
Af0(s): 1.392364502e-004
Af1(s/s): 0.000000000e+000
week: 1446

etc.

Appendix 14: A Continuous UPdating Technique

A Continuous UPdating Technique (CUPT) has been developed as part of this research to loosely couple RTK GPS positions, determined by the SmartStation or the IntegratedPole/SmartPole, with angles and distances measured by a total station. This technique makes use of all RTK positions that could be available during multiple setups of SmartStation or when moving from one point to another using an IntegratedPole/SmartPole and can eliminate the need of two control points to start the survey. Several Matlab functions were written to perform the CUPT calculations and to output an adjustment report and various statistics. A visual overview of CUPT is provided in Figure A14.1.

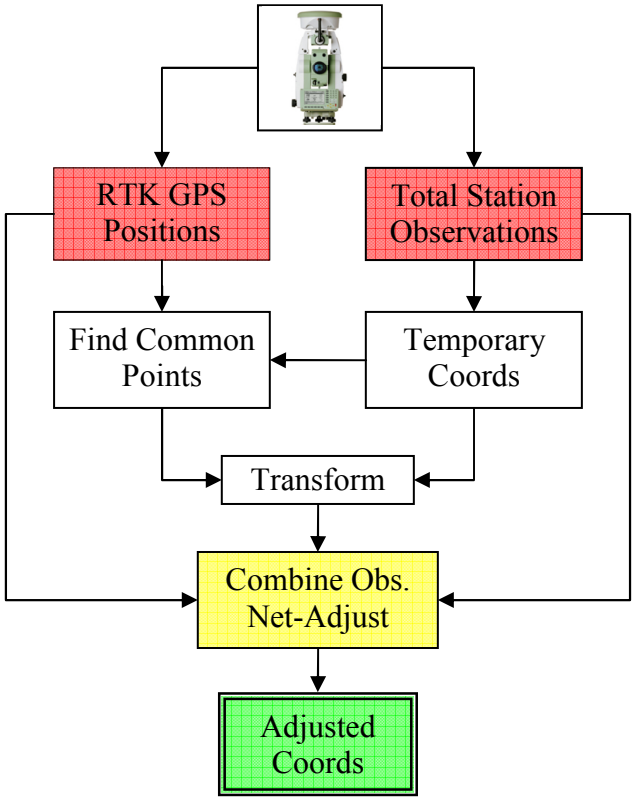

Figure A14.1: Continuous Updating Technique flowchart

The adjusted coordinates in CUPT are continuously maintained and updated as new observations are acquired from the GPS or the total-station. In general, CUPT involves in the following steps:

Step 1: Collect RTK GPS positions wherever available. The user can collect all available RTK GPS positions during the multiple setups of the SmartStation or when moving the IntegratedPole/SmartPole from one point to another.

Step 2: Collect all necessary total-station observations (distances and angles). Also, it is possible to collect multiple measurements (e.g. face left and face right) from one or more stations for the same point.

Step 3: Temporary coordinates calculation. The calculation process starts on the calculation of temporary coordinates in the main Matlab Script (M-Script) of CUPT software. The slope distance (*SD*) and the zenith angle (*Znth*) are used to calculate horizontal distance (*HD*) and height difference (*Dh*) using the formulas:

$$HD = SD * \sin Znth$$

$$Dh = SD * \cos Znth + hi - ht$$

where *hi* is the instrument height and *ht* target height. Then the calculated *HD, Dh* and the measured horizontal angle (*Hz*), used as azimuth (*Az*), are used to compute 3D temporary coordinates (E_T, N_T, Ht_T) using:

$$E_T = E_f + HD * \sin Az$$

$$N_T = N_f + HD * \cos Az$$

$$Ht_T = Ht_f + Dh$$

where E_f = Easting, N_f = Northing and Ht_f = Height are the temporary coordinates of a starting station (e.g. 1000, 1000, 100 respectively).

Step 4: Find common RTK and temporary points. At least two horizontal controls and one vertical control are required to start the transformation. Since it was not possible to collect multiple measurements under the same name, an editing step to correct the name of the SmartStation observation file is required.

Step 5: Transform the temporary coordinates to grid coordinates. Perform a '2d' linear conformal transformation for 'E' and 'N' between the temporary coordinates and the RTK GPS coordinates. A minimum of two common points are required to calculate four transformation parameters (rotation (α), scale (*S*), and translations (T_N and T_E). Using these transformation parameters, the temporary coordinates (E_T and N_T) can be transformed to unadjusted grid coordinates (E_G and N_G) using the formulas:

$$E_G = (S * \cos\alpha) * E_T - (S * \sin\alpha) * N_T + T_E$$

$$N_G = (S * \sin\alpha) * E_T + (S * \cos\alpha) * N_T + T_N$$

The height coordinate can be translated with respect to the height differences between the temporary height and the RTK GPS Orthometric height. The results of this translation will be unadjusted Orthometric heights (Ht_G).

Step 6: Combine observations using the Net_Adjust function. This function performs a 3D network adjustment based on a least squares adjustment. Total station observations, raw RTK GPS coordinates and the unadjusted grid coordinates including the unadjusted Orthometric heights, are combined using observation weights (and correlations between observations) in Net_Adjust software. This creates what is called a complex network.

A least squares adjustment involves two models: a stochastic model and a functional model. In a least squares adjustment, it is essential to select a proper stochastic (weighting) model since it controls the amount of correction received during the adjustment. In order to compute weight for RTK GPS positions and total station observations, standard deviation for each observation is calculated.

As discussed in the SmartStation Overview section, the nominal RTK GPS position precision is given as a horizontal precision of 10mm (a_H) + 1ppm (*bppm*) and a vertical precision of 20mm (a_V) + 1ppm (*bppm*). Furthermore, the RTK GPS position precision could also be affected by SmartStation centring error (σ_i) and other errors such as reference station precision (σ_{RE} East precision, σ_{RN} North precision and σ_{RHt} Height precision) and multipath error. However, in the case of the SmartStation employed, the multipath errors are smoothed by using both the SmartAntenna and the RTK GPS processing algorithms [Leica-Geosystems-AG, 2005d]. Hence, the RTK position standard deviations can be calculated as follows:

$$\sigma_E = \sqrt{\sigma_i^2 + \sigma_{RE}^2 + a_H^2 + (D.bppm)^2}$$

$$\sigma_N = \sqrt{\sigma_i^2 + \sigma_{RN}^2 + a_H^2 + (D.bppm)^2}$$

$$\sigma_{Ht} = \sqrt{\sigma_i^2 + \sigma_{RHt}^2 + a_V^2 + (D.bppm)^2}$$

The standard deviations for the total station observations can be calculated as follows:

- σ_D Standard deviation in the measured distance (*D*) is

$$\sigma_D = \sqrt{\sigma_i^2 + \sigma_t^2 + a^2 + (D.bppm)^2}$$

where σ_i is the instrument centring error, σ_t is the target centring error, *a* and *b* are the instrument's specified precision parameters.

- σ_{Hz} Standard deviation in the measured horizontal angle (*Hz*) is

$$\sigma_{Hz} = \sqrt{\sigma_{ci}^2 + \sigma_{ct}^2 + \sigma_r^2 + \sigma_p^2}$$

where σ_{ci} is the combined instrument centring error, σ_{ct} is the combined target centring errors, σ_r is the reading circle error, and σ_p is the pointing error. More information about the combined instrument and target errors can be found in [Davis, 1981] and [Ghilani and Wolf, 2006] .

- σ_{Znth} Standard deviation in the measured zenith angle (*Znth*) is

$$\sigma_{Znth} = \sqrt{\sigma_r^2 + \sigma_p^2 + \sigma_l^2 + \sigma_{Ihe}^2 + \sigma_{The}^2}$$

where σ_r is the reading circle error, σ_p is the pointing error, σ_l is the levelling of the vertical circle control bubble error, or the instrument's vertical compensator error, σ_{Ihe} is the instrument height error and σ_{The} is the target height error.

The functional model, or mathematical observation equations, relate the measurements and the parameters. In general, there are two basic forms for the functional models: the conditional and parametric adjustments. In a conditional adjustment geometric conditions are enforced on the observations and their residuals. When conducting a parametric adjustment, observations are expressed in terms of unknown parameters that were never observed directly. For example, the coordinate equations are used to model the total station observations (angles and distances). The parametric adjustment yields the most probable values for the coordinates (parameters) which provide the most probable values for the observations. Furthermore, the adjustment by parameters is now the standard solution approach to almost all over-determined systems [Rizos, 1999].

The combination of stochastic and functional models results in a mathematical model for the adjustment. The CUPT mathematical model (implemented in Net_Adjust) can be obtained as follows:

- Obtain initial approximations for the unknowns (X^O -the transformed unadjusted grid coordinates- E_G, N_G and Ht_G).
- Define the weight matrix of observations (*W*). This is a diagonal matrix with elements equal to $(1/\sigma_i^2)$, where σ_i is the standard deviation for the observation. Details of the forming of the weight matrix can be found in [Ghilani and Wolf, 2006].
- Form the Observed minus Computed matrix (*OmC*) for all observations (distances, horizontal angles, zenith angles and RTK GPS E, N and Ht). It should be noted that the observed slope distances should be reduced to mean sea level, with scale correction applied and corrected for the difference between the instrument height and the prism height. Likewise, zenith angles should be corrected for refraction and earth curvature and for the difference between the instrument height and the prism height.
- Compute the elements of the design matrix (A), containing the partial derivatives of the range observations with respect to the unknowns. For any observation '*ij*', the following slope distance equation can be written:

$$D_{ij} + v_{Dij} = \sqrt{\Delta E_{ij}^2 + \Delta N_{ij}^2 + \Delta Ht_{ij}^2}$$

Where v_{Dij} is the residual in the observed slope distance D_{ij}, $\Delta E_{ij} = (E_j - E_i)$, $\Delta N_{ij} = (N_j - N_i)$ and $\Delta Ht_{ij} = (Ht_j - Ht_i)$.

The previous equation is a nonlinear function involving the unknown variables $(\Delta E_{ij}, \Delta N_{ij}, and\ Ht_{ij})$ that can be written as

$$F(\Delta E_{ij}, \Delta N_{ij}, Ht_{ij}) = \sqrt{\Delta E_{ij}^2 + \Delta N_{ij}^2 + \Delta Ht_{ij}^2}$$

A system of nonlinear equations such as slope distance equations can be linearized using a first-order Taylor-series expansion. The linearized slope distance observation can be, after the partial derivatives, written as follows:

$$+\left(\frac{\Delta E_{ij}}{D_{ij}}\right)dE_i+\left(\frac{\Delta N_{ij}}{D_{ij}}\right)dN_i+\left(\frac{\Delta Ht_{ij}}{D_{ij}}\right)dHt_i$$
$$-\left(\frac{\Delta E_{ij}}{D_{ij}}\right)dE_j-\left(\frac{\Delta N_{ij}}{D_{ij}}\right)dN_j-\left(\frac{\Delta Ht_{ij}}{D_{ij}}\right)dHt_j$$

Like slope distance, for any observation '*ij*', the following zenith equation can be written:

$$Znth_{ij}+v_{Znthij}=\arctan\left(\frac{\sqrt{\Delta E_{ij}^2+\Delta N_{ij}^2}}{\Delta Ht_{ij}}\right)$$

where v_{Znthij} is the residual in the observed zenith angle $Znth_{ij}$. The linearized zenith angle observation can be, after the partial derivatives, written as follows:

$$-\left(\frac{\Delta Ht_{ij}.\Delta E_{ij}}{HD_{ij}.D_{ij}^2}\right)dE_i+\left(\frac{\Delta Ht_{ij}.\Delta N_{ij}}{HD_{ij}.D_{ij}^2}\right)dN_i+\left(\frac{HD_{ij}}{D_{ij}^2}\right)dHt_i$$
$$+\left(\frac{\Delta Ht_{ij}.\Delta E_{ij}}{HD_{ij}.D_{ij}^2}\right)dE_j+\left(\frac{\Delta Ht_{ij}.\Delta N_{ij}}{HD_{ij}.D_{ij}^2}\right)dN_j-\left(\frac{HD_{ij}}{D_{ij}^2}\right)dHt_j$$

where HD_{ij} is the horizontal distance and D_{ij} is the slope distance.

Note that RTK GPS position (E, N and Ht) observation equations are linear and that the only nonzero elements of the 'A' matrix are either '1' or '-1'. Besides, linearization of horizontal angle observation equation can be found in [Ghilani and Wolf, 2006].

- Solve for corrections to the initial approximations (ΔX) using:

$$\Delta X=(A^T*W*A)^{-1}*(A^T*W*OmC)$$

where (A^T*W*A) is the normal matrix (N).

- Apply the corrections to the initial approximations. The adjustment values (X) will be:

$$X=X^O+\Delta X$$

where X matrix contains the adjusted coordinates (E, N and Ht).

- Iterate to account for the neglect of higher order terms from the Taylor series. This iterative process requires solving non-linear equations and must stop at appropriate point. The best method for ending the iteration process, described in [Ghilani and Wolf, 2006], is the monitoring of the reference variance and its

change between iterations. This method is used in CUPT for terminating the iteration process.

Least squares adjustment also provides an estimate of the precision parameters (coordinates in this case) through the covariance matrix (Q_{xx}). The covariance matrix contains the variance of each unknown and the covariance of each pair of unknowns and can be calculated using:

$$Q_{xx} = N^{-1} = (A^T * W * A)^{-1}$$

The quantities in Q_{xx} need to be scaled by a reference variance. This reference variance (S_O^2) is related to the weighting matrix and the residuals by the equation:

$$S_O^2 = \left(\frac{A^T * W * A}{r} \right)$$

where *r* is the number of degrees of freedom (i.e., the number of equations minus the number of unknowns).

Adjusting a network with least squares provides a means for statistically testing the observations. As redundant observations are available in CUPT, blunders can be detected by comparing the unadjusted grid coordinates (for new points) with the adjusted grid coordinates (under the same name). After the adjustment, CUPT performs a goodness-of-fit (χ^2) test. Passing or failing this test could be viewed as a warning flag for the adjustment that requires further analysis. Thus the a posteriori residuals can be checked for the presence of large discrepancies or outliers. More information about outlier detection and adjustment analysis can be found in [Ghilani and Wolf, 2006] and [Davis, 1981].

Step 7: The outputs from the adjustment are a report and several figures. The report includes: the goodness-of-fit (χ^2) test result, the observed coordinates and their a priori standard error, the adjusted coordinates and their a posteriori standard error and absolute positional error ellipses, and observed measurements (such as distances and angles) and their a priori and a posteriori standard error. The figures include: one figure with measurements residuals, Histogram plot and normal probability plot, another figure with network geometry and error ellipse, comparison figures with

'truth' coordinates and/or SmartStation coordinates, and another optional figure showing tracking one point over the different solutions within CUPT.

It is worth mentioning that the adjusted coordinates are continuously updated within CUPT as new observations are available from either the RTK GPS or the total-station.

Appendix 15: Results of GPS and Total-Station Integration – Test9 to Test 14

(a) Differences between 'Truth' coordinates and Test9

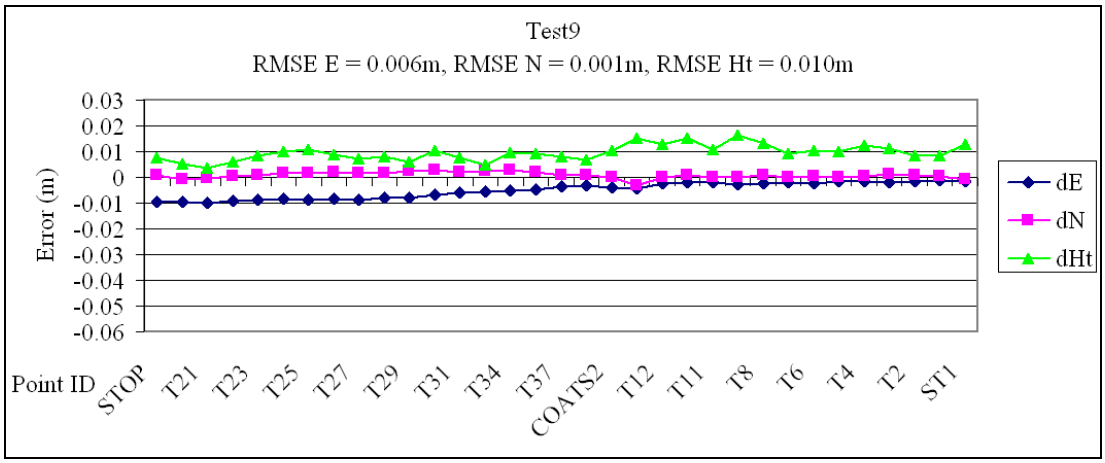

(b) Differences between 'Truth' coordinates and Test10

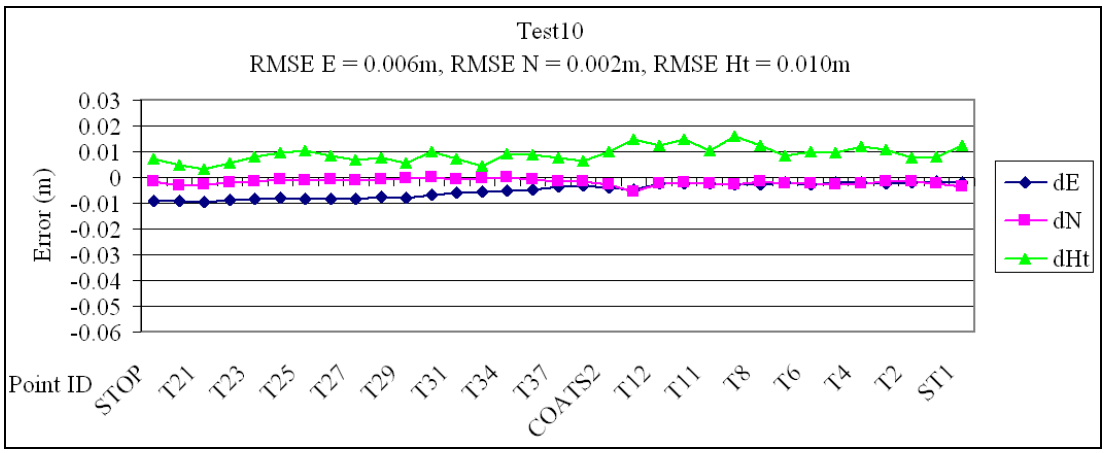

(c) Differences between 'Truth' coordinates and Test11

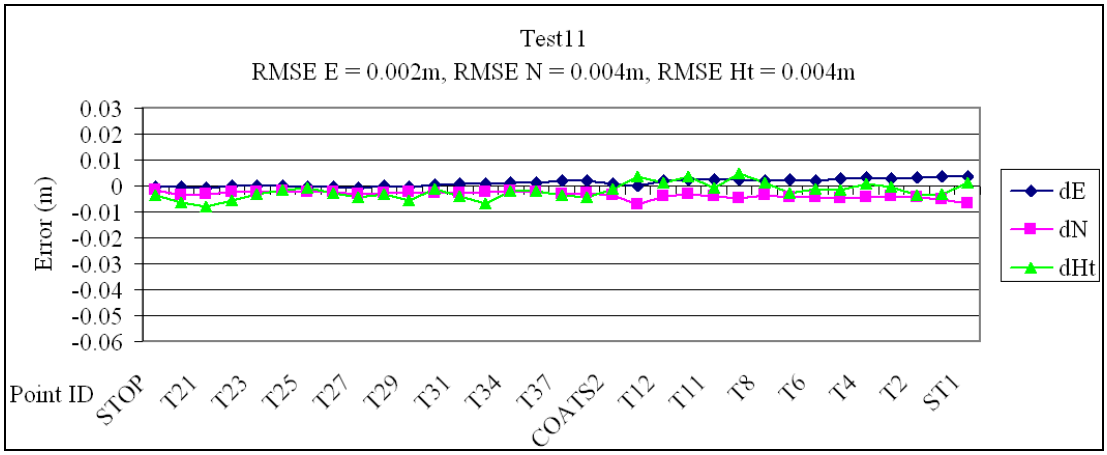

(d) Differences between 'Truth' coordinates and Test12

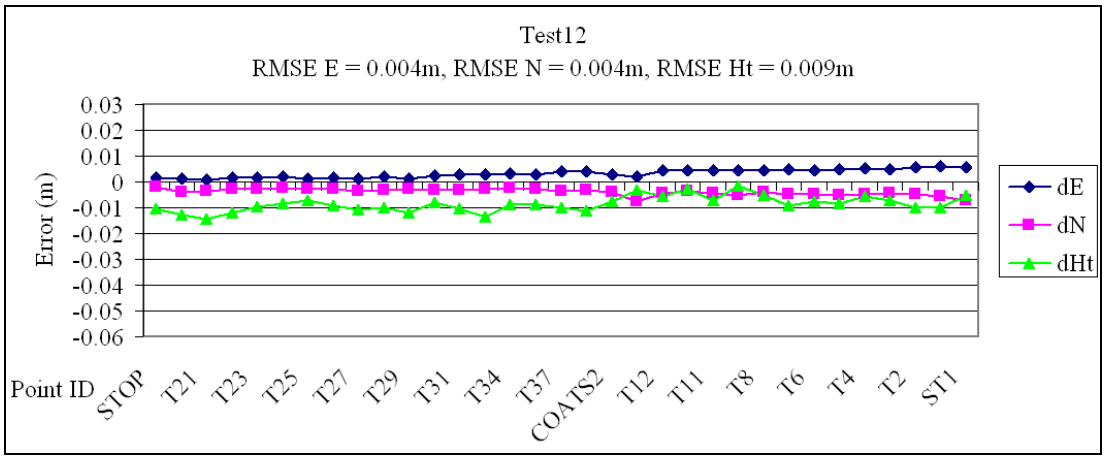

(e) Differences between 'Truth' coordinates and Test13

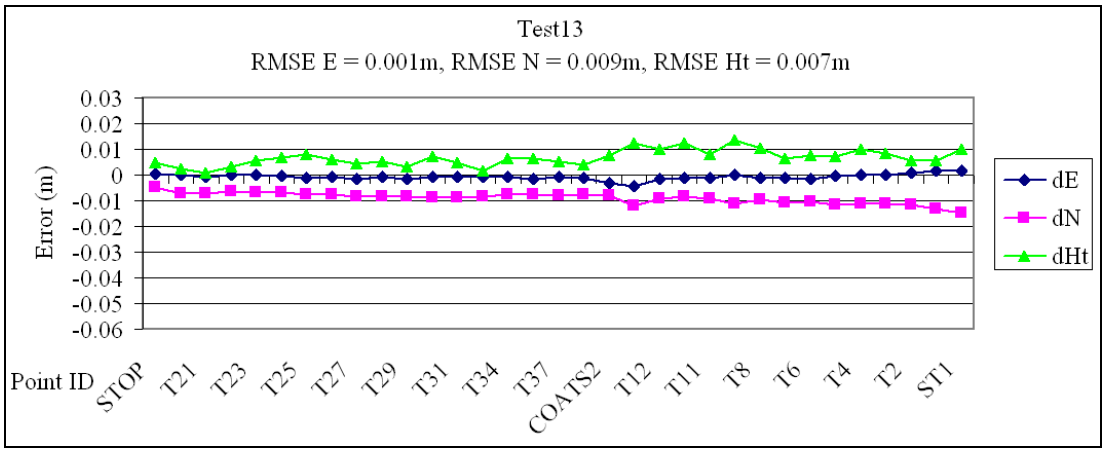

(f) Differences between 'Truth' coordinates and Test14